Neotectonic deformation features in Plio-Pleistocene coastal aeolianites: Palaeoseismology and earthquake hazard implications for the Southern Cape, South Africa

Matthew Sotheron Hodge

Thesis presented for the degree of

Master of Science

Geological Sciences Department

University of Cape Town

September 2013

Supervisor: Dr Åke Fagereng

Abstract

Deformation features within Plio-Pleistocene Bredasdorp Group coastal aeolianites within the Southern Cape, South Africa, have been studied to resolve the neotectonic history of the region, estimate the recent to current upper-crustal stress field, and infer seismic hazard. Previous studies indicate possible Quaternary faulting within the Southern Cape, major faults within the underlying geology, and a horizontal maximum compressive stress (S_{Hmax}) orientated WNW-ESE to NW-SE.

This study utilised geological mapping, small-scale fieldwork, and remote sensing to investigate joints, faults, kink folds, cataclasites, and soft-sediment deformation features within the aeolianites. The majority of these deformation features are found proximal to the inferred traces of the Blomerus and Struisbaai faults. In places along the Blomerus Fault, the aeolianite cross-beds dip at angles of 40 °-90 °, as opposed to dips of <37 ° (the angle of repose for unconsolidated aeolian sands) observed in the rest of the study area.

Possible mechanisms responsible for the aeolianite deformation are: 1) wave action-induced collapse; 2) active sedimentary processes during deposition and consolidation of the aeolian dunes; 3) tectonic activity on underlying faults within the study area. The relative sea level transgression-regression cycles since the consolidation of the aeolianites indicate that the sea level was too low to erode the aeolianites. Likewise, sedimentary processes do not account for the brittle deformation types, non-slope confined deformation, and consistent orientations observed. Normal fault displacement on the Blomerus Fault and the formation of a monocline-type drag fold in the overlying aeolianites, some time between 125 ka - 1.8 Ma, does however account for the steeply dipping cross-beds and deformation features. Limited normal fault displacement on the Struisbaai Fault, some time after 160 ka, may explain the minor aeolianite deformation east of the Blomerus Fault.

An average NW-SE (099 ° - 174 °) orientated S_{Hmax} trajectory for the Southern Cape is inferred from joint orientations. The Blomerus and Struisbaai faults are either well or moderately-well orientated to this stress field for future reactivation as normal faults. The dimensions of the faults indicate palaeomagnitude estimates of M_w > 6.1, with the Blomerus Fault exhibiting a potential maximum M_w∼7.3. From the estimated earthquake magnitudes, the inferred recurrence interval of seismicity for the Southern Cape is on the 100 ka to 1 Ma time-scale, which implies that the possibility of a future earthquake in the next 100-1000 years is low. However, considering the time since the last faulting events, and the potential for large earthquakes (M_w > 6.0) within the region, a low to moderate earthquake hazard is estimated for the Southern Cape.

Acknowledgements

The author would like to acknowledge the friends, colleagues, supervisors, and family who assisted me with the data collection whilst in the field, proof reading of thesis drafts, and tireless support during the thesis writing period. In particular I wish to thank L. Smit and C. Cross for the time spent as my field assistants, and both my Supervisor Dr Åke Fagereng and Marco Andreoli for the invaluable contributions, guidance, and advice over the past two years. I would like to thank the owners of the farms Groot Hagelkraal and Heidehof for accommodating me during the field work. I additionally wish to acknowledge the generous financial support from the Nuclear Energy Corporation of South Africa (NECSA), the University of Cape Town Post Graduate Funding office, the University of Cape Town Geological Sciences Department, and the National Research Foundation (NRF) towards this Masters Thesis.

Contents

Chapter 1

Introduction

Earthquake activity constitutes a considerable hazard to critical facilities (e.g. dams, nuclear power stations, nuclear waste storage sites) particularly if the facilities are located on or near faults capable of earthquake rupture (Andreoli *et al.*, 1996; Gürpinar, 2005; Singh *et al.*, 2011). If there is either a lack of contemporary seismic monitoring, or significant earthquake rupture only occurs episodically separated by extensive time of seismic quiescence (10 ka or more), there is commonly no documentation of regional active tectonics (McCalpin and Nelson, 2009). If no earthquake record for a given area exists, or faults capable of rupture are unidentified, the assessment of earthquake hazard becomes more difficult (Gürpinar, 2005; England and Jackson, 2011).

Intraplate regions such as Southern Africa, are considered to be relatively quiet in terms of active tectonics (Viola *et al.*, 2005), and possess low strain rates relative to the global average strain rate proposed by Pfiffner and Ramsay (1982). Earthquake activity can be temporally clustered on faults with relatively brief episodes of activity, then prolonged recurrence intervals while strain accumulates again (Sibson, 2002; Li *et al.*, 2009). Additionally, the spatial distribution of intraplate earthquakes has been attributed to the preferential reactivation of pre-existing structures, which formed during prior tectonic episodes (Zoback, 1992b). Pre-existing faults will typically reactivate if they are favourably orientated in a prevailing stress field (Sibson, 1985; White *et al.*, 1986). Consequently, any fault exhibiting evidence for palaeoearthquakes and that is also well orientated to fail in the current stress field, could potentially experience a future faulting event.

Given the complexity of many continental intraplate regions and the possible lack of earthquake records for a specific area, the investigation of preserved palaeoearthquakes and recent crustal deformation features can often be the only means to provide a neotectonic history and an earthquake hazard estimation (McCalpin and Nelson, 2009). Neotectonic and palaeoseismological studies have been done in other intraplate regions of the world, for example in the central and eastern parts of the United States of America and in Australia (e.g. Hancock and Engelder, 1989; Cox *et al.*, 2001; Sandiford, 2003; McCalpin, 2005). In the Southern Cape of South Africa, previous structural and neotectonic studies (field investigations and aeromagnetic surveys) have already suggested the following: 1) Past tectonic activity occurred during the Late Tertiary to Quaternary (Andersen and Andreoli, 1990); 2) Major faults are present within the Table Mountain Group sandstones and quartzites, and the Cape Granite Suite units (the underlying geology) (Andersen and Andreoli, 1990); 3) A possible horizontal maximum compressive stress field orientated WNW-ESE to NW-SE for the Southern Cape upper crust (Andreoli *et al.*, 1996).

The Southern Cape falls into the so-called Wegener Stress Anomaly (WSA), recognised through the orientation of the maximum horizontal compressive stress (S_{Hmax}) being almost perpendicular to the S_{Hmax} trajectory for the rest of Southern Africa (Andreoli *et al.*, 1996; Viola *et al.*, 2005; Bird *et al.*, 2006). As there is a lack of stress field data for the Southern Cape region, particularly offshore-onshore stress field integration, this study will add to the stress field data for the WSA. Although previous neotectonic activity was suggested by Andersen and Andreoli (1990) for the Southern Cape, a wider and more comprehensive study within this region, will add to the understanding of South African neotectonics, and potentially for wider intraplate tectonics. The assessment of the reactivation potential of the recognised faults, can provide an earthquake hazard estimation for the Southern Cape. This is particularly important as the study area encompasses a proposed site of a nuclear power station at Bantamsklip.

The aims of this study are therefore: 1) determine whether there is evidence for neotectonic activity within the Southern Cape, and most particularly if palaeoearthquakes can be identified on the previously reported faults, namely the Blomerus, Struisbaai, and Brandfontein Faults (Fig. 4.8); 2) provide local and regional current/neotectonic stress field estimates for the Southern Cape; 3) Suggest palaeomagnitudes for identified past earthquake

events; 4) compare the orientations of faults exhibiting palaeoearthquake evidence to the prevailing stress fields, and consider if these faults possess the potential for reactivation. 5) Postulate a recurrence interval for seismicity within the Southern Cape region, and thus estimate earthquake hazard.

The study concerns the Southern Cape region, which is located within the south-western part of Southern Africa (Fig. 1.1).

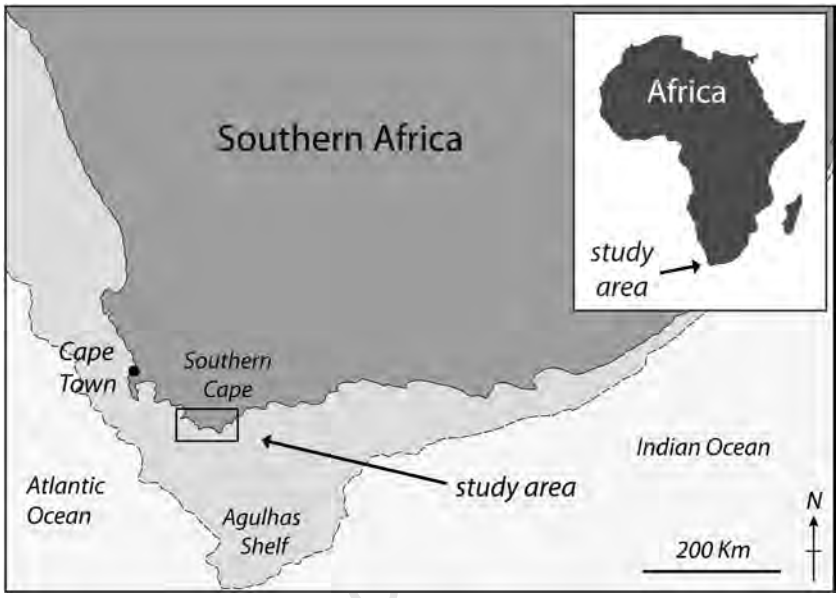

Figure 1.1: The study area is located at the southern-most part of Africa. Regionally the study area is ∼150 kilometres SE of the city of Cape Town, located along the southern coastal area of South Africa.

The Late Pliocene to Lower Pleistocene Wankoe Formation and Upper Pleistocene Waenhuiskrans Formation (of the Bredasdorp Group) coastal aeolianites (Malan, 1990) located proximal to faults previously recognised by Andersen and Andreoli (1990), are the primarily focus of this investigation. The underlying geology is considered only where it may be relevant to deformation of the overlying aeolianites, otherwise it has been ignored for the purpose of this study. Brittle deformation features, such as joints, faults, brittle/kink folds, and breccias within the Wankoe and Waenhuiskrans Formation aeolianites, are the main targets for data collection. Soft-sediment deformation features (if found within the aeolianites) are considered if associated with the recognised faults. The aeolianites located throughout the Southern Cape (not just proximal to the faults), have been examined to provide the horizontal stress field estimates. The underlying geology was not used to provide palaeo-stress

fields, because of its ancient nature and complex deformation history.

The theoretical background required to complete this study has been outlined in Chapter 2 through the following themes: Rock mechanics (brittle deformation, joints, and fault reactivation), crustal and neotectonic stress fields (principal stress axes, horizontal compressive stresses, and stress variability), sedimentary processes able to produce deformation features within aeolian dune bodies, and earthquake hazard (intraplate earthquakes, palaeoseismology, and methodology). This theoretical background was applied during the data collection and interpretation phases of the study.

To place the study within a geological context, the regional and local geological setting of this study is outlined in Chapter 3 through the following: Demarcation of the geographical position of the study area, the large-scale tectonic setting, the regional stratigraphy of the underlying geology, the major tectonic episodes (the Cape Orogeny and the break up of Gondwana) affecting the regional underlying geology, sea-level fluctuations affecting the region's coast line, the stratigraphy and characteristics of the cover geology, and a review of the previous work on the Southern Cape local geology.

A large-scale reconnaissance of the study region was done through remote sensing (satellite imagery, aerial photography, and digital elevation models), to uncover potential large-scale landform disruption features, which together with the geological setting review, delineate the sites of local investigation.

Local-scale field work is initially focussed on the petrology of the aeolianites to determine the specific rock formation (Wankoe or Waenhuiskrans Formations) present within the study areas, and record the sedimentary features (cross bedding and karstic features) within the aeolianites. Subsequently the geology of the local study areas was mapped (maps involve the adaptation of pre-existing maps made by Andersen and Andreoli (1990) for the Southern Cape) and geological cross-sections produced. Field investigation involved the measurement and documentation of deformation features present within the aeolianite units.

The spatial distribution of the Wankoe and Waenhuiskrans Formation aeolianites, and the relative abundance, orientations, deformation style, and distribution of the different brittle deformation and soft-sediment features (within and between the different aeolianite units) can be compared to work previously done by McKee (1979); Haq *et al.* (1987); Hancock *et al.* (1991); Schlische (1995); Willsey *et al.* (2002); Finch *et al.* (2004); Bintanja *et al.*

(2005); Pirrotta and Barbano (2010); Owen *et al.* (2011) to suggest whether sedimentary processes with aeolian dunes, (neo)tectonic activity on underlying faults, or collapse induced by wave undercutting of the aeolianites can account for the origin of these features.

Consequently, if neotectonics is determined as the most likely origin of the deformation features, the reactivation potential of the faults will be obtained by comparing the geometry of the identified faults with the estimated regional and local stress fields. A moment magnitude for the palaeoearthquake(s) will be estimated, and a recurrence interval for seismicity within the Southern Cape, will be estimated from previous work done by Kenner and Segall (2000); Sandiford (2003); Sandiford and Egholm (2008); Li *et al.* (2009) in other intraplate regions of the world. Subsequently, from these findings an estimate for earthquake hazard will be suggested for the Southern Cape.

Chapter 2

Theoretical Background

2.1 Rock Failure

The brittle failure modes of rocks within the upper crust have been studied and described thoroughly within the literature (e.g. Jaeger and Cook, 1976; Sibson, 1998; Ramsey and Chester, 2004). Before an attempt to analyse and interpret observed rock deformation features in this study, and as this investigation involves surfical deposits within the brittle deformation regime (Jaeger and Cook, 1976), the characteristics of brittle failure need to be examined.

2.1.1 Conditions of Brittle Failure

Assuming a rock unit is homogeneous and intact, it will typically obey the Griffith and Coulomb criteria, defined respectively as:

$$\tau^2 = 4\sigma'_n T + 4T^2 \tag{2.1}$$

and

$$\tau = C + \mu_i(\sigma_n - P_f) \tag{2.2}$$

Where τ is the shear stress, σ_n is the normal stress, T the tensile strength of an intact rock unit, C the cohesive strength of intact rock, P_f pore fluid pressure, μ_i the coefficient of internal friction, and σ'_n is the effective normal stress (σ_n - P_f) (Brace, 1960; Jaeger and Cook, 1976). Therefore conditions of failure are controlled by both inherent properties

of a specific rock unit, and the type and magnitude of applied stress. As a result, brittle rock failure can be described using the Mohr diagram and plotted Griffith-Coulomb failure envelope in Fig. 2.1 (Sibson, 1998).

Rock failure typically occurs when the tensile/shear strengths of a given rock unit are exceeded by either applied compressional stress or fluid pressure conditions (Jaeger and Cook, 1976). Given effective principal compressive stresses $\sigma'_1 > \sigma'_2 > \sigma'_3$ (where $\sigma'_1 = \sigma_1 - P_f$ and so forth) within the crust, rock failure can be determined by how the Mohr stress circle (size of the stress circle = (σ'_1 - σ'_3) the effective differential stress) will migrate, by varying the magnitude of the respective principal stresses (towards tensile or compressional normal stress conditions) and the pore fluid pressure, and subsequently intersect the Griffith-Coulomb failure envelope defined by equations 2.1 and 2.2 (Fig. 2.1) (Sibson, 1998). Where along the failure envelope intersection occurs, can be seen in Fig. 2.1. The three Mohr circles labelled A, B and C illustrate the following stress conditions (after Jaeger and Cook, 1976):

A) $\sigma'_3 = -T$; provided that $\tau = 0$ & $\sigma'_n < 0$

B) $\sigma'_3 < 0$ but $-T < \sigma'_3$; provided that $\tau \neq 0$

C) $\sigma'_n > 0$; provided that $\tau \neq 0$

Thus from Fig. 2.1 and the outlined stress conditions, Mohr circle A describes tensile failure within the tensile field, with no shear stress component. Mohr circle C describes compressional-shear failure, with the effective normal stress compressional, and possessing a significant shear stress component. Mohr circle B describes the transition from tensile failure to compressional-shear failure as hybrid tensile-shear failure, including both tensile and shear stress components. (Hancock, 1985; Price and Cosgrove, 1990; Sibson, 1998; Ramsey and Chester, 2004)

2.1.2 Rock Failure and Stress Orientations

Fractures commonly form at specific angles to applied stress (Jaeger and Cook, 1976). Assuming an intact and homogeneous host rock, the angle between the fracture plane and the principal stress axes can be determined from Griffith-Coulomb theory, and is given by the equation below (Jaeger and Cook, 1976; Sibson, 1998):

$$\theta = 45^\circ - \frac{tan^{-1}\mu_i}{2} \tag{2.3}$$

The angle from the fracture to the maximum principal stress (σ_1) is defined as θ, where 2θ represents the acute angle between a conjugate pair of shear fracture planes, and is bisected by σ_1. The 2θ angle can be seen on Fig. 2.1 as the angle made by the line between the point of Mohr circle - failure envelope intersection, and the centre of the Mohr circle.

As seen on Fig. 2.1 as Mohr circle A, tensile failure (fracture) results in a 2θ value of 0° (Fig. 2.2A) (Secor, 1965). Which means the fracture is parallel to σ_1 and σ_2 axes, and perpendicular to σ_3 axis (Secor, 1965). Furthermore the only displacement observed on the fracture will be normal to the failure plane, with no shear displacement (Ramsey and Chester, 2004).

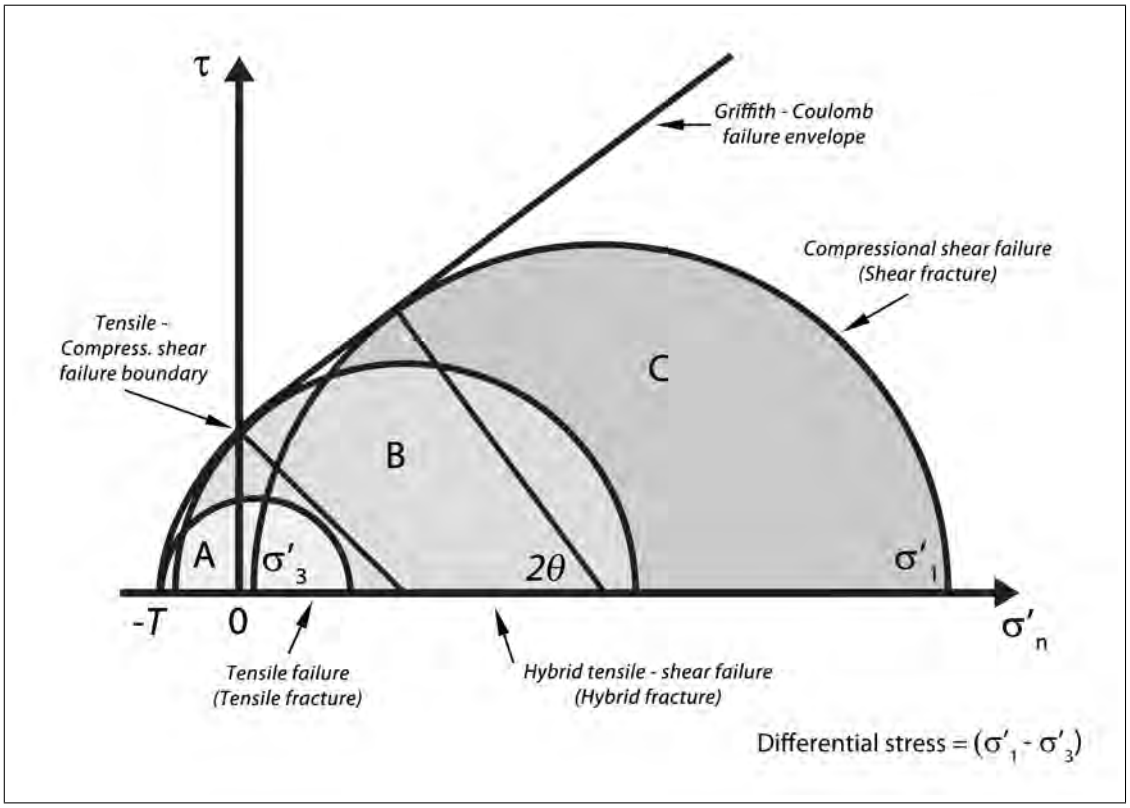

Figure 2.1: Generic mohr diagram with the Griffith-Coulomb failure envelope plotted in shear (τ) versus normal (σ'_n) stress space. Different conditions of brittle failure are shown by the mohr circles: A) Tensile failure, B) Hybrid tensile-shear failure, C) Compressional-shear failure. The angle between the failure plane and σ_1 is described by θ. The positions of σ'_1 & σ'_3 are indicated for Mohr circle C as an example. Modified from Sibson (1998); Ramsey and Chester (2004).

As shown on Fig. 2.1 Mohr circle B, hybrid extensional-shear failure will intersect the failure envelope to typically form a 2θ <60° (Price and Cosgrove, 1990). This results in hybrid tensile-shear fractures (here onwards referred to as hybrid fractures) (Hancock, 1985)

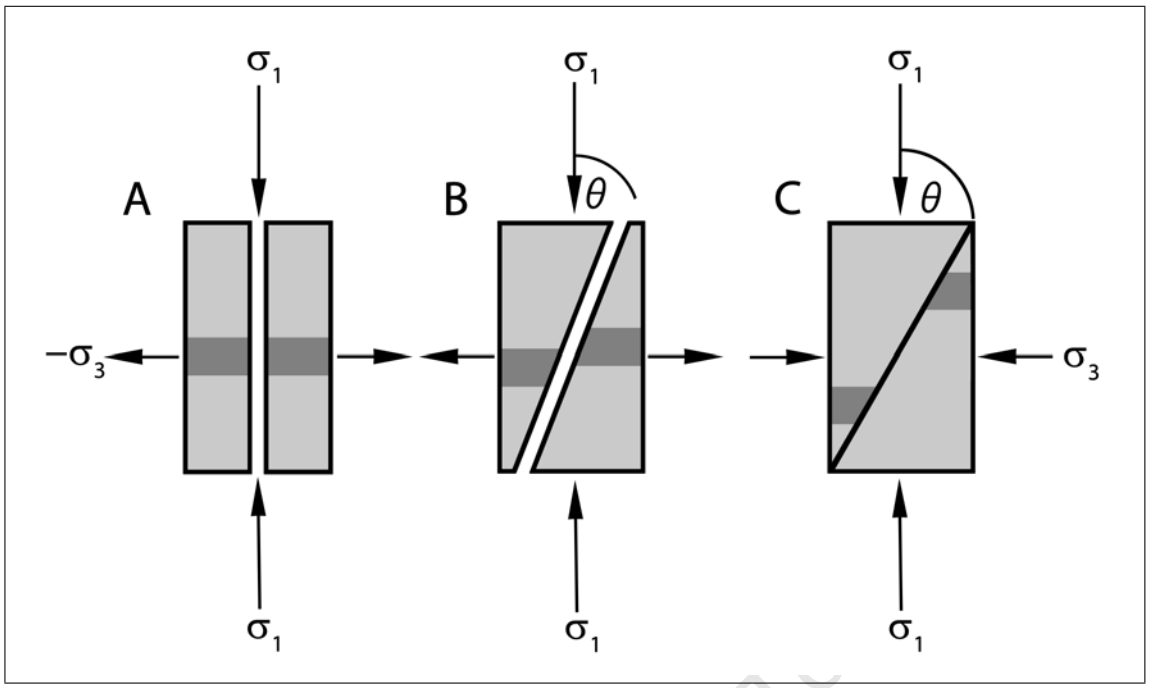

Figure 2.2: Different types of brittle fractures compared to the principal stress axes ($\sigma_1 > \sigma_2 > \sigma_3$) at time of fracture($\sigma_2$ is in the plane of the fractures). The fractures are: A) Tensile fracture, B) Hybrid-shear fracture, C) Coulomb-shear fracture/fault. The angle θ between the fracture surface and σ_1 is indicated in B and C only, as A has $\theta = 0$. Modified from Hancock *et al.* (1991); Ramsey and Chester (2004).

(Fig. 2.2B) with a low θ angle, ($\sim 30^\circ$ or less) (Price and Cosgrove, 1990). Conjugate hybrid fractures (Fig. 2.3) with a small acute angle (2θ) will thus include σ_1 as the acute bisector, and σ_3 as the obtuse bisector, with σ_2 in the plane of the fracture (Dunne and Hancock, 1994)(Fig. 2.3).

Mohr circle C on Fig. 2.1, compressional-shear fractures (otherwise known as faults) intersect the failure envelope to form a $2\theta \sim 60^\circ$, depending on the coefficient of internal friction (μ_i) of the rock mass (Price and Cosgrove, 1990; Sibson, 1998) (Fig. 2.1). The result is compressional-shear fractures (Coulomb-shear), faults, and also conjugate shear fractures. The faults form a θ angle to σ_1 at approximately $\sim 30^\circ$ (Ramsey and Chester, 2004) (Fig. 2.2C) with a typical rock co-efficient of friction $\mu_i = 0.6$ (Brace, 1960). Conjugate faults (Fig. 2.3) form with the 2θ constituting the acute angle between the conjugates, enclosing σ_1 as the acute bisector. σ_3 is thus the obtuse bisector, with σ_2 parallel to the intersection line of the fault planes (Price and Cosgrove, 1990; Hancock *et al.*, 1991; Sibson, 1998).

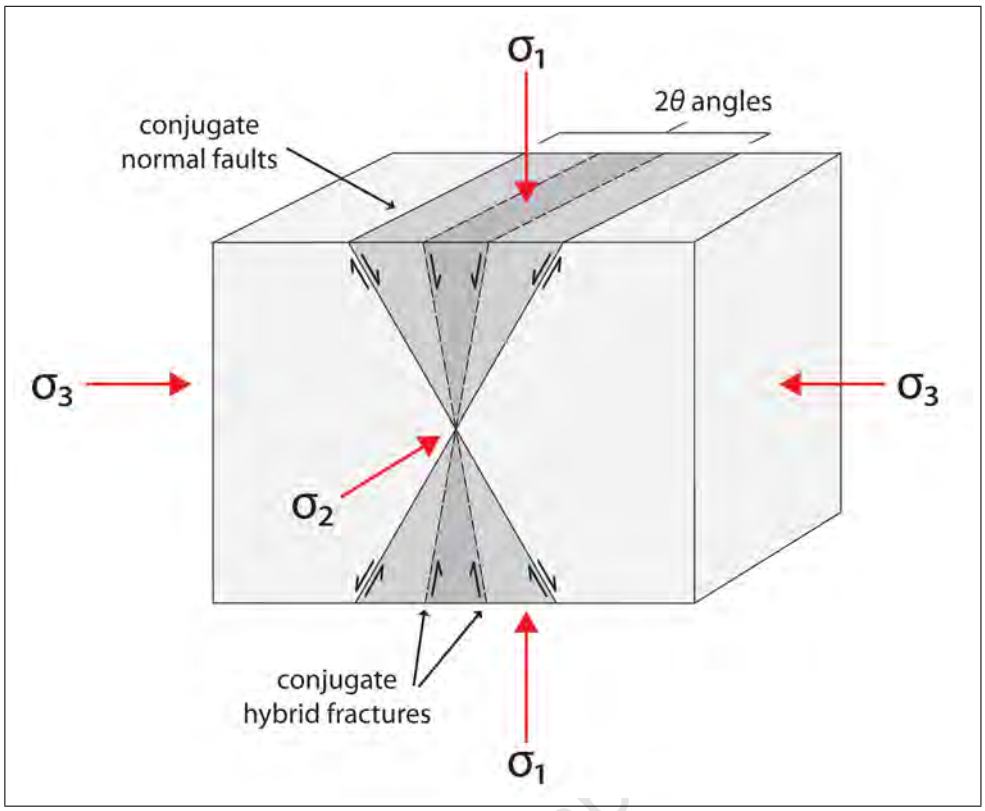

Figure 2.3: The orientation of the acute bisector (σ_1), and the obtuse bisector (σ_3), in comparison to the types of conjugate rock failure planes: Coulomb-shear fractures (normal faults), and hybrid-shear fractures. The intermediate stress axis (σ_2) is in the plane of the fractures. The angle 2θ (dark grey - hybrid fractures, light grey - normal fauts) defines the conjugate fracture angles (read text for explanation). Sense of shear offset indicated. Modified from Hancock *et al.* (1991).

2.1.3 Stress Variability

Conjugate fractures, as discussed before, develop due to either compressional-shear fracture, or hybrid extensional-shear fracture. However another mechanism can cause mutually cross-cutting fractures to form, that being the process of stress swap/exchange during tensile fracture (Caputo, 2005).

Stress swap occurs as a result of σ_1, σ_2, σ_3 stress axes exchange (assuming the state of stress is Andersonian, with σ_v equal to one of the principal stresses (Anderson, 1951)), which if the rock is currently in a state of tensile failure, will cause the orientation of developing tensile fractures to switch orientation by 90° (Caputo, 2005). This swap in the stress axes and fracture geometry will form coeval, mutually cross-cutting orthogonal tensile fractures,

the tensile fractures will therefore appear similar to the conjugate fractures in outcrop (with a large 2θ angle) (Caputo, 2005).

Typically the causes of stress variability and resultant stress axis exchange can be caused by the following processes or characteristics of a rock unit: 1) If the lesser principal stresses σ_2 and σ_3 are relatively similar in magnitude, the magnitude of (σ_3) may increase until it surpasses (σ_2), at which point a stress swap will happen, and orientation of the propagating tensile fracture will switch (Caputo, 1995). 2) A rock unit can also involve different zones of higher or lower tensile strength (commonly attributed to the degree of consolidation and cohesion), and furthermore the presence of pre-existing sedimentary structures and fractures may also influence the stress orientation (compositionally heterogeneous and structurally anisotropic), and hence the ability for stress to vary through space (Jaeger and Cook, 1976; Caputo, 2005).

2.2 Joints

Tensile fractures which exhibit no shear displacement along the fracture surface can be labelled as joints (Engelder and Geiser, 1980; Engelder, 1987; Hancock *et al.*, 1991; Dunne and Hancock, 1994). However, according to Hancock (1985) conjugate hybrid fractures can also be labelled as joints, if no appreciable shear displacement can be observed. This results in a 'joint spectrum' from distinct tensile fractures to conjugate hybrid fractures (Hancock and Engelder, 1989; Dunne and Hancock, 1994). The use of hybrid fractures as joints however is controversial (Hancock *et al.*, 1991), and should be used with care in field studies. For simplicity in this research project, hybrid fractures will be included within the joint category if no shear displacement can be observed across the fracture.

2.2.1 Joint Characteristics and Terminology

Multiple joints ($\geq$3) propagating through an intact rock with a single preferred orientation are known as a joint set (Engelder and Geiser, 1980; Dunne and Hancock, 1994). Joints constituting a joint set can also be described as systematic, in contrast to non-systematic joints which are orientated randomly to one another, and therefore cannot be placed within a

specific joint set (Engelder and Geiser, 1980; Hancock *et al.*, 1991).

As other studies only utilized steeply inclined (45 °- 80 °) (Fig. 4.17A), or sub-vertical (80 °- 90 °) (Fig. 4.17B) joints (e.g. Engelder and Geiser, 1980; Hancock and Engelder, 1989; Hancock *et al.*, 1991), the same criteria will be applied to this study. Joints are commonly planar features, pervasive, commonly form intersecting sets, and are generally consistent in orientation across space (Arlegui and Simón, 2001), for these reasons distinctive joint set orientations can be observed on the local to regional-scale.

When multiple joint sets are observed to propagate through an intact rock, a joint system can be described (Dunne and Hancock, 1994). The joint sets defining a joint system can be coeval (mutually cross-cut), or multi-generational (abutted, cross-cut, and overprinted) (Engelder and Geiser, 1980; Price and Cosgrove, 1990; Hancock *et al.*, 1991). If coeval joint sets intersect consistently to form acute angles, the joints represent either 'conjugate sets' (Hancock *et al.*, 1991) or joints that are related in formation (formed together).

Joints that have been in-filled with a precipitated mineral (such as calcite) from a fluid, become known as joint veins (Caputo, 2005; Bons *et al.*, 2012). A joint vein has the same characteristics as tensile fractures with regards to relationship to the principal stress axes.

2.2.2 Joints as Geological Stress Indicators

Joints are tensile fractures, which therefore propagate normal to σ_3, and parallel to σ_1 and σ_2 (Fig. 2.2A) (Engelder and Geiser, 1980). As there is commonly uncertainty between whether σ_1 or σ_2 is the vertical principal stress axis if the joint plane is vertical or steeply inclined, σ_3 (or the extension direction) is typically the only constrained stress axis. As a result, for multi-generational joint sets, the σ_3 orientation can be tracked over time by studying the oldest to youngest joint set.

Figure 2.4, illustrates two joint system examples with two related steeply dipping joint sets. Both of these joint systems are characterised by a horizontal σ_3 orientation. However, the σ_1 and σ_2 orientations exchange from vertical to horizontal. As such, a horizontal stress component can only be described from the average σ_3 direction. This minimum horizontal stress is known as S_{Hmin}, which will be perpendicular to vertical joints or inclined to steeply dipping joints. The maximum horizontal stress, S_{Hmax}, is at 90 ° to the S_{Hmin} trajectory.

The orientations of the principal stress axes are important to infer, as they indicate the dominant tectonic regime at time of joint formation. If an Andersonian state of stress is assumed, a vertical σ_1 (with a horizontal σ_3) provides evidence for an extensional tectonic regime; a horizontal σ_1 (with a horizontal σ_3), evidence for a strike-slip tectonic regime (Anderson, 1951). Other geological deformation features can provide evidence for the principal stress axes orientation, these being conjugate normal faults or hybrid fractures for example. Sub-vertical joints are limited to providing evidence for S_{Hmin} and S_{Hmax}.

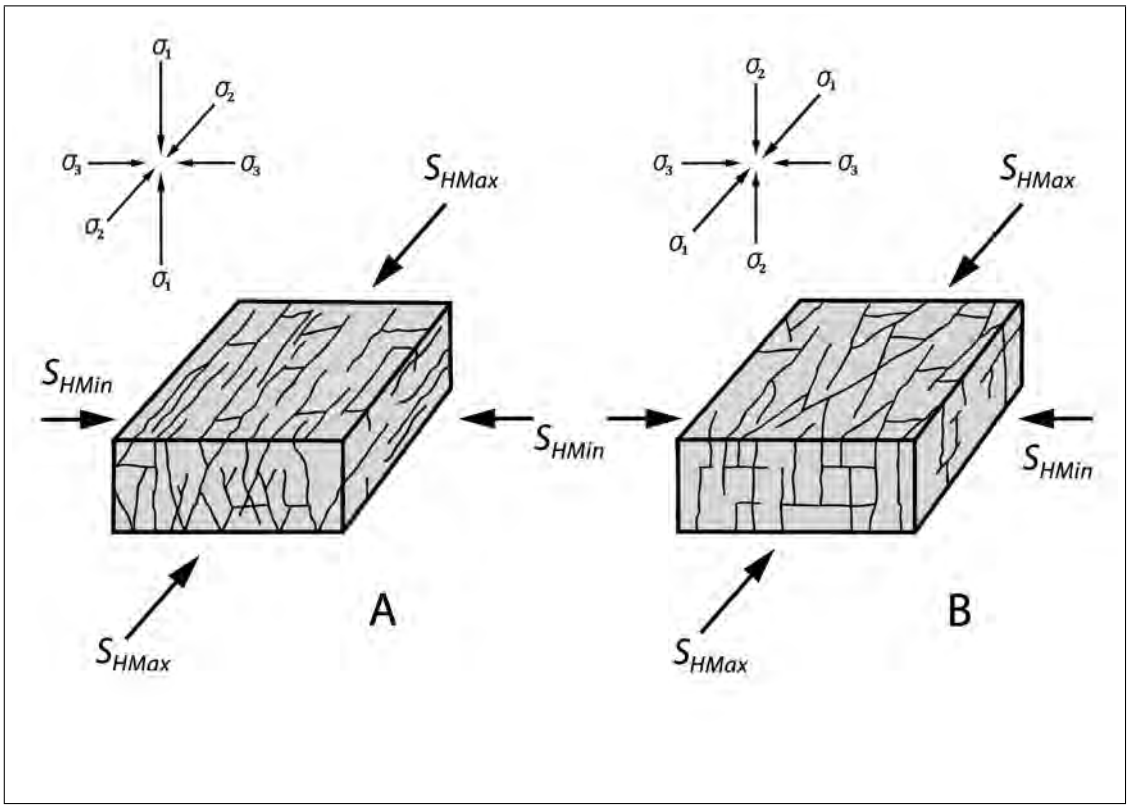

Figure 2.4: Typical joint systems (in 3-D) with indicated principal stress axes ($\sigma_1 > \sigma_2 > \sigma_3$) at time of jointing. Corresponding maximum (S_{Hmax}) and minimum (S_{Hmin}) horizontal compressive stresses are shown. The same S_{Hmax} and S_{Hmin} orientations are given for two different principal stress axes orientations. Converting the 3D stress field to a the horizontal stress field representation, thus overcomes the ambiguity in principal stress orientations. Modified from Hancock *et al.* (1991).

2.2.3 Neotectonic Joints

Neotectonic joints are joints that formed during the same regional/local tectonic regime ongoing at present day, in other words they are recent deformation features (Hancock and Engelder, 1989; Hancock *et al.*, 1991; Stewart and Hancock, 1994). As such, the joints will strike perpendicular to the contemporary or neotectonic S_{Hmin} and parallel to the S_{Hmax} trajectories (Hancock and Engelder, 1989) (if $S_{Hmin} \approx \sigma_3$ and $S_{Hmax} \approx \sigma_1$ or σ_2). Therefore joints determined to be of neotectonic age can be used to estimate the neotectonic stress field, and of pre-neotectonic age used to constrain a palaeostress field (Eyal *et al.*, 2001).

Joints located in rocks consolidated/lithified prior to the Late Cenozoic are typically difficult to define as neotectonic, so commonly the youngest or final joint is inferred to be neotectonic (Hancock and Engelder, 1989). Ancient rock units will have complex deformation histories, which are difficult to constrain in terms of neotectonic deformation (Khadkikar, 2002). However, if the joints are located in recent (Late Cenozoic) and surficial rock units, this uncertainty is removed (Khadkikar, 2002). Recent surface deposits furthermore lack a burial history and with continuous deposition allow for the neotectonic stress field to be temporally constrained over the 1 ka - 10 ka timescale (Khadkikar, 2002). The lower differential stress in the shallow crust and surficial deposits also makes joints the preferred method of strain accommodation (Jaeger and Cook, 1976; Caputo, 2005). Consequently, joints are common deformation features in surface rock units, and can provide neotectonic stress fields.

2.3 Regional Tectonic Stress Fields

The compilation of stress orientations from recent geological evidence (neotectonic joint sets and systems) from local-scale outcrops across a region can allow for the regional contemporary stress field to be estimated (Eyal *et al.*, 2001).

Regional intraplate tectonic stress can originate from both plate boundary forces, such as ridge push (Zoback, 1992b; Eyal *et al.*, 2001), and the resistance to relative plate motion, such as asthenospheric drag (Zoback and Zoback, 1980). Additionally tectonic stress can be derived from within plate interiors, from mechanisms such as ‘swell push’ (for example the ’African Superswell’ in Southern and East Africa) (Nyblade and Robinson, 1994).

Regional intraplate tectonic stress fields are relatively uniform in terms of the orientation of S_{Hmax} and S_{Hmin} (Eyal *et al.*, 2001), with deviations most commonly between 10 ° and 15 ° (Zoback, 1992a). As such, over large intraplate regions, variations of S_{Hmax} orientations are expected, but at the relatively local area scale of the Southern Cape, uniformity in S_{Hmax} and S_{Hmax} trajectories is most likely.

Other techniques deriving contemporary S_{Hmax} and S_{Hmin} are commonly from $in\ situ$ stress measurements (Reynolds *et al.*, 2003). These techniques can involve stress trajectories constrained from borehole-breakout data, focal mechanisms and other geophysical methods (Zoback and Zoback, 1980; Lund and Townend, 2007). These stress indicators are commonly used for constructing regional and global stress pattern maps, for example the World Stress Map (Zoback, 1992a), and can be used to provide context to more localised stress field studies (such as this study).

2.4 Sedimentary Process and Related Deformation

Brittle deformation features observed in sedimentary rock units are not necessarily a consequence of tectonic activity (Owen *et al.*, 2011). The deformation features may also be caused by sedimentary processes either within the rock unit, or external processes applied to the the rock unit (from the surrounding environment) during deposition and consolidation (Pirrotta and Barbano, 2010). Deformation caused by sedimentary processes will commonly be preserved in the consolidated remnant of previously unconsolidated sedimentary units (McKee, 1979).

2.4.1 Soft-sediment Deformation

Unconsolidated sediment ('soft-sediment') is typically cohesionless, with low shear strength (Moretti, 2000). The shear strength is thus easily exceeded with a change in the stress state of the sediment. This leads to inter-granular shear failure and a breakdown of the granular packing structure (Obermeier, 2009). The loss of the internal granular structure and subsequent sediment readjustment results in the formation of deformation features. Soft sediment deformation (SSD) is therefore a common occurrence in unconsolidated to near-consolidated

sediments (such as aeolianites or dune bodies) (Owen *et al.*, 2011).

SSD can derive from sedimentary related process on-going during deposition, consolidation and erosion. Syn-depositional soft sediment deformation is caused by overloading and/or unequal loading of sediments due to bedform topography, or over-steepening of depositional surfaces (Pirrotta and Barbano, 2010; Owen *et al.*, 2011). These deformation processes are typically driven by gravity, and can result in both internal flow within a dune, or mass-movement of the grains on the slope surfaces, to attain a slope angle near/at the angle of repose (Moretti, 2000). Post-deposition related causes of deformation can be attributed to the volumetric expansion of sediment due to thermal stress, pore-fluid increase, or the precipitation of inter-granular cement (Pirrotta and Barbano, 2010).

External causes of SSD can be due to tectonic activity (Owen *et al.*, 2011), typically in the form of earthquake shaking, resulting in deformation preserved as 'seismites' within the sediment units (Moretti, 2000). Wave action can be another significant trigger of SSD in coastal aeolian dunes (Owen *et al.*, 2011), with waves undercutting unconsolidated dune faces (wave action can erode and undercut semi-consolidated to consolidated rock as well).

Common SSD features typically include brittle folds and fractures (discontinuous deformation features), slump structures, autoclastic brecciation, sand dykes, liquefaction deposits, contorted cross-bedding, and overturned bedding (McKee, 1979; Moretti, 2000; Pirrotta and Barbano, 2010; Owen *et al.*, 2011). SSD features are commonly spatially variable in terms of orientation and style, due to the effects of local stress perturbations leading to local slope failure or slumping throughout the dune body (Pirrotta and Barbano, 2010).

2.4.2 Karstic Deformation

Karstic weathering processes cause deformation features (collapse structures) to form in calcareous sediments (Owen *et al.*, 2011), such as coastal aeolianite units rich in marine organism shell fragments composed of calcium carbonate ($CaCO_3$). The weathering occurs through a process of karstic dissolution, whereby calcite cement is removed and re-precipitated elsewhere by water movement through the sediment, thus weakening the source sediment (Owen *et al.*, 2011).

2.4.3 Post-Consolidation Deformation

The method by which sediment is deposited and able to accumulate on slopes, is largely controlled by the angle of repose of that sediment (Allen, 1970). For coastal aeolianites of calc-arenitic (quartz grains and marine organism shell fragments) composition this angle lies between approximately $\sim 32^\circ$ and $\sim 37^\circ$ (Allen, 1970). Therefore $\sim 37^\circ$ is the maximum angle a slope for an aeolianite cross-bed can possess. Any angle greater than 37° indicates some type of deformation (rotation of the cross-bedding) has occurred post-consolidation. Rotation of post-consolidated aeolianite cross-beds, and subsequent deformation could be due to slope failure triggered from under-cutting of slopes through wave action (Flemming, 1965), or tectonic activity, as cemented sediment is susceptible to earthquake-induced slope failure (Keefer, 2002).

2.5 Fault Reactivation

Constraining the orientation and characteristics of larger-scale fault structures in the underlying geology, within the context of the prevailing stress field, is crucial in assessing the reactivation potential of a fault. Reactivation of faults within the brittle crust is typically the preferred means of accommodating strain, rather than formation of new faults (Sibson, 1985) when oriented favourably to imposed stress. To understand how faults are able to reactivate, and how the imposed stress field influences fault reactivation, the condition for re-shear of pre-existing faults needs to be evaluated.

2.5.1 Condition of Reactivation

Faults are known to be potential planes or zones of mechanical weakness within the crust (Scholz, 1990), consequently elastic strain build-up will eventually lead to shear failure if the the fault is conditioned to reactivate (Sibson, 1986, 1992). The conditions for fault reactivation typically involve changes in the prevailing stress state (magnitude and orientation), the fluid pressure, and the level of cohesion of the fault itself (Scholz, 1990).

Reactivation of faults can be best described with the use of Mohr diagrams with plotted frictional failure envelopes. As the Griffith-Coulomb failure envelope describes failure in

intact rock, pre-existing faults (assuming lower cohesion or rock strengths) also reactivate in agreement with Coulomb failure criterion, whereby the frictional reactivation criterion is given as:

$$\tau = C + \mu_s \sigma'_n \tag{2.4}$$

Where τ is the shear stress required for failure, C is the cohesional strength of the pre-existing fault, μ_s is the static co-efficient of rock friction of a fault, and σ'_n is the effective normal stress) (Scholz, 1990; Sibson, 1985, 1998). The τ value is required to overcome the τ_f (shear strength). Both criteria can be plotted and reactivation potential of pre-existing faults assessed (Fig. 2.5 and Fig. 2.6).

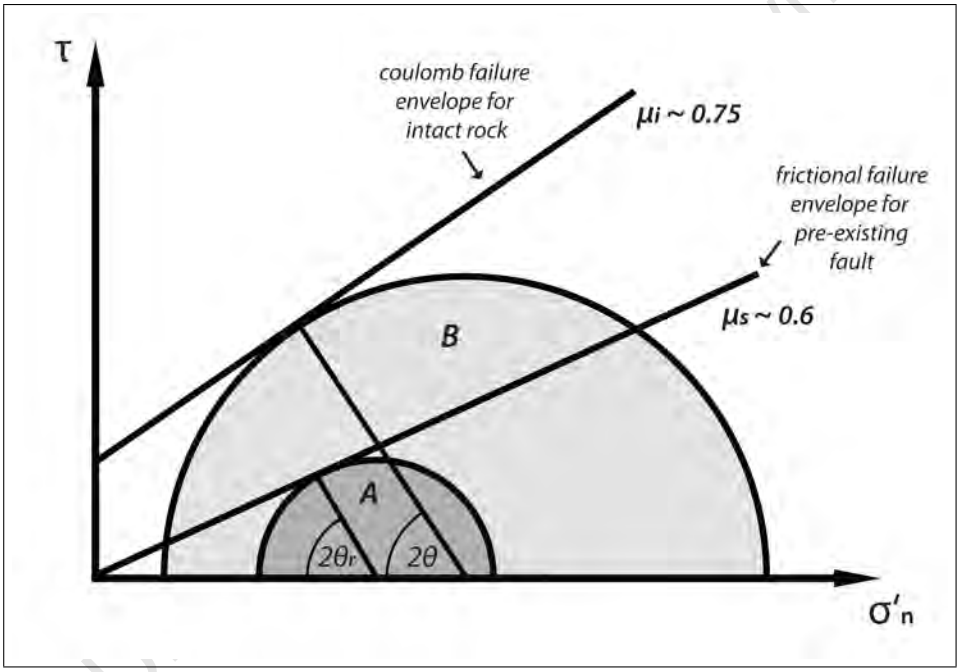

Figure 2.5: Mohr Diagram with both the frictional failure envelope for a cohesionless fault, and Coulomb failure envelope plotted. The condition for reactivation of a pre-existing fault is described by Mohr circle A, with optimal reactivation angle $2\theta_r$. This is in contrast to the condition for formation of a new fault within intact rock shown by Mohr circle B, with optimally orientated fault formation angle 2θ. Note the difference between μ_i and μ_s. Modified from Scholz (1990); Sibson (1998)

In Fig. 2.5 the Mohr Circle B describes shear failure in an intact rock with μ_i = 0.75, whereby the Mohr circle intersects the Griffith-Coulomb failure envelope (refer to section 2.1.1).

Pre-existing faults are locations of prior shear movement, and are commonly seen as "damage zones" quite different to intact rocks (Sibson, 1992). Faults are characterised by brecciated units and gouge rock units, which have typically low cohesion (assumed to be zero for this example) and a lower friction co-efficient (plotted as μ_s = 0.6 on Fig. 2.5) (Scholz, 1990), resulting in a frictional failure envelope with a decreased slope plotted through the τ and σ'_n = 0 origin in stress space (Fig. 2.5) (Etheridge, 1986; White *et al.*, 1986; Scholz, 1990; Dubois *et al.*, 2002; Nortje *et al.*, 2011).

From the frictional failure envelope, pre-existing fault possess a lower shear strength than the surrounding rock, and will typically fail before the surrounding intact rock if the stress orientation is favourable (Etheridge, 1986). Frictional failure (sliding) therefore requires lower differential stress to fail, in comparison to shear failure in an intact rock (Fig. 2.5, Mohr circle A) (Sibson, 1985).

The fault orientation relative to the prevailing stress field affects the potential for a fault to reactivate (Sibson, 1985; White *et al.*, 1986). In Fig. 2.5, Mohr circle A, describes frictional failure of an optimally orientated pre-existing fault (Sibson, 1985; Scholz, 1990). The optimal reactivation angle (θ_r) is provided by the equation:

$$\theta_r = 45^\circ - \frac{tan^{-1}\mu_s}{2} \tag{2.5}$$

Which describes the angle that a pre-existing optimally orientated plane of weakness will make to σ_1 at reactivation (Sibson, 1998). The angle θ_r for most rocks, has been previously determined to be in the range between 25 ° - 30 °, with optimal reactivation occurring at ∼30 ° if μ_s ∼0.6 (Sibson, 1985, 1998). If however a pre-existing fault possesses a θ_r >30 °, reactivation will typically only occur if there is: 1) high P_f, 2) σ_3 is tensile, and 3) low μ_s (<0.5), or the fault will be sufficiently mis-orientated to the prevailing stress field to experience reshear (Sibson, 1985).

Furthermore, within an imposed stress field (Fig. 2.6), the formation of new faults opposed to fault reactivation (Fig. 2.6 at point C), will typically only occur if the pre-existing faults are not enclosed by the 2β angle (Fig. 2.6 between points A & B) in other words, sufficiently mis-orientated for reshear (Etheridge, 1986; Scholz, 1990; Nortje *et al.*, 2011). However, as seen within the range of 2β, there is an ability for non-optimally pre-existing faults to reactivate before new faults form (Scholz, 1990). Therefore, in most cases existing

faults will most likely reactivate before new faults form, provided a favourable orientation to the prevailing stress field, and that conditions of frictional failure (equation 2.3) are met.

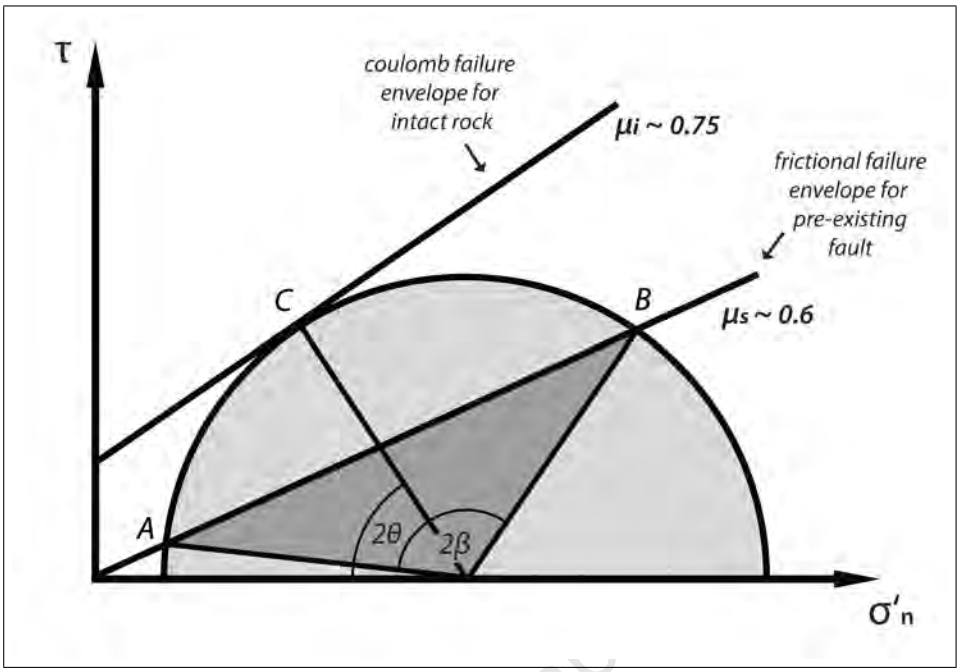

Figure 2.6: Mohr Diagram with both the frictional failure (pre-existing fault) and Coulomb failure (intact rock) envelopes shown. The Mohr circle describes the stress condition for formation of new faults at C, and re-activation at A and B, however pre-existing faults with an orientation within the range of 2β will preferentially reactivate instead of formation of new optically orientated faults given by 2θ. Modified from Sibson (1985); Scholz (1990)

Consequently, a constrained regional tectonic stress field is essential in determining the reactivation potential of pre-existing faults. As such, any fault which has been determined to have previously undergone a faulting event (therefore assumed to be pre-disposed to reshear), favourably orientated in the prevailing stress field, and possessing a shear strength less than the surrounding host rock, will undergo future fault reactivation (Etheridge, 1986; Baudon and Cartwright, 2008; Nortje *et al.*, 2011).

2.5.2 Effect of Fault Reactivation on Cover Sequences

The reactivation of faults in the underlying geology (blind faults) has characteristics which influence the deformation of the overlying undeformed Tertiary and Quaternary deposits.

With reactivation of a pre-existing normal fault (Fig. 2.7 A), vertical displacement may occur through subsidence of the hangingwall, and this displacement translates into the cover sequence. This is shown in Fig. 2.7 A, where the cover sequence (C_1, C_2, C_3) is subsided with the underlying unit (U). This process causes monocline drag folds to develop in the cover sequence (illustrated by a hangingwall syncline, and a footwall anticline) (Schlische, 1995; Finch *et al.*, 2004). These drag folds have hinge lines orientated parallel to the fault and are laterally extensive (Schlische, 1995).

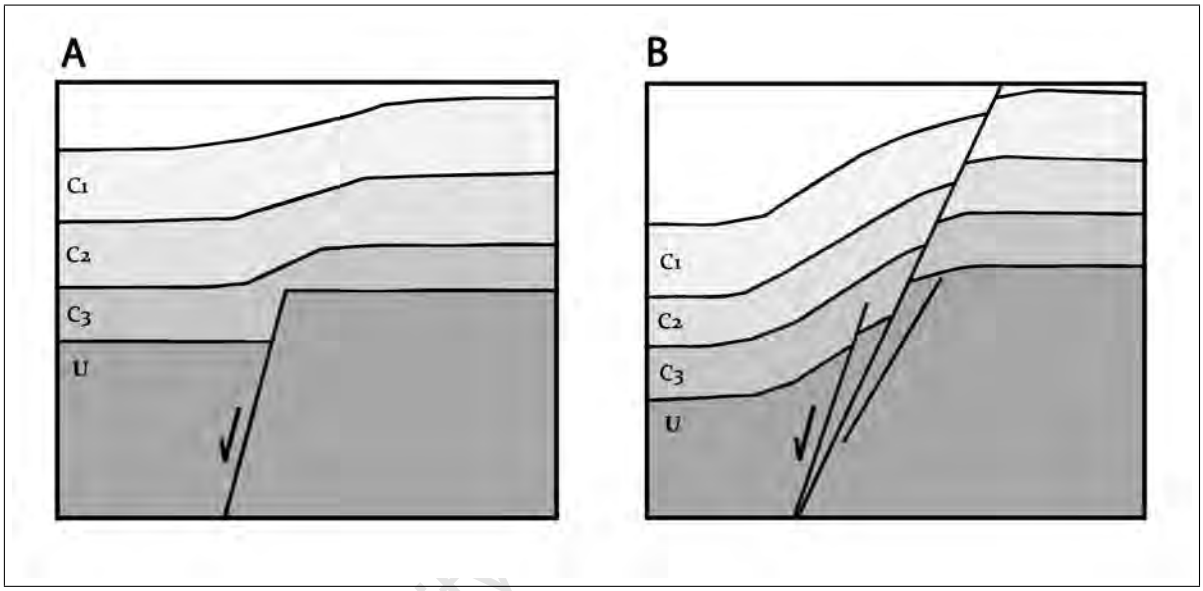

Figure 2.7: The progressive deformation of a cover sequence (C_1, C_2, C_3), by the reactivation of a normal fault in the underlying units (U). A) shows an initial vertical displacement of the hangingwall, with subsequent folding of the cover. B) Continued vertical displacement on the normal fault results in significant rotation of the cover sequence, and internal deformation, with eventual fault breach. Modified from (Schlische, 1995; Finch *et al.*, 2004)

With continued displacement on an underlying blind normal fault, the fault propagates upwards into the cover sequence (Fig. 2.7 B) (Finch *et al.*, 2004). This results in progressive folding of the cover sequence into a more pronounced monocline, with an increasingly widening zone of deformation (characterised by brecciation and brittle deformation) focused on the fault growth upwards (Finch *et al.*, 2004). The normal fault may also become splayed and progressively diffuse, with eventually the monocline faulted through the fold ramp (Finch *et al.*, 2004). Furthermore due to the diminished confining vertical stress, nor-

mal faults are also expected to become steeper, even near-vertical at the surface (Stewart and Hancock, 1994). The end result is a cover sequence that has been rotated from an initially horizontal orientation to a significantly steeper orientation.

The reactivation of strike-slip faults, beneath an undeformed cover sequence, is quite different to normal faults. As strike-slip faults are typically vertical, and sense of off-set is horizontal, commonly no drag folds develop in the overlying geology (McCalpin *et al.*, 2009). The most common large-scale deformation feature associated with blind strike-slip faults are the lateral off-set of rivers, alluvial terraces, fan deposits, and other landform features (e.g. valleys and ridges) (McCalpin *et al.*, 2009). As the Southern Cape is considered a region of extensional tectonics (Andreoli *et al.*, 1996; Bird *et al.*, 2006) (refer to section 3.6) with σ_3 inferred horizontal and σ_1 orientated vertical from the presumed neotectonic normal faults, these faults may still have undergone past reactivated as strike-slip faults and could potentially still reactivate in the future as strike-slip faults. Consequently, possible evidence for past strike-slip fault activity will be investigated in this study.

2.6 Intraplate Seismicity

Intraplate regions are considered to be tectonically stable (Zoback, 1992a), with low strain rates (Kenner and Segall, 2000), typically less than the global average of $4\times10^{-14}.s^{-1}$ (Pfiffner and Ramsay, 1982). Additionally, as the majority of fault displacement is accumulated during reactivation of pre-existing faults occur during earthquake rupture (Sibson, 1986), intraplate regions have relatively slow elastic strain accumulation and low slip rates on faults. This is observed in how only 0.5% of the total recorded earthquake moment release is measured within stable intraplate zones (Sandiford and Egholm, 2008).

The majority of recorded and preserved earthquake activity is concentrated on plate-boundary zones, where seismicity commonly occurs in a quasi-periodic manner due to steady relative plate motion (Sibson, 2002; Li *et al.*, 2009). Intraplate seismicity, in contrast, is spatially concentrated in specific zones and scattered through wide regions, with episodes of clustered seismic activity followed by prolonged quiescent intervals (Li *et al.*, 2009). The quiescent intervals typically extend for tens of thousands of years or more ($\geq$ 10 Ka) (Sibson, 2002).

Intraplate seismicity is more commonly the consequence of reactivation of pre-existing faults formed during a prior tectonic event, than the formation of new faults (Sibson, 2002). This would indicate that the majority of intraplate earthquakes are localised to inherited tectonic structures (for example ancient orogenic and rifted zones) (Sibson, 2002) and have a predictable distribution. The distribution of intraplate seismicity is however, observed to migrate through different fault zones and fault segments over time, and additionally occur on faults located away from inherited tectonic structures, producing complex distribution patterns (Li *et al.*, 2009). The relationship between seismicity and inherited structures as a result remains poorly understood (Li *et al.*, 2009). The need therefore to characterise faults with past (ancient and recent) seismic rupture is crucial in constructing a pattern of intraplate seismicity, thus understanding the occurrence of earthquakes in stable intraplate regions.

2.7 Neotectonics

Neotectonics is the study of recent crustal movements and deformation by the description of the contemporary stress field (through use of geological stress indicators), and identification of active or seismically quiescent geological structures (tensile fractures, faults) (Stewart and Hancock, 1994; McCalpin and Nelson, 2009). This combined with the recognition of faults with a favourable orientation to the contemporary stress field, which could reactivate in the future and generate seismic activity (Stewart and Hancock, 1994). For the Southern Cape, recent crustal deformation is specified to be Late Cenozoic, or specifically post-Miocene in age (McCalpin and Nelson, 2009; Viola *et al.*, 2012).

Geological structures (tensile fractures, faults) can develop and propagate over extended time periods (ka-Ma time-scales) and instantaneously(McCalpin and Nelson, 2009). The instantaneous propagation of crustal deformation features would be due to earthquake rupture and subsequent shaking, which is the reason palaeoseismology is incorporated within the broader field of neotectonics, and utilised to document recent crustal movements (McCalpin and Nelson, 2009).

2.7.1 Palaeoseismology

Seismic activity is common throughout large areas of the Earth's crust, with recent and current seismic activity recorded and described. Back through the geological past however, many seismic events could not be recorded due to the lack of human presence and instrumentation at the time of the earthquake event. These unrecorded earthquakes commonly leave geological evidence (McCalpin and Nelson, 2009), and can be documented using the modern geology research techniques. Following this, the aim of palaeoseimology is therefore an attempt to describe ancient (prehistoric) earthquakes, specifically the location, rupture source, timing, and the possible magnitude of past seismic events (McCalpin and Nelson, 2009).

2.7.2 Methodology and Techniques

Palaeoseismology study techniques involve the investigation of preserved evidence of ancient earthquakes (McCalpin and Nelson, 2009). Preserved earthquake evidence can be subdivided into two categories according to the spatial extent or scale of the deformation features:

1) Landform evidence, where landform disruption has occurred; commonly in the form of geomorphological off-sets, lineaments, fault-scarps, or monocline drag-folds (McCalpin, 2009; McCalpin and Nelson, 2009).

2) Stratigraphic evidence, where lithological deformation features are preserved within the stratigraphic record (blind fault-related deformation or earthquake shaking deformation), typically preserved below the land surface and exposed later due to erosion or human activity (McCalpin, 2009; McCalpin and Nelson, 2009).

The use of remote sensing and digital terrain models (DEM's) can typically delineate landform disturbances (McCalpin, 2009). Geophysical surveys (for example aero-magnetic surveys) and local-scale (outcrop-scale) geological mapping are used to document stratigraphic evidence for past earthquake activity, and expose any trends within the deformation (orientation, style, degree of deformation) (McCalpin, 2009).

The process of investigation needs to start from a regional-scale to a local-scale in order to fully document the extent of the deformation and fault structure reactivated or formed by past seismic activity (McCalpin, 2009). Past-earthquake evidence needs to be constrained in

time, whether this is done with absolute or relative dating techniques (McCalpin and Nelson, 2009). An age of co-seismic deformation is needed to determine the length of the quiescent interval and possible recurrence time, therefore allowing for a seismic hazard assessment (McCalpin and Nelson, 2009).

2.8 Earthquake Hazard

Human records (if they exist) of past earthquakes are typically subjective, and can exaggerate the magnitude of the event, and involve conflicting records of the earthquake timing and magnitude (Gürpinar, 2005). The lack of detailed records of past earthquake activity in many regions, leads to an over-estimation of earthquake hazard in areas of frequent and significant earthquake activity, and under-estimation of seismic hazard in areas of minimal to no recorded seismic activity (periods of quiescence) (Li *et al.*, 2009). Therefore the use of palaeoseismological investigations for quantifying and qualifying earthquake hazard is commonly the most reliable and objective method available (Gürpinar, 2005).

The International Atomic Energy Agency (IAEA), recommends the use of palaeoseismological studies in evaluation of seismic hazard for critical facilities (dams, power stations) (Gürpinar, 2005), and the U.S. Nuclear Regulatory Commission (2007) requires thorough geological investigations of past seismic activity, and faults with reactivation potential at the sites of proposed nuclear power stations. South Africa, which has no standard regulatory document for seismic hazard, therefore makes use of these international regulatory guidelines when evaluating seismic hazard (Singh *et al.*, 2009).

Therefore, through resolving the contemporary regional stress field from geological stress indicators, the recognition of favourably orientated faults to the prevailing stress field, and the assessment of the reactivation potential of the faults, a seismic hazard estimation can be determined. Seismic hazard determination is of critical societal importance, as potential earthquake damage to critical facilities due to poorly constrained local seismic hazard would have serious consequences to general human population living nearby.

Chapter 3

Geological Setting

3.1 Geographic Position of the Study Area

This investigation focusses in on the Southern Cape region, which is positioned within the southern-most part of Southern Africa (in the Republic of South Africa) (Fig. 3.1). The local study area involves the coastal area between the towns of Gansbaai and Waenhuiskrans (Fig. 3.2).

3.2 Tectonic Setting

The position of the study area in relation to the surrounding plate boundaries, and other tectonic plate-scale forces is illustrated by Fig. 3.1. The study area is in an intraplate setting within the larger-scale African plate (Andreoli *et al.*, 1996; Viola *et al.*, 2005). The active tectonics and forces potentially effecting the study area derive from the geodynamics and tectonic characteristics of the African Plate.

3.2.1 The African Plate

The African Plate, as shown in Fig. 3.1 can be sub-divided into two sub-plates, the Nubia and the Somalia plates (Nocquet *et al.*, 2006). Southern Africa is located on the Nubia Plate in close proximity to the suggested sub-plate boundary. The study area is located within the Southern African region.

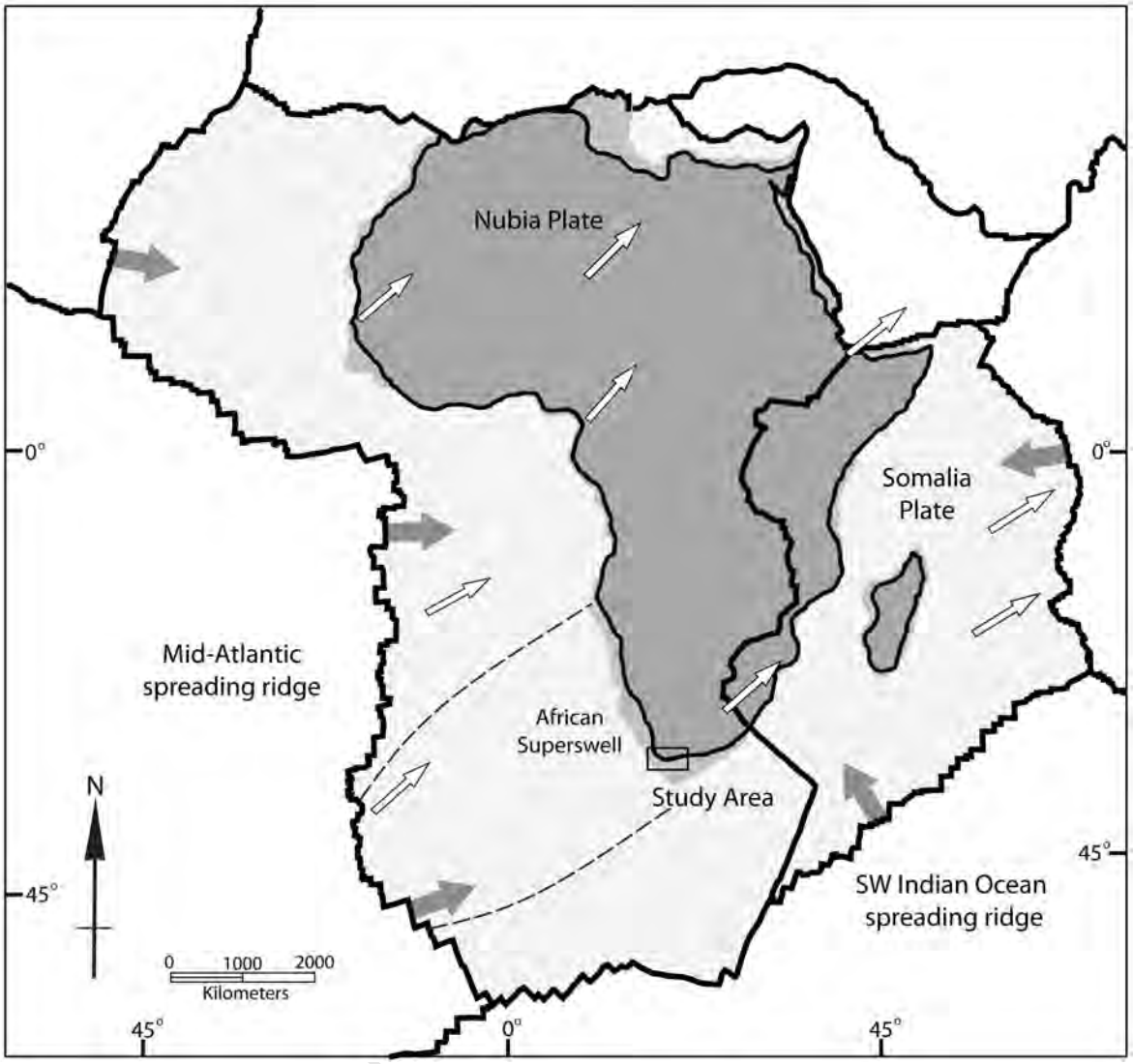

Figure 3.1: The African Plate illustrated with the Nubia and Somalia sub-plate boundaries as provided by Heidbach *et al.* (2010). The African continent and off-shore shelf regions are shown in darker grey. The position and trend of the African Superswell is shown from Nyblade and Robinson (1994). Dark arrows give directions of ridge-push forces deriving from oceanic spreading ridges. White arrows provide plate motion trajectories relative to the surrounding plates as suggested by Nocquet *et al.* (2006). Study area is shown. Figure modified from Viola *et al.* (2005)

The surrounding African Plate boundary is predominately spreading ridges, with the only convergent margin being in North Africa (Viola *et al.*, 2005). In relation to Southern Africa, the closest spreading ridges are the Mid-Atlantic spreading ridge (MASR) and the south-western part of the Indian Ocean spreading ridge (IOSR). Tectonic stress within Southern Africa could be predicted to derived from plate boundary effects such as ridge-push from the MASR and IOSR (as indicated on Fig. 3.1).

Southern Africa is however commonly experiencing an extensional tectonic regime within the African Plate, which is discordant to the expected compressional regime due to the surrounding spreading ridges (Bird *et al.*, 2006). It has been suggested that this discrepancy is a result of an elevated African topography possessing a larger horizontal extensional force than the ridge-push force (Bird *et al.*, 2006).

The elevated topography of Southern Africa, and decreased off-shore bathymetry has been attributed to the 'African Superswell' (Nyblade and Robinson, 1994). This feature, considered a topographical/bathymetric 'high' (relative to the earth geoid, centred on Africa), trends from the SE Atlantic ocean to eastern Africa and possesses on average an elevated heat flow within the underlying lithosphere, relative to the surrounding continental/oceanic lithosphere (Nyblade and Robinson, 1994). Locally, the African Superswell is observed to have an approximate NE-SW trend throughout the Southern Africa region (Fig. 3.1). The African Superswell is suggested to influence the African Plate through 'swell-push' force (Singh *et al.*, 2009) producing vertically orientated stress and large-scale uplift (Lithgow-Bertelloni and Silver, 1998).

Southern Africa, despite the prevailing tectonics, is considered to be a relatively tectonically stable continental region, with low levels of seismicity (Viola *et al.*, 2005). However the African Plate is not a stationary entity, as tectonic migration in response to plate-scale forces is an ongoing and significant process.

3.2.2 Plate Migration

The African Plate is undergoing relative motion approximately towards the NE with respect to the surrounding plates (Fernandes *et al.*, 2004; Nocquet *et al.*, 2006) (Fig. 3.1). This motion would suggest the ridge-push force of the MASR is most significant (Viola *et al.*, 2005).

The Nubia and Somalia sub-plates have distinct relative motion directions, with a current divergence occurring across the East-African rift (EAR) (Nocquet *et al.*, 2006). The divergence and rotation of the Somalia plate away from the Nubia plate has been suggested by Bird *et al.* (2006) to cause an NE-SW crustal lithospheric extensional stress across the incipient rift within the Southern Africa region.

3.3 Underlying Geology

The underlying regional geology of the study area (Fig. 3.2) can be sub-divided into the Syntaxis and Southern Domain of the Cape Fold Belt (CFB) (Söhnge, 1983; Andersen and Andreoli, 1990; Johnston, 2000), and the older Saldanian Belt (Rozendaal *et al.*, 1999). The CFB and the Saldanian Belt involve lithostratigraphic units which have been overprinted by multiple deformation events (Hälbich *et al.*, 1993), and owing to the underlying geology potentially having significant control on the deformation of surficial deposits, the lithostratigraphic units and tectonic events thus need to be characterised and described.

3.3.1 Pre-Cape Orogeny

The rock units deposited and deformed before the Cape Orogeny are the Neo-Proterozoic age Malmesbury Group (Tygerberg Formation) and the Cape Granite Suite rock units (Rozendaal *et al.*, 1999). The Malmesbury Group was deposited during rifting and eventual break-up of Rodinia (from 780 to 600 Ma) (Rozendaal *et al.*, 1999).

The Pan-African orogenic event subsequently deformed the Malmesbury Group units, with the intrusion of the Cape Granite Suite occurring contemporaneously at this time (between 550 to 510 Ma) (Hälbich *et al.*, 1993; Rozendaal *et al.*, 1999) (Tab. 3.1). The deformed Malmesbury Group and Cape Granite constitute the Saldanian Belt ,which trends throughout the south-western and southern margins of Southern Africa (Söhnge, 1983; Rozendaal *et al.*, 1999) (Fig. 3.2).

3.3.2 Cape Orogeny

The Paleozoic Cape Supergroup rocks (Table Mountain Group, Bokkeveld Group, and Witteberg Group), were deposited (unconformably on the Saldanian Belt rocks) within the Cape Basin between the Mid-Cambrian to the Mid-Carboniferous (Shone and Booth, 2005). These Saldanian Belt and the Cape Supergroup rock units preserve the Cape Orogeny effects.

The Permian-Triassic Cape Orogeny involved significant deformation of the Saldania belt and Cape Supergroup rocks between 280 Ma - 235 Ma (Hälbich, 1983; Hälbich *et al.*, 1993), throughout the merging of the Pangea (Singh *et al.*, 2011). The formation of the

CFB occurred during this orogenic event, with the Western Domain, Syntaxis, and Southern Domain sections all developing simultaneously (Johnston, 2000). The study area is primarily situated within the Southern Domain of the CFB.

The deformation of the Southern Domain of the CFB was typically through a north-south compression, resulting in a 120 kilometer shortening of the rock packages (Johnston, 2000). The compressional strain accommodation resulted in intense to gentle folding and steep thrust fault propagation, with common thrust stack development (Söhnge, 1983; Hälbich *et al.*, 1993; Johnston, 2000). The deformation structures have an approximate east-west trend, with northward-verging folds, and southward dipping (bedding-parallel) thrust faults (Johnston, 2000).

AGE (Ma)	ERA	PERIOD/EPOCH	REGIONAL TECTONICS	SEDIMENTARY & VOLCANIC UNITS	INTRUSIVE UNITS
0.012	CENOZOIC	Quaternary: Holocene, Pleistocene	200 metre uplift event 200m epeirogenic uplift along SAA	Sandveld Formation Waenhuiskrans Formation Kleinbrak Formation Wankoe Formation De Hoopvlei Formation (Bredasdorp Group) Quoin Point volcanic complex	
2.6		Neogene: Pliocene, Miocene			
5.3					
23		Paleogene: Eocene			
66					
145	MESOZOIC	Cretaceous	Gondwana extension, rifting and break-up Agulhas - Falklands Fracture Zone development Cape Orogeny thrust fault reactivation Listric normal faults and half grabens	Enon Formation — Uitenhage Group	Cape Dyke Swarm emplacement
201		Jurassic			
252		Triassic	Cape Orogeny Northward directed compression E-W trending folds Bedding parallel thrust faults		
299	PALEOZOIC	Permian			
359		Carboniferous		Witteberg Group Bokkeveld Group Table Mountain Group (Cape Supergroup)	
419		Devonian			
443		Silurian			
485		Ordovician			
541		Cambrian			
635	NEO-PROTEROZOIC	Ediacaran	Gondwana Formed Saldanian belt development, Pan-African Orogenic event	Tygerberg Formation — Malmesbury Group	Cape Granite Suite
850		Cryogenian			

Table 3.1: Summary of the stratigraphy of the south-western part of Southern Africa. Major tectonic events are correlated with deposition and emplacement of lithological units. Details taken from Hälbich (1983), Söhnge (1983), Andersen and Andreoli (1990), Malan (1990), Hälbich *et al.* (1993), Ben-Avraham *et al.* (1997), Rozendaal *et al.* (1999), Johnston (2000), Shone and Booth (2005), Trumbull *et al.* (2007)

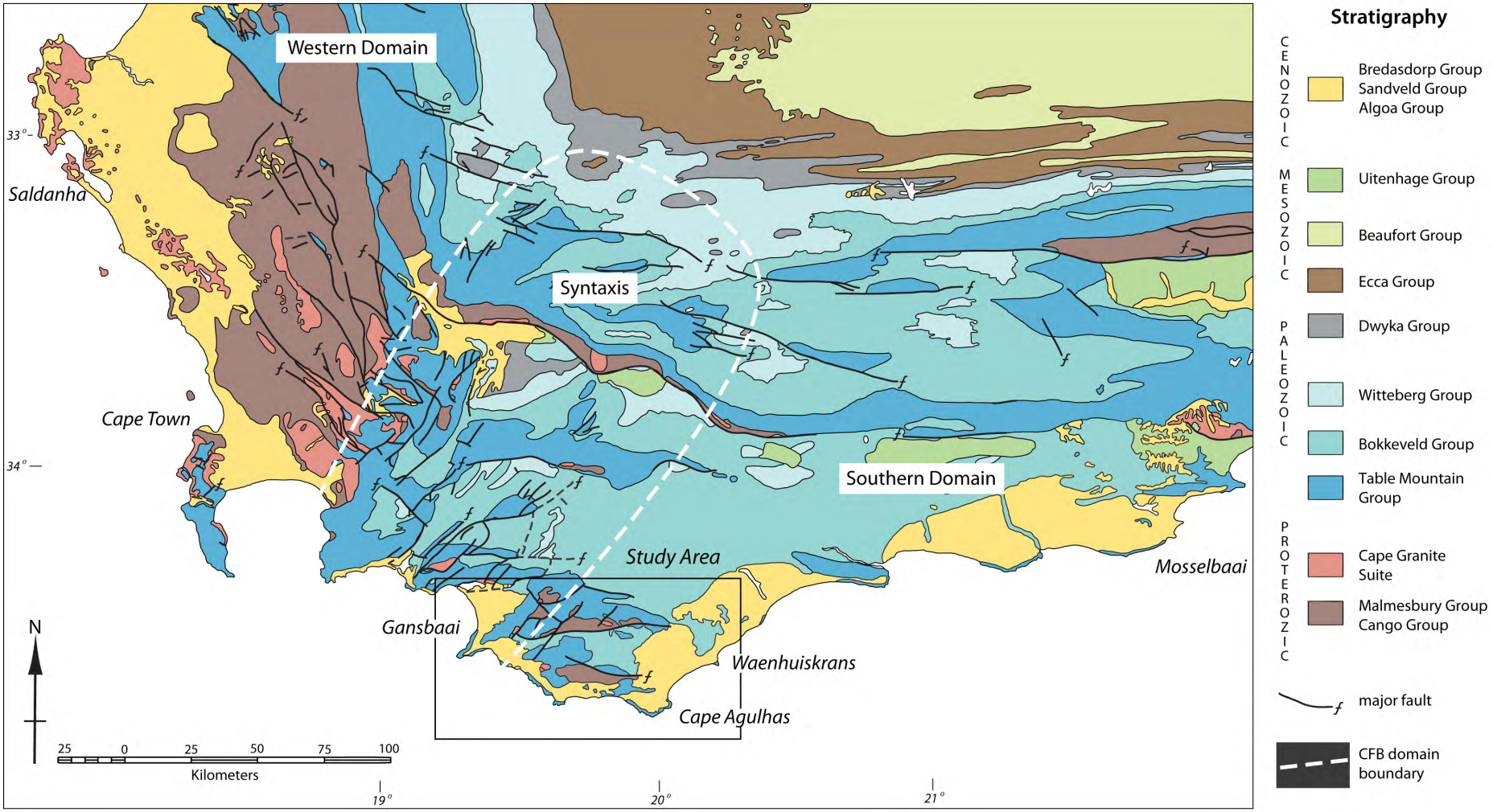

Figure 3.2: Geological map of the south-western part of Southern Africa. Major lithological Groups (Proterozoic to Cenozoic-age) and faults described. The study area over the Southern Cape is indicated. Modified from Coertze et al. (1970).

3.3.3 Gondwana Breakup

The Late-Jurassic to Early-Cretaceous rifting and eventual breakup of the super-continent Gondwana initially resulted in the intrusion of the Cape Dyke Swarm (CDS) between 150 Ma - 130 Ma (Trumbull *et al.*, 2007). The orientation of the dykes developed parallel to the palaeo-stress field at the time (dykes intrude through tension fractures), with a trend NW-SE (Hälbich *et al.*, 1993; Trumbull *et al.*, 2007).

The main rifting phase during 140 Ma - 130 Ma resulted in widespread structural inversion of the CFB, with a north-south to NE-SW extension on average (Hälbich, 1983; Paton, 2006). The continued extension and rifting process resulted in reactivation of the Cape Orogeny thrust faults into normal listric faults (Fig. 3.2) (Paton, 2006). These normal faults (eg. the Worcester and Kango faults) are predominately southward dipping, with numerous antithetic components dipping northward (Hälbich *et al.*, 1993; Paton, 2006).

The separation of the African and South American (Falklands Plateau) continents caused the formation of the Agulhas-Falklands Fracture Zone (AFFZ) (Hälbich *et al.*, 1993; Thomson, 1999). The AFFZ (Fig. 3.3) is a major transform fault zone (dextral strike-slip displacement sense) which was active from 130 Ma to 65 Ma (Ben-Avraham *et al.*, 1997).

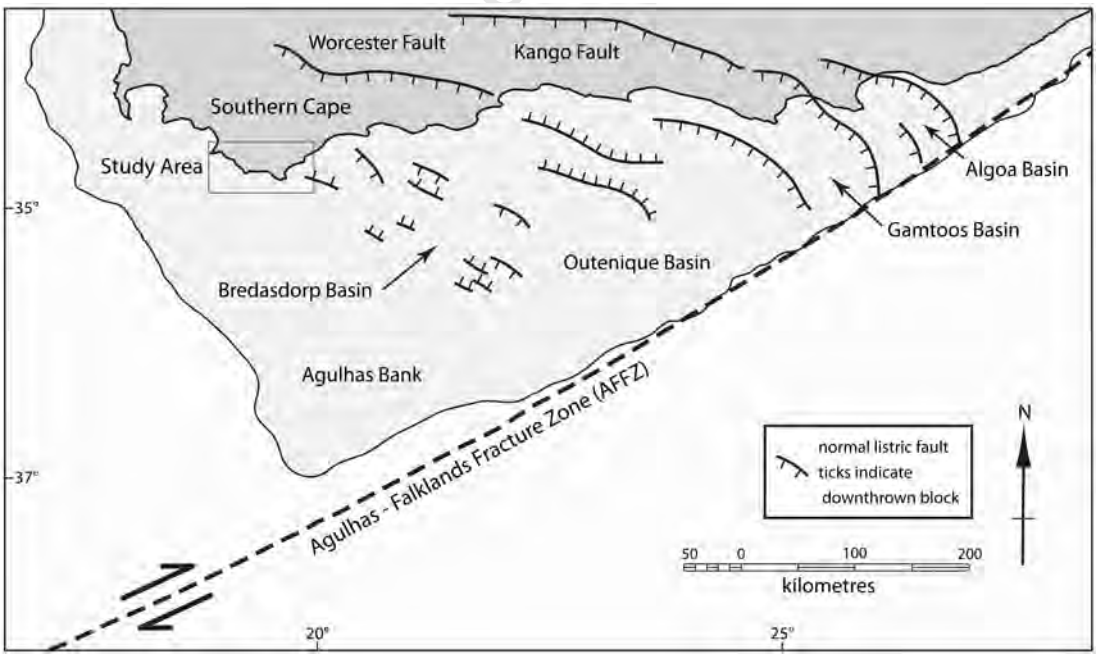

Figure 3.3: Schemmatic figure of major structures constituting the Agulhas-Falklands fracture zone, and major Gondwana breakup related extensional faults. Position of basins within the Agulhas Shelf are indicated. Modified from Thomson (1999); Paton (2006)

Transtension and dextral wrenching (due to the westward migration of the Falklands Plateau relative to the Agulhas Shelf) on the AFFZ caused $en\ echelon$ extensional listric faults to propagate from the AFFZ onto the Agulhas Shelf (Fig. 3.3) (Andersen and Andreoli, 1990; Paton, 2006). The resultant normal faulting (synthetic and antithetic normal fault development) and subsequent half-graben and grabens formed the off-shore Bredasdorp and Outeniqua Basins (Hälbich *et al.*, 1993). The trend of the normal listric faults from the AFFZ is typically NW-SE to E-W towards the study area with southward dipping faults on average (Paton, 2006).

The Gondwana Breakup is seen to be the last major large-scale tectonic episode affecting the region (Viola *et al.*, 2005), with these rift-related extensional structures being the youngest developed faults present in the underlying geology of the study area.

3.4 Post Breakup Tectonics

The Southern Cape developed as a passive continental margin due to the rifting and eventual breakup of the super-continent Gondwana ($\sim$135 Ma) (Bradley, 2008; Leroy *et al.*, 2008). Passive continental margins are typically observed to be stable tectonic features, however substantial post-rift uplift of the continental margin can occur (Leroy *et al.*, 2008). Most applicable to this research project are the most recent regional uplift events over the south-western parts of Southern Africa, which occurred successively during the Neogene.

3.4.1 Neogene Uplift Events

The first significant regional uplift event occurred during the Miocene ($\sim$18 Ma) (Partridge, 1998; Partridge and Maud, 2000). The coastal platform, seen as the Cretaceous-age African Surface (pediplain), was incised significantly by river channels during the Miocene (Holmes *et al.*, 2007). The river terrace development which consequently ensued, provides evidence for epeirogenic uplift of approximately 200 metres throughout the Southern Cape region (Partridge and Maud, 2000; Marker and Holmes, 2005).

The second major regional uplift event occurred during the Pliocene ($\sim$ 5 Ma) (Partridge and Maud, 2000; Holmes *et al.*, 2007). Again the reworking of the African Surface and

river terrace development provides evidence for epeirogenic uplift and seaward tilting of the coastal platform, most distinctly along the so-called Saldanha-Agulhas Axis (SAA) (Andreoli *et al.*, 1996). Regional uplift is considered to be of no more than 200 metres for the south-western part of the Southern Cape (Partridge and Maud, 2000).

Andersen and Andreoli (1990) further suggest that to accommodate this regional uplift, pre-existing structures may have been utilised instead of the uplift being purely epeirogenic in nature, possible fault reactivation after the Jurassic-Cretaceous Gondwana Breakup is expected to have therefore occurred during the Neogene.

Both these uplift events have been attributed to the African Superswell initiation and continued large-scale uplift (Nyblade and Robinson, 1994), however isostatic uplift and thermal uplift of the Southern Africa passive margin are also postulated as possible mechanisms for the regional uplift of the Southern Cape (Partridge and Maud, 2000).

3.4.2 Quaternary Fault Reactivation

Recent and contemporary fault reactivation throughout Southern Africa is well documented (Singh *et al.*, 2009, 2011). Offshore of the West Coast of Southern Africa active fault reactivation has been documented, typically as the development of multiple mud volcanoes (Viola *et al.*, 2005). Active tectonics is also recorded and documented in Namaqualand and South Namibia (Viola *et al.*, 2005, 2012), as well as in the interior of Southern Africa (Koffiefontein, Witswatersrand basin, and Lesotho), typically attributed to mining activity (Singh *et al.*, 2009).

However in the more southern parts of Southern Africa, recorded active tectonics is commonly concentrated on the Ceres-Worcester area, and the Kango-Bavainskloof-Coega faults throughout the CFB (Singh *et al.*, 2009). Other relatively dispersed seismic events are also being recorded seaward of the 'Great Escarpment' along the CFB mountains(Singh *et al.*, 2009). Active tectonics within the CFB appear to be largely restricted to structures inherited from the Cape Orogeny and Gondwana breakup period, with complex intraplate earthquake characteristics (Bird *et al.*, 2006; Singh *et al.*, 2009).

3.4.3 Wegener Stress Anomaly

Through the use of Late-Neogene and Quaternary-age deformation structures, bore-hole breakout data, and geological stress indicators, a regional upper-crustal stress field can be estimated and measured for the south-western part of Southern Africa (Fig. 3.4). This stress field can be described as possessing a S_{Hmax} oriented NW-SE to NNW-SSE for the offshore Namibia and Namaqualand region (Viola *et al.*, 2005, 2012), a WNW-ESE to NNW-SSE oriented S_{Hmax} for the Southern Cape and Bredasdorp Basin region (Andreoli *et al.*, 1996), and an approximate NW-SE oriented S_{Hmax} for the south-western Cape region (Green and Bloch, 1971; Bird *et al.*, 2006).

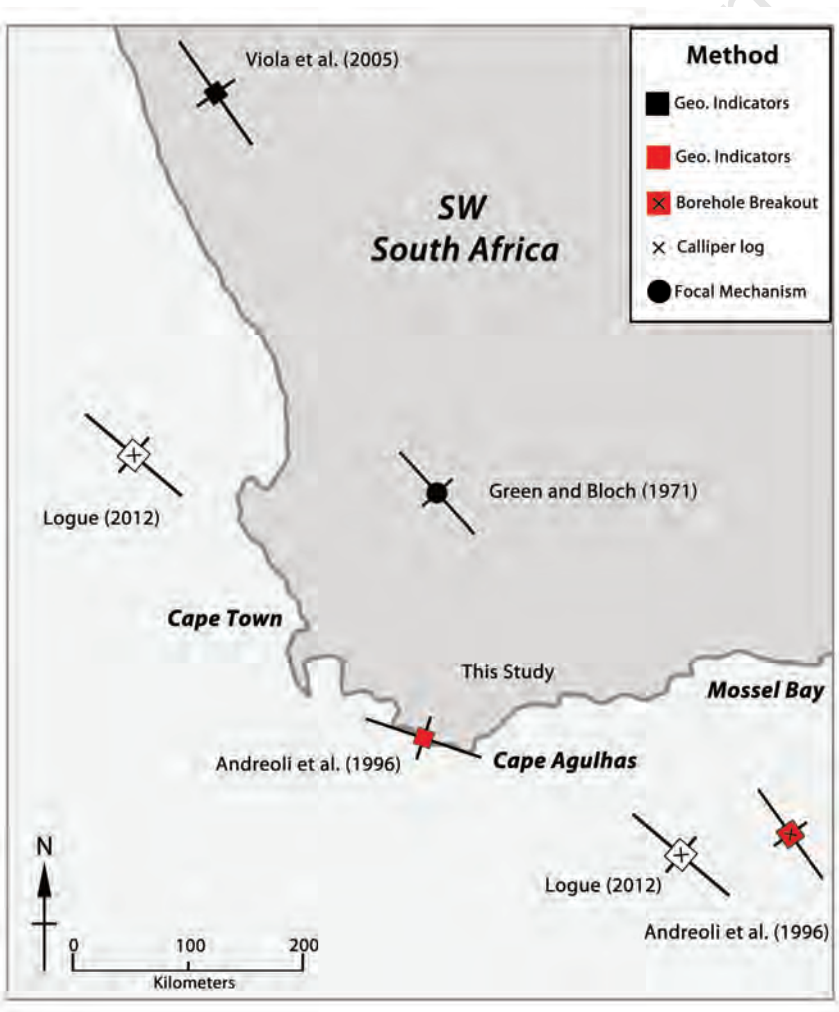

Figure 3.4: Diagram showing the orientation of S_{Hmax} at locations within the south-western part of Southern Africa. Stress orientation data is derived from indicated sources (including Logue *et al.* (2012)). Average trajectory of S_{Hmax} is NW-SE. Figure modified from Bird *et al.* (2006)

The similarity of all S_{Hmax} directions to one another suggests a large-scale stress field prevailing over the south-western region of Southern Africa (Fig. 3.4). The stress field possesses an approximate NW-SE trajectory of S_{Hmax} in a NW-SE trend over the region on average (Bird *et al.*, 2006). The stress field was given the name 'Wegener Stress Anomaly' (WSA) by Andreoli *et al.* (1996), with no solid explanation for its existence available. The WSA is considered to have existed over the region at least since the Cretaceous time from the orientation of the emplaced NW-SE trending Cape Dyke Swarm until present (Andreoli *et al.*, 1996) (Tab. 3.1).

3.5 Late Cenozoic Sea-Level Fluctuations

The Late Cenozoic relative sea-level (RSL) fluctuation (driven by glacio-eustatic sea-level change (Partridge and Maud, 2000; Maud and Botha, 2000)) at the southern continental margin of Southern Africa, needs to be outlined because of the significant effect that RSL fluctuation has on the deposition and erosion of coastal rocks (Marker and Holmes, 2005). The Late Cenozoic and Upper Pleistocene-Holocene RSL fluctuation curves as illustrated in (Fig. 3.5) displays the most recent interglacial - glacial cycles, with the respective marine regressions and transgressions shown.

Since the Late Pliocene, the Southern Cape has experienced several major marine regression/transgression events (Haq *et al.*, 1987). On average, the marine regressions involved $\sim$50 metres below present sea level shoreline shifts, with the marine transgressions typically involving $<$30 metre above present sea level shoreline shifts (Haq *et al.*, 1987). More recently however, the last interglacial at 130 ka - 118 ka resulted in a maximum 6 - 7.5 metres above present sea level shoreline transgression (Clark *et al.*, 2009; Carr *et al.*, 2010), and the last two glacial periods at $\sim$135 ka and $\sim$22 ka, both resulted in successive shoreline regressions of 120 - 130 metres below present sea level (Ramsay and Cooper, 2002; Waelbroeck *et al.*, 2002).

The formation of the Late Cenozoic marine platforms and terraces, as observed within the Southern Cape, are also a consequence of this RSL fluctuation (along with regional continental uplift and tilting events) (Maud and Botha, 2000). It is upon these marine terraces that the Pliocene to Pleistocene Bredasdorp Group deposits are distributed; with the locations

and elevations of the different deposits, and subsequent wave action erosion, being controlled by the relative position of the shoreline over time (Marker and Holmes, 2005).

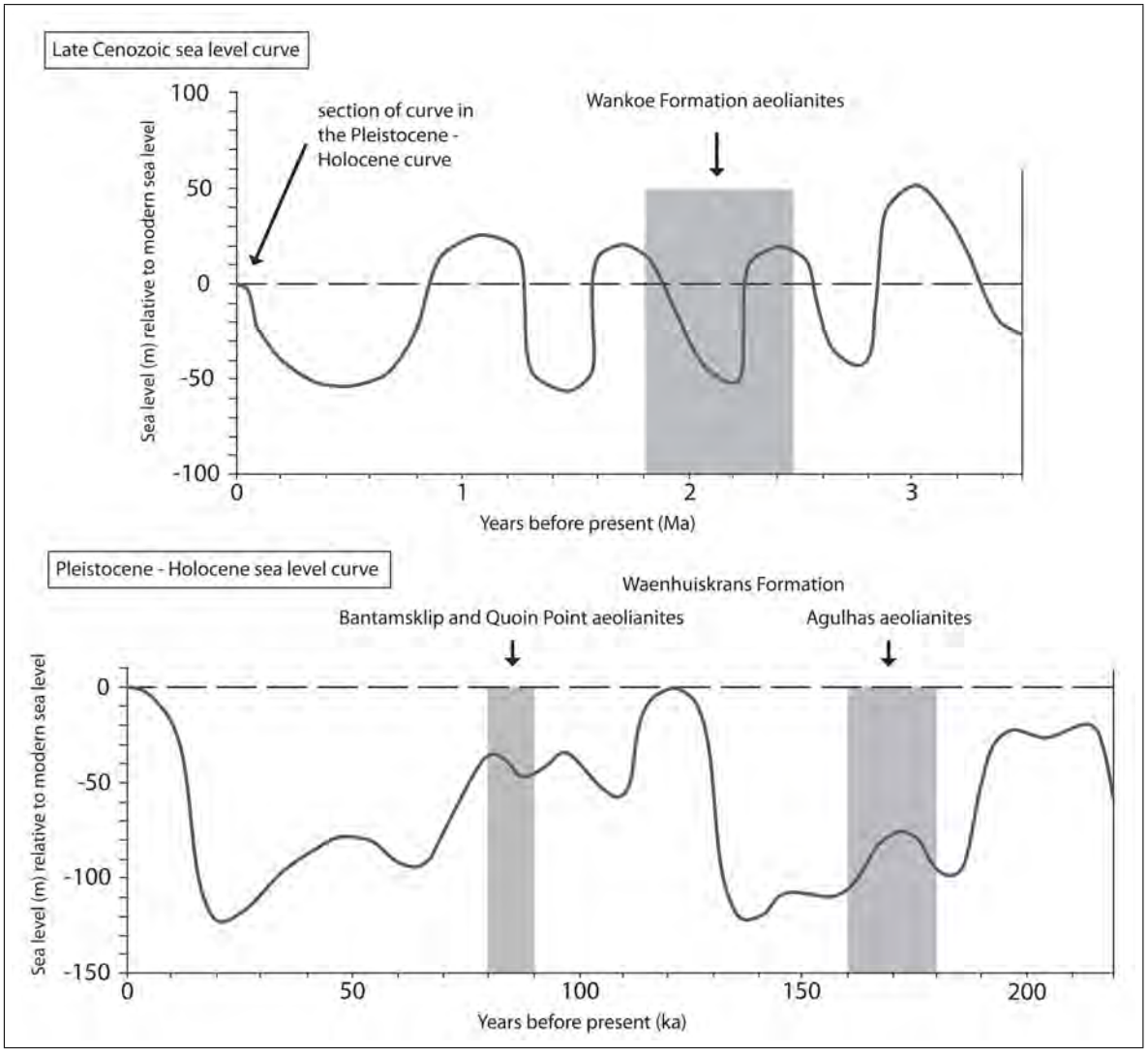

Figure 3.5: Relative sea-level (RSL) curves for the Late Cenozoic (3.5 Ma to Present) and the Upper Pleistocene - Holocene (220 ka to Present). The Late Cenozoic RSL curve illustrates long term regression-transgression cycles, with the approxiamte consolidation period of the Wankoe Formation (grey area) indicated. The Pleistocene - Holocene RSL curve illustrates the last two inter-glacial and glacial cycles (and regression-transgression cycles), with the periods of consolidation for the Waenhuiskrans Formation aeolianites found at Bantamsklip and Agulhas indicated. Ages of consolidation as described by Marker and Holmes (2005) for the Wankoe Formation, and by Bateman *et al.* (2004) for the Waenhuiskrans Formation. Late Cenozoic RSL curve modified from Haq *et al.* (1987), and Pleistocene - Holocene RSL curve modified from Bintanja *et al.* (2005).

3.6 Cover Sequence Geology

The Pliocene to Pleistocene-age cover sequence present along the southern continental margin of Southern Africa, and most specifically the Southern Cape is comprised of the Bredasdorp Group coastal, marine and marginal marine deposits (Malan, 1990).

3.6.1 The Bredasdorp Group

The Bredasdorp Group outlined in Tab. 3.2, is the most recent lithological unit present through the study area (Tab. 3.1), and covers the underlying geology unconformably from Hermanus to Plettenberg Bay (Malan, 1990; Partridge and Maud, 2000) (Fig. 3.2). The succession has a variable width ranging between 0.2 km to 7 km (Roberts *et al.*, 2006), and possesses a total thickness of $\sim$500 metres (Malan, 1990; Partridge and Maud, 2000).

The Bredasdorp Group consists of typically marginal-marine, coastal deposits, with interstitial marine deposits deposited during marine regressions (see previous section) (Partridge and Maud, 2000). The succession is characterised by aeolianites, calarenites, calcerous sandstones, pebbly limestones, beach gravels, and calcretes (Malan, 1990). These lithologies are comparable elsewhere along the south-western continental margin of Southern Africa with the Algoa Group and the Sandveld Group lithologies further to the east and west respectively (Partridge and Maud, 2000).

The Bredasdorp Group was deposited and consolidated during interglacial periods throughout the Pliocene and Pleistocene (Brooke, 2001). Constant sea-level fluctuation and climate change were the main controlling factors for the formation and preservation of the successions (Brooke, 2001; Bateman *et al.*, 2004). The atmospheric conditions during glacial lowstands periods are commonly cooler and winder on average, with sediment predominately mobile; however during interglacial high-stand periods, the warmer and wetter conditions aided in the consolidation and carbonate cementation of the various Bredasdorp Group rock units (Brooke, 2001).

The Bredasdorp Group, although consisting of several different coastal and marginal marine rock Formations (Tab. 3.2), needs to be limited to the Wankoe and Waenhuiskrans Formations, due to these Formations being the most useful for this research project. Both the Wankoe and Waenhuiskrans Formations are the most geographically pervasive throughout

Age (Ma)	Period/Epoch	Lithostratigraphic Unit	Depositional Environment	Lithological Characteristics
0.012	Holocene	Strandveld Formation	Fluvial Colluvial Marine (beach and shoreface) Near-marine Aeolian dune fields Interdune environments	Unconsolidated beach, river, scree, aeolian dune sands Stabilised dune deposits Beach rock Quartz -feldsparthic sands Significant shell fragment content
0.088	Upper Pleistocene	Waenhuiskrans Formation	Coastal (near-marine) Backshore dune fields Aeolian dune corridors Interdune environments	Unconsolidated, semi-consolidated, consolidated, calcified dune rock Well sorted - very well sorted Medium grained Calcarenite, calcerous sands Calcrete layers Large-scale aeolian crossbedded Thickly bedded (3 metres) Terristrial gastropods Well rounded marine shells, foraminifera fragments Maximum thickness 200 metres
0.125		Kleinbrak Formation	Shallow marine Estuarine Beach Lagoonal environments	Consolidated sand, calcarenite, marine gravel, conglomerate, significant shell content. Poorly sorted to well sorted. Pebbly limestone
0.126	Middle Pleistocene			
1.8	Lower Pleistocene	Wankoe Formation	Coastal (near-marine) Backshore dune fields Aeolian dune corridors Interdune environments	Calcified dune rock Well sorted - very well sorted Fine - medium grained Calcarenite, calcaerous sandstone Pebble lenses, calcrete layers Massive, large-scale cross bedded Weathered Terrestrial shells Positive erosive landscape feature, forms prominent ridges Maximum thickness 300 metres
2.6	Late Pliocene	De Hoopvlei Formation	Shallow marine (beach, shoreface, backshore, foreshore) Estuarine, lagoonal environments Deposited on Tertiary marine terrace.	Cemented Beach gravel Poorly sorted Basal pebbly conglomerate, calcarenite, calcerous sandstone Marine shells Average thickness 8 metres

Table 3.2: Summary of the Bredasdorp Group stratigraphy. The different ages of Formations indicated from the late Pliocene to Holocene. Depositional environment at time of formation outlined. Lithological and petrographic characteristics described. Details taken from Malan (1989a), Malan (1989b), Malan (1990), Malan (1991a), Malan (1991b), Bateman *et al.* (2004)

the Southern Cape, and constitute the majority of the Bredasdorp Group. The Formations furthermore possess lithological characteristics which will assist in the analysis of internal deformation features.

3.6.2 Wankoe Formation

The Late Pliocene and Lower Pleistocene-age Wankoe Formation constitutes the majority of the Bredasdorp Group (Partridge and Maud, 2000). It was deposited during the Late-Pliocene sea-level regression between 2.8 Ma - 2.3 Ma (Siesser and Dingle, 1981; Malan, 1989b), with consolidation occurring into the Lower Pleistocene (approximately 1.8 Ma) (Marker and Holmes, 2005) (Fig. 3.5). The Wankoe Formation can be described as an aeolianite-type rock unit (consolidated wind blown dune), which has commonly weathered heavily to become thoroughly calcified on average (Malan, 1989b). The lithological characteristics and depositional environment are summarised in Tab. 3.2.

Numerous prominent topographical highs throughout the Southern Cape are weathered Wankoe Formation ridges, which are commonly positioned relatively distal from the present shoreline (Malan, 1989b). These ridges are most distinctive, and commonly the diagnostic feature used when locating the Wankoe Formation within the Southern Cape region.

3.6.3 Waenhuiskrans Formation

The Upper Pleistocene Waenhuiskrans Formation is the second-most abundant Formation within the Bredasdorp Group (Partridge and Maud, 2000). It was deposited either during the penultimate marine regression between $\sim$180 ka to 160 ka, with consolidation by 160 ka (Agulhas aeolianites), or during the last marine regression between 125 ka and 88 ka, with consolidation occuring up to 80 ka (Bantamsklip aeolianites), as described on Fig. 3.5 (Bateman *et al.*, 2004). The Waenhuiskrans Formation is typically described as an aeolianite-type (consolidated wind blown dune) deposit, which exhibits moderate to heavy degrees of surface weathering (Malan, 1989a). The lithological characteristics and depositional environment is summerised in Tab. 3.2.

The Waenhuiskrans Formation differs most significantly from the Wankoe Formation in the lower levels of weathering, lower unit thickness, and increased content of rounded marine

gastropod shells and foraminifera fragments (Malan, 1989a). The Waenhuiskrans Formation is often observed as wave-eroded cliff faces, with general dune topography, commonly relatively proximal to/or submerged by the present sea-level (Malan, 1989a; Bateman *et al.*, 2004).

3.7 The Study Area and Local Structural Geology

The study area of this research project is located at the most southerly part of Southern Africa, specifically between the coastal towns of Gansbaai and Arniston/Waenhuiskrans within the Southern Cape. The location of the study area is illustrated on Fig. 3.2. The local geology of the area has been previously described by Andersen and Andreoli (1990) in a Atomic Energy Corporation report on the structural geology of the Southern Cape.

3.7.1 Recognised Faults and Landform Disruption

Through previous use of aeromagnetic surveys, numerous underlying faults were detected by Andersen and Andreoli (1990), these being the Elim and Struisbaai Faults, interpreted to be reactivated thrust faults during the extensional regime at Gondwana breakup times. Uilkraal, Celt Bay, and Kleyn Hagelkraal faults, interpreted to be strike-slip in the displacement, are also of Gondwana breakup age (Andersen and Andreoli, 1990). The Donkergat Fault was also initially detected with the use of aeromagnetic surveys and later confirmed through borehole drilling (fault breccia was exposed in the drill core) (Andersen and Andreoli, 1990). The fault was suggested by Andersen and Andreoli (1990) to be strike-slip in nature and possibly related to the development of the AFFZ.

Landform disruptions involve fault scarps to the north of Cape Agulhas, geologically recognised by the superimposition of Table Mountain Group quartzites against Enon Formation silicified conglomerates (of Cretaceous age) (Fig. 3.2) (Andersen and Andreoli, 1990). Furthermore the outcropping Waenhuiskrans Formation dune bodies and ridges are observed to be truncated by both the underlying postulated Blomerus Fault to the north-east of Gansbaai, and by the Struisbaai Fault to the north of Cape Agulhas (Andersen and Andreoli, 1990).

3.7.2 Neotectonic Features

Within the Southern Cape, Andersen and Andreoli (1990); Andreoli *et al.* (1996) recognised recent (neotectonic) joints, faults, and breccias cross-cutting consolidated Pliocene - Pleistocene coastal deposits at Quoin Point (to the east of Gansbaai). The presence of structural deformation in the Waenhuiskrans Formation deposits, having been consolidated since the last interglacial period, provides a maximum age of a deformation event < 88 ka (Andersen and Andreoli, 1990).

Only limited other geological evidence of neotectonic activity has been previously documented within the study area and surrounding region. This study therefore attempts to add to the pre-existing data collected, and contribute towards a further understanding of the neotectonics and tectonic evolution of the Southern Cape.

Chapter 4

Results

4.1 Remote Sensing

An initial remote sensing reconnaissance of the Southern Cape region is necessary to recognise primary evidence of large-scale landform disruption by possible faults. The use of various platforms (e.g. satellite imagery, aerial photography, and digital elevation models (DEM's)) allows for topographical lineaments to be mapped. Lineaments are linear features which cross-cut or truncate landforms in an extensive manner across the Earth's surface (Drury, 1993). Although commonly formed by human activity (fences and roads) or image processing artefacts, lineaments can also be formed by fault activity (Drury, 1993). Faults involve significant deformation of the upper crust, which can result in the surface trace of faults preferentially eroding into linear valleys or depressions; and as the vertical/horizontal displacement of the surface geology along a fault plane can potentially truncate overlying/adjacent landforms, fault traces are often viewable on large-scale imagery of a region (Drury, 1993). Consequently, by applying this correlation between lineaments and faults, possible large-scale faults in the Southern Cape can be identified and subsequently studied in the field at the local level.

4.1.1 Regional Satellite Imagery

Multiple lineaments are identified and mapped on the natural colour (5, 4, 3 spectral band composite) Landsat 7 image of the Southern Cape region (Fig. 4.1), obtainable from the

United States Geological Survey LandsatLook Viewer website (http://landsat.usgs.gov).

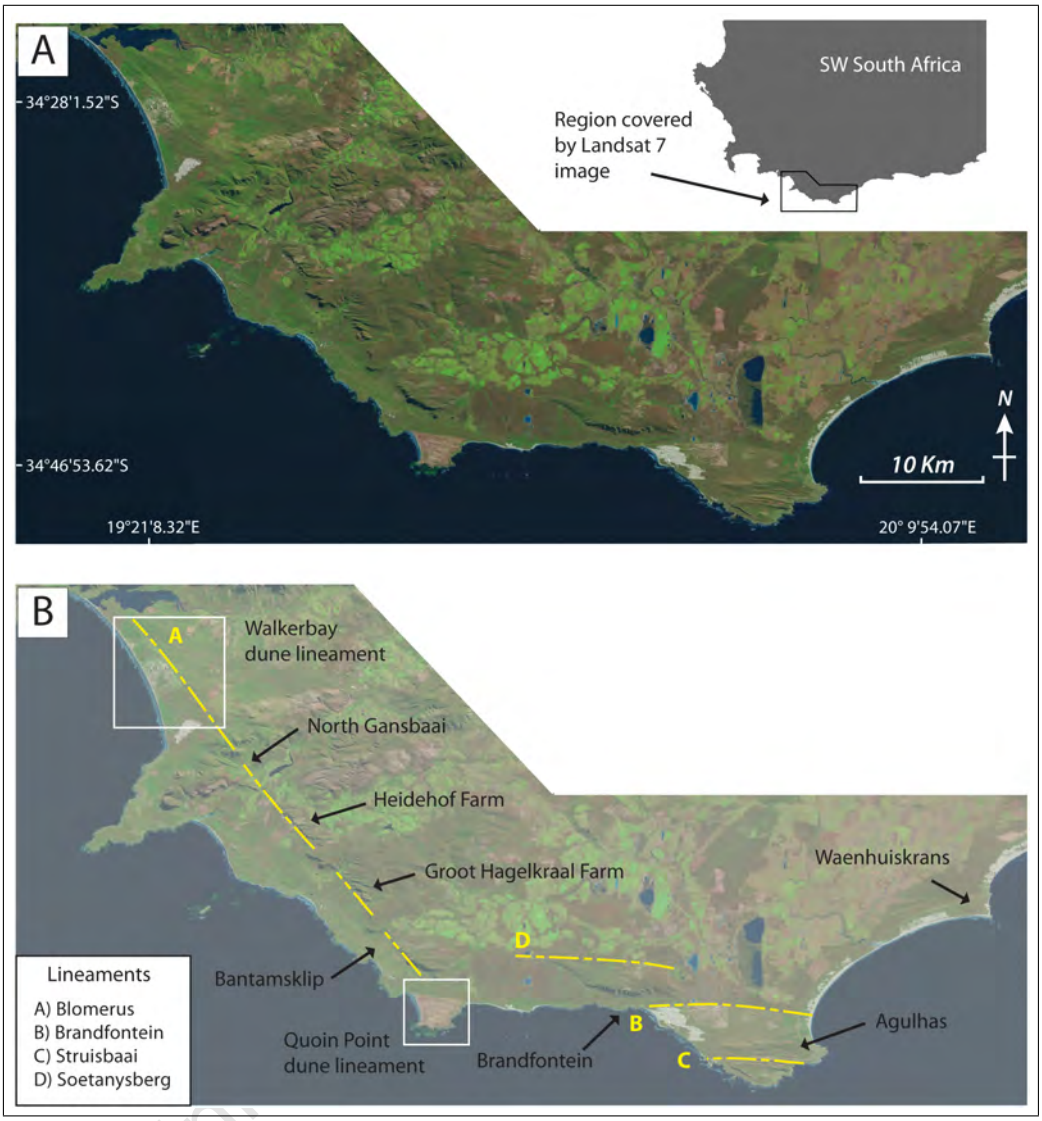

Figure 4.1: Natural colour Landsat 7 image of the Southern Cape. A) Original Landsat 7 image. B) Annotated image with lineaments mapped in yellow. The Blomerus Lineament extends from Walkerbay to Bantamsklip in an approximate NW-SE segmented trend. The Brandfontein, Struisbaai, and Soetanysberg lineaments trend approximately E-W across the respective areas. Locations of observable dune lineaments are indicated, see Fig. 4.3 for lineament locations. Image courtesy of the U. S. Geological Survey (http://landsat.usgs.gov).

The lineaments (Fig. 4.1B: as yellow lines) are identified through the recognition of linearly arranged scarp features, ridges, elongate topographical depressions, and differences in colour tone. Depending on the arrangement of the features, they are subsequently mapped as a single continuous lineament, segmented parts of a single lineament, or multiple discrete lineaments.

The lineament A (Blomerus) is present from the Walkerbay area, through the North Gansbaai area, the Heidehof and Groot Hagelkraal Farm areas, and into the Bantamsklip area. Lineament B (Brandfontein), extends from Brandfontein to North of Struisbaai. Lineament C (Struisbaai) is roughly parallel to lineament B, extending from the west to east of the Agulhas headland. Lineament D (Soutanysberg) is more cryptic in appearance and traces along the north of the Soutanysberg.

The Blomerus Lineament possesses a ∼NNW-SSE trend, with a combined segemented length of ∼35 km and an average segment length of ∼10 km. The Brandfontein and Struisbaai lineaments both trend ∼E-W and have continuous lengths ∼15 km to 10 km respectively. The Soetanysberg Lineament trends ∼E-W with a length similar to the Brandfontein Lineament, ∼15 km.

The lineaments mapped on Fig. 4.1 are either relatively linear lineament segments (transversing the Walkerbay, Heidehof Farm, Groot Hagelkraal Farm, and Bantamsklip areas), or relatively arcuate lineaments (transversing the North Brandfontein, Brandfontein, Struisbaai areas). The orientation and aligned nature of the linear lineament segments suggest a single lineament (the Blomerus Lineament) extending through all these areas (segmentation may be due to the preservation of landforms defining the lineament in certain places only). The arcuate lineaments (e.g. Brandfontein, Struisbaai lineaments) are considered to be discrete lineaments.

Figure 4.1 illustrates that the lineaments cross-cut and truncate both the topographically mountainous areas, and the coastal plain areas. From the geology of the Southern Cape completed by Malan (1990); Andersen and Andreoli (1990) (outlined in Fig. 3.1), both the underlying geology (Cape Granite Suite, Table Mountain Group, Bokkeveld Group), and the more recent Tertiary-Quaternary cover sequence (Bredasdorp Group) are cross-cut/truncated by the lineaments.

4.1.2 Digital Elevation Model

Digital elevation models (DEM's) are topographical representations of the Earth's surface, where the elevation data is obtained through the use of satellite surveys (refer to McCalpin (2009) for details on DEM elevation data acquisition and processing specifics). DEM's can

therefore be used to expose topographical anomalies, most particularly lineaments, which may suggest existing fault structures (McCalpin, 2009). DEM's are therefore used to confirm the lineaments already mapped on the Landsat 7 image.

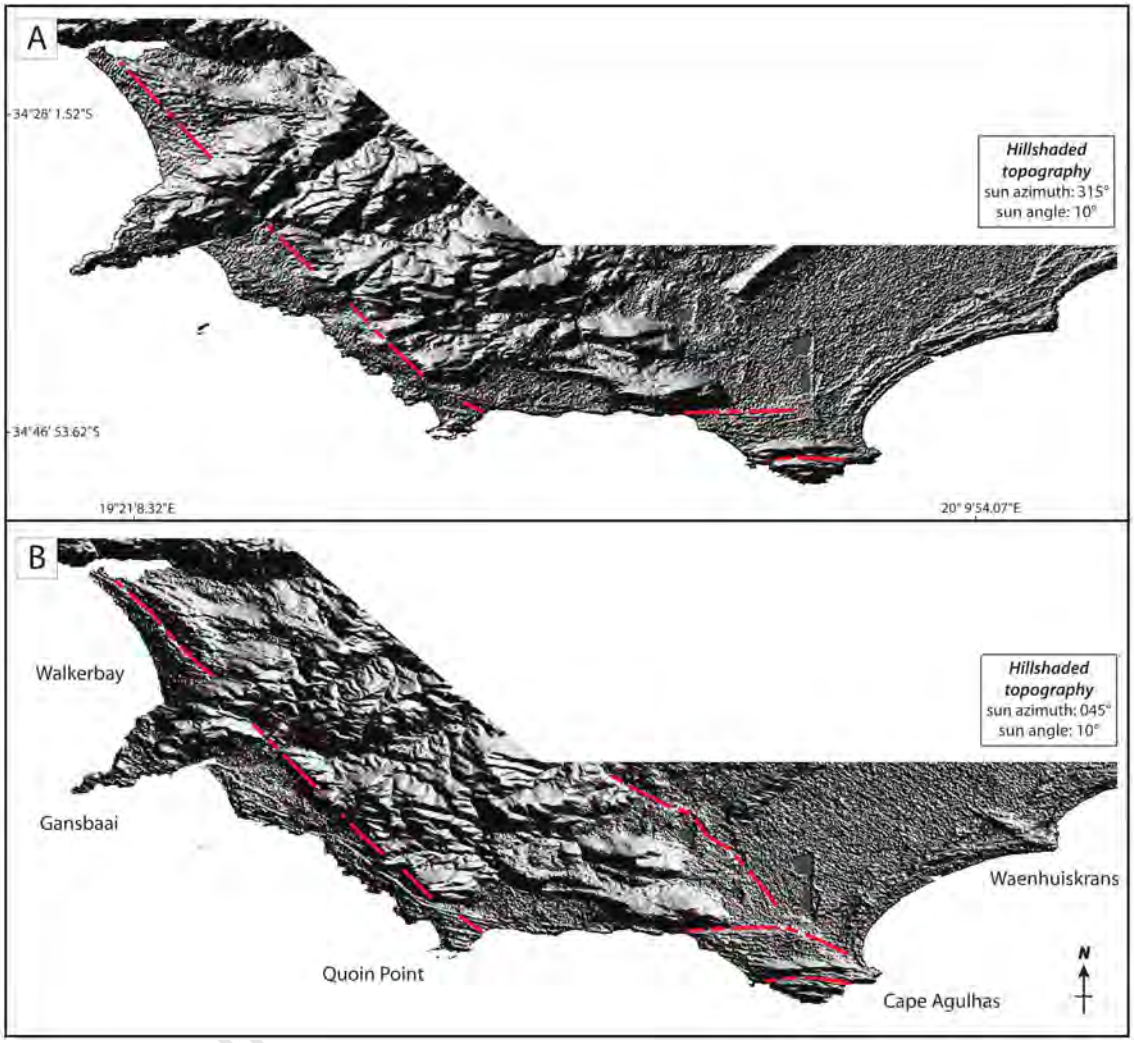

Figure 4.2: 90 metre resolution Digital elevation models for the Southern Cape. DEM's are Hillshaded to expose topographical features. A) Hillshaded with the sun azimuth set to 315 ° with a sun angle of 10 °. Lineaments (traced in red) are mapped from Walkerbay, through Heidehof Farm, Groot Hagelkraal Farm, and Bantamsklip areas to Quoin Point in a NW-SE orientation; Brandfontein, and Struisbaai areas in a E-W orientation. B) Hillshaded with the sun azimuth set to 045 °, with a sun angle of 10 °. Lineaments are mapped from the Walkerbay to Quoin Point, and north of Brandfontein areas, with a NW-SE orientation; Brandfontein and Struisbaai areas with an approximate E-W orientation. All the lineaments mapped on the DEM's confirm the lineaments on the Landsat 7 image. DEM's are georeferenced using the WGS84 datum, and processed in Quantum GIS (version 1.8.0 - Lisboa).

The DEM for the Southern Cape is acquired from the NASA Shuttle Topographical Mission (SRTM), and is obtainable from the CGIAR-CSI SRTM website (http://srtm.csi.cgiar.org) at 90 metre resolution. The DEM is further processed to provide two hillshaded DEM's

(Fig. 4.2) (refer to Chenrai (2012) for specifics on DEM hillshade processing). DEM A as shown in Fig. 4.2 is hillshaded with a sun azimuth of 315 ° and a sun angle of 10 °. The DEM B in Fig. 4.2 is hillshaded with a sun azimuth of 045 °, and a sun angle of 10 °. The different sun azimuths expose different topographical features orientated obliquely to the sun azimuth direction.

DEM A & B in Fig. 4.2 exhibit corresponding linearly arranged scarps, truncated ridges, and linear depression features to the Landsat 7 image (Fig. 4.1), these features can be mapped as lineaments (shown in dashed red on the DEM's). As a result, the lineaments identified and mapped on Fig. 4.1 are confirmed on both DEM A and B. However, the DEM's do provide some additional lineament information: DEM A and B shows evidence for an additional scarp feature in the Quoin Point area on the same line as the Blomerus Lineament. DEM B in particular displays a very distinct scarp feature, in the Walkerbay area (on the Blomerus Lineament). A lineament is also traced ∼NW-SE on DEM B north of the Brandfontein Lineament.

From both the cross-cutting and truncating nature (involving both the underlying and cover sequence geology), and large-scale lengths, the lineaments could suggest the orientation and locations of faults. Furthermore, because the orientations and locations of the Blomerus, Brandfontein and Struisbaai lineaments are significantly similar to the faults already suggested and mapped by Andersen and Andreoli (1990), these lineaments in particular warrant further investigation at the local scale. Therefore, the local-scale study areas will be demarcated in areas that these lineaments traverse through.

4.1.3 Dune Lineaments

'Dune lineaments' are observed in the Walkerbay and Quoin Point areas (Fig. 4.3), where recent Holocene dune bodies are disrupted or preferentially deposited to form linearly arranged depressions and scarps along the Blomerus Lineament recognised on both the Landsat 7 image (Fig. 4.1) and the Southern Cape DEM (Fig. 4.2).

The Walkerbay dune lineament is also distinct on the Google Earth image (Fig. 4.3A). At ground level a clear elongate topographical depression is bounded by Holocene dunes to the south, and a raised topography to the north (Fig. 4.3B). The dune lineament can be

seen to trend NW to the North Gansbaai area to the SE (Fig. 4.3A), and possesses a length of approximately 15 km. The Walkerbay dune lineament is aligned with, and has a similar orientation to the other Blomerus Lineament segments.

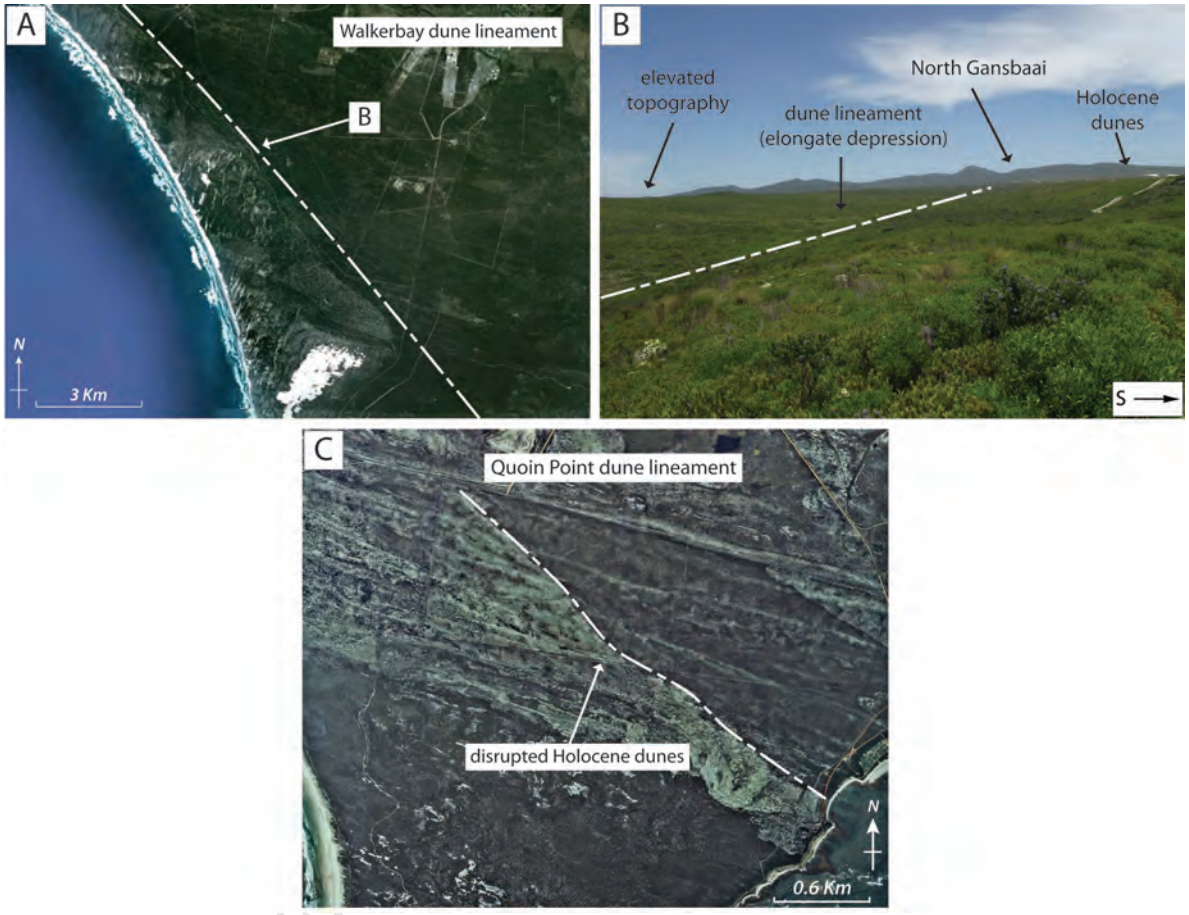

Figure 4.3: Dune lineaments in the Walkerbay and Quoin Point areas (indicated in white). Dune lineament locations are shown on the Landsat 7 image. A) Google Earth image of the Walkerbay dune lineament is shown to disrupt Holocene dunes. The dune lineament is characterised by a linearly arranged depression trending NNW-SSE. B) Photograph (taken facing SE) of the Walkerbay Lineament whilst standing on the edge of linear depression (position shown on the Google Earth image). C) Aerial photograph showing the Quoin Point dune lineament, a linear scarp and depression feature trending NW-SE to NNW-SSE. Aerial photograph courtesy of the Chief Directorate of Mapping and Surveys, South Africa.

The Quoin Point dune lineament is observable on the aerial photograph in (Fig. 4.3C), Holocene transverse dunes are obliquely disrupted by a ∼NW-SE trending elongate depression. The length of the dune lineament is approximately 3.5 km. The Quoin Point dune lineament has the same orientation as, and is aligned with, the Blomerus Lineament (Fig. 4.1).

4.2 Field Observations

4.2.1 Aeolianite Petrology

Outcrops of Bredasdorp Group aeolianites located throughout the Southern Cape study region, have characteristic petrographic features (documented by Malan, 1990) attributed to either the Late Pliocene - Middle Pleistocene Wankoe Formation, or the Upper Pleistocene Waenhuiskrans Formation. The spatial distribution of the Wankoe and Waenhuiskrans Formations has also been suggested by Malan (1989b,a). Therefore, the aeolianites within the different study areas will be investigated to confirm the specific rock units present.

Wankoe Formation

The aeolianites within the North Gansbaai, Heidehof and Groot Hagelkraal farm areas form relatively isolated prominent hills and ridges (sometimes referred to as "koppies") (Fig. 4.4A), typically with ∼150 metres or more height elevations. The hills are located at approximately 40 - 50 metres above present sea level, with the present coastline several kilometres away from the hills. There are no obvious wave-cut cliffs within these aeolianites.

The hills are commonly well vegetated, weathered, and rounded topographical features with cliff exposures on the NE sides of the hills and ridges. Karstified aeolianite and calcrete 'capping' units cover the top surfaces of the hills. Numerous horizons and palaeosol surfaces within the hills exhibit the effect of karstification, and have a similar orientation to the cross-bedding and bounding surfaces (Fig. 4.4B).

Cliff exposures display abundant karstic weathered units, which obliterate the cross-bedding (Fig. 4.4C), in places as karstic dripstone features (Fig. 4.4D). Unkarstified cliff exposures exhibit large-scale tabular cross-bedded, and massive units. The cross bedded units are typically between 1 metre and 10 metres in thickness (Fig. 4.4D). The cross-bedding dip direction is towards the NE-E on average on the eastern sides of the aeolianite units, and towards the SW-W on the western sides.

The aeolianites are characteristically well-consolidated to calcified, with some weathered sections possessing lower levels of cementation. The particles constituting the aeolianite are commonly sand-sized and are of a quartz-rich and calcareous composition. The aeolianite

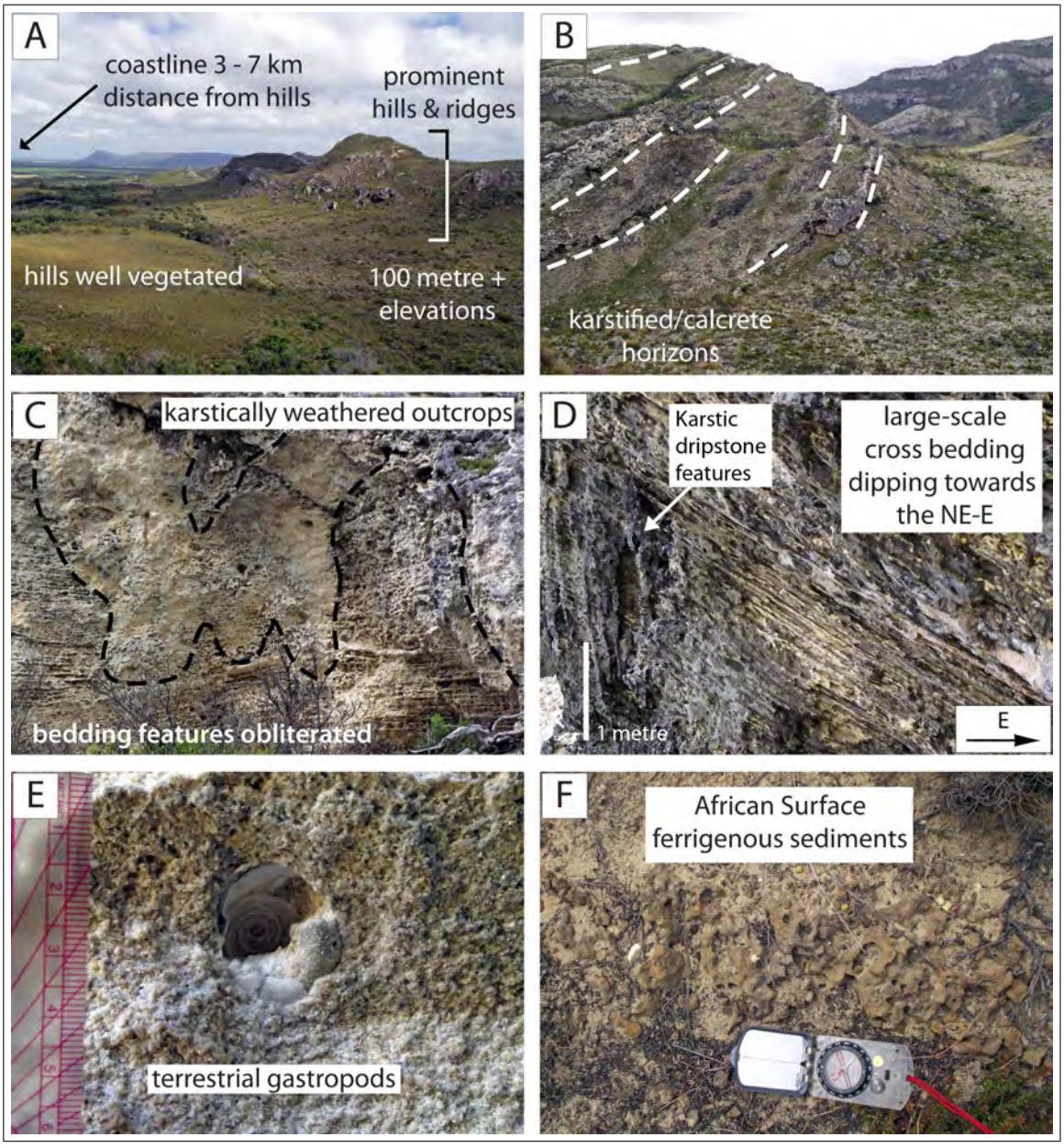

Figure 4.4: Typical macro-scale petrographic features observed in Wankoe Formation outcrops throughout the North Gansbaai, Heidehof, and Groot Hagelkraal farm areas. A) Outcrop position is several kilometres from the present coastline and involves prominent, well vegetated hills. B) Karstification features (internal bedding/palaeosol surfaces) within the rounded outcrops, with predominantly NE-side cliff exposures. C) Weathering features and obliterated sedimentary structures. D) Large-scale cross-bedding dipping towards the NE, and karstic dripstones. E) *In situ* intact terrestrial gastropod shell, distinctive of the Wankoe Formation. F) The aeolianites overlie the African Surface ferrigenious sediments.

units appear grey or yellow to orange, with white calcrete caps or inter-beds. Minor to no biological content can be seen in hand sample, except for isolated terrestrial gastropod shells and fragments (Fig. 4.4E)

Within the study area, these specific aeolianite units unconformably overlie either the African Surface ferrigeneous sediments (as described by Partridge (1998); Partridge and Maud (2000)) or Table Mountain Group sandstone and quartzite units (Fig. 4.4F).

The constituents of the aeolianites involve three main aggregate components: Detrital grains, ooid grains (coated grains), and marine organism skeletal/shell fragments (bioclasts) (Fig. 4.5A & B).

The siliciclastic grains are typically sub-rounded to sub-angular and possess a well-sorted size distribution (Fig. 4.5A). The grain sizes are fine to medium sand, commonly between 0.1mm to 0.5mm. Quartz is the predominant mineral, with relatively minor feldspar and lithic fragments. The grains exhibit minor coating, with grain boundaries in contact with the cement. The detrital material provides a volume percentage of $\sim$20% of the whole aeolianite unit.

The ooid grains (coated grains) exhibit cortices of calcerous minerals (micrite, microspar calcite) surrounding an inner detrital grain nucleus. Most commonly the nuclei of these coated grains are quartz grains. The roundedness of the grains appears to have increased as a result of diagenetic cortex growth (Fig. 4.5A & B) (Adams and MacKenzie, 1998). The size of the nuclei grains are approximately the same as the uncoated siliciclastic grains. The volume percentage of these coated grains in the aeolianite is $\sim$15%. Therefore the overall detritally derived material (detrital grains and superficial ooids) content is $\sim$35%.

The marine organism shell fragments are predominantly constituted by foraminifera skeletal remains or molluscan fragments (gastropod or possible bivalve fragments) (Fig. 4.5E). Typically the bioclasts have a similar roundedness to the siliciclastic material, generally rounded and sub-angular. The size variation between the different bioclasts is within the range of 0.2mm to 1mm, with the molluscan fragments having the larger size distribution on average. The biological content compared to the detrital material and superficial ooid grains is relatively high. The volume percentage of the bioclasts within the aeolianite unit is $\sim$40% on average.

The matrix cementing the detrital grains, superficial ooids, and marine organism frag-

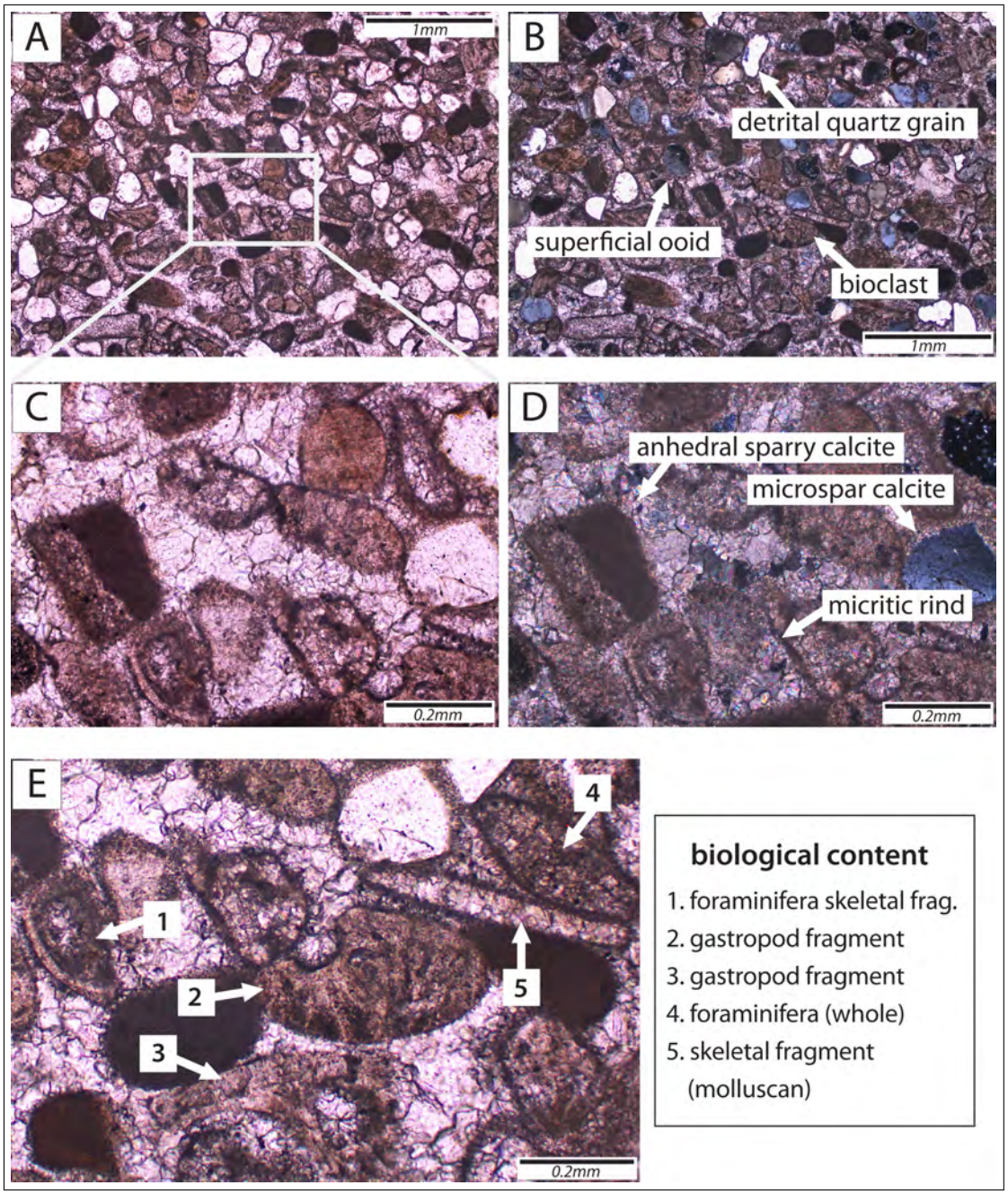

Figure 4.5: Photomicrographs of Wankoe Formation aeolianite, sample taken from an outcrop in the Groot Hagelkraal area. Photographs A, C, and E are in plane-polarised light, with the corresponding cross-polarised light photographs B and D. Typical micro-scale features involve: A and B) A composition made up of detrital grains, superfical ooid grains, and bioclast material; with a well sorted, grain supported texture. C and B) Cement matrix features, involving anhedral sparry calcite, microspar calcite, and minor micrite rinds surround the cemented grains. No significant pore-space is visible. E) Biological content comprised by foraminifera, gastropod, and other unidentifible molluscan skeletal and shell fragments.

ments (Fig. 4.5C & D), is predominantly comprised of anhedral sparry calcite with minor amounts of microspar calcite. The aeolianite in thin section has low amounts of micrite present within the cement, however some micritic rinds coat/surround certain detrital grains. The precipitant cement appears to have infilled the inter-granular pore-spaces completely, with no significant pore-spaces remaining after cementation.

The rock texture is typically grain-supported and well-sorted. The aeolianites are relatively homogeneous (with little to no variation in the clastic and matrix composition between different outcrops and different samples). The presence of sparry calcite and microspar calcite is evidence for neomorphism of the primary micrite cement during diagenesis.

Considering the work already completed by Malan (1989b, 1990) on the Bredasdorp Group (refer to Tab. 3.2), and the observations of this study, the following points can be made: The outcrop position relative to the present coastline suggests at least one marine transgression may have eroded away aeolianites closer to the present coastline since the time of deposition (Fig. 3.5). The high levels of karstification and calcification of the aeolianites, and the sparry calcite cementation (neomorphism) imply that these are relatively old aeolianite units. From the above, the aeolianites in the North Gansbaai, Heidehof Farm and Groot Hagelkraal Farm belong to the Wankoe Formation.

Waenhuiskrans Formation

The aeolianite units within the Bantamsklip, Agulhas, and Waenhuiskrans areas, form elevated hills or mounds, commonly shaped by wave action to form sea cliffs (Fig. 4.6A). The pervasive aeolianite units are typically proximal to the current coast line, with isolated outcrops further inland in low elevation areas. The aeolianites at the coast are not well vegetated, with the inland mound outcrops exhibiting somewhat higher levels of vegetation.

The aeolianite mound or hill outcrops possess height elevations between $\sim$2 metres to $\sim$10 metres (Fig. 4.6B). The maximum thickness of the aeolianite units are found within the Agulhas area, with a thickness up to a 100 metres in places.

Karstic weathering of the aeolianite outcrops is typically limited, with the sea cliffs appearing relatively unweathered (Fig. 4.6C). However, the aeolianite outcrops further inland commonly exhibit more karstic weathering (Fig. 4.6D), with some karstic dripstone features

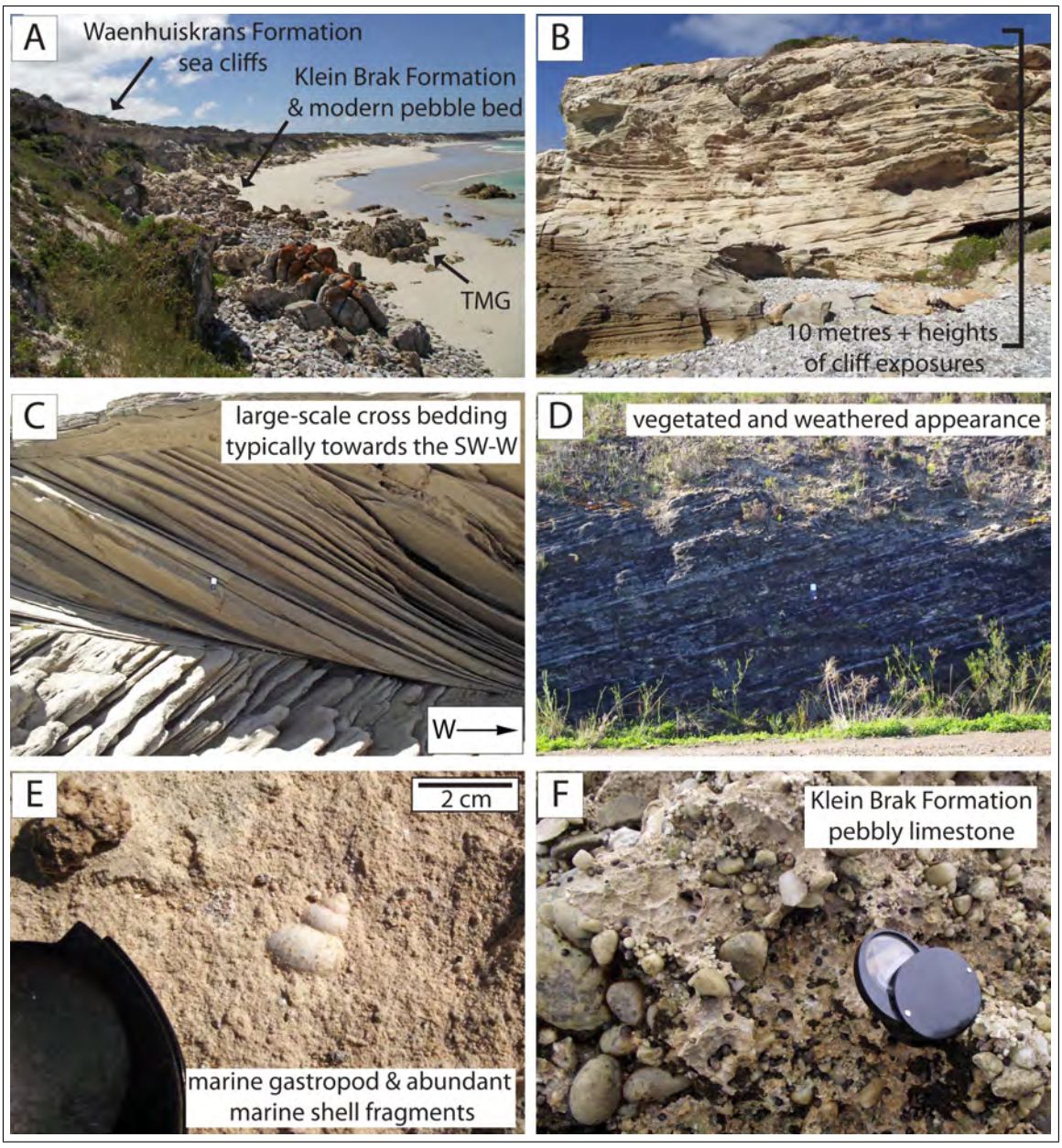

Figure 4.6: Typical macro-scale petrological features of the Waenhuiskrans Formation in the Bantamsklip, Agulhas, and Waenhuikrans areas. A) Outcrops are on or relatively proximal to the present coastline. B) Wave-cut cliffs in the Waenhuiskrans area, with elevation heights $\sim$10 metres or more in places. C) Large-scale cross-bedding dipping towards the SW on average, also exhibiting low levels of karstic weathering. D) Cross-bedded aeolinite exhibiting higher levels of karstic weathering. Outcrop is situated further inland of the coast. E) $In\ situ$ intact marine gastropod shells, distinctive of the Waenhuiskrans Formation. F) Underlying the base of the Waenhuiskrans Formation, the Klein Brak Formation pebbly limestone.

observed. Karstic cap units are commonly seen covering the surfaces of the aeolianites.

In the majority of the aeolianite outcrops the sedimentary cross-bedding features remain relatively intact and not obliterated by karstic weathering. The sedimentary features involve large-scale tabular cross-bedded units within the aeolianites, which predominantly dip towards the SW (Fig. 4.6C). The thickness of the beds containing the cross-bedding are between 1 - 3 metres on average.

The aeolianite units are typically semi-consolidated to well-consolidated, with the well-weathered outcrops exhibiting the lowest levels of consolidation. The composition of the aeolianites are calc-arenitic, with quartz grains and calcereous marine shell fragments being the main constituents. Cemented quartz grains and marine shell fragments are medium to course sand-sized (<2mm), with larger cemented marine gastropod shells (Fig. 4.6E). The weathered aeolianite outcrops appear light-brown or yellow to grey.

Within the study area, the aeolianite units either overlie the Table Mountain Group quartzites and sandstones unconformably, or conformably overlie the Kleinbrak Formation pebbly limestones (previously recognised by Malan, 1990)(Fig. 4.6F).

The aeolianites typically involve two major aggregate components: coated detritial grains, and bioclastic fragments (Fig. 4.7A & B).

The rounded to sub-angular siliciclastic grains are constituted predominantly by quartz grains, with minor feldspar and lithic fragments (Fig. 4.7A & B). The sizes of the siliciclastic material is medium to course sand sized, with diameters commonly between 0.2mm to 0.7mm. The grains are rounded to sub-angular and are relatively well sorted with only minor variations in grains size distribution. The detrital grains exhibit widespread micrite coating (Fig. 4.7C & D), which increases the level of roundness of the grains. The volume percentage of the siliciclastic material is 35% - 40% of the overall aeolianite rock units.

The bioclastic material is constituted by a wide range of marine organisms' shell and/or skeletal fragments (Fig. 4.7E). The fragments derive predominantly from foraminifera, mollusc, and echinoderm species. The degree of fragmentation is greatest in the larger gastropod and bivalve bioclasts (molluscan). The fragments are rounded to sub-angular in shape on average. The typical diameter size distribution is between 0.2mm and 1mm (with some shell fragments up to $\sim$2mm in diameter), a relatively moderate level of size sorting of the material. The bioclastic fragments are coated with micrite, the same as the detrital grains

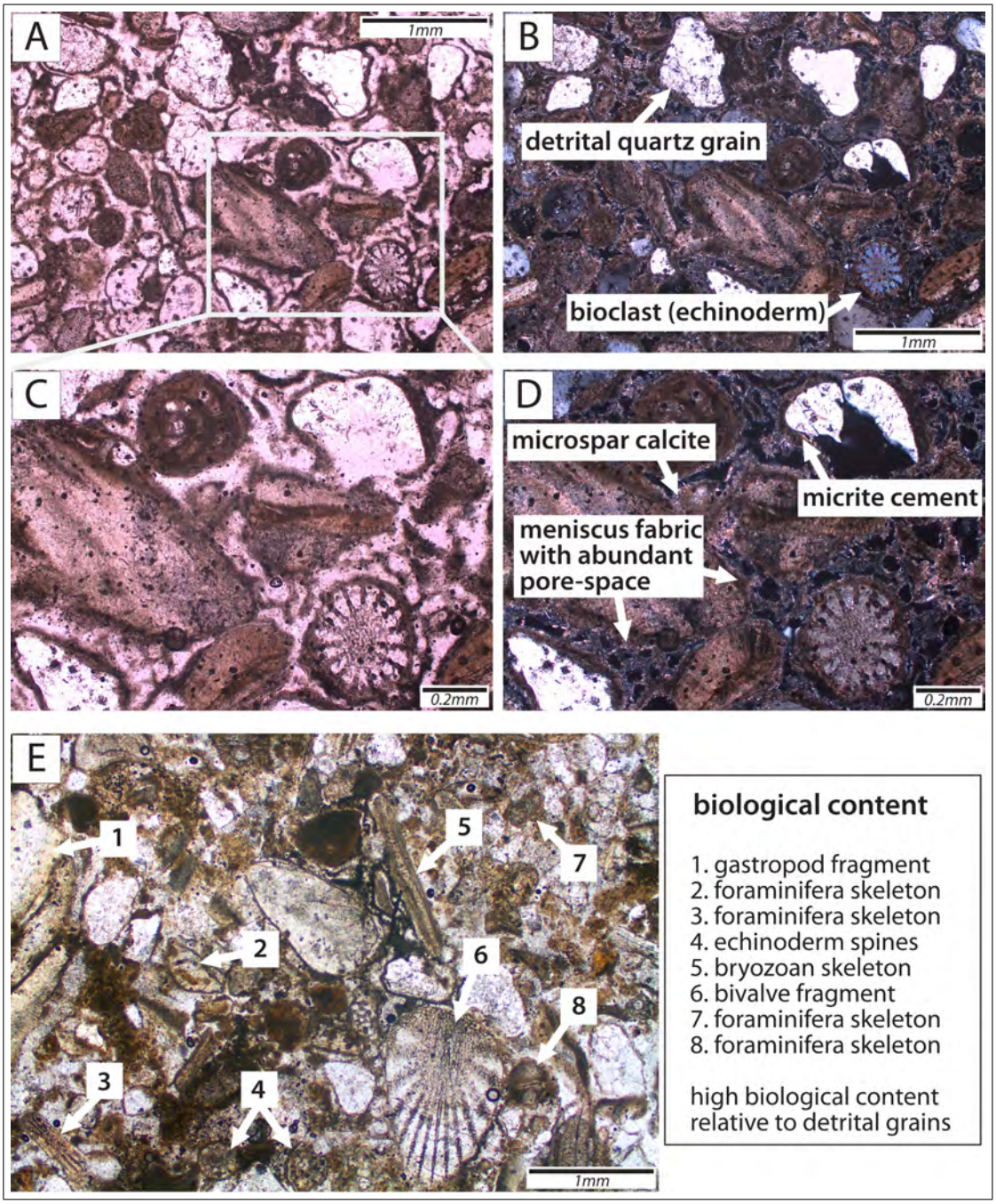

Figure 4.7: Photomicrographs of Waenhuiskrans Formation aeolianite. Sample taken from the Bantamsklip study area. Photographs A, C, and E are taken in plane-polarised light, photographs B and D are the corresponding cross-polarised light images. A) & B) The two main clastic components making up the aeolianites: detrital grains exhibiting micrite coating, and bioclastic material also exhibiting micritic coating. C) & D) Cement is predominantly micrite with minor microspar calcite. Cement is located on the grain boundary contacts, with abundant rounded pore-spaces. E) Biological content, mostly foraminifera, molluscan, and echinoderms (also view in C & D). Shell and skeletal fragments constitute a high volume percentage of the whole aeolianite unit.

(Fig. 4.7C & D). The aeolianites exhibit a relatively high biological content relative to detrital material, with >50% of the overall rock being shell/skeletal fragments.

The cementing matrix is constituted almost entirely by clay sized (<5μm) micrite ($\sim$95%), with minor amounts of microspar calcite (Fig. 4.7C & D). The cement is predominantly distributed at the grain-boundary contacts of the detrital grains and bioclastic material, forming meniscus-type rounded pore-spaces. The cement (and significant pore space) has a volume percentage of $\sim$5% - 10% of the aeolianites.

The overall rock texture is grain-supported and well-sorted. The aeolianite is relatively homogeneous (the rock composition does not vary significantly between different outcrops and different samples). The lack of neomorphism is evident through the high micrite content of the cement (no sparry calcite is observed in thinsection from any of the aeolianites sampled), providing evidence for only minor levels of diagenesis.

Considering the work already completed by Malan (1989a, 1990) on the Bredasdorp Group (refer to Tab. 3.2) and the observations of this study the following can be said: The lower average level of consolidation and karstification of the aeolianites, the volume content of bioclastic material, the lack of neomorphism, all suggest a younger aeolianite deposit. The outcrop position of the aeolianites relative to the present coastline implies a lower sea level at time of deposition (Fig. 3.5) compared to the Wankoe Formation. These characteristics suggest that the aeolianites observed in the Bantamsklip, Agulhas, and Waenhuiskrans areas belong to the Waenhuiskrans Formation rather than the Wankoe Formation.

4.2.2 Geological Maps and Cross Sections

The regional geology of the Southern Cape (Fig. 4.8), is described in Chapter 3 (sections 3.3-3.7), and was initially geologically mapped by Andreoli *et al.* (1988). Further spatial distribution and petrological characteristics of the Bredasdorp Group aeolianites, and details on observed geological structures (faults) collected during the field investigation and remote sensing, have been added to the original geological map of the Southern Cape.

The geological maps for the North Gansbaai (Fig. 4.9), Heidehof Farm (Fig. 4.10), Groot Hagelkraal Farm (Fig. 4.11), and Bantamsklip (Fig. 4.13) cover the areas traversed by the Blomerus Lineament (Fig. 4.1 & Fig. 4.2). The postulated Blomerus Fault (Andersen and Andreoli, 1990) is suggested to extend approximately along the same trace. The Blomerus Lineament and the Walkerbay and Quoin Point dune lineaments can thus be assumed to indicate the inferred surface trace of the Blomerus Fault. As such, the Blomerus fault is implied to trace ∼NW-SE (in a possibly segmented manner) from the Walkerbay area through to the Quoin Point area (Fig. 4.8). The length of the Blomerus Fault is considered to be at most ∼50 km in length (on land), but could potentially extend offshore from Quoin Point.

The Agulhas geological map (Fig. 4.14) covers the area in which the Brandfontein and Struisbaai lineaments are mapped (Fig. 4.1 & Fig. 4.2). The Brandfontein and Struisbaai faults were originally mapped with the use of aeromagnetic surveys (Andersen and Andreoli, 1990) and are in approximately the same orientations and positions as the mapped lineaments. As such, the lineaments can be considered to indicate the respective fault surface traces. The Brandfontein Fault has an arcuate trend roughly WNW-ESE to E-W from Brandfontein to the north of Struisbaai. The Struisbaai Fault possesses a similar trend across the Agulhas headland. Both the Brandfontein and the Struisbaai Faults potentially continue offshore, as suggested by Andersen and Andreoli (1990).

The North Gansbaai (Fig. 4.9), Heidehof (Fig. 4.10) and Groot Hagelkraal Farm (Fig. 4.11) geological maps reveal Wankoe Formation aeolianites overlying the inferred trace of the Blomerus Fault. The typical outcrop pattern for the Wankoe Formation is most distinct on the Heidehof and Groot Hagelkraal Farm maps; with isolated rounded hills on the SW-side of the Blomerus Fault trace, and larger more laterally extensive ridges on the NE-side of the Fault trace. The smaller hills are separated from the larger ridges by NW-SE trending

linear valleys approximately aligned to the Blomerus Fault trace, this topography can also be viewed on the geological cross sections (Fig. 4.12).

The cross sections in Fig. 4.12, show the Blomerus Fault exhibiting a SW dip of $\sim 60^\circ$ (the fault orientation has been inferred from large-scale listric normal faults in the Bredasdorp Basin (Paton, 2006)). The down-thrown block is on the SW-side, with the footwall on the NE-side having negligible vertical displacement in comparison. Multiple NE-dipping antithetic normal faults are inferred (Fig. 4.12) off of the main Blomerus Fault, defining a fault zone (breccia and gouge units delineating the fault zone on surface). The downward slip displacement of the Blomerus Fault is inferred to be significant (several metres at least) towards the SW, with similar displacements on the antithetic faults towards the NE. This displacement is estimated from the space required to accommodate the rotation of the overlying Wankoe Formation units (between $\sim 20^\circ$ - $\sim 40^\circ$). The rotation is estimated from the cross-bedding dip angles.

In both the geological maps (Fig. 4.10 & Fig. 4.11) and the geological cross sections (Fig. 4.12), the typical dip directions of the cross-bedding within the Wankoe Formation aeolianites is towards the NW-W-SW on the SW-side of the Blomerus Fault trace, and towards the NE-E-SE on the NE-side. The cross-bedding in the aeolianites on the SW-side possess a steeper dip relative to the aeolianites on the NE-side (refer to section 4.2.4).

The Wankoe Formation in the North Gansbaai (Fig. 4.9), Heidehof (Fig. 4.10), Groot Hagelkraal Farm (Fig. 4.11) areas have been, in places, mechanically and chemically weathered and eroded into surficial deposits (reworked deposits). These surficial deposits are commonly semi-consolidated to unconsolidated. Distinct alluvial terrace deposits define two topographical terrace levels, the higher is typically on the NE-side, and the lower on the SW-side of the mapped areas.

The Bantamsklip (Fig. 4.13), Agulhas (Fig. 4.14), and Waenhuiskrans (Fig. 4.16) geological maps predominantly involve the Waenhuiskrans Formation aeolianites. These deposits overlie the Blomerus Fault in the Bantamsklip area, and the Brandfontein and Struisbaai faults in the Agulhas area. The aeolianites are shown to outcrop proximally to the coast line, and are commonly overlain by active Holocene dunes. The outcrop pattern is areally extensive low-lying hill and mound-shaped outcrops (refer to section 4.2.1).

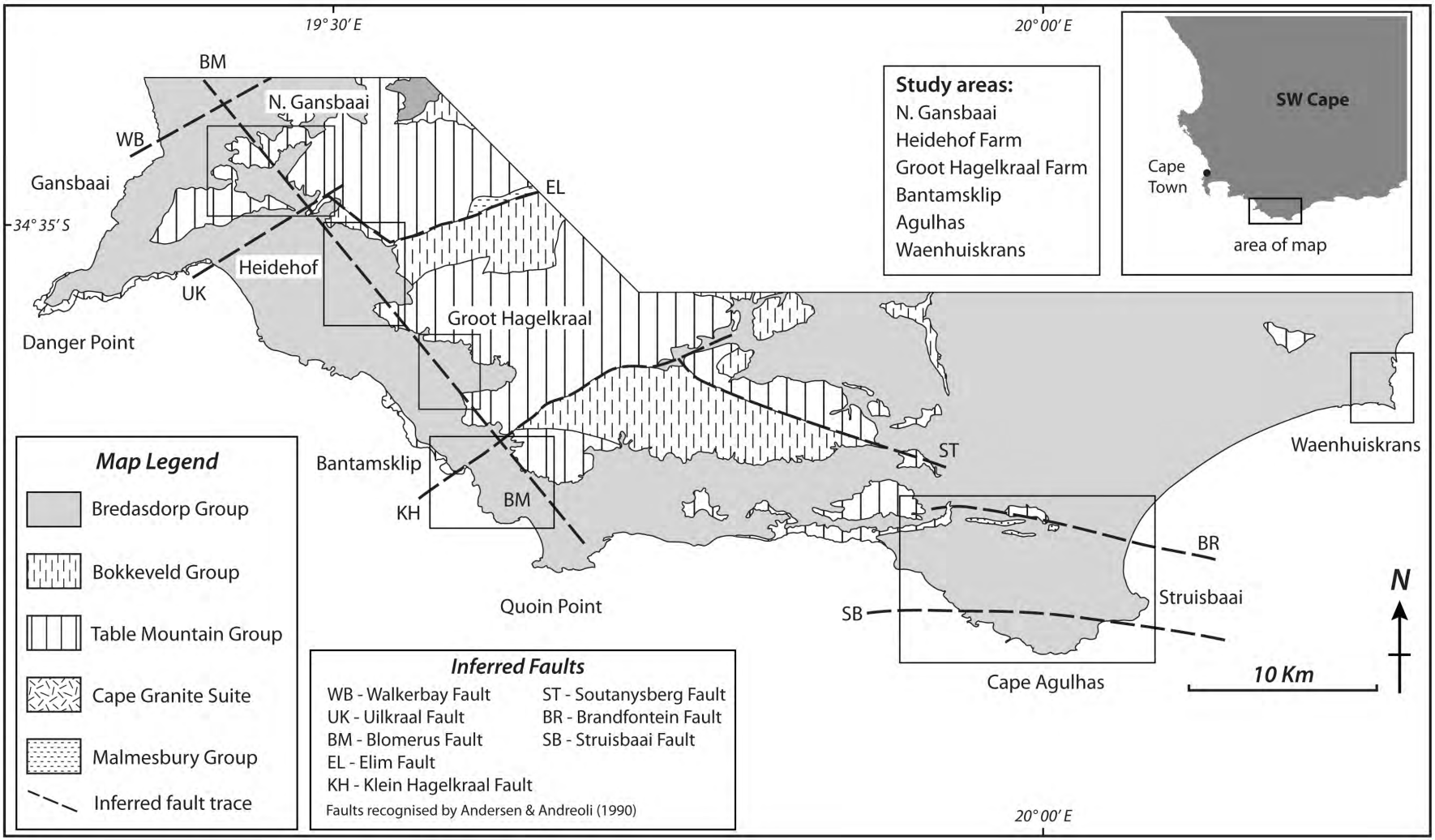

Figure 4.8: Overview geological map of the Southern Cape. Region originally mapped by Andreoli *et al.* (1988), with additions from remote sensing and field observations. The locations of the study areas and smaller-scale geological maps are indicated. Positions of faults previously recognised by Andersen and Andreoli (1990) are inferred. The Blomerus, Brandfontein, and Struisbaai faults are mapped from the orientation and length of the corresponding lineament.

The cross-bedding in the Waenhuiskrans Formation aeolianites is consistent in all the mapped areas, with dip direction towards the SW on average. The presence of the underlying Brandfontein and the Struisbaai faults in the Agulhas area does not appear to affect the cross-bedding orientation in the overlying aeolianites (Fig. 4.14).

The geological cross section for the Agulhas study area (Fig. 4.15) illustrates the Waenhuiskrans Formation overlying the inferred traces of the Struisbaai and Brandfontein faults. The orientation of the faults is provided by similar faults surveyed offshore in the Bredasdorp Basin (Paton, 2006). The faults dip towards the south with $\sim 60^\circ$ dip angles.

The Waenhuiskrans Formation is typically semi-consolidated in the Bantamsklip area, with more consolidated outcrops located in the Agulhas and Waenhuiskrans areas. However, in all the study areas, abundant mechanical and chemical weathering and erosion of the Waenhuiskrans Formation aeolianites have resulted in overlying unconsolidated surficial deposits.

Enon Formation ferrigenous conglomerates and silcretes (silicified conglomerate) (Fig. 4.23A) known to date to the Late Jurassic - Early Cretaceous Gondwana break-up (Dingle, 1973) are observed in the northern parts of the Agulhas field area, NE of the Brandfontein Fault (Fig. 4.14).

The Enon Formation units crop out to the south of the inferred trace of the Brandfontein Fault with an outcrop trend approximately E-W, parallel to the Brandfontein Fault. The geological cross section of the Agulhas study area (Fig. 4.15) includes the inferred position of the Enon Formation relative to the Brandfontein and Struisbaai faults in basins formed from half-graben development. The down-thrown hangingwall of the faults is thus suggested to be on the southern side of the faults.

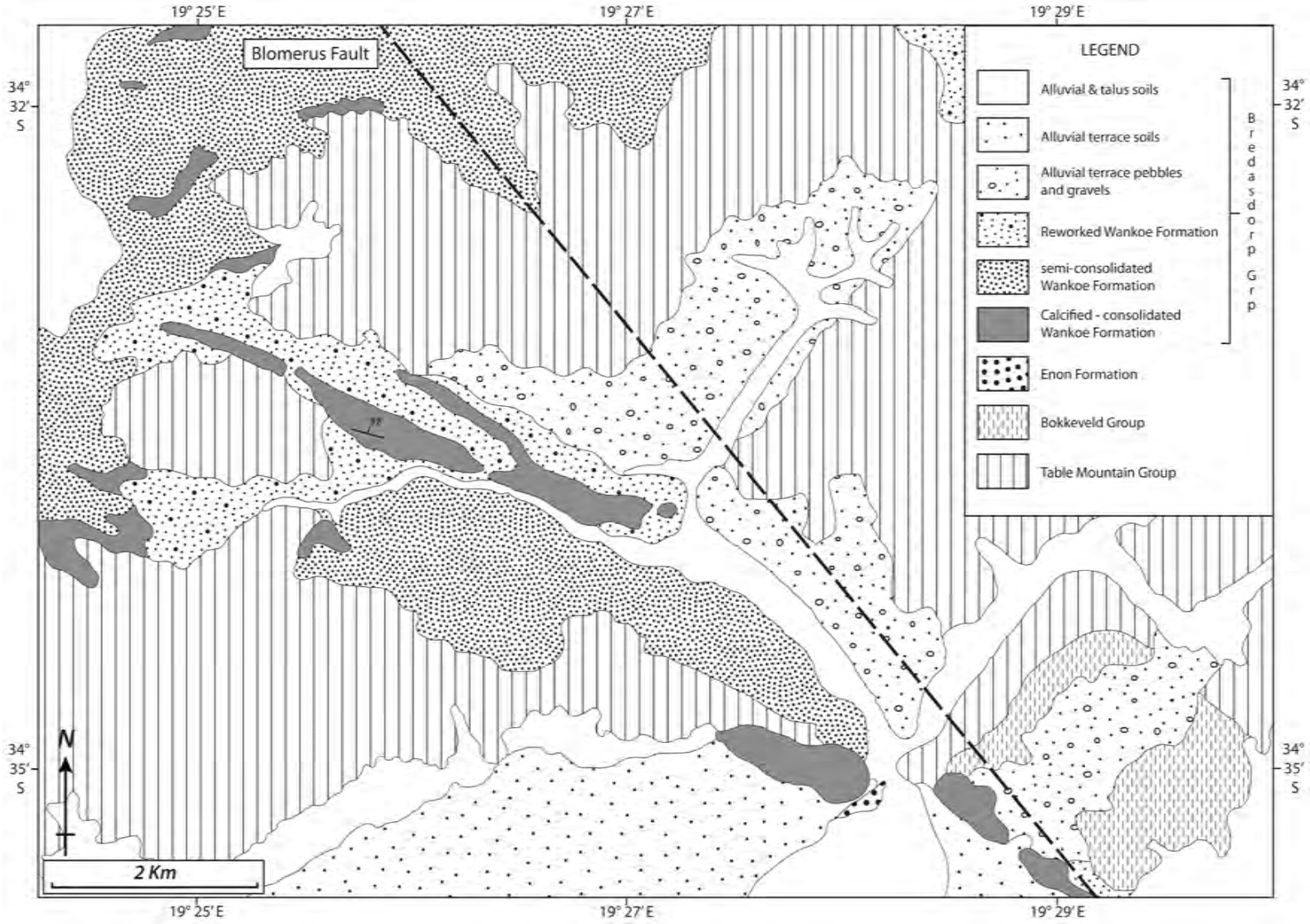

Figure 4.9: Geological map of the North Gansbaai study area. Area originally mapped by Andreoli *et al.* (1988), with additions from remote sensing and field observations. The inferred trace of the Blomerus Fault is seen to traverse the mapped area. Strike/dip symbols represent cross-bedding orientations.

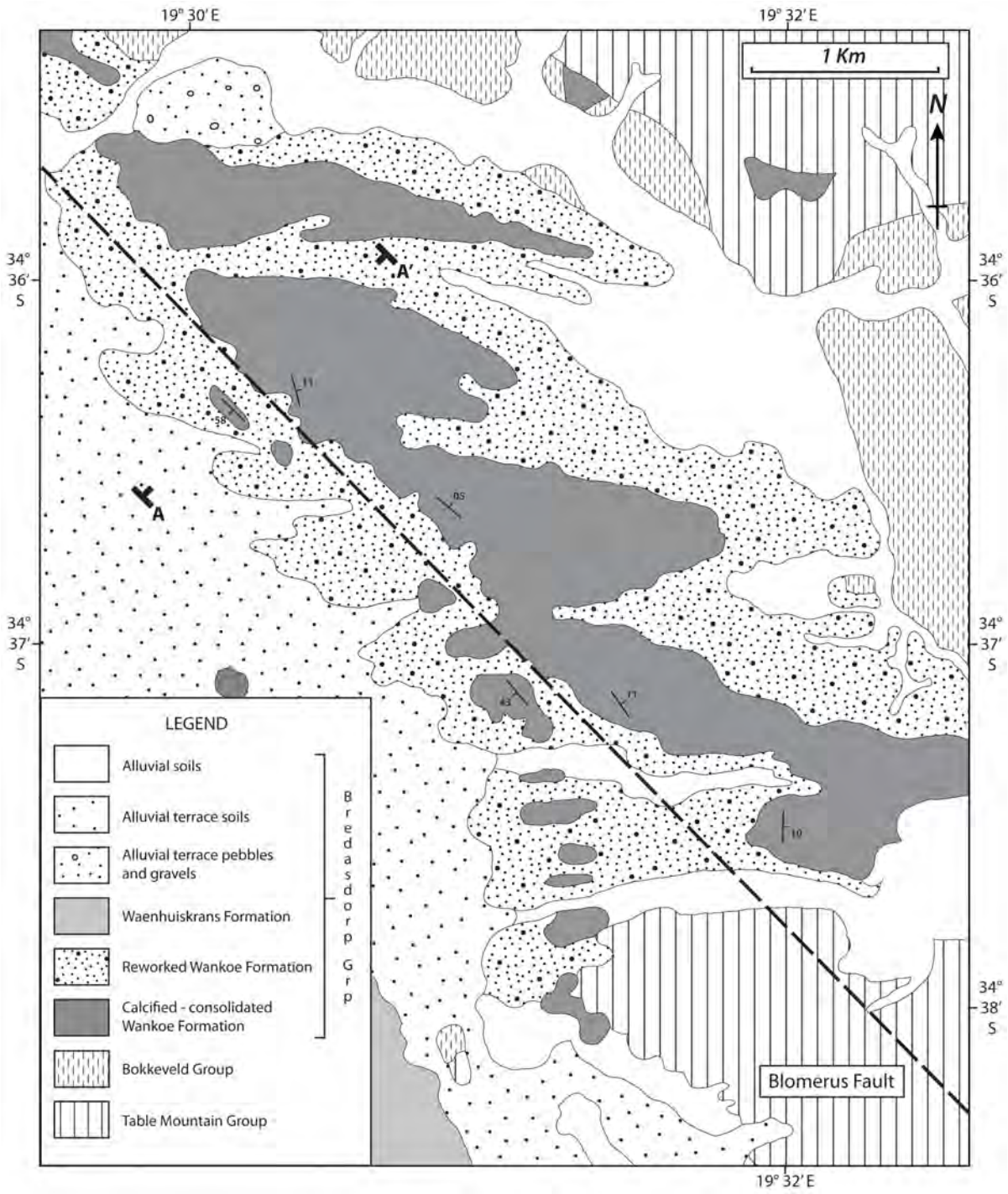

Figure 4.10: Geological map of Heidehof Farm study area. Area originally mapped by Andreoli *et al.* (1988), with additions from remote sensing and field observations. The inferred trace of the Blomerus Fault is seen to traverse the mapped area. Strike/dip symbols represent cross-bedding orientations. The cross section A - A' trace is indicated on the map.

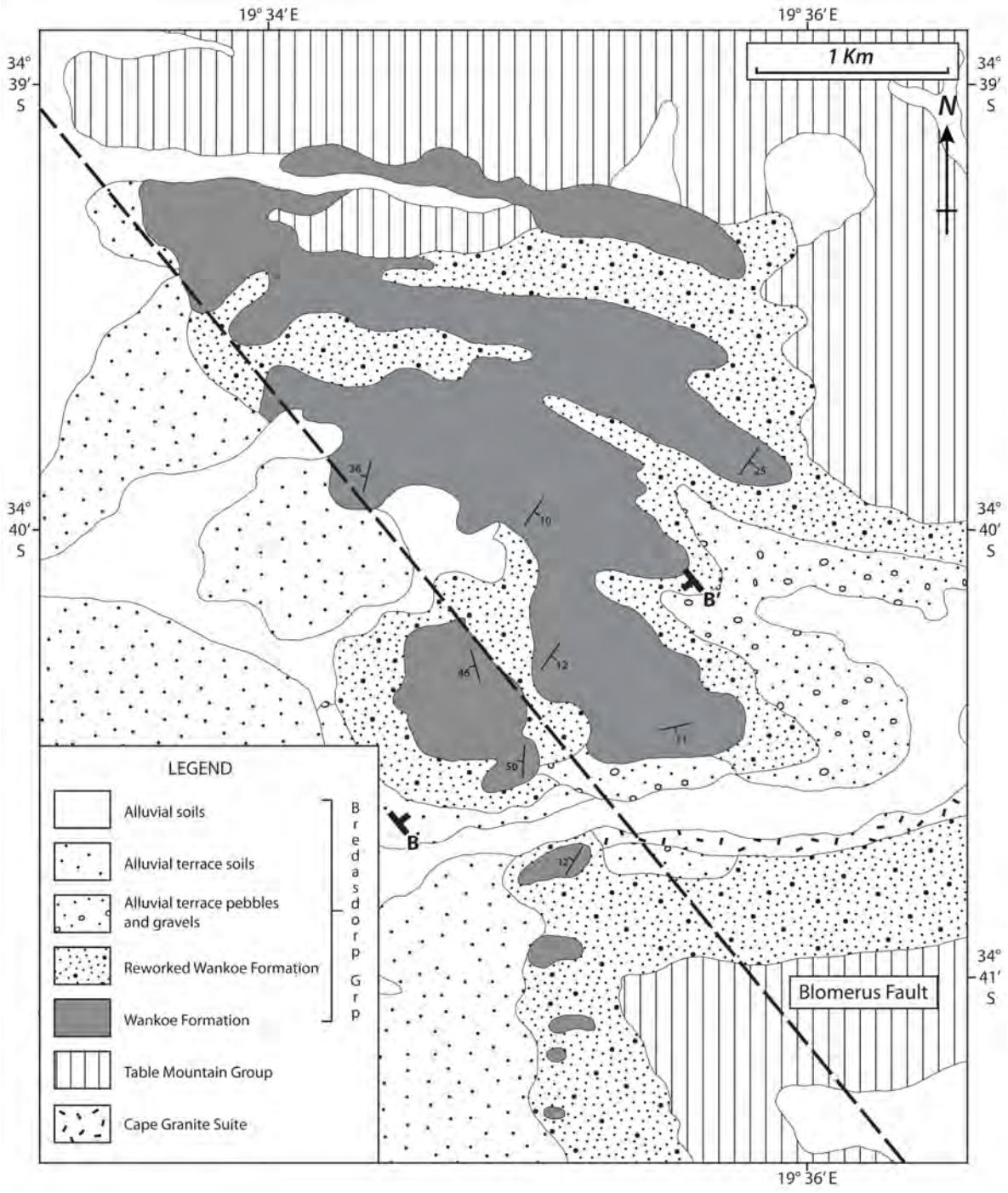

Figure 4.11: Geological map of Groot Hagelkraal Farm study area. Area originally mapped by Andreoli *et al.* (1988), with additions from remote sensing and field observations. The inferred trace of the Blomerus Fault is seen to traverse the mapped area. Strike/dip symbols represent cross-bedding orientations. The cross section B - B' trace is indicated on the map.

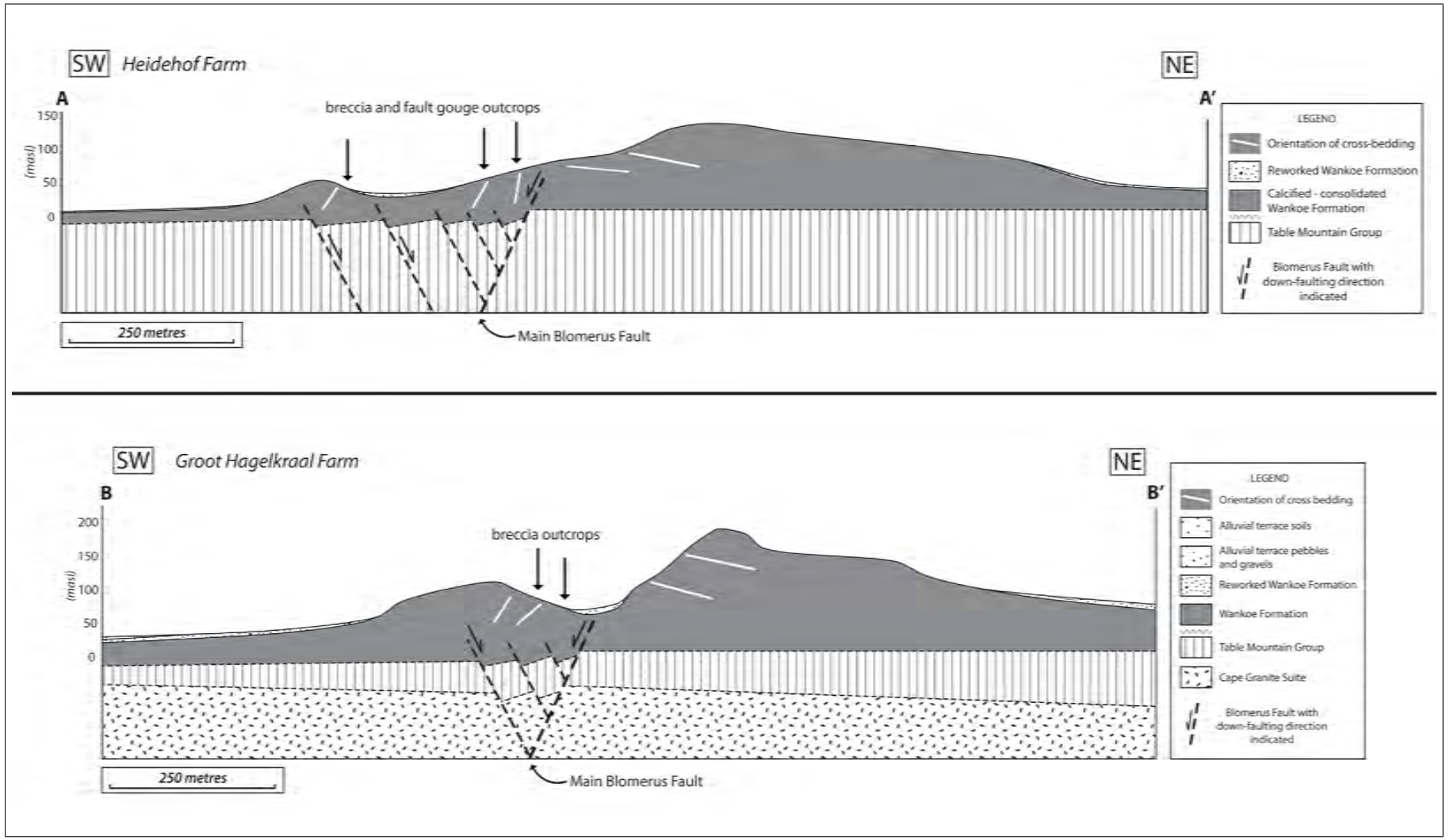

Figure 4.12: Geological cross sections of the Heidehof farm and Groot Hagelkraal Farm study areas. Breccia and fault gouge outcrops and variations in cross-bedding orientations are indicated. Vertical exaggeration is 1x. A) Cross section trace between A - A', as indicated on the Heidehof Farm geological map. B) Cross section trace between B - B', as indicated on the Groot Hagelkraal geological map.

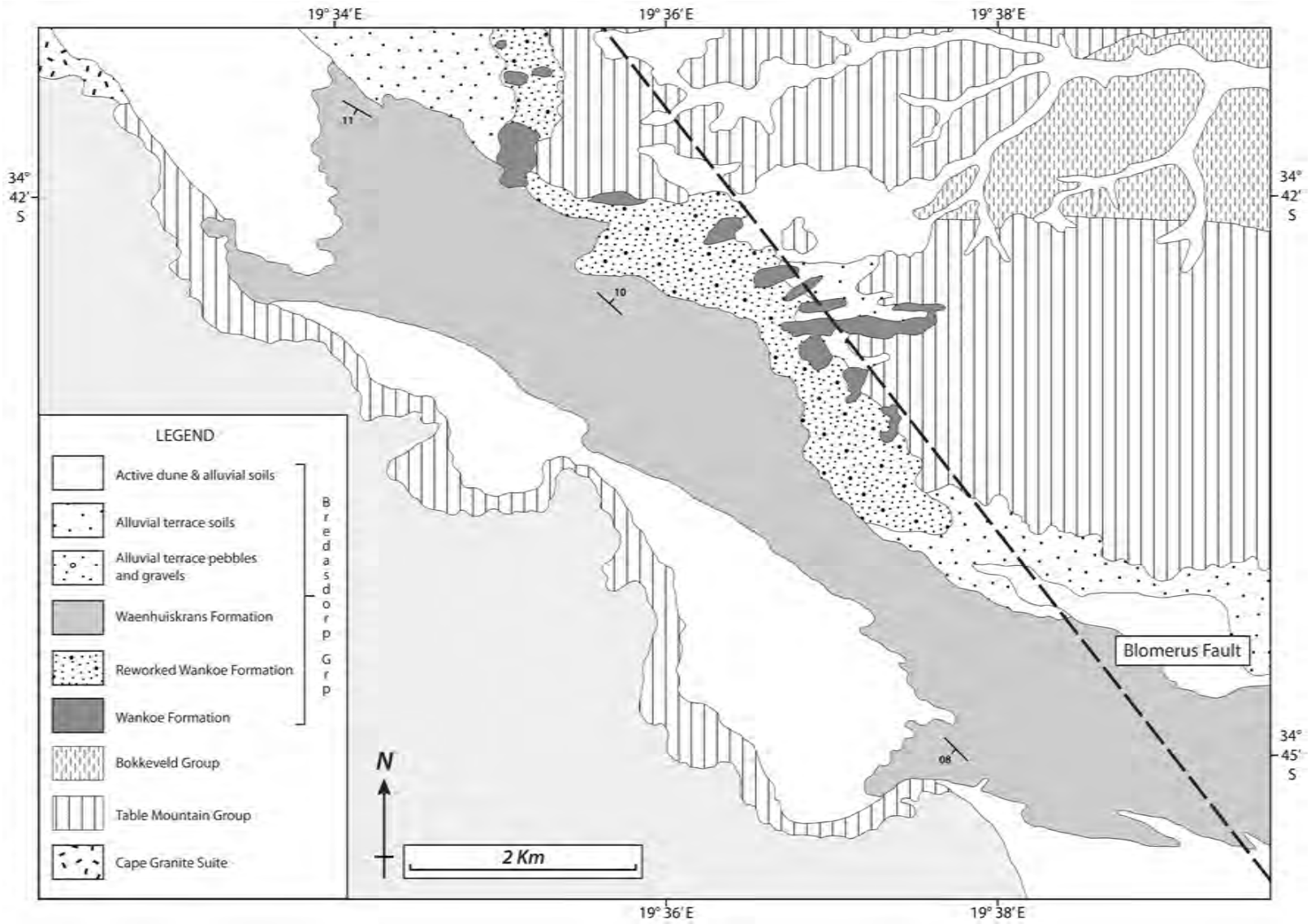

Figure 4.13: Geological map of the Bantamsklip study area. Area originally mapped by Andreoli *et al.* (1988), with additions from remote sensing and field observations. The inferred trace of the Blomerus Fault is seen to traverse the mapped area. Strike/dip symbols represent cross-bedding orientations.

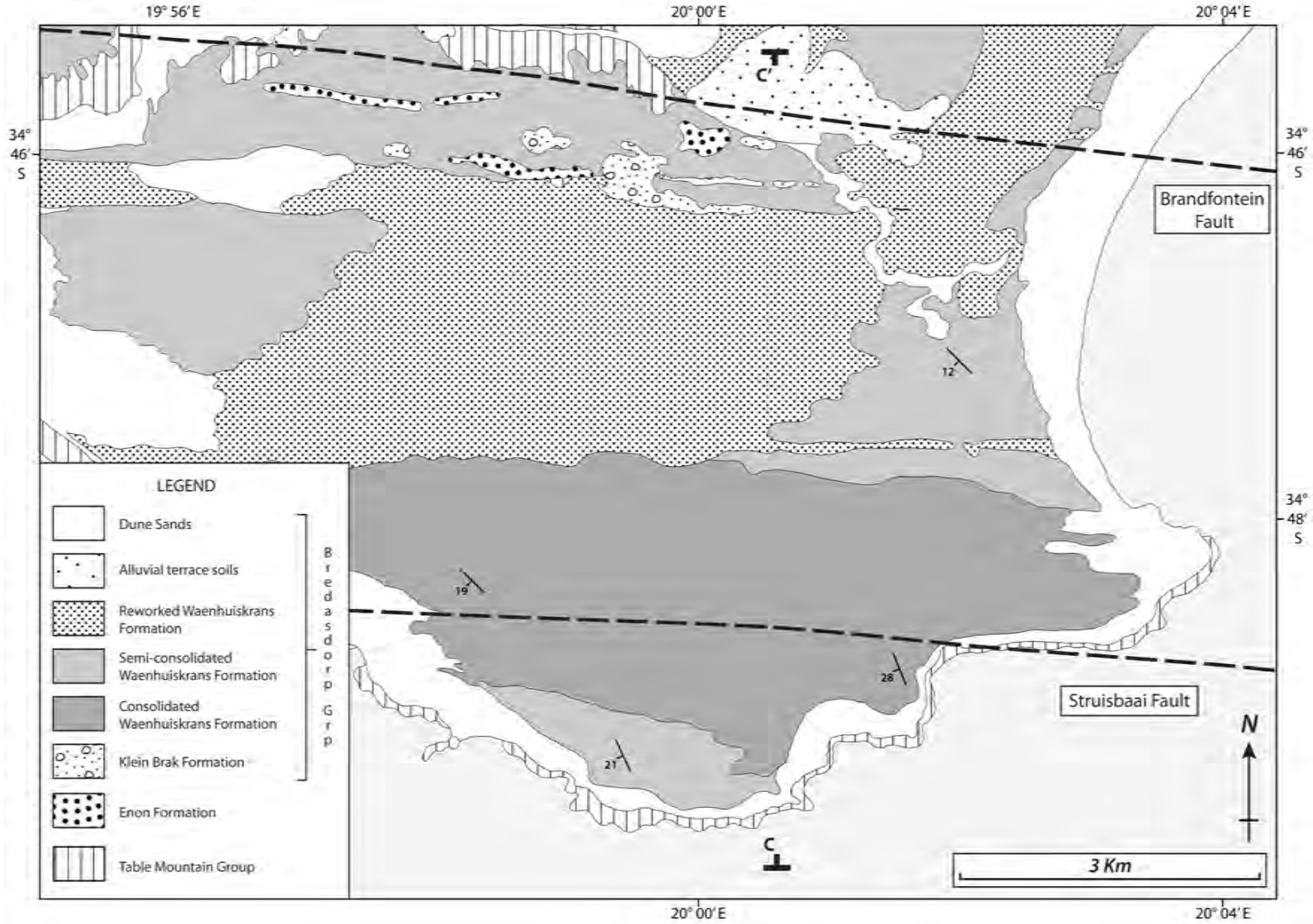

Figure 4.14: Geological map of the Agulhas study area. Area originally mapped by Andreoli *et al.* (1988), with additions from remote sensing and field observations. Strike/dip symbols represent cross-bedding orientations. The inferred traces of the Brandfontein and Struisbaai faults are seen to traverse the mapped area. Outcrops of Enon Formation observed south of the Brandfontein Fault. Cross section traced between C - C'.

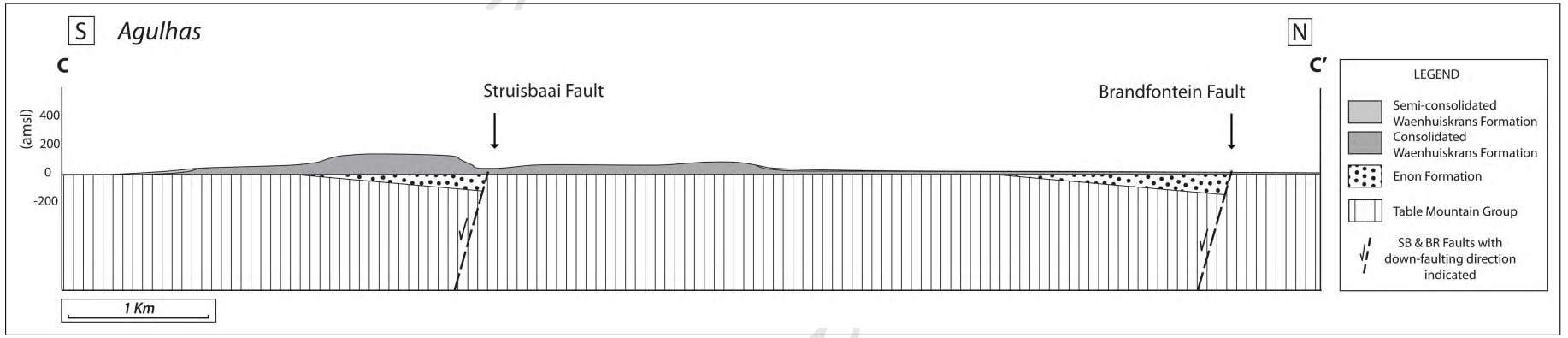

Figure 4.15: Geological cross sections of the Agulhas study area. The locations, within the Waenhuiskrans Formation aeolianites, of the Struisbaai and Brandfontein faults are indicated. Vertical exaggeration is 1x. Cross section is traced between C - C', as indicated on the Agulhas geological map. The presence of Enon Formation as normal fault basin fill is particularly notable. Cross-bedding orientations are indicated on the geological map.

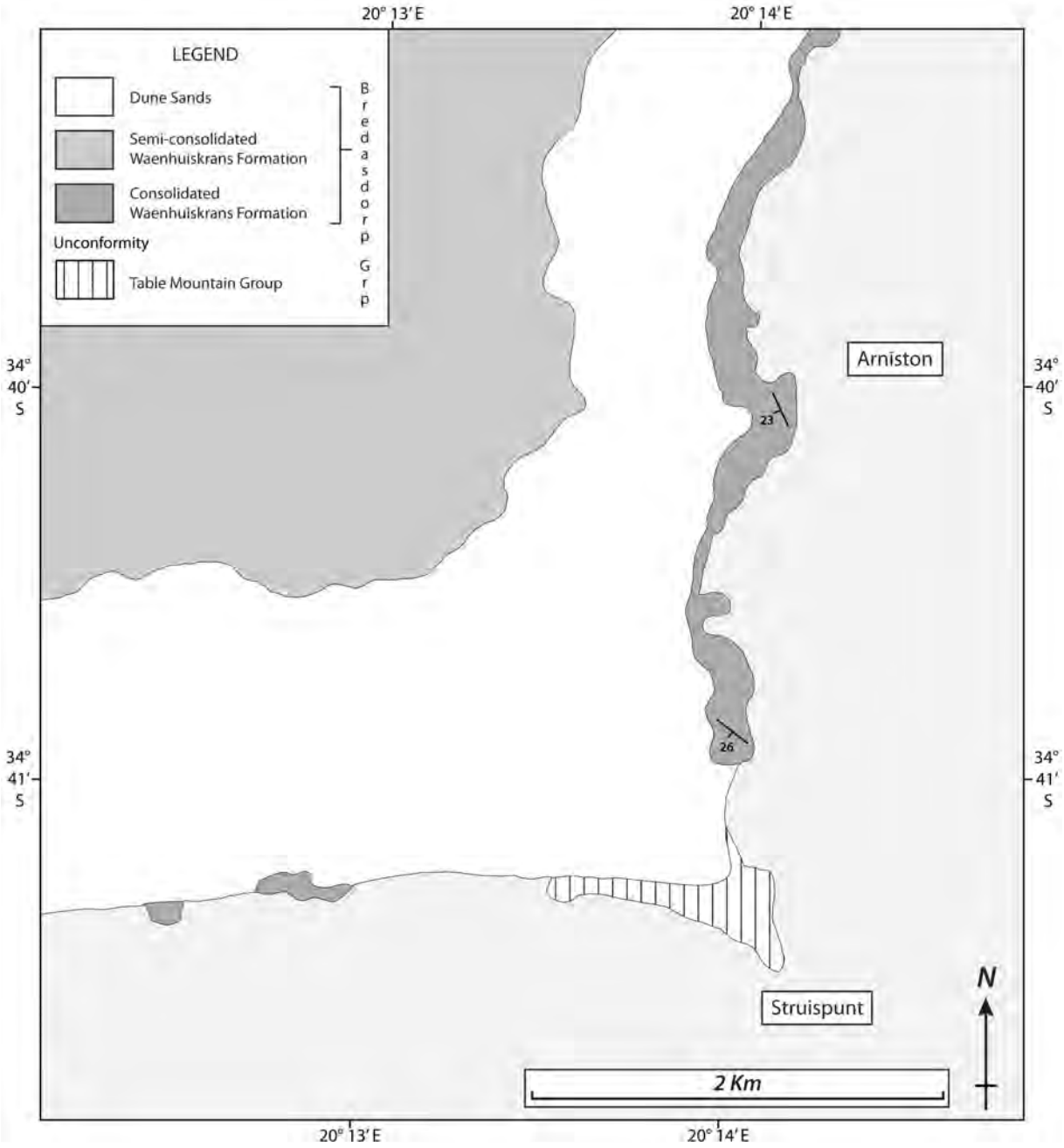

Figure 4.16: Geological map of the Waenhuiskrans study area. Area originally mapped by Andreoli *et al.* (1988), with additions from field observations. This is the type locality of the Waenhuiskrans Formation, as described by Malan (1989a). Strike/dip symbols represent cross-bedding orientations.

4.2.3 Joints and Faults

The most abundant brittle deformation features found within the Southern Cape region, in both the Late Pliocene to Lower Pleistocene Wankoe Formation, and the Upper Pleistocene Waenhuiskrans Formation aeolianites, are pervasive joints. Faults on the other hand are relatively rare in comparison. The characteristics and orientation trends of both these deformation features will be outlined through the following sections.

Joint Characteristics

Joints are approximately planar discontinuities which cut through intact aeolianite units, with no appreciable shear displacement across or along the fracture plane (refer to section 2.1). The joints dip steeply at angles ranging from 60 ° to 90 °, with an average dip angle of ∼75 ° (Fig. 4.19). The joints in the aeolianites are predominantly metre long features. However, in specific locations throughout the Southern Cape, joints have variable lengths from several centimetres (Fig. 4.17B), to tens of metres (Fig. 4.23D).

The joints are open fractures or in-filled with secondary calcite precipitate. The joints fracture through bedded aeolianites, and can become obliterated by karstification of the upper sections of aeolianite outcrops. The bedding features (cross-bedding and bedding planes) are predominantly cross cut by the joints. The veins commonly form positive erosive features in outcrop, while open fractures form negative erosive features.

Joints are parallel to sub-parallel to one another, constituting distinctive joint sets (defined as J_0, J, J'). The aeolianites display either a single joint set or multiple joint sets (Fig. 4.17). Distinctive joint sets observed at a single aeolianite outcrop do not necessarily continue without change to adjacent outcrops (some local variation in joint systems). Joint set nomenclature is therefore outcrop-based and should not be applied to whole areas or regionally.

The Wankoe Formation aeolianites exhibit two distinct joint sets (J & J'), although in places three joint sets are also seen, typically as an orthogonal joint set to the dominant J (at Heidehof Farm). Similarly, the Waenhuiskrans Formation aeolianites commonly exhibit two joint sets (J & J') and less commonly three joint sets (J_0, J & J').

A typical example of a two joint set system (J & J') in the Wankoe Formation aeolianites

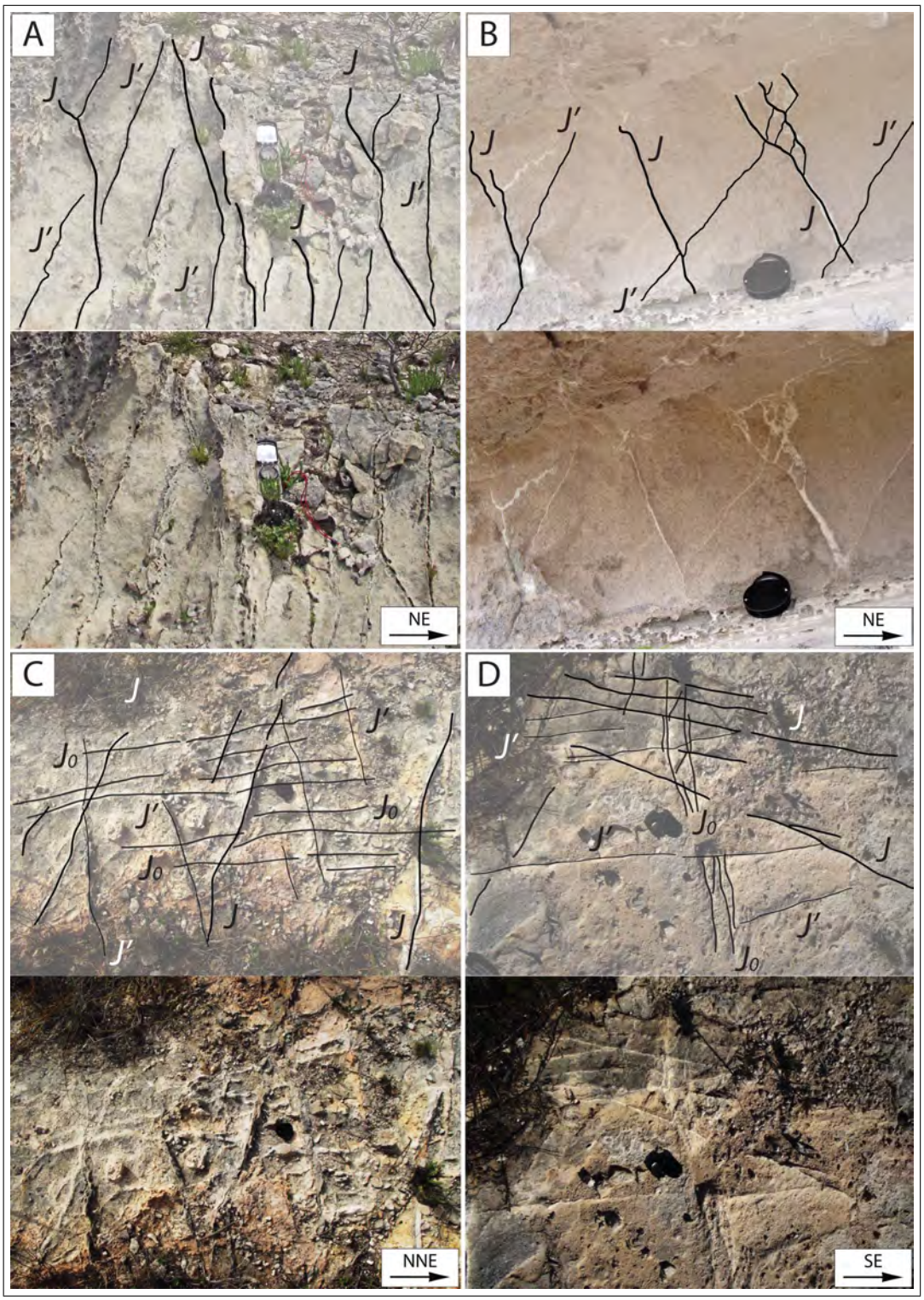

Figure 4.17: Joint systems observed in the Southern Cape. Vertical cliff exposures exhibiting: A) Intersecting joint sets (J, and J') within Wankoe Formation aeolianite. B) Intersecting joints (J, and J') in Wankoe Formation aeolianites. Horizontal surface exposures exhibiting: C) Three sets of steeply dipping joint veins, J_0, J, and J' cross-cut Waenhuiskrans Formation aeolianite. J_0 is cross-cut by coeval J, and J'. D) A similar joint pattern as seen in (C), at a proximal outcrop. (A), (B), (C) and (D) show J as the dominant joint set, with J' terminating and abutting up against J. See text for more details. Geological compass and hand lens for scale.

(Fig. 4.17A & B), involve two joint sets mutually cross cutting or abutting against each other. In most examples, J is typically the dominant joint set with J' abutting up against J (also seen in the Waenhuiskrans Formation). An example of a three joint set system (J_0, J, and J') in the Waenhuiskrans Formation aeolianites (Fig. 4.17C & D), involve joints cross-cutting each other (J_0 is cross-cut by J & J') and abuttment (J and J' only, with J' commonly terminating at the point of intersection with J).

The 'joint sets' which mutually cross-cut and intersect to form low acute angles ($\sim 30\,^\circ$ or less), such as those seen in Fig. 4.18 B (Waenhiskrans Formation) and Fig. 4.18C (Wankoe Formation), can be considered possible hybrid fractures (refer to section 2.1). The fractures firstly appear coeval, with neither of the fractures offsetting the other, and the cross-bedding has no visible offset across the fractures. Typically the possible hybrid fractures possess an acute intersection angle with an orientated sub-vertical bisector, and a sub-horizontal obtuse bisector.

The joints within the Wankoe Formation, in the Heidehof and Groot Hagelkraal areas, are predominantly within the tilted aeolianites or towards the SW of the inferred Blomerus Fault, with significantly less in adjacent untilted aeolianite units. In the North Gansbaai area, Wankoe Formation aeolianites exhibit lower abundance of joints but a similar level of systematic joint expression relative to the Heidehof and Groot Hagelkraal areas. The joints in the Waenhuiskrans Formation are most abundant in the aeolianites in the Bantamsklip area with slightly less in the Agulhas area. Relative to the Bantamsklip and Agulhas areas, the Waenhuiskrans area possesses the least amount of joints. All the Waenhuiskrans Formation aeolianites exhibit similar systematic joint patterns.

Fault Characteristics

Faults within the Wanhuiskrans Formation and Wankoe Formation aeolianites are less abundant than joints. The lengths of the faults are typically on the metre-scale to tens of metres-scale range depending on the location and fault pattern (e.g. conjugate faults are shorter (in terms of lengths) than single normal faults on average). The faults all cross-cut the sedimentary structures and cross-bedding features of the respective aeolianite units (Fig. 4.18A, Fig. 4.23C, Fig. 4.24C).

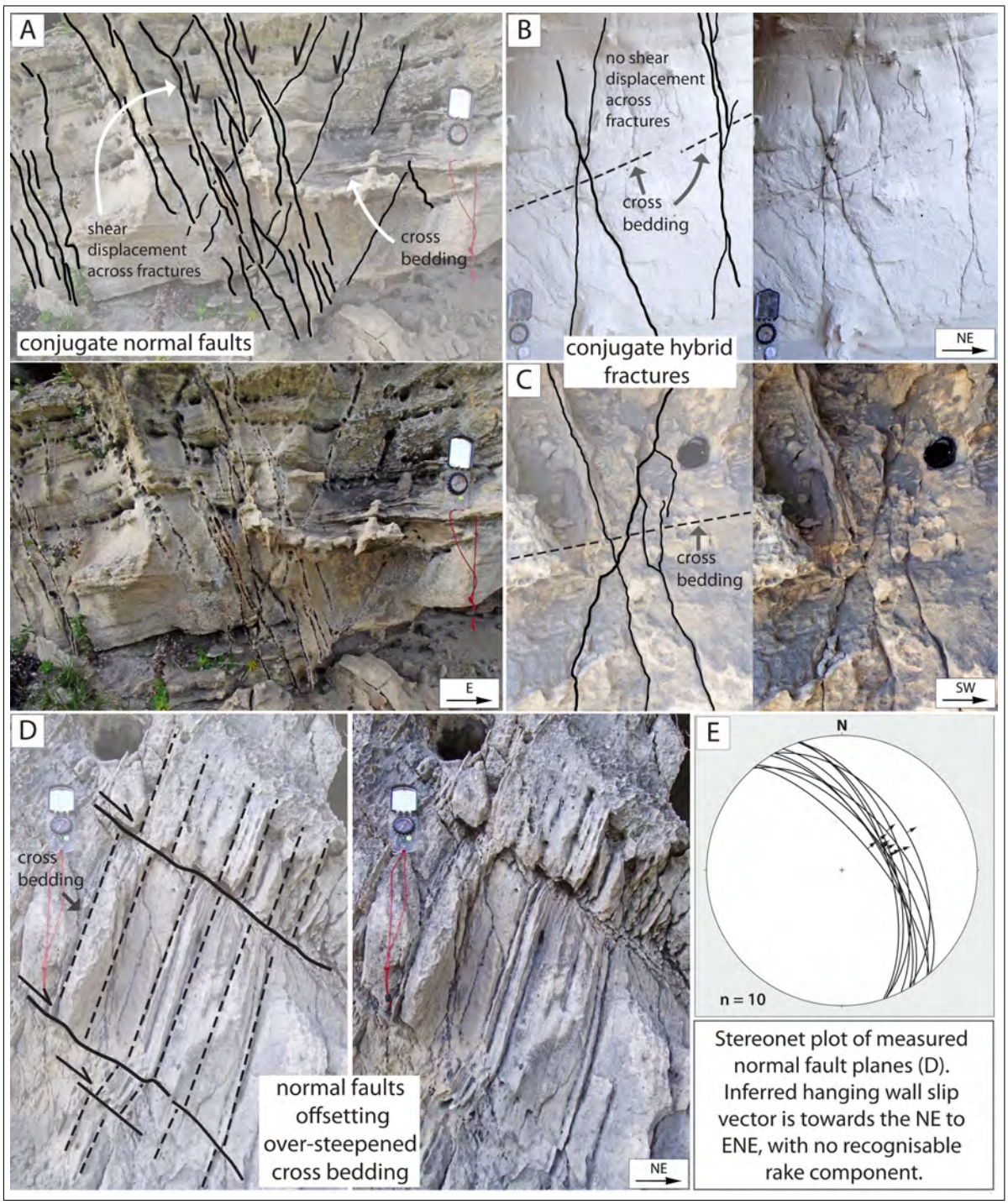

Figure 4.18: A) Conjugate normal faults intersect to form a sub-vertical to vertical orientated acute angle bisector, with a sub-horizontal obtuse angle bisector orientated NE-SW. Normal faults cross-cut and offset the cross-bedding of Wankoe Formation aeolianite. B) Possible conjugate hybrid fractures in Waenhuiskrans Formation aeolianite with no significant shear off-set across the fracture planes. C) Another example of possible hybrid fractures in Wankoe Formation aeolianite, with no significant shear off-set across the fracture planes, similar to (B). In both (B) and (C) possible conjugate hybrid fractures intersect to form a small acute angle (2θ<30 °), and exhibit similar acute and obtuse bisector orientations as (A). D) Multiple parallel normal faults off-setting significantly oversteepened cross-bedding, outcrop located on the inferred trace of the Blomerus Fault, on the Heidehof farm. E) Stereonet showing orientations and fault slip directions of the normal faults from the outcrop in (D). All photographs are taken of vertical cliff faces, geological compass, and hand lens for scale.

Conjugate normal faults are observed in the Wankoe Formation in the Groot Hagelkraal and Heidehof areas (Fig. 4.18A). The shear displacement along the normal faults is typically minor, on the centimetre-scale. The line of intersection between the conjugate faults has a trend direction approximately NW, with a shallow dip of approximately 10 °- 15 ° on average. The conjugate normal faults in both the Heidehof and Groot Hagelkraal areas are commonly located near to heavily jointed aeolianite.

Normal faults are also observed in the Wankoe Formation within brittle folds (kink folds) and significantly oversteepened cross-bedded aeolianite units (Fig. 4.18D). The faults which have typical lengths on the metre-scale, possess shear displacement towards the NE, between 5 - 10 centimetres on average. An isolated normal fault is observed in the Waenhuiskrans Formation aeolianites on the inferred trace of the Struisbaai Fault in the Agulhas area (Fig. 4.23C). This normal fault possesses a length of several metres, with shear displacement on the centimetre-scale towards the north.

Reverse faults are found within brittlely folded Wankoe Formation aeolianites in the Heidehof area (Fig. 4.24C). The shear displacement is towards the NE on average, and involves cross-bedding offsets on the centimetre-scale. The reverse faults only appear in aeolianites which are significantly over-steepened and folded.

Orientation of Joints and Faults in the Aeolianites

The measured orientations of joints and faults within the Waenhuiskrans or Wankoe Formation can be compiled graphically. The orientations of all the joints are displayed on the stereonet in Fig. 4.19, and the joint strike trends are shown in the strike azimuth frequency plots (positioned spatially) on Fig. 4.20. The different study areas each exhibit preferential trends in the orientation (strike and dip) of the joint planes, where the orientation trends relate to specific joint sets in the field (the highest frequency of joint strikes on the strike azimuth plots equates to the dominant joint set). These trends will be outlined in the following:

The Agulhas, Bantamsklip, Groot Hagelkraal, and Heidehof Farm joint distributions all display discrete joint set orientations (Fig. 4.19 & Fig. 4.20):

• The Groot Hagelkraal and Heidehof Farms study areas both have joint sets intersecting at $\sim 30^{\circ}$ (Fig. 4.17A & B), with the Heidehof Farm joints exhibiting an additional third set

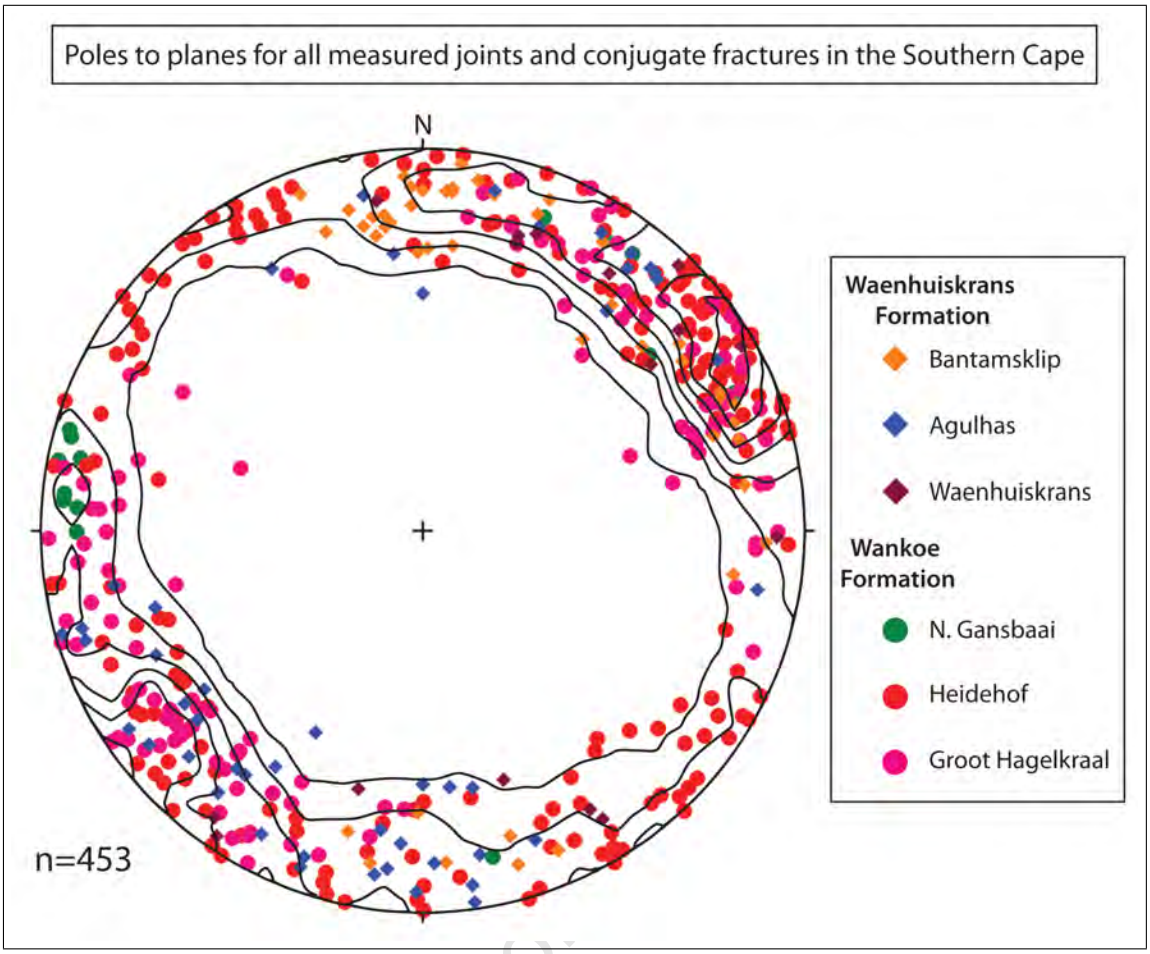

Figure 4.19: Poles to planes stereonet plot of all measured joints and conjugate fractures (faults and hybrid fractures). Displayed data is collected from all study areas, with study area designated by colour, and rock formation by symbol. The plot is Kamb contoured, with 2σ intervals, at a significance level of 3σ.

orthogonal to the dominant joint set. The Groot Hagelkraal and Heidehof areas' dominant joint set dips towards the NE, with the less dominant joint set towards the SW. The orthogonal joint set in the Heidehof area dips towards the NW and SE equally.

• Joint sets in the Bantamsklip area (the sets J and J' as seen in Fig. 4.17C & D, J_0 assumed to not be the most recent deformation features, thus ignored for this study), intersect at $\sim 70^\circ$ with the dominant joint set striking E-W. The dominant joint set dips towards the S-SSW, with the less dominant joint set towards the SW.

• The Agulhas area has two distinctive joint sets, orientated $\sim 45^\circ$ apart, with the acute bisector orientated WNW-ESE. The dominant joint set dips towards the NE, with the less dominant dipping towards the SW.

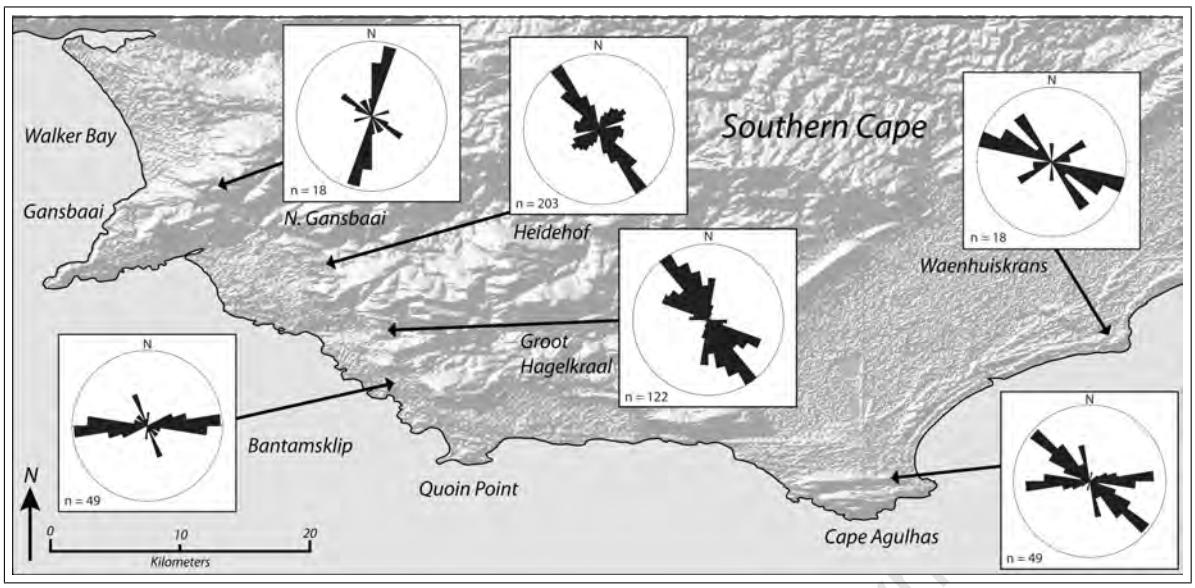

Figure 4.20: Joint strike azimuth frequency plots for locations of Wankoe and Waenhuiskrans Formation outcrops throughout the Southern Cape. The strike azimuth frequency plots display at least two sets of joints for all locations. The trend of joint set orientations typically range between E-W to N-S with the dominant direction approximately NW-SE. The frequency of joint plane strike varies in a clockwise manner through space from an E-W to NW-SE to N-S azimuth from Cape Agulhas/Waenhuiskrans to Bantamsklip, Groot Hagelkraal Farm, Heidehof Farm, and eventually North Gansbaai. The azimuth frequency plots are superimposed on a hill-shade DEM of the Southern Cape, illustrating the topographical features in relation to the study areas.

The North Gansbaai, and Waenhuiskrans areas both have trends in joint set orientations (Fig. 4.19) (Fig. 4.20), but due to the small sample sizes, joint sets can only be inferred approximately from the stereonet and strike azimuth frequency plots:

• North Gansbaai area plot displays a NNE-SSW dominant joint set, with a subordinate joint set approximately NW-SE. The dominant joint set dips towards the ESE, with the less dominant joint set towards the NNE-NE.

• The Waenhuiskrans area has a dominant joint set WNW-ESE and another minor set orientated NW-SE. The dominant joint set dips towards the SSW, with the less dominant joint set towards the SW.

The mean strike orientation of joints within the Southern Cape can be summarised as the following: Both the Waenhuiskrans and Agulhas plots exhibit predominant joint strikes WNW-ESE to NW-SE, Bantamsklip has a preferred joint strike approximately E-W, the Groot Hagelkraal and Heidehof Farm area joints strike approximately NW-SE to NNW-SSE, North Gansbaai has a N-S to NNE-SSW preferred joint strike. Therefore the dominant

strike trend from the azimuth frequency plots for all the study areas in the Southern Cape is approximately NW-SE.

The measured fault planes, from all study areas within the Southern Cape, on average share a similar orientation to the measured joints. The faults have an overall strike trend NW-SE. The significant difference in orientation between the joints and faults however, is the steepness of the dip angle. The normal faults are typically less steeply dipping than the joints on average, with the faults possessing dip angles of $\sim$60° (e.g. Fig. 4.18E) and the reverse faults having dip angles of $\sim$65°-70° (Fig. 4.24C).

4.2.4 Aeolianite Cross-Bedding Orientations

Two particular study areas, the Heidehof and Groot Hagelkraal Farm areas, exhibit different orientations of cross-bedding within the aeolianite units. In both, the Wankoe Formation aeolianites display significant change in both dip direction and dip angle of the cross-bedding across the inferred surface trace of the Blomerus Fault; which constitutes a NW-SE axis across both study locations (Fig. 4.21 & Fig. 4.22).

As seen on Fig. 4.21, the Heidehof Farm displays a variation in cross-bedding dip direction and angle with location. The aeolianites on the SW-side of the Blomerus Fault possess a relatively steep dip between 42° to 82° SW (Fig. 4.21A). The cross-bedding within the aeolianite units directly on the inferred trace of the Blomerus Fault has an increased dip angle between 67° - 88° towards the SW-W (Fig. 4.21B). The aeolianites on the NE-side of the Blomerus Fault display a relatively shallow dip angle between 3° - 11° towards the NE (Fig. 4.21C). The respective strike and dip of the cross-bedding is represented on the stereonet plots in Fig. 4.21.

The Groot Hagelkraal Farm exhibits a similar variation in cross-bedding dip direction and angle to the Heidehof Farm area (Fig. 4.22). The SW-side of the inferred surface trace of the Blomerus Fault consists of aeolianite units dipping between 34° - 57° towards the SW (Fig. 4.22A). The aeolianite units on the NE-side of the inferred surface trace of the Blomerus Fault display cross-bedded units dipping relatively shallowly at 11° - 28° towards the E on average (Fig. 4.22B). This variation in cross-bedding orientation can be viewed on the stereonet plots in Fig. 4.22.

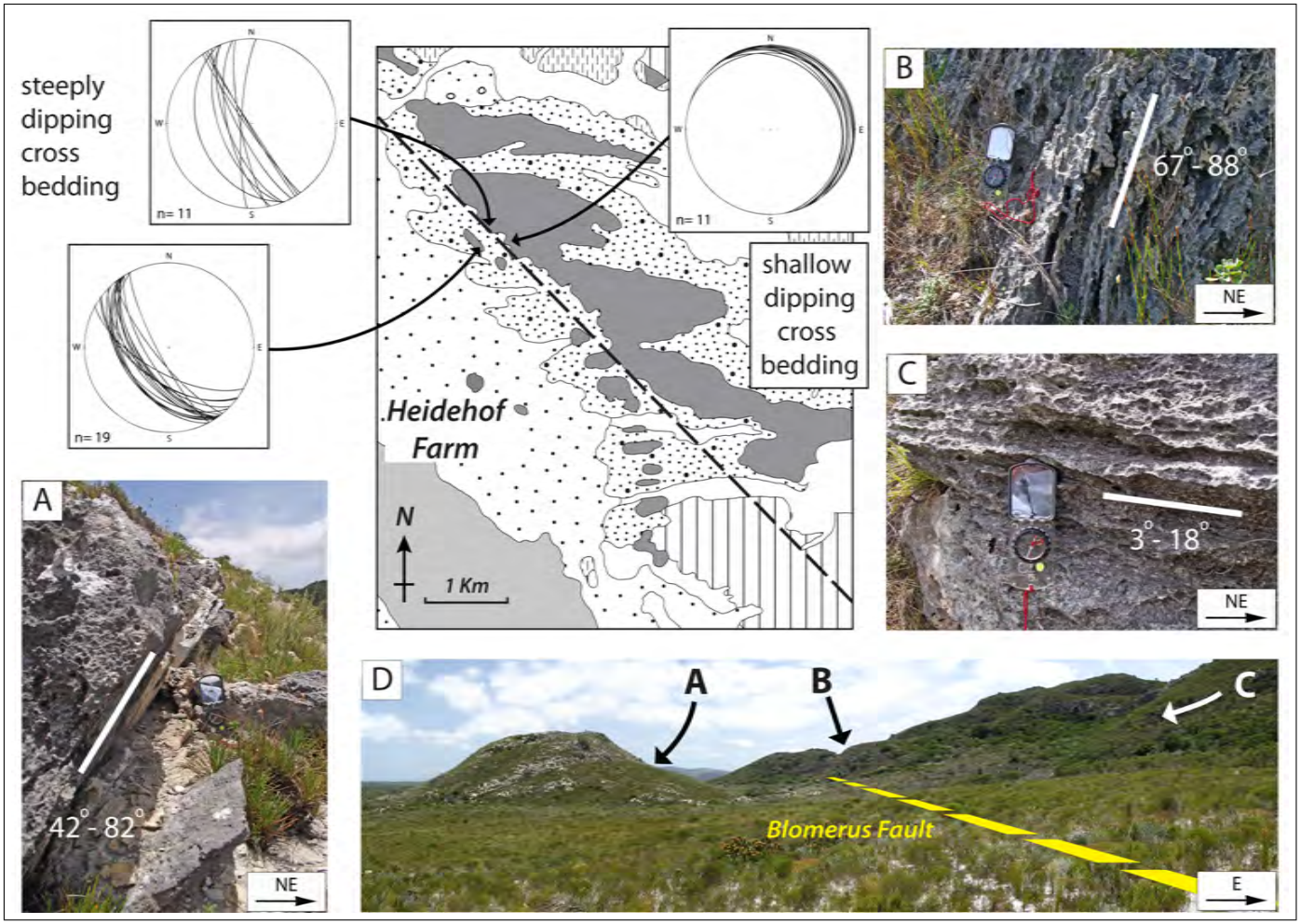

Figure 4.21: The Heidehof area exhibits a change in cross-bedding dip orientation over the inferred trace of the Blomerus Fault. In both (A) and (B) cross-bedding dips are observed to exceed the angle of repose of unconsolidated sediments ($\sim 37°$) towards the SW. The dip orientation is seen to be the most steep (sub-vertical to vertical) in (B) which overlies the inferred Blomerus Fault trace. (C) displays shallowly dipping cross-bedding towards the NE. A change of dip direction and dip angle is thus observed over the inferred fault trace. (D) provides a cross profile view of the inferred fault trace, with cross-bedding outcrop locations (A, B, C) on the Heidehof farm.

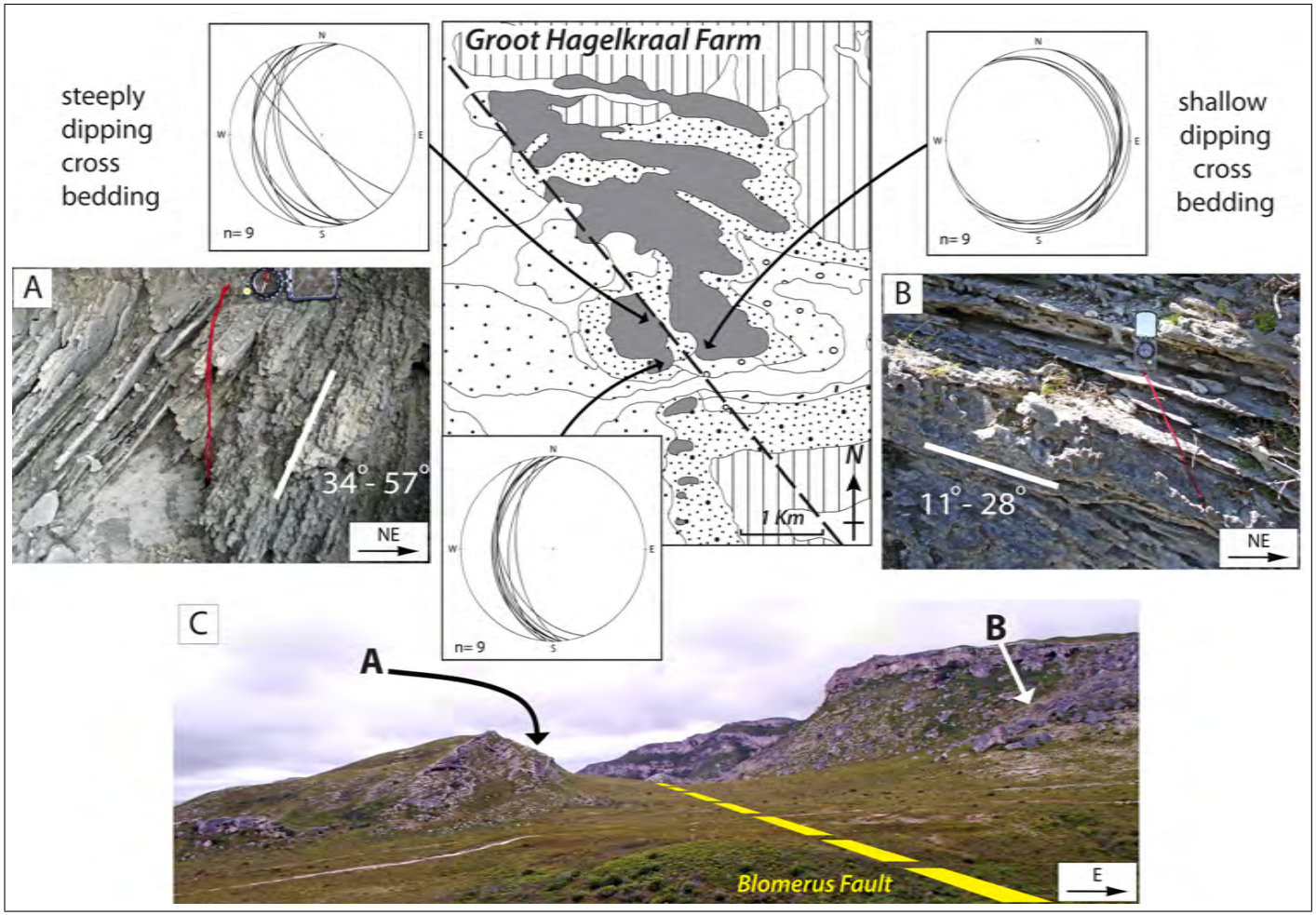

Figure 4.22: The Groot Hagelkraal area exhibits a change in cross-bedding dip orientation over the inferred trace of the Blomerus Fault. In (A) cross-bedding dips are observed to exceed the angle of repose of unconsolidated sediments ($\sim 37\,^{\circ}$) towards the SW. In (B) cross-bedding is seen to dip shallowly towards the NE & ESE. A change of dip direction and dip angle is thus observed over the inferred fault trace. (C) provides a cross profile view of the inferred fault trace, with cross-bedding outcrop locations (A, B) on the Groot Hagelkraal Farm.

Both the study locations (Heidehof Farm and Groot Hagelkraal Farm), have abrupt changes in cross-bedding dip direction and dip angle across the inferred surface trace of the Blomerus Fault. The aeolianites found on the SW-side of the Blomerus Fault have dip angles typically in excess of the angle of repose for unconsolidated sediments (37°), and up to sub-vertical in locations (significantly over-steepened), towards the SW-W. In contrast, the aeolianites found on the NE-side of the Blomerus Fault typically have cross-bedding dip angles less than the angle of repose for unconsolidated sediments, and dip towards the E on average.

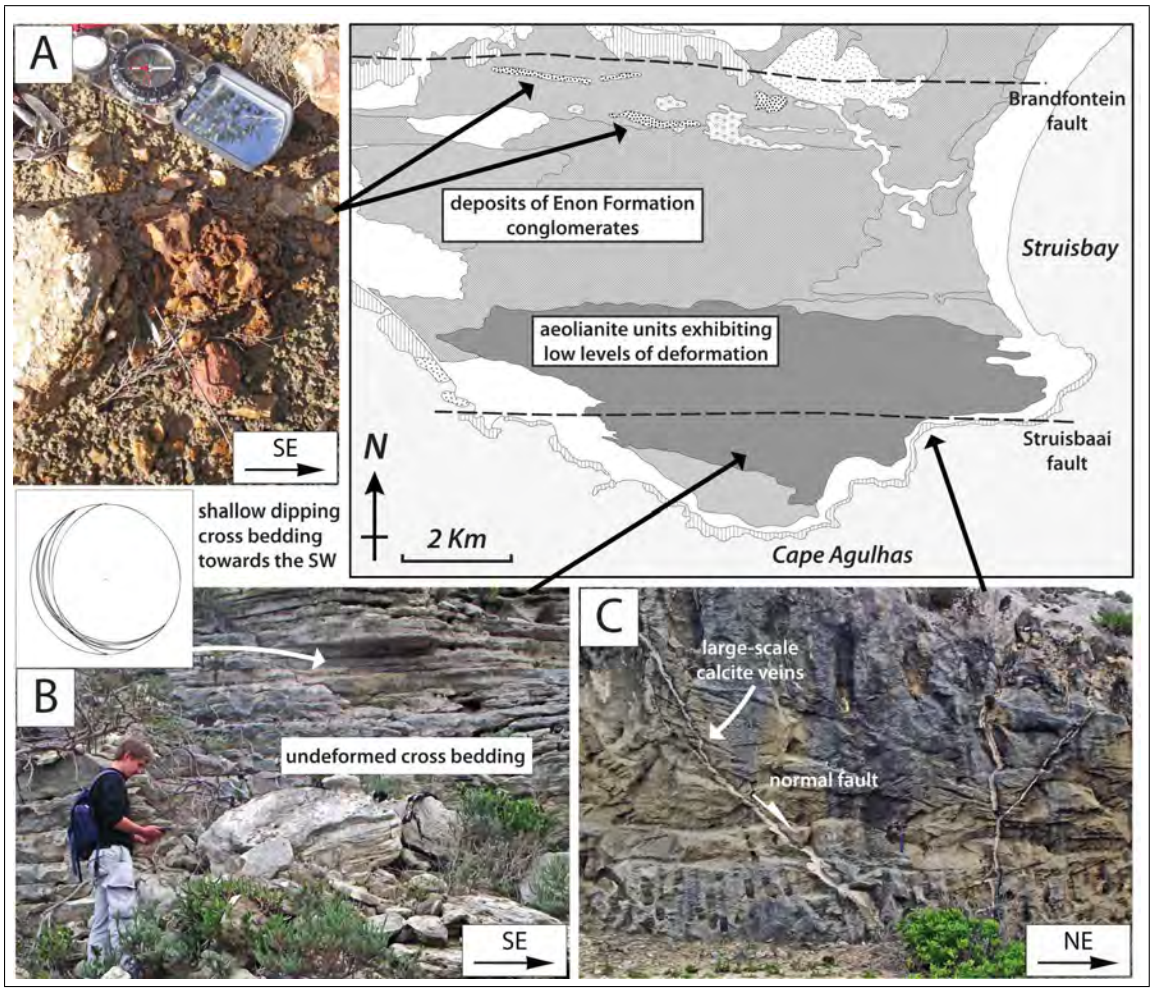

Figure 4.23: Geological features associated with the Cape Agulhas area. A) Enon Formation (ferrigenous sediments and silicified conglomerates) found in association with the inferred Brandfontein Fault exposed at surface. B) Typically shallow dipping cross-bedding of the Waenhuiskrans aeolianites located in the Agulhas area (refer to stereonet). No cross-bedding over the angle of repose ($\sim 37°$) is observed throughout the Cape Agulhas aeolianites. C) Minor deformation features are observed, with joints, conjugate hybrid joints (Fig. 4.18B) and metre-scale normal faults observed proximal to the inferred trace of the Struisbaai Fault. The aeolianites are generally undeformed, and found to be in the same state as at time of consolidation, except for natural weathering and erosion effects.

The change in cross-bedding dip angle and direction across the NW-SE axis of the inferred surface trace of the Blomerus Fault is observed to be a laterally extensive trend both to the NW of the Heidehof Farm area, and to the SE of the Groot Hagelkraal Farm area. As such, this cross-bedding orientation trend is considered to be a significant feature on the hundred metres to kilometres-scale across the western part of the Southern Cape.

The large-scale and significant variability in orientation of the cross-bedding is only observed in the Wankoe Formation, and exclusively in close proximity to the inferred surface trace of the Blomerus Fault. This is in contrast to the lack of significant changes in cross-bedding orientation observed in the Waenhuiskrans Formation (other than 'natural' minor variation in cross-bedding), for example as seen in the Agulhas study location (Fig. 4.23B). Consequently, a relatively consistent cross-bedding dip angle and dip direction towards the SW is seen in the Waenhuiskrans Formation throughout the Southern Cape.

4.2.5 Brittle Folds and Kink Folds

The folds as seen in the Wankoe Formation aeolianites, in the Heidehof and Groot Hagelkraal Farm areas, most commonly involve two distinct types:

Kink folds are relatively small-scale features, involving tens of centimetres to half a metre fold widths (Fig. 4.24A & B). The observed kink folds involve localised angular folding across a single hinge (kink plane) or two hinges (kink band) (e.g. Fig. 4.24A) (as discussed by Ramsay, 1967). The deflection of the cross-beds typically forms kink bands with reverse shear-sense displacement along the kink planes (Fig. 4.24A & C). This sense of deflection of the cross-beds within the kink folds (kink bands) is consistent throughout the study areas. However, normal shear-sense kink bands are also observed in a localised area of the Heidehof Farm (Fig. 4.24B).

The brittle folds are typically metre-scale features, and involve the angular folding of cross-bedded aeolianite through multiple hinges (zone of kink folds and fractures) (Fig. 4.24D). The brittle fold are consistently heavily fractured, almost brecciated in places. Monocline-type brittle folds, as seen in Fig. 4.24C (the larger structure), exhibit southward dipping (oversteepened) cross-beds of aeolianite deflected to a sub-horizontal orientation. The deflected cross-bedding is cross-cut by faults through the hinge. Throughout the Heidehof and

Groot Hagelkraal Farm study areas, only a few examples of brittle folds are observed.

The cross-bedded aeolianite units typically host the brittle folds and kink folds, with no brittle folds observed within the massive or karstified aeolianite units. Furthermore, the brittle folds and kink folds are typically concentrated in the aeolianites exhibiting steeply dipping cross-beds. For example, Fig. 4.24A shows a kink band in comparatively shallow dipping cross-beds, whilst the kink folds shown in Fig. 4.24B are within very steep to sub-vertical dipping aeolianite cross-beds.

Figure 4.24: Brittle folds and kink folds in Wankoe Formation aeolianite. A) Relatively steep dipping cross-bedding fractured and kink folded, with fracture along the planes of maximum flexure (kink planes). B) Kink band in significantly oversteepened cross-bedding, with significant deformation within the 'hinge-zone'. C) Steeply dipping cross-bedding brittlely folded to a relatively horizontal plane, with multiple reverse faults cross-cutting the cross-bedding across the hinge. Some small-scale kink folds are observed within the structure. D) Brittle fold with multiple fractures (almost brecciated) through the hinge. Brittle folds and kink folds appear to involve consolidated cross-bedded aeolianite only. All pictures taken of vertical cliff exposures, with geological compass/hand lens for scale.

The orientation of the brittle folds, kink folds, and kink bands within the aeolianites on the Groot Hagelkraal Farm and Heidehof Farm areas has two main trends in fold axes. The fold hinges typically plunge relatively shallowly towards either the SE or NW, the fold hinges being approximately parallel to the strike of the host cross-bedding. The other less frequent plunge direction is towards the SW (illustrated in Fig. 4.24A), with the plunge angle typically steeper than the NW to SE plunging folds (illustrated Fig. 4.24B and C).

The spatial distribution of the brittle folds and kink folds is also commonly adjacent or proximal to the brecciated aeolianite units. In places, a gradual change from brittlely folded cross-beds to cataclastically deformed (brecciated or gouged) aeolianite is seen.

Although relatively sparsely observed, brittle folds and kink folds are recognised in two study areas only, the Heidehof Farm and the Groot Hagelkraal Farm. The deformation is therefore concentrated to the Wankoe Formation, with no brittle folds or kink folds observed in the Waenhuiskrans Formation aeolianites. The brittle folds and kink bands are also located only in the aeolianite units to the SW of the inferred Blomerus Fault axis striking NW-SE through these two study locations (as seen previously in Fig. 4.21 & Fig. 4.22).

4.2.6 Cataclasites

Cataclastic rocks (cataclasites), as described by Davis and Reynolds (1996), are characterised by pervasive fractures and exhibit typically sharp, angular grains and fragments, which have formed as a result of cataclasis. Cataclasites can be sub-divided into two categories: Gouge which exhibits $<$30% of the the whole rock unit as angular fragments, and breccias which exhibit $>$30% of the whole rock unit as angular fragments (Sibson, 1977).

Breccias and gouge units are only observed cross-cutting Wankoe Formation aeolianites on the Heidehof and Groot Hagelkraal Farm study areas. Furthermore, the spatial distribution of the cataclasites is typically localised in the aeolianites proximal to the inferred surface trace of the Blomerus Fault (Fig. 4.25). The breccias are not limited to the SW-side of the NW-SE Blomerus Fault trace, and also occur on the NE-side. However, the majority of breccia and gouge outcrops are on the SW-side of the Blomerus Fault and within the steeply dipping aeolianites (refer to section 4.2.4).

The characteristics of the brecciated aeolianites vary throughout the two study areas:

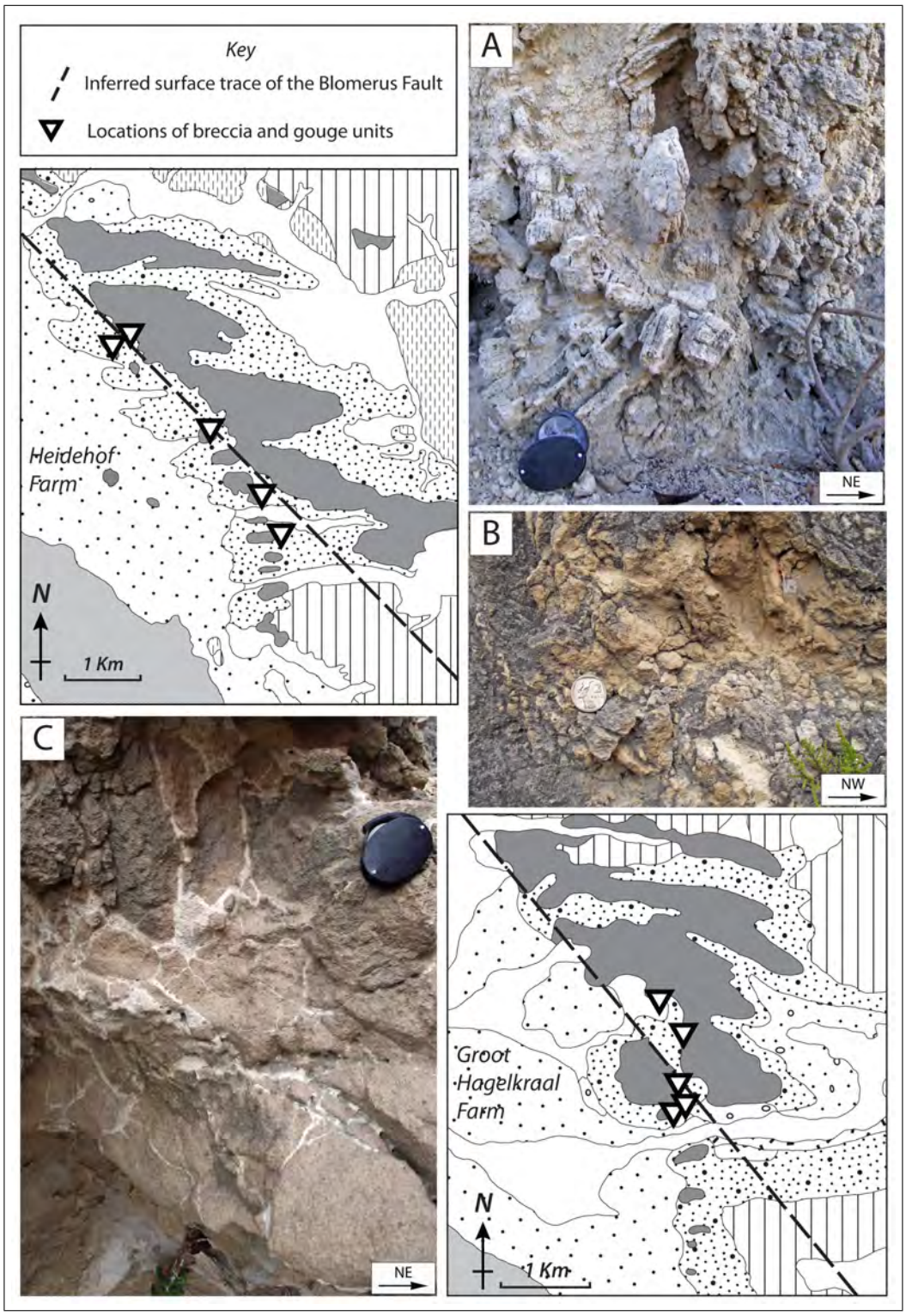

Figure 4.25: Locations and breccia types observed throughout the Heidehof and Groot Hagelkraal farm areas. A) Blocks of cross-bedded Wankoe Formation, off-set and rotated relative to surrounding unbrecciated aeolianite, cemented by finer gouge and massive calc-arenitic sands. B) Gouge involving angular to sub-rounded fragments of aeolianite, with the majority of the cross-bedding features obliterated. Cohesion of the gouge is low on average, and erodes preferentially. C) Angular fragments of fragmented aeolianite cemented together with calcite veins, in a typical breccia. Locations of the breccias and gouge units relative to the inferred trace of the Blomerus Fault are indicated on maps. The breccias are in close proximity to the fault trace. Photographs all taken of vertical cliff exposures.

Most commonly, the breccias comprise rotated and off-set coarse fragments of cross bedded aeolianite set in a finer-grained calc-arenite matrix (Fig. 4.25A). The angular fragments constitute >50% of the whole brecciated aeolianite unit. The angular fragments are typically heavily fractured, with the cross-bedding within the blocks exhibiting significant deflection and off-set from the surrounding unbrecciated aeolianite cross-beds. The matrix is typically semi-consolidated sediment grains, being comprised of sand-sized particles derived from the aeolianites. The matrix lacks significant internal cohesion and consolidation, and is preferentially eroded relative to the angular cross-bedded aeolianite fragments.

Less commonly, the brecciated units are characterised by coarse angular and heavily fractured fragments of aeolianite set in a much finer calcite matrix (Fig. 4.25 C). The angular fragments comprise of massive or cross-bedded aeolianite, with minor rotation or off-set of the angular fragments to the surrounding unbrecciated aeolianites. The fragments generally constitute >60% of the whole breccia units. The matrix is a fine-grained secondary calcite in-fill, precipitated into the interstitial fractures between the angular fragments. The matrix typically erodes preferentially, although in places the angular fragments (depending on the level of consolidation of the fragments) will erode preferentially. However, the whole brecciated unit has a low cohesion on average, and will erode preferentially compared to the surrounding unbrecciated aeolianite.

The aeolianite gouge units (Fig. 4.25B) predominantly crop out at specific localities on the Heidehof Farm, with only minor gouge units seen on the Groot Hagelkraal Farm (usually in association with breccia units). The gouge consists of relatively fine-grained (typically on the millimetre to centimetre-scales) angular to sub-rounded fragments. The fragments constitute the entire gouge unit with no differentiable matrix component. All sedimentary structures within the aeolianite units are obliterated, with the gouge exhibiting significant pulverisation. The gouge units possess low cohesion and consolidation, and are preferentially eroded compared to the surrounding ungouged/unbrecciated aeolianites.

The breccias and gouge units crop out of the aeolianites, and are not observed to be surface features on the inclined slope of the aeolianite hills. The cataclasites in places are eroded down on the slopes, and form debris flow deposits. The breccias and gouge units continue into the aeolianites to some depth (observation is made with the aid of an excavation trench on the Heidehof Farm).

The orientation of the different cataclasite units is inferred from the outcrop pattern along the E to SE facing slopes of the aeolianite hills, throughout both the Heidehof and Groot Hagelkraal Farm study areas. The breccias and gouge units outcrop in an approximately NW-SE direction on average, roughly parallel to the inferred surface trace of the Blomerus Fault (Fig. 4.25).

4.2.7 Soft-sediment Deformation

Soft-sediment deformation (SSD) features are localised to the Heidehof Farm study area and only observed in the Wankoe Formation aeolianites. The SSD features on the Heidehof Farm area are in close proximity to the inferred surface trace of the Blomerus Fault (Fig. 4.26E). The features are only observed in the relatively steeply dipping aeolianites on the SW-side of the NW-SE trace of the Blomerus Fault.

The SSD features, although relatively similar, do have some variation in the style of deformation. As shown in Fig. 4.26A, the downward deflection and rotation of cross-beds form two 'bowl-shaped' features. The deformed cross-bedding is incorporated within the SSD features as internal layering, which is subsequently ductily deformed and fractured within the different 'bowls'. The 'bowls' have a massive inter-bed laterally separating the two features, which the 'bowl-shaped' features cross-cut and pinch-off. The cross-beds below the features exhibit some structural disruption, whilst the cross-beds above these features are relatively undeformed.

The SSD feature as seen in Fig. 4.26B involves cross-bedding that has been deflected and rotated downwards by a centre 'plug-shaped' feature. The 'plug' does cross-cut some of the surrounding cross-bedding, although predominantly the cross-bedding is displaced downwards in a ductile manner. The feature possesses some cryptic internal layering, but is relatively massive compared to the surrounding cross-bedding. The 'plug' is cross-cut and laterally pinched-out by the above undeformed cross-bedded aeolianite.

Figure 4.26C shows a significantly more weathered example of the SSD features. The deformation feature can also be described as an elongate 'plug-shaped' or 'wedge-shaped' feature, which deflects, and downwardly displaces the surrounding cross-bedding. The cross-bedding is nearly obliterated within the structure, with a relatively massive appearance.

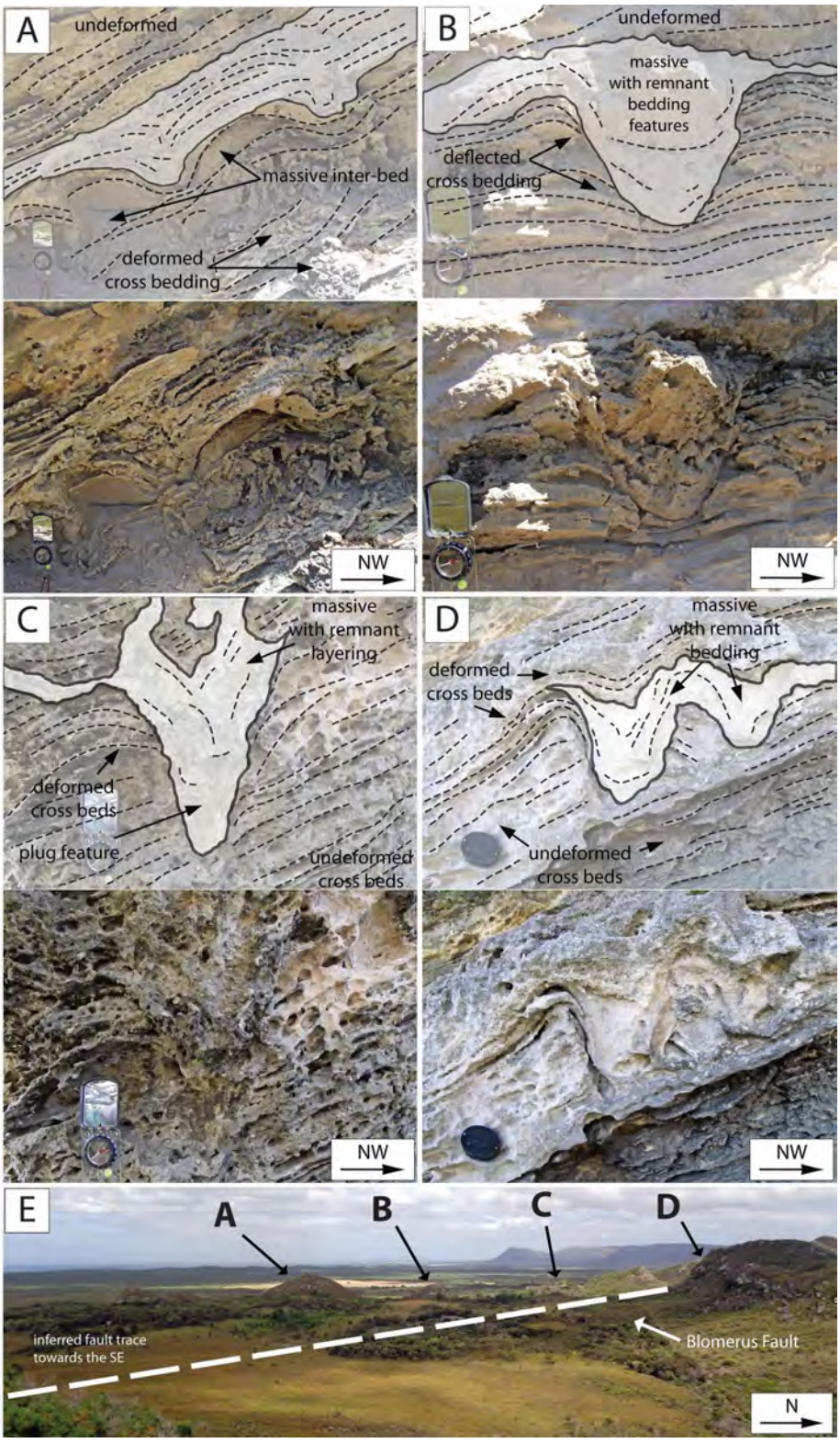

Figure 4.26: Soft-sediment deformation features observed in the Heidehof farm area. Cross-beds are deformed in a ductile manner, around central 'plug'/'wedge'/'bowl-shaped' features. The cross-beds are deflected/rotated downwards to form a 'plug'/'wedge-shape' (B) and (D), or are cross cut by the 'plug' body (C). There is remnant cross-bedding features within the 'bowl-shaped' bodies, generally off-set and exhibiting ductile deformation (A) and general loss of cohesion. The cross-bedding appears to continue undeformed above the 'plug' features. E) The locations of the soft-sediment deformation features relative to the Blomerus Fault (inferred trace).

Figure 4.26D also shows a multiple 'plug-shaped' SSD feature similar to Fig. 4.26A. The surrounding cross-bedding is also deflected downwards in a ductile manner around the 'plugs'. The feature is predominantly massive internally, with only minor remnant bedding present. The feature is also cross-cut by the above typically undeformed cross-bedded aeolianites, but some downward collapse of the above cross-bedding can be seen into the SSD feature.

The SSD features typically possess a heterogeneous internal structure; the remnant cross-bedding (or layering) visible within the 'plugs' or 'bowls' can be traced to the surrounding undeformed cross-beds. The features usually involve ductile deformation features (folding of the sedimentary structures), with no brittle deformation structures visible. The SSD features are found to be typically small-scale, with most of the features possessing widths/lengths on the tens of centimetre to metre-scales.

The orientation of the SSD features are in the same orientation as the surrounding inclined cross-bedding beds of the aeolianites. The 'bowls' feature in Fig. 4.26A shows this most clearly, with the 'bowls' parallel to the SW dipping cross-bedding below and above the feature. The outcrop distribution of the features is in an approximately NW-SE trend across the Heidehof Farm.

Chapter 5

Discussion

5.1 Petrology

The Late Pliocene - Lower Pleistocene Wankoe Formation and the Upper Pleistocene Waenhuiskrans Formation aeolianites require discussion in terms of aeolian dune deposition, accumulation, and past consolidation processes, to explain the present outcrop pattern and the internal sedimentary structures. The cross-bedding orientation trends within the Wankoe Formation aeolianites on the Heidehof and Groot Hagelkraal farms, need to be resolved in terms of the expected characteristics of aeolian dunes, and what mechanisms would account for the oversteepened cross-bedding orientations. The outcrops of Enon Formation within the Agulhas area also need to be explained and related to recognised underlying fault structures, thus helping to constrain the structural history of the Southern Cape.

5.1.1 The Aeolianites

Both the Wankoe and Waenhuiskrans Formation aeolianites formed from the accumulation of aeolian dunes (Malan, 1989b, 1990). Characteristics of aeolian dune formation and internal structure are therefore important to understand when considering observed internal deformation features.

The aeolianites in the Heidehof and Groot Hagelkraal Farm areas both have two preferred cross-bedding dip directions (Fig. 4.4), with the predominant cross-bedding dip direction towards NE-E. Aeolian dunes which form in areas with two seasonal wind directions will

typically exhibit an internal structure which reflects this variability (McKee, 1979) (Fig. 5.1). This is because of alternating accumulation of lee slope and windward slope deposits with subsequent season (Leeder, 2011). The Southern Cape during the Quaternary is known to have seasonal variability in wind direction (Bateman *et al.*, 2004).

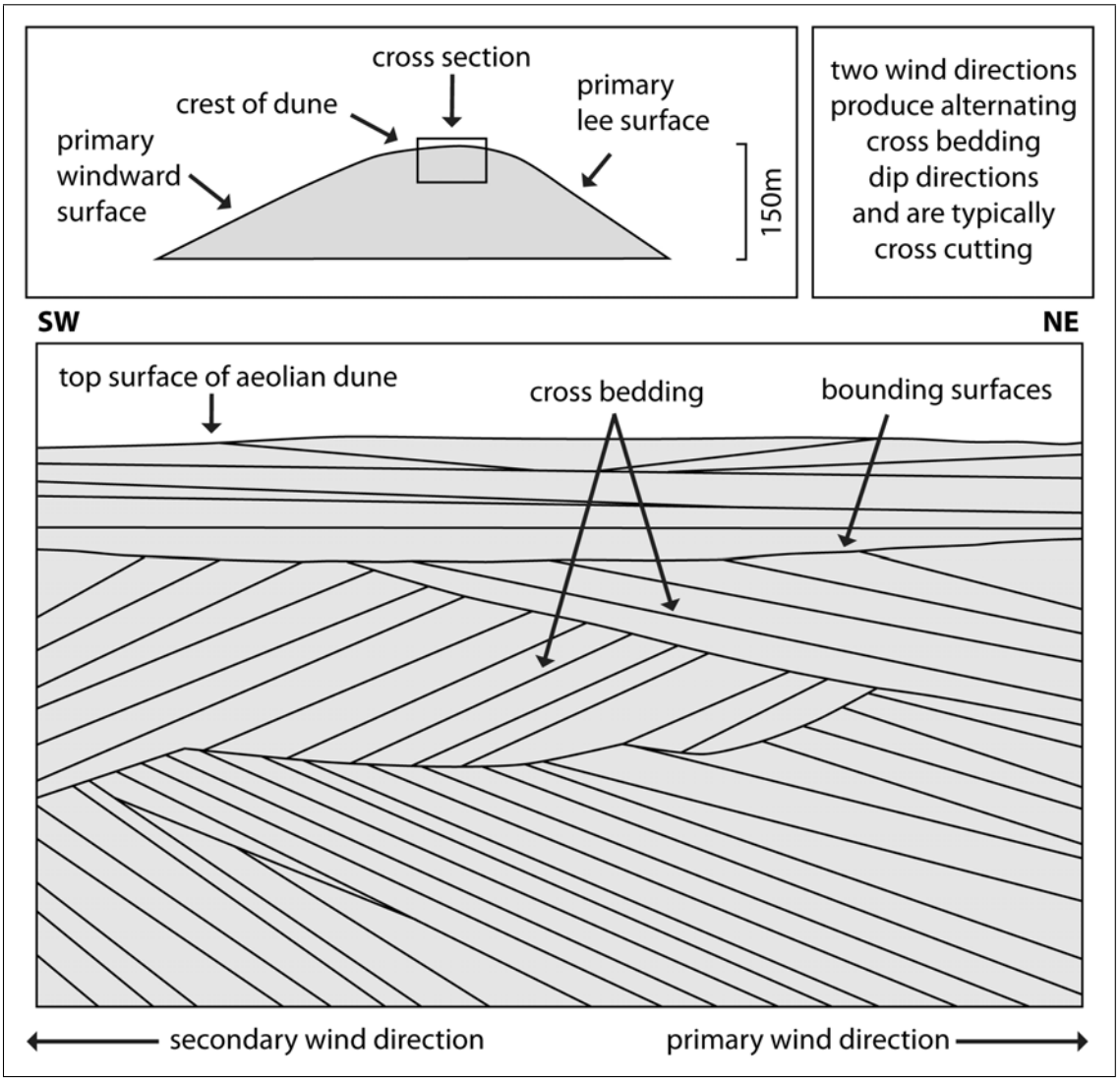

Figure 5.1: The internal structure of aeolian dunes found in regions of seasonal wind variability. The dominant/primary wind direction (shown towards the NE) results in a preferred cross-bedding direction reflecting the primary lee slope, whilst the less dominant/secondary wind direction (shown towards the SW) will result in cross-bedding in the opposite direction (dune migration therefore varies seasonally). The alternation of cross-bedding orientation is preserved as cross-cutting cross-bedded units. Figure adapted from McKee (1979)

As the aeolianites exhibit cross-bedding consistent with the expected aeolian dunes, the aeolianites which outcrop on the SW-side of the inferred Blomerus Fault (cross-bedding dips

towards the W on average), and the ridges on the NE-side (cross-bedding dips towards the E on average) would have originally been a single continuous dune body. Hence, the large-scale cross-bedding on either side of the dune body will be near the angle of repose (or less) for unconsolidated aeolian sand (<37 °) (Allen, 1970).

The Wankoe Formation aeolianites before consolidation were reversing-type dunes, with a typical transverse ridge-type form (after descriptions provided by McKee, 1979). These dunes formed extensive backshore dune fields, which covered much of the Southern Cape coastal plain during the Late Tertiary (Malan, 1989b). The aeolianite outcrops in the North Gansbaai, Heidehof, Groot Hagelkraal, and to the North of Bantamsklip may have been a semi-continuous dune field before and at the time of consolidation.

The Waenhuiskrans Formation aeolianites in the Bantamsklip, Agulhas, and Waenhuiskrans areas possess a predominant cross-bedding dip direction SW, which indicates a dominant westerly wind direction during the Upper Pleistocene; this palaeowind direction is also suggested by Bateman *et al.* (2004). The dunes accumulated in headland by-pass dune fields, and were relatively extensive during the Upper Pleistocene sea regression (Marker and Holmes, 2005).

5.1.2 Tilted Cross-Bedding

Unconsolidated aeolian dunes at the time of formation, require the lee slopes (sand avalanche slopes) to possess dip angles commonly between 30 ° - 34 ° (McKee, 1979), and with a maximum of 37 ° (Allen, 1970). Shallower dipping cross-beds are also typical (<30 °), with bounding surfaces between beds of cross-bedding commonly dipping between 20 °-26 ° (Fig. 5.1).

In places the aeolianites at the Heidehof and Groot Hagelkraal farms however exhibit cross-bedding dips angles >37 ° (Fig. 4.21 & Fig. 4.22). The aeolian sediments could not have achieved these dip angles whilst unconsolidated, therefore these aeolianites must have been tilted once the aeolianites were at least semi-consolidated to achieve cross-beds with dip angles >37 °.

The similarity in the tilted cross-beds found on both the Heidehof and Groot Hagelkraal farms indicate a widespread tilting event post-consolidation (Fig. 4.12). The tilted beds are

only found to outcrop on the SW-side of the inferred Blomerus Fault (see section 4.2.4 and geology maps Fig. 4.10 & Fig. 4.11).

The cross-beds have been tilted between 20° and ∼50° (Fig. 4.21 & Fig. 4.22), with aeolianite units on the ten - hundred metres-scale dimensions exhibiting tilting. The process which caused the large-scale tilting of the cross-beds needs to have occurred once the aeolianites were consolidated to semi-consolidated, and would have needed to simultaneously created space into which the units of cross-bedding could rotate/tilt into.

Figure 5.2 illustrates a simplified 2D representation of the cross-bedding rotation problem as observed in the field. The pre-tilted aeolianite (Fig. 5.2A) possess cross-beds which dip towards the SW at angles at or below the angle of repose. For this example the aeolianite has been limited to a 10 metre long horizontal unit, with an overall orientation expected at time of deposition and consolidation. The unit is than tilted to 20° (Fig. 5.2B), the cross-bedding now possess steeper than 37° dip angles, which is contrasted against actual cross bed orientations taken from Groot Hagelkraal Farm (on stereonet). A continued tilting to 40° (Fig. 5.2C) shows a now significantly over-steepened unit of cross-bedded aeolianite, which is similar to what is observed in the Heidehof Farm area (on stereonet).

The downward space required to rotate a 10 m long unit of aeolianite 20° and 40° (Fig. 5.2) can be determined by applying the trigonometrical relationship:

$$\tan\theta = \frac{(NE - SW\ length)}{(vertical\ height)} \tag{5.1}$$

A 20° rotation of a 10 m long block would require a vertical space below the block of approximately 3.6 m, whilst a 40° rotation would require a space of approximately 8.4 m.

Therefore a subsidence of between ∼3.5 m and ∼8.4 m or more is required to achieve the cross-bedding orientations as measured in some locations in the Heidehof and Groot Hagelkraal Farm areas.

The rotation of the aeolianites (as seen in the field) is however a larger-scale situation than the example above. Scaling these calculations up to accommodate the 20° rotation of the ∼200 m NE-SW length sections of tilted aeolianite (eg. Fig. 4.11), would require a subsidence of ∼73 m. This is an unrealistic amount of space required beneath the aeolianite units to accommodate the tilting.

The other possible means of achieving the observed tilting of the aeolianites, is through

multiple smaller-scale block segments rotating independently (more similar to the example used in Fig. 5.2). This method appears to fit the field observations, such as the tilted aeolianites at the NW-corner of the Heidehof Farm exhibit, over a 200 m NE-SW distance, a progressively decreasing tilt angle towards the SW. This implies that discrete sections (blocks) of the aeolianite tilted differently with respects to one another. Similar observations are found in multiple localities on the Heidehof and Groot Hagelkraal Farms.

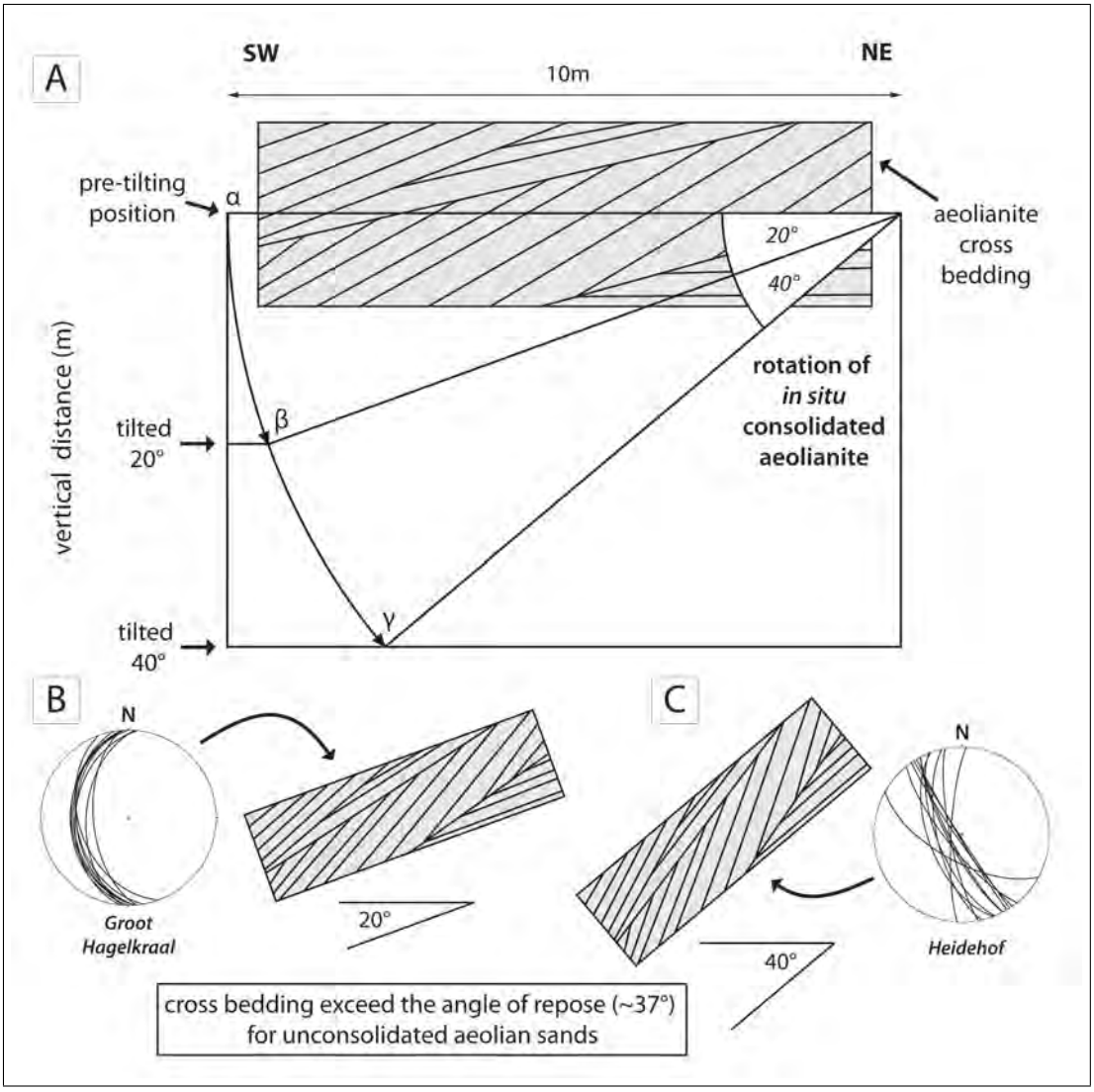

Figure 5.2: Schematic 2D diagram of a cross-bedded unit of aeolianite undergoing different degrees of tilting. The dip angle of the cross-bedding can be observed to steepens progressively with tilting. See text for details.

5.1.3 Enon Formation

The Late Jurrasic - Early Cretaceous Enon Formation, as described by Dingle (1973); Viljoen (1992); Domoney (2009), is a alluvial fan and scree conglomerate deposit, and can also be observed as silcretes in the Southern Cape (Andreoli, M. pers. comm. 18 Jan 2012). The Enon Formation was later ferrigenized during the Cretaceous African Surface planation event (Holmes *et al.*, 2007), which can be seen in the Agulhas area.

The conglomerates are commonly found in normal fault-bound extensional basins, such as the Heidelberg/Riversdale basin (Viljoen, 1992), and localities along the Worcester and Kango Faults (Domoney, 2009). These basins formed as a result of the breakup of Gondwana (the separation of Africa and South America) and the formation of the AFFZ, which resulted in large-scale normal fault-related half-graben development (Hälbich *et al.*, 1993)(refer to section 3.3.3).

The outcrops of Enon Formation within the Agulhas study area (Fig. 4.14, Fig. 4.23), could be accounted for by two possible scenarios: 1) The Enon Formation outcrops are $in\ situ$ and represent the presence of an underlying normal fault-related half-graben basin, or that these Enon Formation outcrops have been transported from elsewhere, reworked, and deposited within the study area. 2) The presence of the inferred Brandfontein Fault (proposed from aeromagnetic survey work by Andersen and Andreoli (1990)) E-W striking surface trace to the north of these Enon Formation outcrops indicate that the Enon Formation conglomerates are normal fault-related half-graben in-fill deposits. The outcrop pattern furthermore reflects an extensive deposit in a E-W manner across the Agulhas headland, which would further support the presence of a large-scale normal fault to the north trending in a similar orientation.

5.2 The Deformation Features

The various deformation features observed in the Wankoe and Waenhuiskrans Formation represent the progressive deformation history of the aeolianites since consolidation. The aim of this section is therefore to determine how these features formed, with a particular look at the stress-state within the aeolianites at the time of rock failure. The outcrop pattern of the

deformation features, and specific trends in the orientation and spatial distribution will also be discussed and related to large-scale geological structures where applicable.

5.2.1 Joints, Hybrid Fractures, Faults and Conjugate Faults

The Joints

Systematic joints/joint veins (considered synonymous) and joint sets, all cross-cut sedimentary structures, with some joints cross-cutting other deformation features (kink folds and breccias). The joints do not cause ductile deformation of the surrounding bedding through deflection or rotation of the sand grains. The joints are not infilled by unconsolidated sand, and don't exhibit ductile collapse of the joint walls. As a result, the joints most likely propagated through already consolidated, or at least partially consolidated aeolianite at the time of failure. Individual joint sets possibly formed at subsequent times, with some joints (joint sets) on the Heidehof and Groot Hagelkraal areas appearing to have been rotated with the cross-bedding, whilst other joints do not.

The penetrative nature of the joints through the aeolianites indicate that the joints are not an exterior/surface phenomenon affecting the aeolianites, as would be expected with diagenetic, thermal, or weathering-type processes (volumetric changes) (Pirrotta and Barbano, 2010). The presence of multiple joints cross-cutting the aeolianite rock units, thus involve the internal brittle deformation of a significant volume of rock.

Aeolianites which are cross-cut by both a dominant joint set (J) and a less dominant joint set (J') (Fig. 5.3), commonly have deviation/deflection of J' around the joints in J, or otherwise abutting up against J (Fig. 4.17) (refer to section 4.2.3). An explanation for joint deflection or abutment against the dominant joints is provided by Hancock *et al.* (1991), who described the dominant joint as the primary joint that formed first in a previously intact rock and within a presumably undisturbed stress field. Consequently, later joints formed in a rock unit which was no longer isotropic and intact, and now possessed an altered internal stress field (Hancock *et al.*, 1991; Caputo, 2005) (joint deflection is discussed in more detail later).

Mutually cross-cutting joints on the other hand, may also be the result of stress field variation at time of failure. A stress state change occurs instantaneously as the primary joint forms, with the secondary joint forming subsequently. The orthogonal joint set in the

Heidehof Farm area may also have formed because of low differential stress, with principal stresses (σ_2 & σ_3) switching orientation during rock failure (refer to section 2.1.3) (Caputo, 2005), this would account for the 90 ° change in the joint orientation.

The orientations of the specific joints and the corresponding joint sets (Fig. 5.3) were described previously in section 4.2.3. The stress conditions at time of deformation can be inferred, provided that conditions required for Griffith-tensile failure are still assumed (refer to section 2.1 on Mohr-Griffith-Coulomb theory) (Fig. 2.1). Because the joints are tensile fractures (Hancock and Engelder, 1989), and assuming the host aeolianites are relatively homogeneous, isotropic, and intact, this implies the joints formed at or near the tensile strength of the aeolianites, and propagated normal to σ_3 (Secor, 1965; Sibson, 1998).

Assuming the joints are near to the same orientation as at the time of formation, the joints within the same joint set provide an σ_3 trajectory specific to that joint set, this can then be combined with other joint sets to produce an average σ_3 trajectory for an outcrop. Because the joints are typically steeply inclined to vertical in outcrop (Fig. 4.17), a near to horizontal σ_3 trajectory throughout the majority of jointed aeolianites can be suggested. This relatively horizontal σ_3 orientation supports an Andersonian stress-state for the study area (after Anderson, 1951).

In Fig. 5.3 the dominant (and assumed primary) joint set, J, indicates a σ_3 trajectory orientated NNE-SSW to E-W on average for the Southern Cape, with the less dominant joint sets providing σ_3 trajectories NE-SW on average. All the joints were previously plotted on the stereonet (Fig. 4.19), with Kamb contoured poles to the joint planes providing a σ_3 trajectory towards the NE-SW on average (local stress fields will be discussed in greater detail in section 5.6.1).

The differences in orientation and abundance of joints within either the Wankoe or Waenhuiskrans Formation can be viewed on Fig. 5.3. The joints strike typically more E-W in the Waenhuiskrans Formation, when compared to the Wankoe Formation. The Wankoe Formation (Heidehof and Groot Hagelkraal study areas in particular) have minor joint sets which reflect the Waenhuiskrans Formation joint strike trends, which implies the Wankoe Formation underwent the same episode of joint formation as the Waenhuiskrans Formation. Moreover, the Wankoe Formation is also significantly more jointed than the Waenhuiskrans Formation, indicating a longer deformation history.

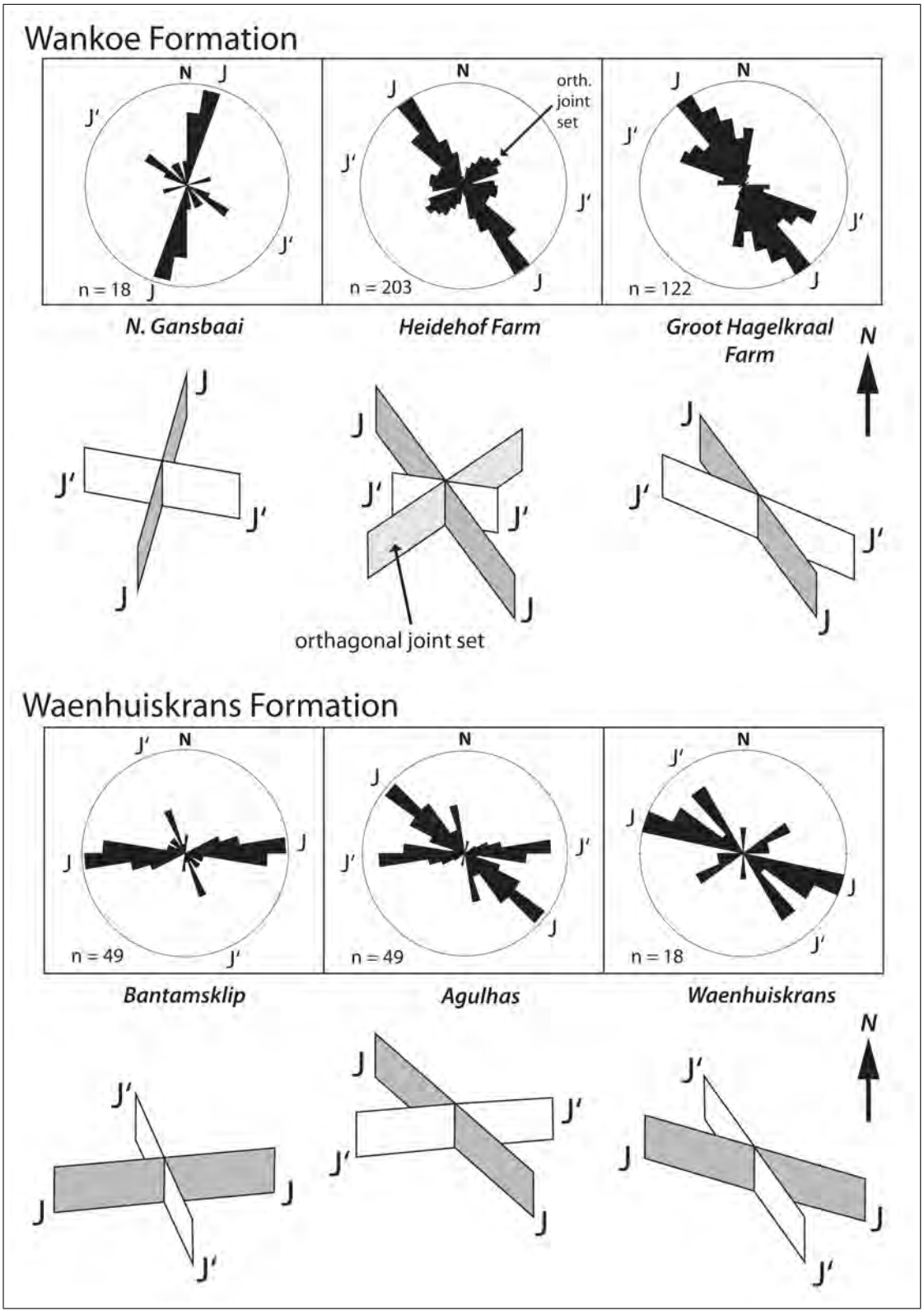

Figure 5.3: Joint strike trends for the study areas plotted as azimuth frequency plots. Discrete joint sets are indicated as J if the dominant joint set, and J' for the less dominant joint set, with the orthogonal joint set (Heidehof study area) indicated. The joint sets are simplified schematically as 3D planar representations. The least principal stress (σ_3) is assumed to be orientated perpendicular to the joint planes.

Faults and Conjugate Faults

The relatively small-scale faults (fault plane lengths on the metre-scale) on the Heidehof, Groot Hagelkraal, and Cape Agulhas study areas can be sub-divided into three groupings: normal and reverse fault arrays, isolated normal faults, and conjugate normal faults.

The normal fault array within the steeply tilted aeolinites on the Heidehof Farm (as shown on Fig. 4.18D), caused brittle deformation (deflection and offset) of the surrounding cross-bedding (refer to section 4.2.3) during fault displacement. Extension fractures in the corresponding footwalls (orientated at $\sim 30^\circ$ off of the normal fault planes) are most probably a result of shear displacement on the fault, and also cross-cut the cross-bedding. Thus the faults must have formed post-consolidation of the aeolianites, and most likely during the tilting of the aeolianites.

The normal faults have a similar orientation and fault offset directions (Fig. 4.18E), with a preferred fault dip angle of $\sim 60^\circ$. The hangingwall slip vectors are towards the ENE on average, which indicates the faults accommodated an ENE-WSW extension of the aeolianites. Moreover, the relative abundance of the normal faults within the tilted aeolianites implies a significant amount of ENE-extension may have occurred syn-tilting of the aeolianites. Therefore the normal faults may have initially been sub-vertical joints which underwent rotation post-formation (tilted with the cross-bedding) and experienced simultaneous shear to become normal faults.

The reverse fault array (as seen in Fig. 4.24C) in the tilted aeolianites, exhibit a significant difference to the normal faults; the faults are located within a section of oversteepened aeolianite which has been folded horizontal (the reverse faults are associated with brittle folds). The faults most likely formed as a consequence of the folding within the tilted aeolianite. This folding would have caused localised shortening within the fold hinges, and as the aeolianites are rheologically brittle, reverse faults formed to accommodate the resultant strain (discussed in more detail in section 5.2.2). The hangingwalls of the reverse faults offset the cross-bedding towards the NE, with brittle deformation of the sedimentary structures. The reverse fault arrays within Wankoe Formation aeolianites appear to be rare, as no other examples are found preserved elsewhere or in the Waenhuiskrans Formation.

The isolated normal fault in the Agulhas area (Fig. 4.23C) has a similar orientation and

hangingwall slip direction to the Heidehof Farm normal faults. A similar extension of the aeolianites ∼N-NE must have occurred. The single, longer normal fault in the Agulhas area, appears to have accommodated the extension of the aeolianites instead of an array of shorter normal faults (such as seen on the Heidehof Farm). The lack of tilting of the Waenhuiskrans Formation aeolianites at this locality, additionally indicates a lower level of overall deformation.

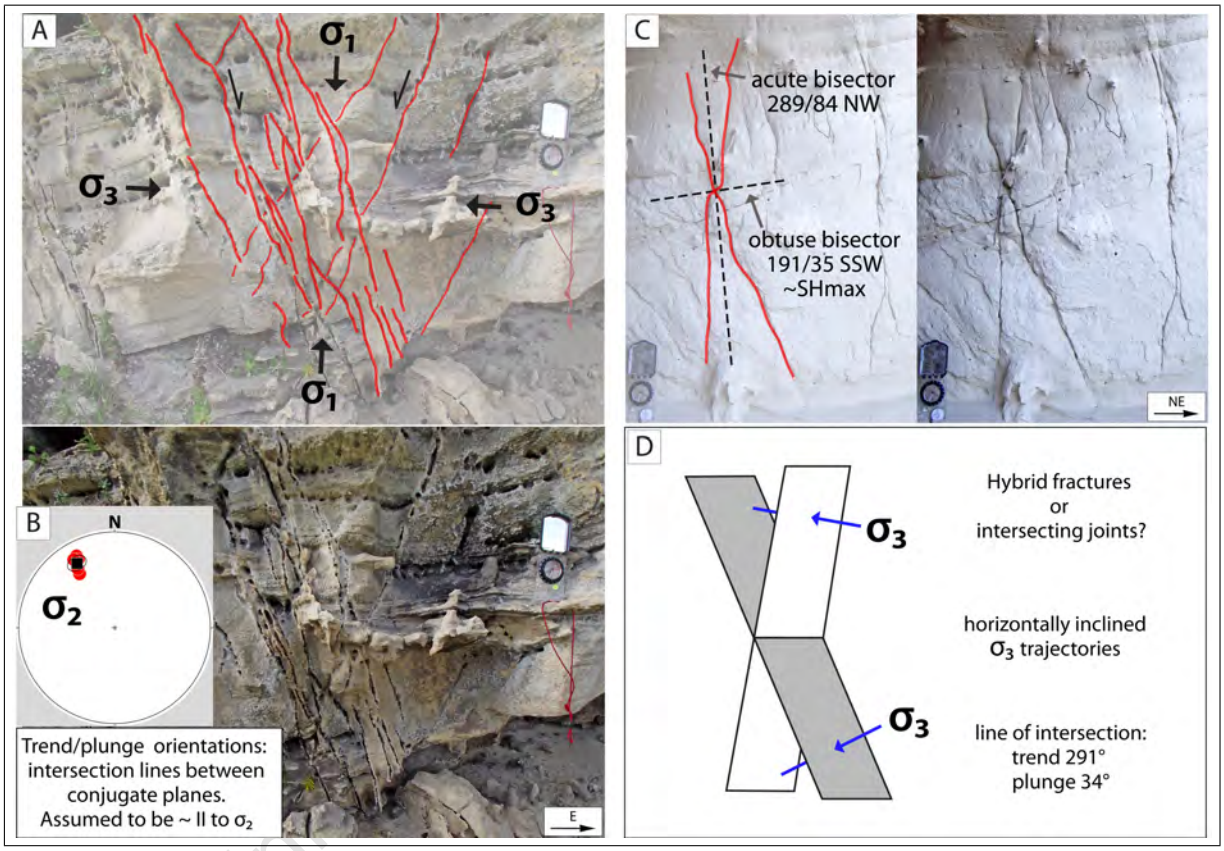

Figure 5.4: Composite interpretive figure derived from the field observations in the Groot Hagelkraal and Agulhas study areas. The principal stress axes provided, are assumed to possess orientations similar to the stress orientations at the time of fracture propagation. A) The orientation of the principal stresses in relation to an example of observed conjugate normal faults. A sub-vertical σ_1 direction and sub-horizontal σ_3 direction can be derived from the faults. B) The mean line of intersection (taken from the planes of the faults) indicate a sub-horizontal σ_2 trending ∼NW. C) Vertically intersecting joints or possible hybrid fractures (no significant observable shear) in the Agulhas area, with bisecting acute and obtuse bisectors orientated sub-vertically and sub-horizontally respectively. D) Hybrid fractures acute/obtuse bisector lines provide the respective σ_1/σ_3 orientations. On the other hand, vertically intersecting joint sets would possess σ_3 directions perpendicular to the joint planes, which consequently provide an average σ_3 orientated near horizontal. Refer to text for more details.

The conjugate normal faults on the Groot Hagelkraal and Heidehof Farms (Fig. 4.18A) are within aeolianites exhibiting lesser degrees of tilt than the aeolianites hosting the normal

and reverse fault arrays. The conjugate normal faults both cross-cut and brittlely off-set the cross-bedding, which indicates a post-consolidation time of shear fracture formation.

The dihedral angles (acute intersection angle between 45 and $\sim$50 °) as described in section 4.2.3, would suggest a 2θ angle similar to the expected $2\theta > 45$ ° angle for conjugate normal faults forming in homogeneous and intact rock (in agreement with the Coulomb-shear failure criterion) (Sibson, 1998; Ramsey and Chester, 2004) (Fig. 2.1).

Assuming the deformation features have not significantly rotated or been translated since formation, the acute bisector σ_1 is orientated sub-vertically, with the obtuse bisector σ_3 orientated sub-horizontally at time of shear failure (Fig. 5.4A). The intersection line of the fault planes indicate a $\sim$NW trending σ_2 sub-horizontal direction estimate (Fig. 5.4B & refer to Fig. 2.3). Other examples of conjugate normal fault in the Groot Hagelkraal Farm have similar orientations, and thus describe similar stress conditions.

The conjugate normal faults indicate a horizontal aeolianite extension NE-SW on average, throughout the Groot Hagelkraal and Heidehof farms. Considering the abundance of conjugate normal faulting, this implies that there was significant extension syn-tilting of the aeolianites. This extension direction is also similar to what is observed from the normal fault arrays in the steeper tilted aeolianites on the Heidehof Farm. The presence of normal fault arrays in the steeply tilted aeolianites, and conjugate normal faults in the less steeply tilted aeolianites, could indicate the degree of aeolianite tilting controls the type of fault and fault pattern.

The Hybrid Fractures

Steeply dipping fractures, which appear coeval and mutually intersect to form small dihedral angles (typically <30 °), are observed in the aeolianites on the Agulhas, Groot Hagelkraal and Heidehof farms (Fig. 4.18B & C) (see section 4.2.3). Similarly to other joints, these fractures cross-cut all sedimentary structures, suggesting the fractures formed post-consolidation.

As the fractures intersect at low angles to one another, as in the case of Fig. 4.18C, the following three explanations can possibly account for these deformation features: 1) Vertical joints propagating through non-intact rock, experience joint deflection because of stress variability, and eventually intersected one another. 2) There are low differential stress mag-

nitudes at time of fracture initiation, where σ_1-σ_3 is too low for shear fractures to form and too high for strictly tensile fractures to form. The two fractures therefore represent conjugate hybrid fractures (with assumed micro-scale shear off-set across the fractures) (after Hancock, 1985), refer to section 2.1.2 (Fig. 2.1). 3) An alternative method of steeply dipping conjugate hybrid fracture formation is considered by Hancock and Engelder (1989); Ramsey and Chester (2004), as when two proximal sub-vertical joints link together by crack propagation, typically via minor $en\ échelon$ joints between the main joints to form conjugate hybrid fractures.

Assuming these deformation features are at a similar orientation at present as at the time of formation, the orientation of the conjugate hybrid fractures/intersecting joints indicate either a sub-vertical orientation of σ_1 (acute bisector), and a sub-horizontal σ_3 (obtuse bisector) at time of fracture initiation, if considered hybrid fractures (Fig. 5.4C); if two intersecting joints, the σ_3 orientations would be sub-horizontally inclined (Fig. 5.4D).

Variability in Brittle Fractures

Variation in deformation styles and orientation of deformation features can be discussed in terms of the assumptions made about the host rocks, and the prevailing stress-state. Because joints, faults, and hybrid fractures are interpreted using the Mohr-Griffith Coulomb failure criteria (Fig. 2.1) (refer to section 2.1.1), three main assumptions are required:
1) That there is compositionally and structurally homogeneous, intact, and isotropic host rock (Sibson, 1998). 2) Stress is uniform and homogeneous through the host rock (Sibson, 1998). 3) An Andersonian stress-state prevails through the region (after Anderson (1951)).

These assumptions however do not always apply to 'real-world' geological situations, and therefore by how much the aeolianites' rock properties deviate from 'ideal' conditions (the assumptions above) for rock failure may have implications for the observed rock deformation.

Rock homogeneity and isotropy has been widely assumed thus far, however in terms of sedimentary rocks, the rock components (quartz, shell fragments, lithic fragments, calcite cement - refer to section 4.2.1), and the proportion of the said components may result in significant heterogeneity through the rock (Caputo, 2005). As each of the components have

a specific tensile/shear strengths, the volume proportion of each of the components to the whole rock, will have an effect on the overall strength of the rock unit (Jaeger and Cook, 1976; Caputo, 2005). Similarly, a bedded sedimentary rock may have varying rock strengths through subsequent beds containing different proportions of components (e.g. layers rich in calcite cement) (Caputo, 2005).

Tensile strength and stress fields are influenced by the level of cohesion and consolidation of sediments and also by rock stratification, with sedimentary structures/depositional fabrics resulting in rock heterogeneity and structural anisotropy (Jaeger and Cook, 1976; Amadei, 1996). Rock discontinuities (e.g. joints) influence the level of rock isotropy, and result in alterations to the stress field to accommodate the new discontinuities (most particularly if formed in a previously intact rock) (Caputo, 2005). Consequently, rock heterogeneities and anisotropy can effect stress, and lead to non-uniform stress fields within rocks (Amadei, 1996; Sibson, 1998).

Variability in the stress field orientation, and resulting variation in the joint/fracture/fault patterns and orientations, can occur through the exchange of principal stresses at time of rock failure (Caputo, 2005). By varying the the stress axes containing σ_1, σ_2, σ_3, will cause differently orientated fractures to form (such as possibly the case with orthogonal joint sets on the Heidehof Farm, and in Fig. 5.4D). The fractures may appear to be coeval, but could represent a temporal shift of the stress axes (possible on time-scale of seconds) (Caputo, 2005).

An Andersonian stress-state requires a planar earth surface (Anderson, 1951), which deviates from the aeolianites' concave-down and undulating surfaces on average. The vertical and horizontal stresses will adjust orientation to account for this surface and the overburden stress (follows Anderson, 1905), possibly resulting in an non-Andersonian state of stress within the aeolianites. The non-planar surface of the aeolianites result in progressively more 'Andersonian' deformation features near the centre of the aeolianite hills (higher confining stress), with altered orientations towards the edges.

All the above may account for local changes in joint and fault characteristics, and indicate a deviation from the initial assumptions made. Considering that there is some minor and local variability, the joints, faults, and possible hybrid fractures do still do exhibit significant trends in the orientation (as reflected in Fig. 5.3) and deformation style of the features

over the Southern Cape. Therefore, the assumptions with respect to the homogeneity of the aeolianites (the aeolianites are compositionally homogenoeous on average), and the Andersonian state of stress (joints and faults orientations tend to agreement with σ_v=σ_1/σ_2/σ_3) are considered to approximate well for the Southern Cape. The aeolianites are nevertheless anisotropic in places, and consequently this could have and effect on stress fields and the deformation features orientations.

5.2.2 Kink folds and Brittle Folds

Kink folds (see section 4.2.5) are angular straight-limbed folds (Fig. 4.24A & B) which involve strain accommodation along a single kink plane (defining the hinge and axial plane) or two parallel kink planes forming a kink band (Ramsay, 1967). Kink bands will form as a consequence of shear strain across cross-bedding, whilst a single kink plane forms if there is cross-bedding-parallel shortening (Ramsay, 1967). Therefore, the normal fault arrays could be related to the formation of the kink bands, due to the similar sense of shear.

As the kink folds deform the aeolianites cross-beds in a brittle manner (brittle fracture along the kink planes is common), the kink folds most likely formed post-consolidation of the aeolianites. Additionally, as the kink folds are found only in the tilted sections of the aeolianites, with the kink plane orientation varying from vertically to inclined (dip towards the NE) with the increase in aeolianite tilt, implies these features are related to the tilting event.

Alternatively, the brittle folds are different when compared to the kink folds (Fig. 4.24C & D), typically owing to the larger limb-to-limb fold widths on average (see section 4.2.5), and a more diffuse brittle deformation across the 'hinge-zone' of the folds (opposed to a single or two parallel kink planes in the kink folds/bands). The 'hinge-zone' breakages typically manifest as either reverse faults (Fig. 4.24C), breccias (intense non-systematic fracturing and cataclasis) (Fig. 4.24D), or multiple kink folds. The brittle folds also brittlely deformation aeolianite cross-beds, with no ductile features present. As the brittle folds are only found in the tilted aeolianite, this likewise implies a post-consolidation/and possible syn-tilting time of formation. From the orientations and distribution of the folds within the tilted aeolianites, these folds are the result of internal shortening and resultant buckling of the aeolianites

during tilting.

Principal stress orientations can be estimated from kink bands, with σ_1 orientated between the parallel to fold limb (orientation of the cross-bedding planes) and the normal to the kink band (the kink planes are planes of maximum shear) (Hudleston and Labao, 1993). Consequently, the kink folds suggest a horizontally orientated σ_1 in the less tilted aeolianites and a vertically inclined σ_1 in the steeply tilted aeolianites, at time of kink formation (both provide a compression direction approximately NE-SW) (Fig. 4.24A & B). Likewise the shortening direction is typically almost parallel to the angle of tilt in the aeolianites. The principal stress orientations for the brittle folds are not realistic to estimate due to the significant deformation involved in fold formation (Hudleston and Labao, 1993), but the similarity to the orientation of the kink folds suggest an approximate shortening direction NE-SW, which is near parallel to the tilt angle of the cross-bedding.

5.2.3 Cataclasites

The cataclasites (breccias and gouge units) on the Heidehof and Groot Hagelkraal Farms (Fig. 4.25) are predominantly found in the tilted aeolianites. These features cross-cut and penetrate the sedimentary structures, brittle folds, and joints (refer to section 4.2.6). The cataclastic rocks can thus be seen to have formed both post-consolidation and after the formation of the folds, joints, and faults; therefore towards the late stages of aeolianite deformation. Some joints do cross-cut the breccias in places, implying a further late extension through the aeolianites.

The fine-grained fragments in the gouge units reflect a significant level of crushing/pulverisation and particle-size reduction during cataclasis (Scholz, 1990) (Fig. 4.25C). The obliteration of original sedimentary structures during gouge formation further indicates substantial levels of deformation (Hausegger *et al.*, 2010). The sub-rounded fragments found within the gouge, imply some minor rotation (abrasive wear and erosion rounding) of the fragments during gouge formation (Hausegger *et al.*, 2010), this could indicate significant movement during cataclasis.

Alternatively, the breccias involve lower levels of deformation on average to the gouge units, which is distinguishable by the lack of total pulverisation and significant size reduction

of the fragments. The breccias which do crop out nearest to the steeply tilted aeolianites, do exhibit rotation and some pulverisation of the block fragments (Fig. 4.25A). The breccias which crop out within the least tilted aeolianites just exhibit significant unsystematic fracturing and minor off-set of the angular fragments (Fig. 4.25C). The breccias tend to crop out of the less tilted aeolianites on average, when compared to the gouge units.

As suggested by Hausegger *et al.* (2010) carbonate cataclasites (typically associated with fault action) exhibit a deformation gradient from a core zone, characterised by more gouge-rich units (the comparatively $most$ deformed rocks), to breccias ($less$ deformed rocks), into the damage zone, characterised by brittlely deformed host rocks (the $least$ deformed in comparison). Within the study areas, the distribution of the gouge, breccia, and brittlely deformed units commonly agree with this same deformation gradient. There is a gradual decrease in the degree of deformation, away from the most tilted aeolianites, towards the less tilted aeolianites in the SW.

As seen in Fig. 4.25, the outcrops of breccia and gouge units define an approximate NW-SE trend on both the Heidehof and Groot Hagelkraal Farms. The gouge units are limited to the most steeply tilted aeolianite units, and breccias to the less tilted aeolianites (and untilted aeolianites in places). The outcrop trend corresponds to the NW-SE orientation and distribution trends of the joints, faults, and folds, which implies a similar mechanism of formation.

Considering the above, the cataclasites may be the result of the following:

1) The tilting of the aeolianites caused internal buckling, extension, and flexure along discrete zones of weakness within the aeolianites (which accounts for the spatial distribution of the cataclasites). The zones of weakness would preferentially undergo brittle failure and cataclasis, separating sections of aeolianite (multiple blocks) with increasing tilt towards the NE. The tilted blocks of aeolianite would therefore be bound by localised zones of cataclasites. Additionally, the degree of tilt would change the amount of overburden stress (σ_v), by an increase of overburden by rotation-thickening of the overlying aeolianite, thus localising higher magnitudes of stress in the more steeply tilted aeolianites. Consequently, as the amount of tilt would influenced the stress distribution within the aeolianites, it will also control the level of rock deformation (which accounts for the deformation gradient).

2) Cataclasites are typical fault rocks (Scholz, 1990; Heilbronner and Keulen, 2006) which

form at low pressure and temperature conditions (Heilbronner and Keulen, 2006). The possibility of past fault activity deforming the tilted aeolianites can therefore be suggested. Cataclasites formed during earthquakes will thus crop out near and along fault surfaces (Heilbronner and Keulen, 2006), which is seen by the spatial distribution of the breccias and gouge units along the inferred trace of the Blomerus Fault (Fig. 4.25). A cataclasitic deformation gradient is also a common feature of fault zones (Caine *et al.*, 1996), and does account for the gradual decrease in the level of deformation away from the inferred trace of the Blomerus Fault.

The presence of breccias and gouge units may further explain the topography of the Heidehof and Groot Hagelkraal study areas. Cataclasites can be more incohesive and possess lower rock strengths than uncataclastically deformed rock, and will erode more easily as a result (Scholz, 1990). The valleys which extend NW-SE across the two study areas, presently separate the tilted aeolianite from the non-tilted aeolianite (Fig. 4.10, Fig. 4.11). As the tilted aeolianite possess the most deformation features, preferential erosion of the cataclasites and brittlely deformed units (within a once continuous aeolianite dune body) may have occurred since the formation of the cataclasites.

5.2.4 Soft-sediment Deformation Features

The soft-sediment deformation (SSD) features on the Heidehof Farm (Fig. 4.26) are different from the other deformation features already discussed. The ductile bending and deflection of the cross-bedding around the 'bowl' or 'plug-like' features and the distinct lack of brittle failure structures, imply these features formed in pre-consolidated aeolian dunes. The SSD features have a similar sense of rotation as the cross-bedding, indicating the tilting of the aeolianites occurred post-formation of the SSD features.

The SSD features have internal layering which either correspond to partially intact aeolian cross-beds (which exhibit off-set and ductile deformation), or are relatively massive with only remnant sedimentary structures. As a result, the SSD features all exhibit some sort of disruption, or obliteration of the primary sedimentary features. The type, method, and extent to which SSD features deform (and thus preserve layering) is controlled by the moisture content (influences internal cohesion), and the level of compaction and consolidation of

sand particles (McKee, 1979; Van Loon, 2009). The formation of SSD structures within the aeolianites on the Heidehof Farm could thus have three possible origins:

1) The SSD features are products of ancient plant (rhizoliths) or animal activity (burrows) (Klappa, 1980; Van Loon, 2009). However, the lack of root casts, karstic mineralisation, petrified roots, and palaeosol horizons which typify rhizoliths (Klappa, 1980) would indicate that this is not the origin. Animal burrows (or trace fossils) would exhibit total reworking of the interior sediments within the 'bowl', or 'plug-like' features, with no layering or partial layering preserved (Bordy, E. pers. comm. 25 Jan 2013). The evident layering of the SSD features does suggest that animal activity is not the mechanism of formation.

2) Sedimentary associated processes during aeolian dune deposition is a common cause for SSD feature formation (McKee, 1979; Moretti, 2000; Pirrotta and Barbano, 2010; Owen *et al.*, 2011). As outlined in section 2.4.1, soft-sediment deformation will typically occur as a result of overloading on slopes, gravity flows of sediment, slumping, and wave action on coast lines (McKee, 1979; Obermeier, 2009; Owen *et al.*, 2011). The SSD features are confined within dipping cross-bedding (Fig. 4.26), which indicates the SSD features formed on existing dune slopes at the time of deformation. The SSD features have a similar appearance to high-angle asymmetric folds, and slump structures (particularly the 'bowl-shaped' structures), which are commonly observed near the base of aeolian dune slopes McKee (1979). The slump and fold SSD structures form through compression of moist sediments due to sediment loading (McKee, 1979), triggered by gravity acting on the slope (Owen *et al.*, 2011). These sedimentary processes could provide a possible origin for the SSD features.

3) SSD features can also form as a consequence of earthquake activity (Moretti, 2000; Montenat *et al.*, 2007; Pirrotta and Barbano, 2010; Owen *et al.*, 2011). Seismic shaking of unconsolidated to semi-consolidated sediments can produce a wide variety of SSD features known as seismites (Montenat *et al.*, 2007). Seismites can form from suddenly applied horizontal shear stress, which causes thixotropy of the sediments and thus creates 'bowl', 'plug', and 'wedge-shaped' structures (Montenat *et al.*, 2007; Pirrotta and Barbano, 2010). Thixotropy causes a loss of internal cohesion and liquefaction of the sediments (assuming pore-space water is present), which subsequently results in disruption or obliteration of sedimentary features (Montenat *et al.*, 2007; Obermeier, 2009; Pirrotta and Barbano, 2010). Owing to

the SSD features being spatially distributed proximal to the inferred trace of the Blomerus Fault, seismically-triggered slope failure (after Owen *et al.* (2011)) or seismically-induced thixotropy of the unconsolidated aeolian sediments could account for the features. Moreover, as the SSD features on the Heidehof Farm (Fig. 4.26) do appear to be quite similar to these thixotropic wedges as described by Montenat *et al.* (2007); Pirrotta and Barbano (2010), a seismic origin for the SSD features is therefore also a possibility.

5.3 Origin of the Brittle Deformation Features

The majority of the brittle deformation features observed throughout the Southern Cape is located within the tilted Wankoe Formation aeolianites (on the Heidehof and Groot Hagelkraal Farms). Owing to this, the mechanism(s) responsible for the tilting of the aeolianites would likewise explain the origin of the deformation features. The tilting of the aeolianites and the deformation features can therefore have three postulated origins, these being the following: 1) Wave action induced undercutting of the consolidated to semi-consolidated aeolianites and eventual sea cliff collapse. 2) Sedimentary-related processes during deposition and consolidation of the aeolianites. 3) Tectonic movements within the underlying geology, possibly during and after the consolidation of the aeolianites (i.e. neotectonics). The aim of this section is therefore to compare and contrast the characteristics of each of the alternative theories, and arrive at the most plausible explanation(s) for the origin of the deformation features.

5.3.1 Wave undercutting

The Wankoe and Waenhuiskrans aeolianites are proximal to the Southern Cape coastline, and therefore could have been eroded by wave-action since the time of deposition and consolidation. As such, the undercutting and eventual collapse of the aeolianites through hydraulic wave action, would require the sea waves to be in contact with the aeolianite units (at least within the tidal range). The variation of the relative 'height' of the past sea level can thus be compared with the onshore elevation at which the aeolianites are distributed, allowing for an assessment of whether wave action could account for the tilting of the aeolianites and the

deformation features.

The Wankoe Formation was deposited and consolidated between the Late Pliocene to Lower Pleistocene (∼2.3 Ma - 1.8 Ma) (Siesser and Dingle, 1981; Malan, 1989b; Marker and Holmes, 2005) (section 3.6.2). The Late Cenozoic sea level curve in Fig. 3.5 illustrates how the relative sea level experienced two major sea transgressions (at ∼1.7 Ma & ∼1.0 Ma) since the consolidation of the Wankoe Formation (Haq *et al.*, 1987). During these subsequent marine transgressions, the sea level rose to ∼20 m - 30 m above modern sea level (Haq *et al.*, 1987). As the Wankoe Formation aeolianites distributed on the coastal shelf at ∼50 m+ above modern sea level (Heidehof & Groot Hagelkraal Farms) (Fig. 4.4), the possibility of wave undercutting the aeolianites would be unlikely. The last marine transgression possible of reaching and eroding the Wankoe Formation aeolianites was between ∼3.0 Ma - 3.1 Ma (Haq *et al.*, 1987) (Fig. 3.5).

The Waenhuiskrans Formation involved two episodes of deposition and consolidation during the Upper Pleistocene, with the Agulhas aeolianites possessing an age of ∼160 ka and the Bantamsklip aeolianites possessing a consolidation age of ∼88 ka (Bateman *et al.*, 2004) (section 3.6.3). As illustrated by the Upper Pleistocene sea level curve (Fig. 3.5) the relative sea level has undergone a single marine transgression (∼120 ka) since the consolidation of the Agulhas aeolianites, and a marine regression (∼20 ka) since the consolidation of the Bantamsklip aeolianites, with the sea level transgressing since then to the present sea level (Bintanja *et al.*, 2005). The sea level has only reached approximately the present relative sea level (0 m) during this last marine transgression (Bintanja *et al.*, 2005). The Waenhuiskrans Formation aeolianites in the Agulhas area are distributed 20 m+ above modern sea level, and the Bantamsklip area aeolianites are located at elevations of ∼50 m above modern sea level. Wave undercutting of the Waenhuiskrans is therefore only limited to the Waenhuiskrans Formation aeolianites that are at sea level (Waenhuiskrans and Quoin Point), which exhibit prominent sea cliffs but minimal deformation features (Fig. 4.6).

Although uncertainties exist regarding relative sea level reconstructions (Bintanja *et al.*, 2005), the curves utilised in this study (Fig. 3.5) correspond adequately with relative sea level research from around the world (e.g. Lambeck and Chappell, 2001; Bard *et al.*, 2002; Ramsay and Cooper, 2002; Miller *et al.*, 2012). Wave undercutting-induced collapse and resulting tilting of the aeolianites is therefore an unlikely candidate to explain the deformation

features observed in both the Wankoe and Waenhuiskrans Formation aeolianites.

5.3.2 Sedimentary Processes

Sedimentary processes potentially responsible for the deformation features have previously been outlined in section 2.4, and discussed in section 5.2.4 (SSD features).

The sedimentary processes that exist in aeolian sand dunes during deposition and consolidation, can cause faulting, folding, breccia formation, and contorted bedding of aeolian sediments (McKee, 1979). However, because the deformation processes are associated with deposition, initial consolidation and compaction of sediments, the sediments are required to be unconsolidated to at most partially consolidated at the time of deformation (Owen *et al.*, 2011). Furthermore, sedimentary processes responsible for deformation within aeolian dunes are typically restricted to slopes (McKee, 1979; Pirrotta and Barbano, 2010; Owen *et al.*, 2011).

The deformation features pervasively penetrate the interior of the Wankoe and Waenhuiskrans Formation aeolianites, and crop out on either side of the outcrops. The deformation features are therefore not confined to the original aeolian dune slope (the cross-bedding planes) processes such as overloading, sediment avalanche (semi-consolidation), or mass debris flows (post consolidation). Moreover, the deformation features all involve the brittle deformation of consolidated aeolianite. This implies that the SSD features are the only observed syn-deposition deformation of the aeolianites (section 5.2.4).

Additionally, sedimentary processes commonly produce deformation features which are randomly distributed and orientated, with irregular/varying deformation styles (depending on specific slope conditions, moisture content, compaction of sediment) (McKee, 1979). In comparison, the observed deformation features in both the Wankoe and Waehuiskrans Formation exhibit significant trends in orientation, and exhibit distinct similarities within specific deformation feature types, throughout the different study areas (tens to hundreds of km's apart).

Karstic dissolution does cause deformation of carbonate rocks, with collapse features being formed by the dissolution of $CaCO_3$ (Owen *et al.*, 2011) (refer to section 2.4.2). However, karstic collapse structures would likewise possess random distributions, deforma-

tion styles, and orientation trends. This would differ greatly to the observed systematic and consistent brittle deformation features.

The coincidence of Wankoe Formation aeolianites, at both the Heidehof and Groot Hagelkraal farms, exhibiting the same deformation features and rotation of the aeolianites (the Farms are situated significantly distantly apart (Fig. 4.8)) implies that the tilting of the consolidated aeolianites is unlikely to be the consequence of sedimentary processes, or mass debris flows. Sedimentary processes are therefore unlikely to be responsible for the brittle deformation features observed throughout the Southern Cape. For this reason, the geological evidence indicates that another larger-scale and pervasive process is responsible for both the tilting and deformation of the aeolianites.

5.3.3 Neotectonics

Considering both wave induced collapse and sedimentary process have been shown to inadequately account for both the tilting and deformation features observed in the field areas, a neotectonic source is required to be examined. Tectonic movements within the underlying geology would cause significant deformation of a cover sequence (Schlische, 1995; Willsey *et al.*, 2002; Finch *et al.*, 2004) (as outlined in section 2.5.2). Potential earthquake sources (faults) and the geometry and extent of these faults need to thus correspond accordingly with the observed distribution of deformation features and the tilted units within the Wankoe and Waenhuikrans Formation aeolianites (the cover sequence).

Faults previously suggested by Andersen and Andreoli (1990) within the underlying geology, and the remote sensing images (Fig. 4.1, Fig. 4.2) indicate three potential faults within the study areas. These are the Blomerus, Struisbaai, and Brandfontein faults, which have the respective inferred traces viewable on Fig. 4.8.

The position of the tilted aeolianite units in the Heidehof and Groot Hagelkraal Farm areas relative to the Blomerus Fault, can be viewed on the maps in Fig. 4.10, Fig. 4.11 and on the geological cross section Fig. 4.12. The tilted aeolianite units are located proximal to the inferred trace of the Blomerus Fault in both study areas, with the most tilted aeolianites positioned directly on the fault trace. The degree of tilt of the aeolianites can be seen to also increase from the SW to the NE towards the inferred trace of the Blomerus Fault, with

the aeolianites on the NE-side of the fault trace exhibiting no tilt (refer to section 4.2.4, and section 5.1.2). The Blomerus fault can therefore be considered an axis over which the aeolianites change from an un-tilted state, to being significantly rotated.

As discussed by Willsey *et al.* (2002), fault displacement on an underlying blind fault (reverse or normal displacement sense) will produce drag-folds in the overlying strata (section 2.5.2). Both the orientation of the tilted cross-beds and the downward space required to rotate the aeolianites to the degree observed, can be accounted for by the formation of a monocline-type drag fold (Willsey *et al.*, 2002). The monocline drag fold would be produced by a blind normal fault in the underlying geology (down-faulted hangingwall on the SW-side of the inferred Blomerus fault trace running ∼NW-SE) (Willsey *et al.*, 2002). Whether the Blomerus Fault is a normal fault will be discussed later, however the tilting of the aeolianites does seem to be associated with the Blomerus Fault, with past fault movement being the cause of rotation.

The joints on the Heidehof and Groot Hagelkraal Farms have strike trends, which on average are parallel or inclined to the inferred trace of the Blomerus Fault. The conjugate normal faults (Groot Hagelkraal Farm), and possible hybrid fractures (Agulhas area), both possess intersection lines (between shear fracture planes) which trend approximately parallel to the Blomerus Fault and the Struisbaai Fault respectively. These deformation features indicate a NE-SW extension over the Blomerus Fault trace, and a ∼N-S extension over the Struisbaai Fault trace.

Joints are known precursory features to fault development (Peacock, 2001; Blenkinsop, 2008) and can imitate the pre-faulting stress field (Peacock, 2001). Joints forming syn-fault movement (co-seismic), will reflect the related stress field and geometry of the fault (Peacock, 2001). As the joints commonly increase in abundance towards the inferred Blomerus and Struisbaai Fault traces, it could be suggested that at least some of the joints are associated with past fault movement (co-seismic or post-seismic related extension features) (Peacock, 2001). The spatial distribution of the joints in the North Gansbaai and Bantamsklip study areas, although in the vicinity of the inferred trace of the Blomerus Fault, do not have strike trends which correlate with the fault trace, as do some joints found on the Heidehof and Groot Hagelkraal study areas (non-seismic deformation features).

There is a significant lack of joints cross-cutting aeolianites away from the inferred fault

Blomerus and Struisbaai fault traces. The joints observed in the Waenhuiskrans study area do not correlate with any known or inferred faults, which implies these joints formed as a consequence of prevailing regional extensional stress and resulting strain.

The spatial distribution and orientation of brittle folds, kink folds, small-scale faults, and cataclasites on the Heidehof and Groot Hagelkraal Farms are predominantly found within the tilted aeolianite units, and have orientation trends similar to the inferred trace of the Blomerus Fault. The level of deformation, most particularly with regards to the breccias and gouge units, increase towards the NE on the SW-side of the inferred trace of the Blomerus Fault. This deformation gradient is a common feature of the surface expression of a fault zone (Scholz, 1990; Heilbronner and Keulen, 2006). The deformation features are therefore related to fault movement on the Blomerus Fault within the underlying geology.

The tilting of the aeolianites (Heidehof and Groot Hagelkraal study areas) and the brittle deformation features (North Gansbaai, Heidehof, Groot Hagelkraal, and Bantamsklip study areas) can be linked to tectonic movement on the Blomerus Fault, at some time post-consolidation of the aeolianites. However, drag folds can form because of readjustment of a cover sequence to movement on an underlying blind normal fault (Fagereng, A. pers. comm. 2 Sept 2013). Consequently, there is a difference in strain rate between the formation of a monocline drag fold and the faulting within the underlying geology. And as such, some deformation features, related to the readjustment of the Wankoe Formation aeolianites, may have formed some time after the actual faulting event (post-seismic features).

The brittle deformation features found in the Agulhas study area can additionally be linked to past movements on the Struisbaai Fault, at some time post-consolidation of the aeolianites. It is important to note, however, that no evidence for past tectonic activity can be linked to the Brandfontein Fault (lack of deformation features on or near the fault trace).

The SSD features proximal to the inferred trace of the Blomerus Fault, could likewise have been produced by fault movement and subsequent seismic shaking on the Blomerus Fault (Montenat *et al.*, 2007; Pirrotta and Barbano, 2010; Owen *et al.*, 2011). The presence of possible 'seismites' could thus indicate an initial fault movement during the deposition of the aeolianite units on the Heidehof Farm. The origin for the SSD features is nevertheless not definitely tectonic, with sedimentary processes a plausible alternative for the formation of these features.

Considering the deposition and consolidation ages of the Wankoe and Waenhuiskrans Formation, neotectonics can therefore be considered the most likely cause for the tilting and brittle deformation features within the respective aeolianite units.

5.4 The Large-scale Faults

The brittle deformation features and the tilting of the aeolianites have been linked to either the Blomerus or Struisbaai faults. As a neotectonic cause for the deformation features has been shown most likely, the faults proposed as palaeoearthquake sources need to be better understood. An examination of the faults will explain how and why the cover sequence (Wankoe and Waenhuiskrans Formations) deformed during palaeoearthquake(s). The aim of this section is thus to discuss the geometry of the faults, the faults characteristics, how the faults formed/origin, and integrate the field evidence with remote sensing evidence and theory. As the majority of deformation features and aeolianite tilting is associated with the Blomerus Fault, this fault will be the main focus of this section, with the other faults discussed in lesser detail.

5.4.1 Blomerus Fault

As already outlined in section 3.3.3, the underlying geology of the Southern Cape underwent the last major extensional tectonic episode during the Break-up of Gondwana and the subsequent development of the Agulhas-Falklands Fracture Zone (AFFZ), between 140 Ma to 65 Ma (Hälbich, 1983; Paton, 2006). This extensional tectonic episode resulted in numerous onshore and offshore S to SW-dipping listric normal faults, with hangingwall down-faulting towards the south (Von Veh, 1992; Paton, 2006) (Fig. 3.3).

Normal faults typically strike E-W within the Southern Domain of the Cape Fold Belt and NW-SE within the Syntaxis domain (Von Veh, 1992). The sub-surface geometry of the normal faults was determined by Viljoen (1992); Paton (2006), with the onshore and offshore normal faults exhibiting fault plane dip angles of $\sim 60^\circ$ on average (Fig. 5.5B). As the Blomerus Fault is within the zone of post-Gondwana extensional fault development, other Cape Fold Belt/Gondwana breakup-related normal faults can be used as geometric analogies

for faults within this study (assumed to be the similar if not the same).

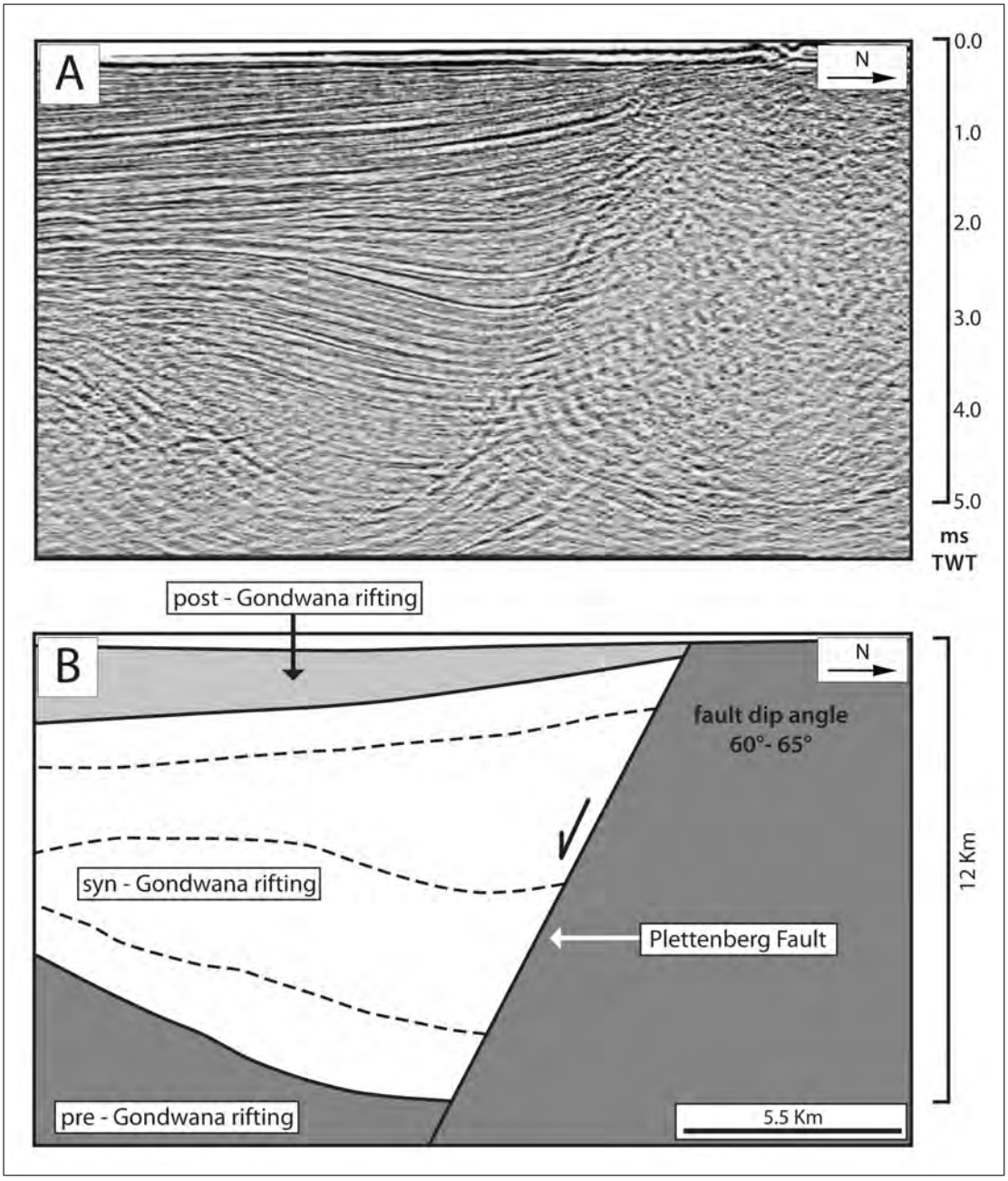

Figure 5.5: Seismic section of the Plettenberg Fault within the Outeniqua Basin offshore the Southern Cape. A) Two way time seismic section. B) True depth section annotated with the (pre, syn, and post) Gondwana rift sediments. The planar nature and dip angle of the fault is used as an approximation of the faults found onshore in the Southern Cape. The figure is adapted from Paton (2006)

As illustrated in Fig. 5.6 (and postulated in section 5.3.3), the down-faulting of the hangingwall on the SW-side of the Blomerus fault would displace the overlying aeolianites downward. During hangingwall subsidence, the aeolianites would be expected to either tilt simul-

taneously or readjust over time to form a monocline-type drag fold (Schlische, 1995). The level of rotation in the aeolianites is determined by the relative horizontal distance from the propagating fault plane and fault tip (Willsey *et al.*, 2002). The greatest rotation of rock units is above the centre of the fault within the hangingwall (and within the cover sequence) (Schlische, 1995; Willsey *et al.*, 2002) (Fig. 5.6D). Less tilted aeolianites are expected above the fault tip, and away from the fault plane (Fig. 5.6A & F), with minor rotation to no tilting of the footwall units (Fig. 5.6F) (Schlische, 1995). The tilted aeolianites in the Heidehof and Groot Hagelkraal study areas conform with a monocline fold over a blind normal fault (Willsey *et al.*, 2002).

The smaller-scale normal fault arrays in the very steeply dipping aeolianites (Fig. 5.6D) dip at $\sim 60^\circ$ towards the NE on average. The main Blomerus fault plane is assumed to dip towards the SW with a dip angle of $\sim 60^\circ$. The dip orientation of the smaller-scale normal fault arrays ($\sim 60^\circ$ is the expected angle for Andersonian normal faults to form in homogeneous and intact rock (Anderson, 1951)). If formed during the tilting event, the faults are co-seismic deformation features, and can be considered to be secondary antithetic faults off of the main Blomerus Fault (the faults have formed at the expected 2θ angle to σ_1 for Mohr-Coulomb shear failure (Ramsay, 1967)). These secondary faults accommodated the aeolianite extension during monocline folding and rotation during hangingwall subsidence, by forming fault-bound blocks in the hangingwall with decreasing rotation levels away from the fault plane (Fig. 5.6) (refer to section 5.1.2).

The kink folds and brittle folds can be linked to the both the formation of the fault-related monocline fold and to shear on the antithetic normal faults. A monocline drag fold above a blind normal fault can be sub-divided into an anticline component in the footwall and above fault-tip, and a syncline component in the hangingwall (Schlische, 1995). The monocline components will have zones of shortening related to fold curvature, with these zones within the base of the footwall anticline, and within the top of the hangingwall syncline (Ramsay, 1967). To accommodate this shortening the aeolianites developed kink and brittle folds. The kink folds may also have formed to accommodate shear strain at the tips of the antithetic normal faults (Ramsay, 1967). The brittle folds and kink folds are consequently syn-drag fold deformation features.

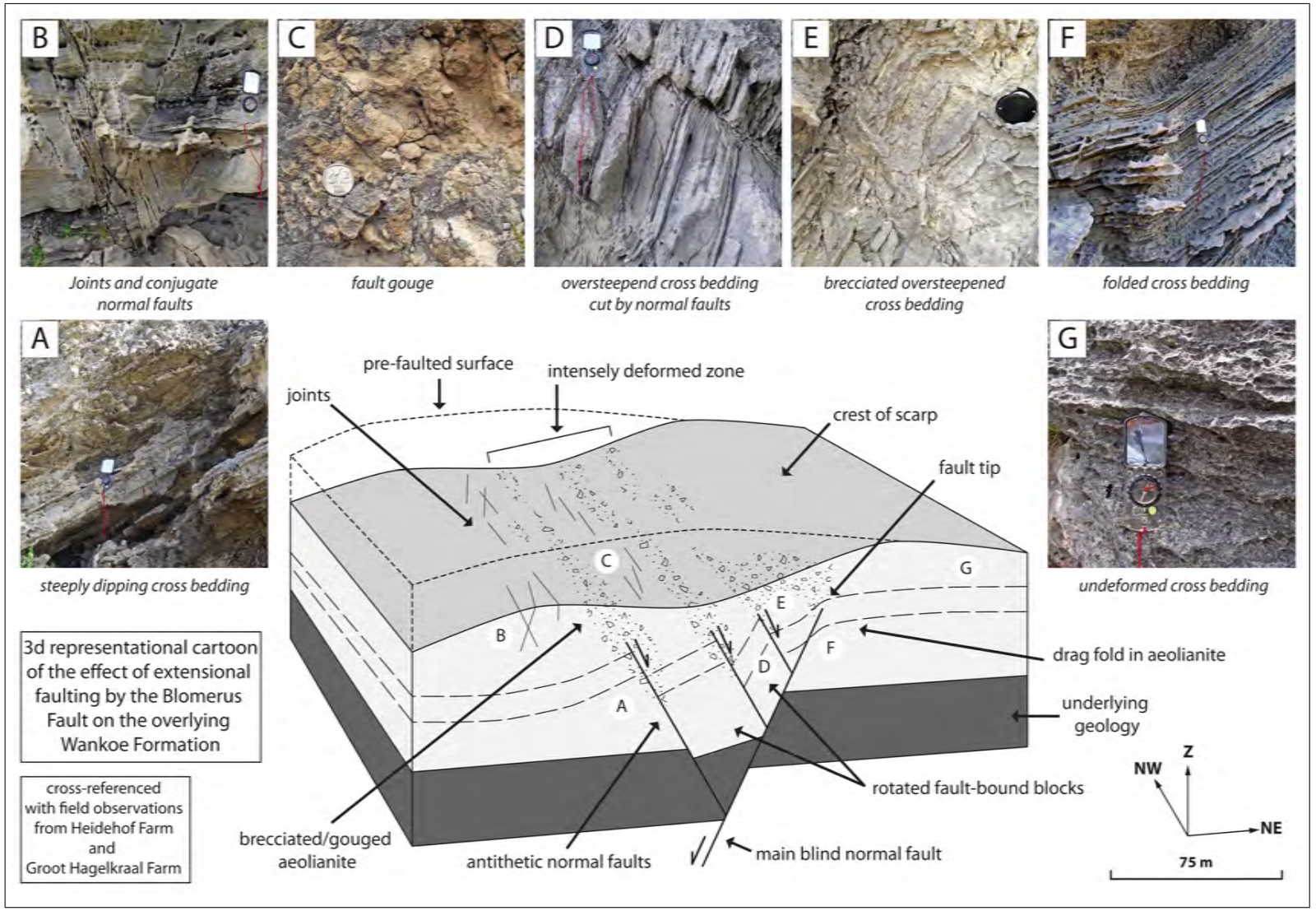

Figure 5.6: Annotated 3D cartoon describing the effect of fault movement on the Blomerus Fault to the overlying aeolianites (the cover sequence). Actual field observations (A - G photographs) are linked to features in the fault diagram. The main Blomerus Fault is assumed planar for this example. See text for more details. Figure orientated to the actual field setting and vertically exaggerated.

The joints which formed as a result of aeolianite extension during monocline fold development are located proximal to, and on the Blomerus Fault (section 5.3.3). These deformation features provide an average sub-horizontal least compressive stress (σ_3) $\sim$NE-SW, or approximately perpendicular to the Blomerus Fault. Assuming an Andersonian state of stress, and that the co-seismic stress field at the time of faulting is reflected in the joints, a σ_3 direction orientated horizontally perpendicular to the fault plane, would further support the Blomerus Fault as a blind normal fault rather than a strike-slip fault (Anderson (1905, 1951)).

The cataclasites distributed along the Blomerus Fault (Fig. 5.6C & E) have already been shown to be the result of brittle flexure of the aeolianites during tilting (fold breccias), and possibly by brittle shear failure of the aeolianites themselves during active fault movement (as previously discussed in section 5.2.3). As breccias and gouge units are typically the result of earthquake activity on a fault (Heilbronner and Keulen, 2006), the distribution of the cataclasites delineate the surface fault zone associated with the Blomerus fault. Additionally, the outcrop distribution which characterises the cataclasites around the inferred trace of the Blomerus Fault, could indicate the Blomerus Fault is not a single fault plane, but multiple antithetic faults, and possible splays. This reasoning agrees with the field evidence, with the smaller-scale normal faults are interpreted as antithetic to the main Blomerus Fault. The cataclasites can therefore be assumed to be the surface expression of the Blomerus Fault (and possible splay faults) and the secondary antithetic faults.

From the work done by Andersen and Andreoli (1990); Viljoen (1992); Paton (2006) and the field evidence from this study, the Blomerus Fault is most likely a normal fault with a SW-dipping fault plane (or possibly multiple SW-dipping fault splays) possessing an inferred dip angle of $\sim$60 $^\circ$ on average, with NE dipping antithetic normal faults. At depth the Blomerus Fault may dip less steeply, with a typical listric geometry (as observed in other Gondwana breakup normal faults (Paton, 2006)), but considering the near surface scope of this study, the listric geometry cannot be confirmed.

The length of the Blomerus Fault can be estimated from the lineaments through the aeolianites, as shown on Fig. 4.1 and Fig. 4.2 and the inferred fault trace on the maps (Fig. 4.8, Fig. 4.9, Fig. 4.10, Fig. 4.11, Fig. 4.13) indicating a fault length of $\sim$30 km. This fault length can be further extended into the Walkerbay and Quoin Point areas if the associated

dune lineaments are taken into account.

Dune lineaments have been linked to faults previously by De Beer (2012), as where holocene dune deposits collect along buried fault scarps Fig. 5.7. The Walkerbay and Quoin Point dune lineaments possess a combined length of ∼20 km, and orientations of ∼140 ° and 135 ° respectively. The dune lineaments are therefore similar to the Blomerus Fault trace orientation and lie on the same line as the Blomerus Fault across the Southern Cape. Consequently, the dune lineaments can be suggested to be surface expressions of the Blomerus Fault through the Walkerbay and Quoin Point areas. The Blomerus Fault thus extends from the Walkerbay area to Quoin Point in a potentially segmented manner (refer to remote sensing section 4.1); a length of ∼50 km or more (if the fault extends off shore).

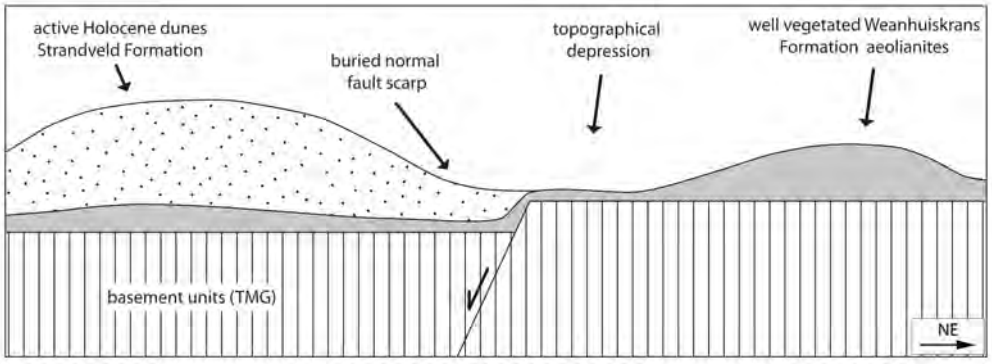

Figure 5.7: A cartoon cross section through a dune lineament. An older fault scarp, formed from normal faulting, acts as a sand transport obstacle, allowing younger unconsolidated aeolian sediments to accumulate at the base of the scarp. The collecting sediment will eventually result in significant dune development parallel to the buried fault scarp. Figure not to scale, and adapted from De Beer (2012).

The Blomerus Fault trends ∼140 ° (approximately NW-SE on average) across the Southern Cape (see section 4.2.2). The orientation of the Blomerus Fault initially suggests it is part of the Cape Fold Belt Syntaxis-related faults (as observed in the change in orientation of the Worcester Fault to the north of the Southern Cape) (Von Veh, 1992) (Fig. 3.2). The other known normal faults in Southern Cape are predominantly orientated E-W to ENE-WSW within the Cape Fold Belt Southern Domain (e.g. the Elim Fault), with a southward change in strike as the Syntaxis Domain is approached (Andersen and Andreoli, 1990; Von Veh, 1992). The orientation of Blomerus Fault is therefore somewhat anomalous within the Southern Cape, and also appears to cross-cut the NE-SW trending fold structures which characterise the Syntaxis (Von Veh, 1992).

The Blomerus Fault is orientated approximately parallel to the strike of the Agulhas Falklands Fracture Zone (AFFZ) related normal faults (extensional direction orientated NE-SW) (Fig. 3.3), and parallel to both the Cape Dyke Swarm dykes (trend NW-SE), and the magnetic anomalies related to Mesozoic-age sea floor spreading to the SW of South Africa (trend NW-SE) (Von Veh, 1992; Thomson, 1999; Paton, 2006). The similarity of the Blomerus Fault to the Gondwana break-up related dykes and the sea floor spreading pattern, indicates the Blomerus Fault formed during the rifting of Gondwana and the subsequent extensional-tectonics and not by the reactivation of a Cape Orogeny thrust fault (an origin similarly postulated for the other known NW-SE trending normal faults in the Southern Cape (Andersen and Andreoli, 1990; Von Veh, 1992)). As a result, the Blomerus Fault can be considered an onshore AFFZ-related normal fault. The age of the dykes (refer to section 3.3.3) is given between 150 Ma - 130 Ma (Trumbull *et al.*, 2007), which combined with the AFFZ being active from 130 Ma to approximately 65 Ma (Ben-Avraham *et al.*, 1997), provides a potential age for the Blomerus Fault within the underlying geology.

5.4.2 Brandfontein Fault

The Brandfontein Fault is already postulated from aeromagnetic surveys done by Andersen and Andreoli (1990), with the corresponding lineament viewable on Fig. 4.1 and Fig. 4.2, and the inferred fault trace mapped on Fig. 4.14. Unlike the Blomerus Fault, the Brandfontein Fault is well in the Southern domain of the Cape Fold Belt (Von Veh, 1992) (Fig. 3.2), and possesses an approximately ESE-WNW strike across the Agulhas headland (see section 4.2.2).

The Enon Formation (as already discussed in section 5.1.3) is found to crop out to the south of the inferred trace of the Brandfontein Fault. The presence of the Enon Formation as a known half-graben in-fill deposit (Viljoen, 1992), indicates that the Brandfontein Fault plane has a southward dip. This interpretation was already considered on the geological cross section Fig. 4.15 and from the field evidence, which corresponds to Fig. 5.5B. The geometry of the fault would therefore be considered similar to the AFFZ normal faults mapped offshore in the Bredasdorp - Outeniqua Basin (Fig. 3.3 (Paton, 2006). The Brandfontein Fault can therefore be suggested to also be an AFFZ-related normal fault, and due to having syn-rift

deposits (Enon Formation) associated with it, was reactivated or formed during the Late Jurrasic - Early Cretaceous break-up of Gondwana (Viljoen, 1992).

As previously mentioned in section 5.3.3, no neotectonic structures are associated with this fault, but the confirmation of an onshore Gondwana breakup age faults within the study area, does suggests that the presence of other Gondwana breakup faults can feasibly exist within the Southern Cape.

5.4.3 Struisbaai Fault

The Struisbaai Fault is also already postulated from aeromagnetic surveys done by Andersen and Andreoli (1990), with the corresponding lineament viewed on Fig. 4.1 and Fig. 4.2, and the inferred fault trace mapped on Fig. 4.14. This fault possesses a similar orientation (approximately WNW-ESE to E-W fault strike) to the Brandfontein Fault and thus also to the offshore AFFZ-related normal faults (Fig. 3.3) (refer to section 4.2.2).

The Struisbaai Fault exhibits an arcuate trace, with the fault strike becoming more WSW-ENE as it traverses westward; which is considered a common feature of faults within the Southern Cape as they approach the Cape Fold Belt Syntaxis from the Southern domain (Fig. 3.2) Von Veh (1992). The underlying geology of the Agulhas headland is characterised by a E-W trending northward-verging over-turned anticline (Von Veh, 1992). The fold has also been suggested to be through-faulted by a south-dipping thrust fault (Von Veh, 1992). The Struisbaai Fault therefore initially formed as a thrust fault during the Cape Orogeny (Johnston, 2000; Paton *et al.*, 2006). From the aeromagnetic survey and structural analysis work by Andersen and Andreoli (1990), the Struisbaai fault reactivated during the Gondwana breakup (the geophyiscs indicate significant down-faulting of the hangingwall on the south-side of the Struisbaai Fault).

Cape Orogeny thrust faults which reactivated as normal faults during later extensional tectonics, can have fault plane dips between 45 ° - 60 ° (Paton *et al.*, 2006). The Struisbaai Fault consequently could have a shallower dipping fault plane geometry than the Blomerus Fault (<60 °).

The deformation features in the Waenhuiskrans Formation at Agulhas can additionally provide some indication of the subsurface geometry of the Struisbaai Fault. The isolated

normal fault observed in the Agulhas area (located on the inferred trace of the Struisbaai Fault) indicates an extensional direction approximately N-NE (refer to section 5.2.1). Down-faulting of the hangingwall of the Struisbaai Fault would cause subsidence and extension on the south-side of the fault, and extension of the aeolianites over the fault trace. The isolated normal fault could thus be an antithetic secondary fault to the main Struisbaai Fault (similar to what is observed in the Heidehof Farm area). The possible hybrid fractures observed to the south, and in close proximity to the inferred fault trace, may also indicate a splaying upwards of the Struisbaai Fault, with joints and hybrid fractures developing within the hangingwall cover sequence due to lower vertical stress (Sibson, 1998; Finch *et al.*, 2004).

The Waenhuiskrans Formation aeolianites are not tilted in the Agulhas area, indicating no fault-related drag folding of the cover sequence, and a relatively lower level of deformation in comparison to the aeolianites proximal to the Blomerus Fault. The limited reactivation of the Struisbaai Fault (minor displacement on the fault) may be linked to the dip angle of the fault. The fault is not optimally orientated to reshear given a prevailing palaeostress field (after (Sibson, 1985)). The Struisbaai Fault (and related deformation features) however does show evidence of neotectonic activity in the Agulhas area since the deposition and consolidation of the Waenhuiskrans Formation aeolianites.

5.5 Relative Timing and Age of Deformation Events

The cross-cutting relationships between different deformation features and the sedimentary features of the Wankoe and Waenhuiskrans Formation, provide a relative timing for the formation of the deformation features (deformation sequence), and the age of the deformation event(s). Owing to the abundance of preserved deformation features within the Heidehof and Groot Hagelkraal study areas (Blomerus Fault), these areas will provide the predominant information towards constraining the deformation sequence related to normal faulting. The differences in types of deformation features associated with the individual faults, implies there are different deformation levels and deformation sequences between the Blomerus and Struisbaai faults. Therefore, this section aims to outline a deformation sequence for the Blomerus Fault, and compare it to the Struisbaai Fault. Moreover, this section will provide a relative age for the preserved palaeoearthquakes on the Blomerus and Struisbaai faults.

5.5.1 Deformation Sequence

The Blomerus Fault appears to have deformed the overlying Wankoe Formation (and the Waenhuiskrans Formation in the Bantamsklip study area) in at least one faulting event; although if the SSD features are considered seismites, at least two Blomerus Fault-related palaeoearthquakes can be suggested. Similarly, the Struisbaai Fault appears to have deformed the overlying Waenhuiskrans Formation aeolianites in at least one faulting event.

The deformation sequence for the Blomerus Fault-associated deformation features in the Wankoe Formation aeolianites (and on Fig. 5.6) is illustrated in Fig. 5.8. The deformation sequence is sub-divided into pre-consolidation deformation, post-consolidation deformation, pre-seismic deformation, co-seismic deformation, and post-seismic erosion to fully describe the sequence of deformational events.

The sequence initiates (Fig. 5.8A) during the Late Tertiary marine regressional phase (Siesser, 1972; Malan, 1989b), with the initial accumulation and deposition of aeolian sands over the Blomerus Fault (effectively creating a blind normal fault). Before consolidation, either sedimentary-related processes or an initial faulting event causes soft sediment deformation (SSD) structures to form in the overlying aeolian sands (Owen *et al.*, 2011) (Fig. 5.8B).

Consolidation of the aeolian sands (Fig. 5.8C) during the subsequent Lower Pleistocene marine transgression phase (Bateman *et al.*, 2004), preserved the internal sedimentary structures and the SSD structures.

Regional tectonic stress fields within the upper crust propagate into the surficial consolidated aeolianites (Fig. 5.8D). Extensional stress conditions results in wide-spread elongation of the aeolianites, which is accommodated by subsequent joint formation (Engelder, 1987). These joints cross-cut the sedimentary features and constitute the pre-seismic deformation features (alternatively known as non-seismic tectonic deformation).

Regional stress acting on the Blomerus Fault (assumed to have been favourably orientated to the prevailing stress field) causes elastic strain build-up and eventual shear failure of the Blomerus Fault (Sibson, 1985; Etheridge, 1986). Shear failure of the fault results in hangingwall subsidence, which in turn causes an initial NE-SW extension and subsidence of the overlying Wankoe Formation aeolianites above the Blomerus Fault (Fig. 5.8E). The aeolianite extension is accommodated by conjugate normal faults and joints (Blenkinsop,

2008). The subsidence of the aeolianites induces initial tilting, and possible early brecciation of the aeolianites. A fault-related drag fold begins to form within the cover sequence (Willsey *et al.*, 2002).

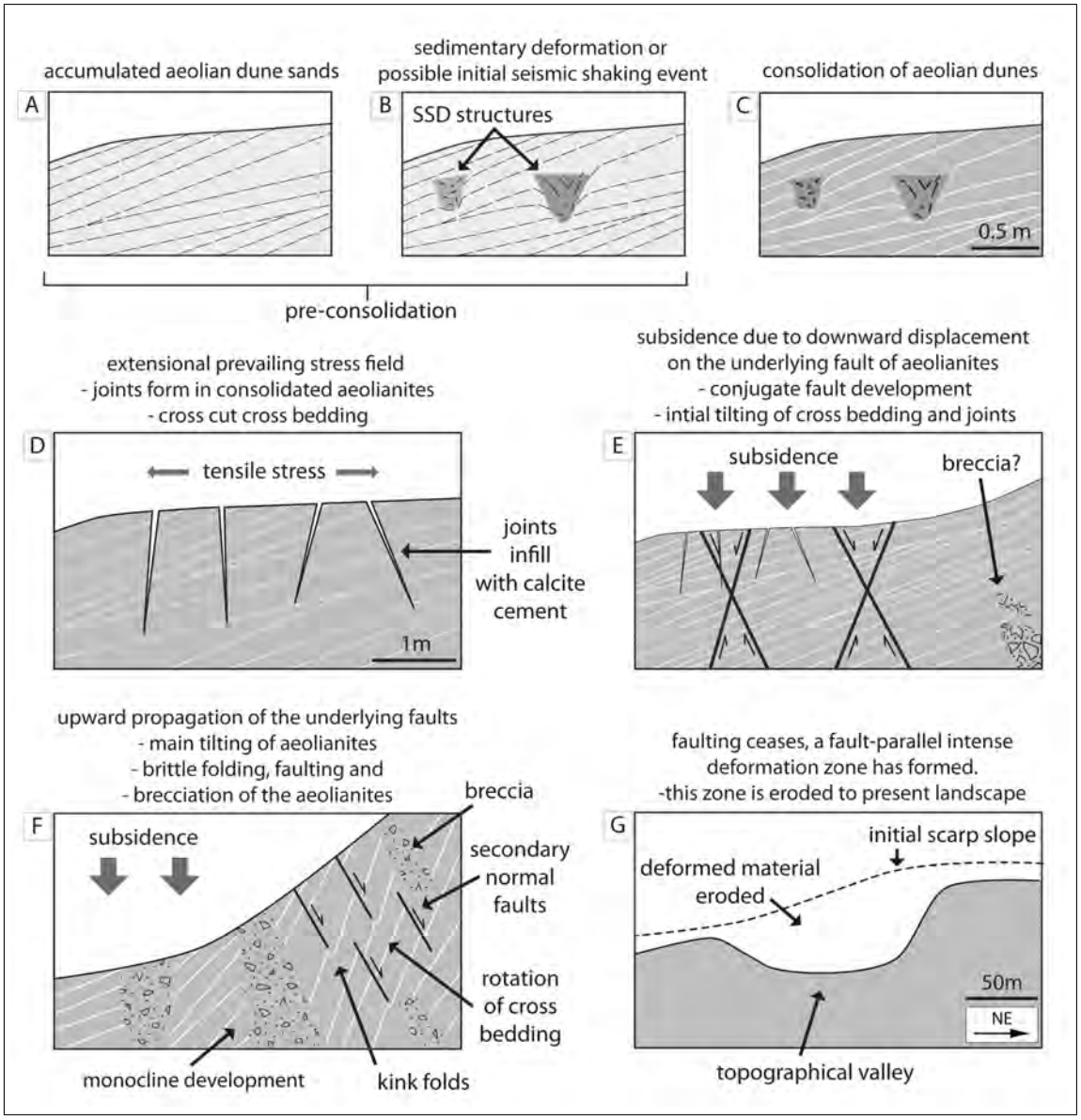

Figure 5.8: A cartoon representation of the deformation sequence as seen in the Blomerus Fault affected Wankoe Formation aeolianites. All representation figures are vertical cross-sections of the aeolianites, and are not necessarily to scale. Refer to the text for details regarding the different deformation stages.

With continued displacement on the Blomerus Fault (Fig. 5.8F), the fault propagates upwards into the Wankoe Formation aeolianites (Schlische, 1995; Willsey *et al.*, 2002; Finch

et al., 2004). During and after fault propagation, the subsiding hangingwall causes significant rotation and tilting of the aeolianites (Willsey *et al.*, 2002), with related brittle folding. Contemporaneously to the rotation of the aeolianites, secondary antithetic faults develop (cross-cut the tilted cross-bedding) to the main Blomerus Fault, with subsequent kink folding of the aeolianites. The combination of upward fault propagation and aeolianite drag folding, results in abundant brecciation and formation of gouge units. The breccias and gouge units obliterate all sedimentary features and delineate the fault zone of the Blomerus Fault (Heidbach *et al.*, 2010). With post-faulting readjustment of the Wankoe Formation aeolianites to the underlying geology over time, the monocline drag fold now fully develops. Drag fold-related late extension related joints cross-cut the breccias and kink folds in places (Ramsay, 1967; Willsey *et al.*, 2002).

The post-seismic phase involves the erosion of the heavily deformed aeolianites, which surround the upward propagated Blomerus Fault core (Fig. 5.8G). The low rock strength and cohesion of the breccias, gouge units, and heavily jointed and faulted aeolianites, leads to preferential erosion of these units (Scholz, 1990). The erosion forms topographical valleys (and scarps/truncated aeolianite outcrops in places) delineating the trend of the Blomerus Fault in the present landscape. Surviving breccia, gouge units, antithetic normal faults, and joints are still viewable in the less tilted aeolianite units (which have lower levels of deformation, and thus higher preservation potential).

The deformation sequence describes a general increase in differential stress (and strain) over time. The joints characterise the pre-seismic deformation features due to low differential stress, and with higher stress magnitudes, shear fractures, folding, and cataclasites preferentially form (Jaeger and Cook, 1976). It can therefore be suggested a palaeoearthquake on the Blomerus Fault lead to a transient increase of the differential stress, with consequent relatively high strain rates (Sibson, 1986). Owing to the brittle rheology of the aeolianites, relatively high differential stress and high strain rates, at low temperatures (earth surface conditions) abundant brittle deformation features formed within the Wankoe Formation.

The relatively lower levels of deformation in the Bantamsklip study area indicate the deformation sequence only progressed up to the point of Fig. 5.8D, with the Waenhuiskrans Formation aeolianites either not proximal enough to the Blomerus Fault itself (The joints are not co-seismic deformation features), or only formed joints as a consequence of prevailing

regional stress. The aeolianites in the Agulhas study also appear to have only involved a deformation sequence up to (at most) the stage described by Fig. 5.8E, or significantly less slip occurred on the Struisbaai Fault (with consequently lower deformation levels) than the Blomerus Fault.

The deformation sequence as outlined by this section can be suggested to adequately describe the aeolianite deformation sequence, as a response to neotectonic fault activity on the Blomerus and Struisbaai faults. However, as noted by McCalpin and Nelson (2009), there is inherent uncertainty when interpreting whether several deformation features represent a single relatively large magnitude earthquake event, or multiple low magnitude earthquake events. A significant length of time (1ka - 10Ka) after the formation of deformation features, with active mechanical and chemical weathering of the host rock and deformation features, can make multiple palaeoearthquakes appear to be a single event through the preserved evidence (McCalpin and Nelson, 2009). Thus the deformation sequence could potentially represent several faulting events, but this cannot be confirmed within the scope of this study.

5.5.2 Age of Deformation Events

Providing an age for the deformation features associated to the Blomerus and Struisbaai faults, is crucial in inferring the neotectonic history of the Southern Cape. As recognised by McCalpin and Nelson (2009), the typical method of dating palaeoearthquakes is by constraining the possible maximum (oldest) and minimum (recent) ages at which the deformation features could have formed. The dating of the deformation events thus needs to take into account the ages of the Wankoe and Waenhuiskrans Formation aeolianites, and any calibrated ages derived for the consolidation times of the lithologies (McCalpin and Nelson, 2009).

As the deformation features in both the Wankoe and Waenhuiskrans Formation aeolianites formed post-consolidation, the deformation features must be younger than the consolidation times of the respective units. The Wankoe Formation (refer to sections 3.5.2) consolidated by $\sim$1.8 Ma, during the Lower Pleistocene (Marker and Holmes, 2005). The Waenhuiskrans Formation (refer to sections 3.5.3) in the Bantamsklip study area has a consolidation age of $\sim$80 ka, and in the Agulhas study area a consolidation age of $\sim$160 ka

(Bateman *et al.*, 2004). These consolidation ages therefore provide upper age constraints for the palaeoearthquakes.

The Blomerus Fault has been linked to the deformation features cross-cutting the Wankoe Formation aeolianites in the North Gansbaai, Heidehof, and Groot Hagelkraal study areas; and possibly the Waenhuiskrans Formation aeolianites in the Bantamsklip study areas (if the joints are co-seismic or post-seismic deformation features). The Blomerus Fault has additionally been linked to two fault scarps (Walkerbay and Quoin Point dune lineaments) possibly involving Waenhuiskrans Formation (off-set) and recent Holocene dunes. Consequently, the palaeoearthquake(s) on the Blomerus Fault could potentially have two age scenarios:
1) If the joints within the Waenhuiskrans Formation at the Bantamsklip study area are considered tectonic deformation features (due to either seismic shaking, fault movement beneath the aeolianites, or cover sequence readjustment to fault movement); and if the dune lineaments are considered to be defined by scarps in the Waenhuiskrans Formation, in both the Walkerbay and Quoin Point areas, a faulting event on the Blomerus Fault occurred some time after 80 kya.
2) If the joints observed in the Bantamsklip study area associated to prevailing regional stress fields (non-seismic tectonic deformation features), and if the dune lineaments are fault scarps involving the underlying geology, an earlier faulting event is most likely. The palaeoearthquake(s) must have happened before the deposition and consolidation of the Waenhuiskrans Formation, with deformation of the Wankoe Formation aeolianites only. This event occurred after 1.8 Ma and some time before 125 ka (the deposition age of the Waenhuiskrans Formation (Bateman *et al.*, 2004)). The joints cross-cutting the Bantamsklip area Waenhuiskrans Formation aeolianites do however provide evidence for neotectonic stress fields and resulting deformation younger than 80 ka.

As none of the fault-related (drag fold) deformation features are observed in the Waenhuiskrans Formation aeolianites in the Bantamsklip study area, the Blomerus Fault therefore has evidence for a palaeoearthquake(s) event during the Lower to Middle Pleistocene.

On the other hand, the deformation features observed in the Waenhuiskrans Formation aeolianites in the Agulhas study area must have formed some time after 160 ka. The Struisbaai Fault therefore has evidence for an Upper Pleistocene-aged palaeoearthquake. This age is consequently the youngest relatively dated evidence for neotectonic fault activity doc-

umented for the Southern Cape study region.

5.6 Stress Fields

The use of joints as geological stress indicators to constrain palaeostress fields and contemporary stress fields, is widely applied within the field of neotectonics (Engelder and Geiser, 1980; Hancock and Engelder, 1989; Hancock *et al.*, 1991; Eyal *et al.*, 2001; Khadkikar, 2002; Roberts and Myrvang, 2004) (refer to section 2.2). Owing to how joints propagate normal to σ_3 (Secor, 1965), the prevailing stress field in which the joint formed can be determined (refer back to section 5.2.1). Conjugate shear fractures and faults can additionally be used to determine the stress field of a given rock unit (Hancock and Engelder, 1989), but because joints have a high abundance (within the Southern Cape), joints are the preferred stress field indicator for this study. This section thus aims to constrain the local and regional stress fields for the Southern Cape, and provide possible explanations for any spatial and temporal variation of the respective stress fields. Furthermore the estimated regional stress field will be compared to the Wegener Stress Anomaly (WSA) (Andreoli *et al.*, 1996), and any differences between the two discussed.

5.6.1 Local and Regional Stress Fields

The joint planes measured throughout the different study areas have been plotted on the streonets in Fig. 5.9 as pole-to-plane data. The orientation density of the joint data has been subsequently Kamb contoured with 2σ contour intervals, at a 3σ significance level (where σ in this case represents standard deviation rather than a principal stress axis) (follows after Kamb (1959)).

The joint pole to plane data assumed to represent σ_3 trajectories, display variable orientations for σ_3 (distributed spread of data on the stereonets). As a consequence, the data points are averaged to provide mean σ_3 orientations for the study area/region. This is done through statistical calculation of eigenvectors by stereonent software, and involves the following method:

From Watson (1966), the stereonet is considered a spherical projection, with each data

point representing a unit mass on the sphere surface. A rotation axis (through the centre of the sphere) with the least distance to the points of mass on the surface of the sphere, would thus possess the least moment of inertia (Watson, 1966; Lisle, 1989; Whitaker and Engelder, 2005). Conversely, the moment of inertia is dependant on the orientation of the rotation axis, and the distribution of the mass points relative to the rotation axis (Lisle, 1989; Whitaker and Engelder, 2005). An orientation tensor (refer to Watson (1966) pg: 788 for the tensor matrix derived from the direction cosines of the pole to joint plane data) therefore produces eigenvectors (E_1, E_2, E_3) which define a three mutually perpendicular axis system so that the eigenvector E_1 corresponds to the point of lowest moment of inertia (rotation axis closest to all of the data points), E_3 to the point of highest moment of inertia, and E_2 the intermediate moment of inertia (Watson, 1966; Whitaker and Engelder, 2005). The axis that defines the lowest moment of inertia and the E_1 eigenvector is consequently the mean statistical point within the data points (Whitaker and Engelder, 2005). The E_1 eigenvector thus approximates the mean σ_3 principal stress axis for a given number of joints.

As the joints measured in the field study areas only provide σ_3 principal stress directions, the ambiguity between the orientations of σ_1 and σ_2 require the stress field to be reduced to the horizontal compressive stress components, S_{Hmin} and S_{Hmax} (Zoback and Zoback, 1980; Hancock *et al.*, 1991) (refer to section 2.3.1). As the joints are relatively vertical planar features, the eigenvector E_1 therefore also approximates the S_{Hmin} direction. Considering S_{Hmax} is perpendicular to S_{Hmin} the two horizontal compressive stress directions can be constrained (S_{Hmax} will additionally correspond closely to either E_2 or E_3 if the eigenvector is relatively horizontal).

Local Stress Fields

The joint data for the study areas has been organised in Fig. 5.9 by study area, and firstly displays the Wankoe Formation and subsequently the Waenhuiskrans Formation stress field data. The Kamb contoured poles to joint planes stereonet plots correspond to Fig. 5.3, where data clusters correlate to specific joint sets cross-cutting the aeolianite outcrops. The local horizontal compressive stress field is duly estimated for the respective study areas.

The North Gansbaai study area (Fig. 5.9A) stereonet plot for the joints, exhibit two clus-

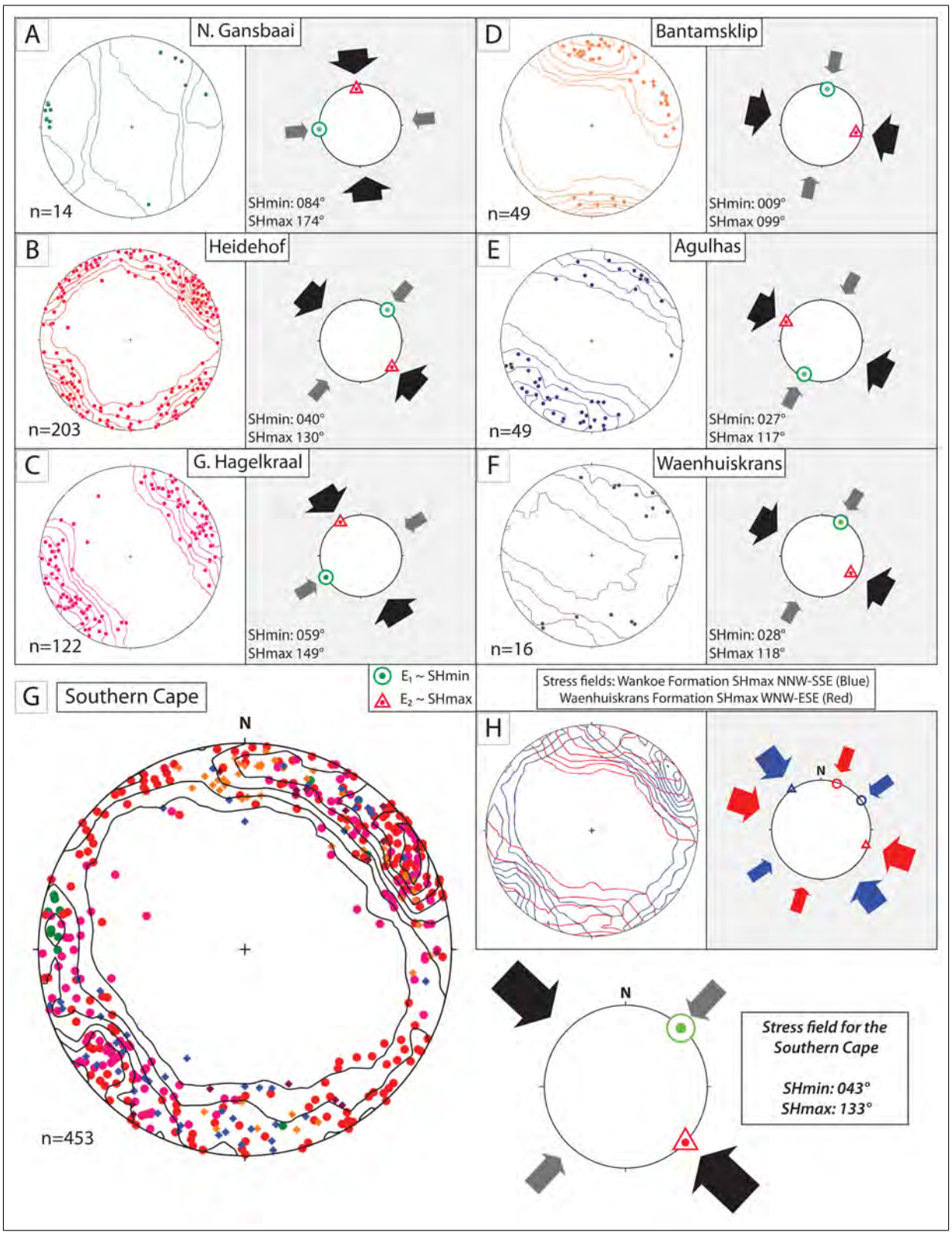

Figure 5.9: Stereonets with plotted pole to joint planes, Kamb contoured to express orientation density trends. The respective statistical eigenvector plot is provided, with the approximated S_{Hmin} and S_{Hmax} stress fields. See text for details on stereonets, statistics, and the local, regional, and age-related stress fields.

ters of poles in the WNW and the NE. The calculated eigenvectors indicate a horizontal E_1 WSW, and the horizontal E_2 NNW. The approximate local horizontal stress field for the North Gansbaai area is: S_{Hmin} azimuth trend 084 ° and S_{Hmax} azimuth trend 174 °.

The Heidehof study area (Fig. 5.9B) stereonet plot for the joints exhibit six clusters of poles, in a descending order of abundance, in the NE/SW, NW/SW, and NNE/SSW. The calculated eigenvectors indicate a horizontal E_1 NE, and the horizontal E_2 SE. The approximate local horizontal stress field for the Heidehof area is: S_{Hmin} azimuth trend 040 ° and S_{Hmax} azimuth trend 130 °.

The Groot Hagelkraal study area (Fig. 5.9C) stereonet plot for the joints exhibit four clusters of poles, in a descending order of abundance, in the NE/SW, and the NNE/SSW (approximately the NE and SW quadrants). The calculated eigenvectors indicate a horizontal E_1 SW, and the horizontal E_2 NW. The approximate local horizontal stress field for the Groot Hagelkraal area is: S_{Hmin} azimuth trend 059 ° and S_{Hmax} azimuth trend 149 °.

The Bantamsklip study area (Fig. 5.9D) stereonet plot for the joints exhibit three clusters of poles, in a descending order of abundance, in the N/S, and the ENE. The calculated eigenvectors indicate a sub-horizontal E_1 NNE, and the sub-horizontal E_2 ESE. The approximate local horizontal stress field for the Bantamsklip area is: S_{Hmin} azimuth trend 009 ° and S_{Hmax} azimuth trend 099 °.

The Agulhas study area (Fig. 5.9E) stereonet plot for the joints exhibit two dispersed clusters of poles, in a descending order of abundance, in the SW-S, and in the NE (approximately the NE and SW quadrants). The calculated eigenvectors indicate a sub-horizontal E_1 SSW, and the horizontal E_2 WNW. The approximate local horizontal stress field for the Agulhas area is: S_{Hmin} azimuth trend 027 ° and S_{Hmax} azimuth trend 117 °.

The Waenhuiskrans study area (Fig. 5.9F) stereonet plot for the joints exhibit two dispersed clusters of poles, in a descending order of abundance, in the NNE-WNW, and in the SSW-SSE. The calculated eigenvectors indicate a horizontal E_1 NE, and the sub-horizontal E_2 SW. The approximate local horizontal stress field for the Waenhuiskrans area is: S_{Hmin} azimuth trend 028 ° and S_{Hmax} azimuth trend 118 °.

The local stress fields as described above can be geographically positioned on Fig. 5.10A. The stress fields for the different study areas exhibit a trend of the S_{Hmax} and S_{Hmin} trajectories, with a average S_{Hmin} direction orientated NE-SW. There is however significant

variation of the S_{Hmax} and S_{Hmin} trajectories. The S_{Hmax} direction can be seen to vary from the eastern to the western parts of the Southern Cape; there is a more WNW-ESE S_{Hmax} trajectory in the Waenhuiskrans, Agulhas, and Bantamsklip areas, changing progressively to a more NNW-SSE S_{Hmax} in the Groot Hagelkraal, Heidehof, and North Gansbaai areas. The shift in stress field trajectory is therefore a clockwise rotation from east to west.

The variability in the stress field through the Southern Cape, may be due to various measuring bias, such as abundances differences of joints in specific study areas relative to the other study areas (Wankoe versus Waenhuiskrans Formations). The geometry of aeolianite outcrops furthermore also effect the measuring of joints (joints parallel to outcrop slopes are typically eroded away and not measurable). The systematic errors associated with data collection (compass, data recording errors) may additionally influence the calculated stress field variability.

However, if the variability in stress field over the Southern Cape is assumed to exist, this variation may be due to the following effects:

1)Topographical effects, primarily on the outcrop scale and secondly on a regional scale. The aeolianite ridges which constitute the study outcrops, have variable shapes in the different study areas. Therefore the geometry of these ridges may influence the internal stress fields (within a prevailing regional stress field) and consequently the fracture patterns (Miller and Dunne, 1996) (also refer to section 5.2.1 on variation in deformation features). On a regional scale, the NW part of the Southern Cape possesses higher topographical features (the Cape Fold mountains) than the SE to E part of the Southern Cape (Bredasdorp coastal plain) (refer to the DEM on Fig. 5.10A). The disturbance of the prevailing regional stress field though induced compressive/tensile stresses, or rotation of the stress trajectories, can significantly effect the fracture patterns observed through the Southern Cape (Miller and Dunne, 1996; Roberts and Myrvang, 2004).

2) The effects of pre-existing geological structures in the underlying geology. Stress has been known to be effected by pre-existing structures and crustal anisotropies within a given region (Zoback and Zoback, 1980; Zoback, 1992b). Residual stress from the formation of ancient crustal anisotropies (orogenic belts such as the Cape Fold Belt) are however, not considered to significantly effect the contemporary (neotectonic) stress field (Zoback, 1992a). Nevertheless, the assumption that the pre-existing Cape Fold Belt related structures themselves

(folds, faults within the underlying geology) can influence the prevailing regional stress field, would therefore control the orientations of the local stress fields within the Southern Cape. The clockwise rotation of the stress field does appear to correspond to the transition from the Southern domian to the Syntaxis domain of the Cape Fold Belt (Fig. 3.2); indicating a possible link between regional underlying crustal anisotropy and stress fields.

Regional Stress Field

The joints measured at all the study areas have been compiled on a single stereonet, and plotted as poles to joint planes (Fig. 5.9G). The poles are Kamb contoured for the orientation density of the joints. The data points on the stereonet are colour-coded to study area, and symbol-coded for host rock, being either the Wankoe or Waenhuiskrans Formations (the data colour and symbol key is viewable on Fig. 4.19).

The Southern Cape region stereonet plot exhibits a dispersed clustering of pole to plane data throughout the azimuth range, but a significantly higher density of poles in the NE and SW quadrants. The calculated eigenvectors indicate a sub-horizontal E_1 NE, and the horizontal E_2 SW. The approximate horizontal stress field for the Southern Cape is: S_{Hmin} azimuth trend 043 ° and S_{Hmax} azimuth trend 133 °.

In order to account for different levels of representation (sampling bias) of the the joints for the local study areas, a mean S_{Hmin} azimuth trend is taken from the means of the local S_{Hmin} azimuth trends (Caputo, 2005), this provides an additional S_{Hmin} azimuth trend for the Southern Cape of 039 °, with a corresponding S_{Hmax} azimuth trend of 129 °. The 'mean of the means' stress field azimuth trend is sufficiently similar to the stress field orientation calculated form the Southern Cape composite stereonet (Fig. 5.9G) to be considered the same (within the errors inherent to data collection).

The difference between the stress fields estimated from the Wankoe and Waenhuiskrans Formations, could possibly indicate a temporal shift in the stress field between consolidation and deformation of the respective aeolianite formations. The data collected from the Wankoe and Waenhuiskrans Formation aeolianites are compiled and Kamb contoured (Fig. 5.9H), with the resultant eigenvectors providing S_{Hmax} orientations for the Wankoe Formation NNW-SSE and the Waenhuiskrans Formation WNW-ESE. This indicates a shift

towards a more E-W orientated S_{Hmax} from the Late Pliocene - Lower Pleistocene to the Upper Pleistocence.

The Kamb contours for the different aeolianite formations do exhibit significant overlap which could imply the temporal shift in the stress field is a consequence of standard deviation in joint data (both respective E_1 eigenvectors are within range of the 4σ and 6σ contours for each of the data sets), the effect of sampling bias, where more data is available for the Wankoe Formation, is also a possible source of the stress field variation.

5.6.2 Wegener Stress Anomaly

The Wegener Stress Anomaly (WSA) as described by Andreoli *et al.* (1996); Viola *et al.* (2005); Bird *et al.* (2006), is a NW-SE trending region over the south-western part of Southern Africa with a S_{Hmax} stress direction orientated on average NW-SE (Fig. 3.4). This WSA relative to the larger-scale Southern Africa stress field, and the sources of the stress field are not fully understood (Bird *et al.*, 2006) (refer to section 3.4.3).

The S_{Hmax} and S_{Hmin} stress field orientations determined for the individual study areas and for the Southern Cape correspond to the stress field estimates provided by the following: Green and Bloch (1971); Andreoli *et al.* (1996); Brandt *et al.* (2005); Viola *et al.* (2005); Logue *et al.* (2012) (Fig. 5.10B), for areas within the south-western part of Southern Africa and the offshore continental shelf. These estimates, derived from earthquake focal mechanisms, bore-hole breakout orientations, and fault slip derived stress orientations, all indicate an ∼NW-SE orientated S_{Hmax} with extension S_{Hmin} orientated ∼NE-SW.

As the stress fields in this study agree with the larger-scale NW-SE trending S_{Hmax} WSA stress field (Bird *et al.*, 2006), the mechanisms responsible for the intraplate tectonic stress field for the SW part of Southern Africa can likewise apply to the Southern Cape. The regional stress field of the Southern Cape may be a product of one of the following mechanisms or a combination of some/all of the mechanisms: 1) Ridge-push derived horizontal compressive stress originating from the surrounding mid-oceanic spreading ridges (Viola *et al.*, 2005). 2) High continental topography induced horizontal extensional stress (Bird *et al.*, 2006). 3) Swell-push as a consequence of the 'African Superswell' resulting in vertical compressive stress (Singh *et al.*, 2009). 4) Different relative plate motion of the Somalia

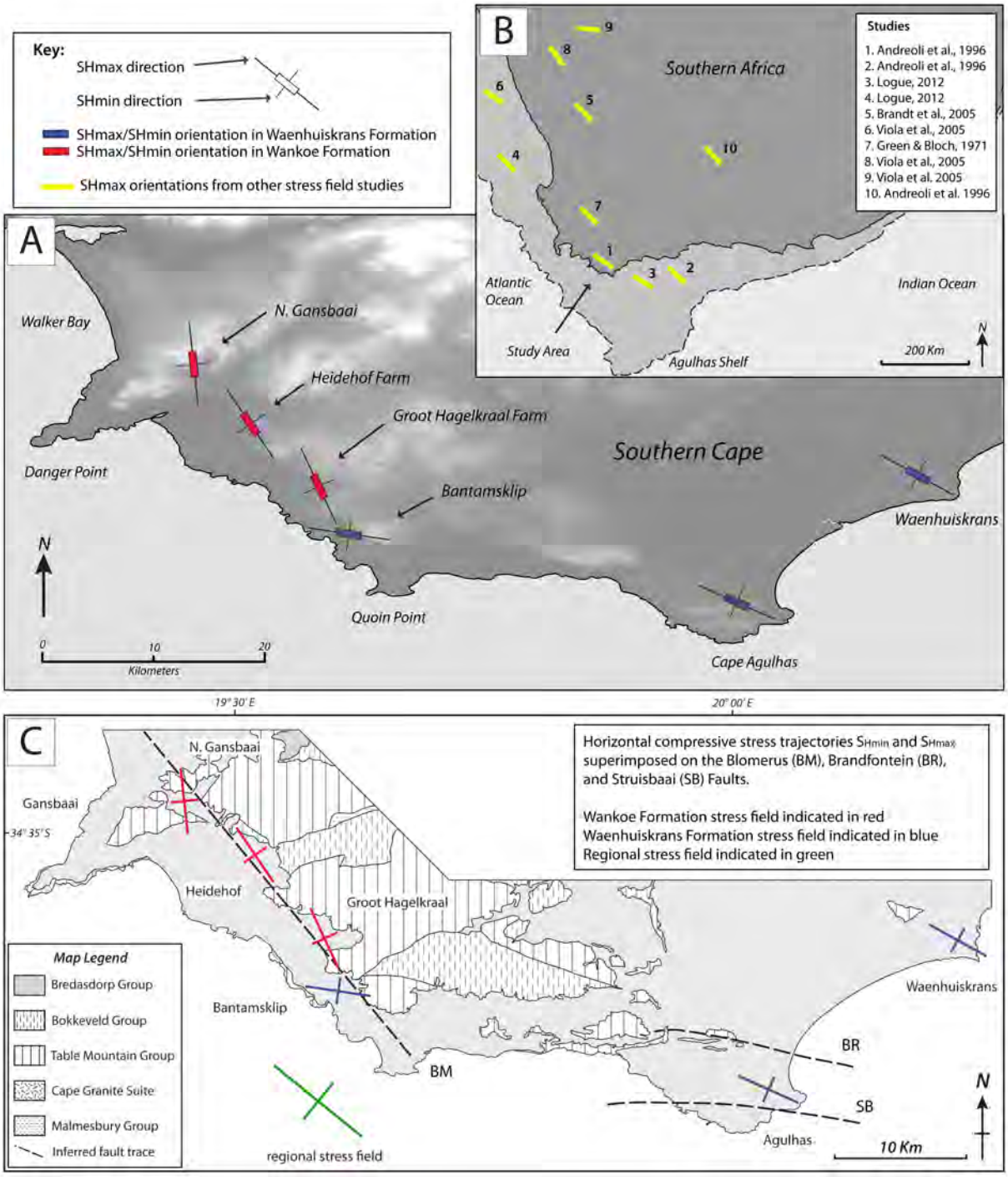

Figure 5.10: Maps illustrating the spatial distributions of the respective stress fields and the fault reactivation potential of the different faults. A) Local stress fields in relation to the study areas plotted on a DEM for the Southern Cape. Lighter areas on the DEM represent higher topography. B) Literature provided S_{Hmax} orientations for the SW part of Southern Africa, indicate the NW-SE S_{Hmax} orientated Wegener Stress Anomaly. C) Local Stress fields and the regional stress field plotted adjacent to the proposed faults in the Southern Cape to indicate fault reactivation potential. See text for more details.

Plate in contrast to the Nubia Plate, causing stress to accumulate as a result of incipient plate boundary formation through intact lithosphere (Bird *et al.*, 2006).

The WSA is poorly understood (Andreoli *et al.*, 1996), the stress field derived from this study can therefore add to the previous WSA stress field orientation estimates for the SW part of Southern Africa. More research is needed to fully understand the mechanisms behind the origin of the WSA in terms of global tectonics, but this study does consequently reinforce the understanding of the WSA as a neotectonic and contemporary stress field feature (Andreoli *et al.*, 1996; Viola *et al.*, 2012).

5.7 Earthquake Hazard

Faults are typically recognised as planes of mechanical weakness in the crust (White *et al.*, 1986; Nortje *et al.*, 2011). Hence any faults which are unable to further accommodate elastic strain accumulation, and are favourably orientated to a prevailing stress field, will preferentially reactivate instead of the formation of a new fault (Sibson, 1985; Baudon and Cartwright, 2008). This section will thus compare the orientations of the faults which are associated with neotectonic deformation features and exhibiting prior shear failure (the Blomerus and Struisbaai faults, with the Brandfontein Fault therefore excluded from this section), against the orientations of the local and regional Southern Cape stress fields. The type of fault reactivation will also be discussed, and as no evidence for compressional (thrust or reverse) faulting has occurred in the recent geological time within the Southern Cape (Bird *et al.*, 2006), whether the faults could potentially reactivate as normal or strike-slip type faults will need to be determined. Finally, estimates for palaeomagnitudes of the past faulting events and a possible recurrence interval for Southern Cape seismicity will be provided.

5.7.1 Reactivation Potential of the Recognised Faults

The reactivation potential of the Blomerus and Struisbaai faults is dependant on the cohesion and shear strength of the faults, the value of the static frictional co-efficient (μ_s), and the orientation of the faults to the prevailing stress field (assuming an Andersonian state of stress,

and conditions for Mohr-Coulomb shear failure) (Sibson, 1985, 1986, 1998; Nortje *et al.*, 2011) (refer to section 2.5.2).

As the Blomerus and Struisbaai Faults formed at the time of Gondwana rifting and subsequent formation of the AFFZ (during the Jurassic-Cretaceous), both the faults can be considered relatively mature. Therefore, the co-efficient of static friction can be assumed to be relatively low on the Byerlee rock friction range $0.6 < \mu_s < 0.85$ (Byerlee, 1978; Sibson, 1998). If the assumed value of $\mu_s \approx 0.6$, then the fault should reactivate when the fault plane is approximately 30 ° to σ_1 (Sibson, 1985).

The Blomerus 'fault plane' (the fault may involve significant splays) is found to be orientated approximately 140 ° across the study areas (Fig. 5.10C). The local stress field S_{Hmax} orientations that encompass the area that the Blomerus Fault transverses through, include the following: North Gansbaai - 174 °; Heidehof Farm - 130 °; Groot Hagelkraal Farm - 149 °; Bantamsklip - 099 °. The regional stress field S_{Hmax} is orientated 133 ° with the 'mean of means' azimuth trend 129 ° (Fig. 5.10C).

The deformation features associated with the Blomerus fault (normal faults, conjugate normal faults (section 5.2.1)) typically have a sub-vertical σ_1 direction, which indicates that the S_{Hmax} trajectory approximates the σ_2 and S_{Hmin} trajectory approximates σ_3 (a normal faulting regime). This implies, if the Blomerus fault is orientated parallel to the S_{Hmax} trajectory or within a close range of this stress field trajectory and is assumed to dip at ∼60 °, that the fault is suitably orientated to fail in the neotectonic stress field (Zoback, 1992b). The Blomerus Fault is orientated between 34 °-41 ° to the local North Gansbaai and Bantamsklip S_{Hmax} trajectories respectively, and orientated <10 ° to the Heidehof and Groot Hagelkraal S_{Hmax} trajectories. Additionally the Blomerus Fault is orientated ∼10 ° to the regional S_{Hmax} trajectory. The Blomerus Fault is therefore favourably orientated to reactivate as a normal fault in the estimated regional stress field, but at a local level could preferentially reactivate in the Heidehof and Groot Hagelkraal areas rather than in the North Gansbaai and Bantamsklip areas (segmented reactivation).

The Struisbaai Fault is inferred to have a shallower fault plane dip relative to the Blomerus Fault (refer to section 5.4.3). The lower dip angle of the fault plane would influence the reactivation potential, as reactivating thrust faults as normal faults needs $\mu_s < 0.55$ because of the higher reactivation angle (θ_r) (refer to section 2.5.1 and Fig. 2.5), and a tensile σ_3

or high fluid pressure required (Sibson, 1985). This notwithstanding, the Struisbaai fault is considered to have formed as a steep angled thrust fault (Andersen and Andreoli, 1990), which implies that the required conditions of reactivation would not be too dissimilar as those required to reactivate the Blomerus Fault.

Similar to the Blomerus Fault, the Struisbaai Fault posses associated deformation features (possible hybrid fractures and normal faults (refer to section 5.2.1) which suggest a sub-vertical σ_1 orientation. As a consequence, the Struisbaai Fault plane would also need to be relatively aligned to the S_{Hmax} trajectory (containing σ_2) direction. The Struisbaai Fault's arcuate orientation 088°-100° is typically less than 30° off of the local S_{Hmax} trajectory. The more eastern parts of the Struisbaai Fault are orientated <30° off of the regional S_{Hmax} trajectory. Therefore, the Struisbaai Fault is moderately orientated to fail as a normal fault in the prevailing local and regional stress fields. The fault geometry and the conditions of reactivation required to cause reactivation, both suggest a limited future reactivation is more likely when compared to the Blomerus Fault.

Considering Green and Bloch (1971); Andreoli *et al.* (1996); Viola *et al.* (2005) all suggest strike-slip faulting regimes for regions within the SW part of South Africa (where S_{Hmax} = σ_1 and S_{Hmin} = σ_3), the possibility of the Blomerus and Struisbaai faults reactivating as strike-slip faults also needs to be discussed. As previously stated above, optimal reactivation of a fault will occur when σ_1 is orientated 30° to the fault plane (provided the fault is conditioned for reshear, refer to section 2.5.1) (Sibson, 1985). As shown on Fig. 5.10C, the local stress fields in both the North Gansbaai and Bantamsklip areas are orientated ∼30° to the Blomerus Fault, and the Agulhas stress field is orientated <30° to the Struisbaai Fault. If the Blomerus Fault could reactivated as individual fault segments, both the North Gansbaai and Bantamsklip areas would have favourably orientated stress fields for near optimal strike-slip faulting. The Struisbaai Fault also has a moderate potential of reactivating as a strike-slip/oblique normal fault. However, the observed field evidence (refer to sections 5.2 & 5.4) all suggests that a normal faulting regime is dominant for the Southern Cape (thus faults will reactivate as normal faults rather than a strike-slip faults). Andreoli *et al.* (1996) also determined a normal faulting regime for the Southern Cape, which implies it is tectonically different (fault regime and the orientations of the principal stresses) from other parts of the SW Southern Africa and the Wegener Stress Anomaly region (refer to section 5.6.2).

5.7.2 Palaeomagnitudes and Earthquake Recurrence Interval

Both the Blomerus and the Struisbaai faults are considered moderately to well orientated to reactivate as normal faults, given the current/neotectonic stress fields. And as past fault movement is associated with these faults (observed neotectonic deformation features), the magnitude of the preserved palaeoearthquakes can be inferred. The recurrence intervals assessed from similar magnitude events in other intraplate tectonic settings (central U.S.A., and SE Australia) can be used to estimate a recurrence interval for the Southern Cape.

Palaeomagnitudes

The palaeomagnitudes of past faulting events on the Blomerus and Struisbaai faults can be estimated by the appraisal of the geological evidence (assumed to only represent a single palaeoearthquake on the faults), which involves the following: Length of surface faulting (truncated, deformed, and folded aeolianite; dune lineaments; aeromagnetic survey imaging, and remote sensing), rotation of the aeolianite cross-bedding, and the displacement along secondary faults to estimate slip displacement (Wells and Coppersmith, 1994; McCalpin and Nelson, 2009).

The Blomerus Fault is inferred to possess a whole fault rupture length of approximately 50 km and an average fault segment length of 10 km (segment length derives from the average lineament length mapped through remote sensing, refer to section 4.1). The Struisbaai Fault is inferred to have a rupture length of approximately 20-30 km. The down-dip fault rupture width is inferred from the continental seismogenic zone, being at most $\sim$10 km (the Southern Cape is an ancient rift zone, and situated on a passive continental margin) (Sibson, 2002). The inferred range of possible average fault slip displacements ($\bar{D}$) on the Blomerus Fault is estimated from the space required to rotate the aeolianites and form dune lineaments, which provides $\bar{D}$ = 2m, 4m, and 8m. The low level of deformation and lack of rotation of the aeolianites proximal to the Struisbaai Fault, and the minor displacement on the secondary normal fault on the fault trace provides an inferred $\bar{D}$ range of 0.2m and 0.5m.

The first palaeomagnitude determination method involves initially calculating the seismic moment (M_o) (total energy released during a faulting event), from the following equation (where shear modulus $\mu = 3\times10^4$ MPa for faults found in continental crust, and A= rupture

surface length of the fault×rupture down-dip fault width) (provided by Hanks and Kanamori, 1979; Kanamori and Brodsky, 2004):

$$M_o = \mu \times \bar{D} \times A \tag{5.2}$$

The resulting M_o value for the range of $\bar{D}$ values for the respective faults can subsequently be used to calculate the moment magnitudes (M_w) with the following equation (Kanamori and Brodsky, 2004):

$$M_w = \frac{\log M_o}{1.5} - 6.07 \tag{5.3}$$

From equation 5.3 the M_o values for different values of $\bar{D}$, and from equation 5.4 the resultant M_w values can be viewed in the table below:

Table 5.1: Palaeoearthquake seismic moments and magnitude results

Fault:	$\bar{D}$ (m)	M_o (Nm)	M_w
Blomerus	2	3×10^{19}	6.9
Fault (whole)	4	6×10^{19}	7.1
	8	12×10^{19}	7.3
Blomerus	2	6×10^{18}	6.4
Fault (seg.)	4	12×10^{18}	6.6
	8	24×10^{18}	6.8
Struisbaai	0.2	0.18×10^{19}	6.1
Fault	0.5	0.45×10^{19}	6.4

There is a correlation between surface rupture length and the magnitude of a given earthquake (Scholz *et al.*, 1986; Wells and Coppersmith, 1994). Consequently, the lengths of Blomerus Fault and Struisbaai Faults would provide inferred estimates of palaeomagnitudes for past faulting events. Therefore to make the palaeomagnitude estimates above more robust, a second method using the log-linear regression determined by Wells and Coppersmith (1994) is utilised. The regression between moment magnitude and surface rupture length is

given by:

$$M_w = 5.08 + 1.16 \times \log\left(Fault\ Length\right) \tag{5.4}$$

The Blomerus Fault with a 50 km whole fault length (presumed to have ruptured), provides a M_w of $\sim$7.0, whilst a 10 km fault segment length provides a M_w of $\sim$6.2. The Struisbaai Fault with a fault length of approximately 30km (presumed to have ruptured), provide a M_w of $\sim$6.7. These estimates appears to agree with the inferred values calculated in Table. 5.1.

Two palaeoearthquake end-members can thus be postulated for the Blomerus Fault: 1) There was a M_w $\sim$7.0 rupture along the entire fault length in a single seismic event. 2) There were multiple subsequent M_w $\sim$6.2 ruptures on each of the fault segments, progressively along the entire fault length. Although in the scope of this study it is difficult to determine which rupture scenario is true for the Blomerus Fault, the Landsat 7 imagery and DEM's do provide evidence that the Blomerus Fault is segmented. The Struisbaai Fault however, does not have similar remote sensing evidence to suggest fault segmentation (refer to section 4.1).

The following uncertainties attached to the determined M_o and M_w values need to be discussed and are dependant on the fault rupture length, width, and fault displacement:

The Blomerus and Struisbaai faults are assumed to have ruptured along the entire lengths of the determinable fault trace or subsequently as individual segments (the Blomerus Fault only). Whether this assumption is realistic depends on the abundance of faulting-related deformation along the fault trace. The Blomerus Fault exhibits neotectonic deformation features in the Heidehof and Groot Hagelkraal study areas, and dune lineaments (buried fault scarps) in the Walkerbay and Quoin Point areas. The Struisbaai Fault only exhibits potential co-seismic deformation across the Agulhas headland (offshore deformation features can be assumed to either not exist, or are long since eroded away).

The down-fault plane rupture width of $\sim$10 km (to the base of the seismogenic zone of a ancient rift zone, provided by Sibson (2002)) would appear to be a reasonable approximation, as earthquakes of typically M_w > 5.5 - 6.0 possess mainshock hypocentres near the base of the regional seismogenic zone (Wells and Coppersmith, 1994; Sibson, 2002). The depth of 10 km should be considered an upper-bound estimate, as the seismogenic crust in the Southern Cape is potentially thinner.

The $\bar{D}$ values are estimated from the level of tilt (space required for rotation) of the

aeolianites in the Heidehof and Groot Hagelkraal areas, deformation features (secondary antithetic fault displacement), and the formation of dune lineaments (buried fault scarps) by the Blomerus and Struisbaai Fault. As the Blomerus and Struisbaai Faults are blind normal faults, no accurate measurement of fault slip on an actual discrete fault plane can be made. Consequently, the provided $\bar{D}$ values are only rough indications of displacement on the fault planes. Because of these uncertainties, the second method of producing M_w values (provided by equation 5.4) is considered the most reliable, due to the use of fault rupture lengths and not slip values in the calculation.

Earthquake Recurrence Interval

Earthquake recurrence intervals, derived for intraplate regions in other parts of the world, can be used as possible analogues for the Southern Cape region (also situated within an intraplate region, refer to section 3.2).

The central and eastern parts of the United States of America (U.S.A.) are a typical intraplate tectonic environment (Li *et al.*, 2009), and are characterised by a seismically active region known as the New Madrid Seismic Zone (NMSZ) (Liu and Zoback, 1997; Kenner and Segall, 2000). Modelled recurrence times for large earthquakes (M_w>6) within the NMSZ are within the 100 to 1 ka years time range (Kenner and Segall, 2000). The NMSZ is known to have a relatively short recurrence interval, and as such, is considered a seismic zone where seismicity preferentially clusters in time and space (Li *et al.*, 2009). The recurrence interval provided for this region can thus be considered the 'low bracket' of the recurrence interval spectrum.

The SE part of Australia is also considered an intraplate tectonic environment (Sandiford and Egholm, 2008), where the Murray Basin is a particularly seismically quiet region (Sandiford, 2003). Slip rates on faults found within the Murray Basin are of the magnitude of $\sim$ 0.015mm.year^{-1} (Sandiford, 2003). Considering the fault slip rate relationship to earthquake recurrence intervals provided by Scholz *et al.* (1986); Sibson (2002), large earthquakes (M_w>6) would only recur on the 100 ka to 1 Ma years time range. The recurrence interval provided for this region can thus be considered the 'high bracket' of the recurrence interval spectrum.

The lack of multiple preserved palaeoearthquakes within the Wankoe and Waenhuiskrans Formation in the Heidehof, Groot Hagelkraal, and Agulhas study areas, indicates long recurrence intervals, more in line with the Murray Basin high bracket (100 ka - 1 Ma year time-scale) applies to the Southern Cape. However, the assumption that approximately same size (M_w) earthquakes will occur at regular intervals (provided by the recurrence interval) is not necessarily true for all faults (McCalpin and Nelson, 2009). The temporal and spatial distribution of intraplate earthquakes is also significantly complex (Li *et al.*, 2009), and as such, the recurrence interval provided for earthquake rupture on the Blomerus and Struisbaai Faults should be considered an estimate only.

The Blomerus and Struisbaai Faults are therefore well to moderately-well orientated to the prevailing Southern Cape local and regional stress fields (neotectonic to contemporary) to reactivate as normal faults. The deformation features, estimated slip displacements, and respective fault lengths all indicate relatively large (M_w>6) palaeoearthquakes have occurred during the neotectonic time period within the Southern Cape. Considering the recurrence interval for seismicity on the Blomerus and Struisbaai faults is on the 100 ka and 1 Ma years time-scales, the possibility of a future earthquake occurring in the next 100-1000 years is low. Nevertheless, as the age of the palaeoearthquake on the Blomerus Fault is between 125 ka - 1.8 Ma, and the Struisbaai Fault is less than 160 ka, the Southern Cape may possibly be over-due for an earthquake event. Consequently, a low to medium earthquake hazard can be estimated for the Southern Cape. However, as there is a high level of uncertainty associated with such an assessment in an intraplate tectonic setting, this conclusion can only be postulated as a tentative estimate.

Chapter 6

Conclusions

The following conclusions can be drawn from this study:

1) The brittle deformation features cross-cutting the Wankoe Formation aeolianites within the Heidehof and Groot Hagelkraal study areas, express higher levels of deformation than Wankoe Formation aeolianites in the North Gansbaai study area. The joints, faults, brittle/kink folds, cataclasites documented in the Heidehof and Groot Hagelkraal study areas, are considered to have formed post-consolidation of the aeolianites, predominantly during a rotation/tilting of the aeolianites during a single palaeoearthquake event. Some joints (e.g. in the North Gansbaai area) formed initially from regional prevailing stress and resultant crustal extension before active faulting, and thus are not associated with displacement on the Blomerus Fault (non-seismic deformation features). Furthermore, throughout the Southern Cape, the Wankoe Formation appears to be more deformed than the Waenhuiskrans Formation on average.

2) The aeolianites in the Heidehof and Groot Hagelkraal areas were rotated during the development of a monocline-type drag fold, which formed as a consequence of normal fault movement on the underlying blind Blomerus Fault. This monocline fold formed within the aeolianites over and parallel to the Blomerus Fault, and significantly tilted the aeolianites on the SW-side of the inferred fault trace. The substantial amount of space required to accommodate the tilting of a single block of hangingwall aeolianite is considered problematic; however, the space requirement may have been minimised through the rotation of relatively small blocks of aeolianite within the hangingwall of the propagating Blomerus

Fault. The progressive decrease in the degree of rotation from the NW to the SW, away from the Blomerus Fault trace as seen in the Heidehof and Groot Hagelkraal areas, agrees with multiple aeolianite block rotation and the expected tilt of strata within a normal fault-related monocline drag fold.

3) The brittle deformation features observed cross-cutting the Waenhuiskrans Formation aeolianites within the Bantamsklip, Agulhas, and Waenhuiskrans study areas, express comparably lower levels of deformation than the Wankoe Formation units. The joints, fault, and possible hybrid fractures are all considered to have formed post-consolidation of the aeolianites. Within the Bantamsklip area, the joints cross-cutting the Waenhuiskrans Formation aeolianites are suggested to be non-seismic, as the Blomerus Fault is believed to have only deformed the overlying Wankoe Formation in the Heidehof and Groot Hagelkraal areas (in a single palaeoearthquake event) before the deposition and consolidation of the Waenhuiskrans Formation. The deformation features in the Agulhas area are considered the result of a single palaeoearthquake on the Struisbaai Fault, with only minor movement on the fault in comparison to the Blomerus Fault. The joints observed in the Waenhuiskrans area are considered as non-seismic deformation features similar to the Bantamsklip area.

4) Soft-sediment deformation features observed in the Heidehof area, are probably the result of either sedimentary processes associated with aeolian dune deposition, or seismites formed within unconsolidated aeolian sand due to seismic shaking on the Blomerus Fault. If the SSD features are seismites, it implies an initial palaeoearthquake event occurred prior to the preserved faulting event which rotated and deformed the consolidated Wankoe Formation aeolianites in both the Heidehof and Groot Hagelkraal areas. The seismites would have also needed to have formed some time between $\sim$2.3 Ma to 1.8 Ma, during the deposition and consolidation of the Wankoe Formation. However, in the scope of this study the origin of these SSD features is uncertain.

5) The Cretaceous-Jurassic Enon Formation crops out south of the inferred trace of the Brandfontein Fault (Agulhas study area), and indicates that Gondwana break-up age faults are present in the Southern Cape. Likewise the Blomerus and the Struisbaai Faults are inferred to have formed during the break-up of Gondwana and the formation of the Agulhas Falklands Fracture Zone (AFFZ). The Gondwana rift-related Cape Dyke Swarm, and the offshore magnetic anomalies that formed during post-rift sea floor spreading, both strike

parallel to the orientation of the Blomerus Fault, and implies a possible age of fault formation at ∼130 Mya.

6) There is a difference in strike between joints in the respective aeolianite units. The joints within the Wankoe Formation aeolianites are found to strike more NNW-SSE to NW-SE, compared to the more WNW-ESE joint strike within the Waenhuiskrans Formation aeolianites. The Hybrid fractures and conjugate normal faults have similar strike orientations to the joints on average. In places, the extension directions (inferred parallel to the least compressive stress σ_3) provided by the deformation features, were shown to be perpendicular to the respective inferred fault traces, which imply at least some of the joints, hybrid fractures, and conjugate normal faults are co-seismic features and thus reflect the prevailing stress field during an earthquake.

7) As the Wankoe Formation and Waenhuiskrans Formation aeolianites have consolidation times in the Pleistocene, the orientation of the neotectonic joints can be assumed to reflect the Quaternary crustal stress conditions for the Southern Cape region. Because joints are tensile fractures, they provide σ_3 trajectories, and as joints are common features throughout the aeolianites in the Southern Cape, local and regional stress fields can be estimated. The local stress fields were found to have preferred S_{Hmax} trends WNW-ESE to NNW-SSW, with a clockwise stress field rotation from east to west across the Southern Cape. Although the clock-wise stress field rotation could be influenced by measurement/data collection errors, the effects of topography and the the underlying geological structures on propagating stress in the crust are suggested as the most likely causes of the stress field variation. The regional stress field, possessing a S_{Hmax} trend ∼NW-SE, agrees with the other previously measured stress fields for the SW of Southern Africa (refer to Bird *et al.*, 2006), otherwise known as the Wegener Stress Anomaly (WSA).

8) The Southern Cape region is demonstrated to possess a normal faulting regime (S_{Hmax}=σ_2 & S_{Hmin}=σ_3) type stress state. This is different to other parts of the WSA, which generally possess a strike-slip faulting regime (S_{Hmax}=σ_1 & S_{Hmin}=σ_3). This determined orientation of the principal stresses within the Southern Cape indicates that the tectonic nature of the WSA is heterogeneous in terms of stress-state, and thus can be considered a complex crustal stress feature.

Thus, the two key conclusions of this study are the following:

9) Analysis of discontinuous deformation features within the Plio-Pleistocene Wankoe and Waenhuiskrans Formation aeolianites, distributed throughout the Southern Cape of South Africa, indicate that neotectonics, in contrast to either wave under-cutting induced collapse or sedimentary processes within the aeolianites, would be the most likely origin for the observed deformation features. This is due to the orientation, spatial distribution, and deformation style of the deformation features and the tilted aeolianite cross-beds all significantly correlate to either the Blomerus or Struisbaai Faults. The proposed age of the neotectonic activity (palaeoearthquakes and nonseismic deformation) for the Blomerus Fault associated features, had occurred some time after 1.8 Ma and before 125 ka; and for the Struisbaai associated deformation features, some time after 160 ka. No evidence of palaeoearthquake activity could be attributed to the Brandfontein Fault, which, as such, is assumed to be seismically immobile since the break-up of Gondwana.

10) Comparison of the neotectonic horizontal stress field with the geometries of the Blomerus and Struisbaai faults, shows that the faults are orientated at low angles to (S_{Hmax}) (Blomerus Fault is $\sim$10 $^\circ$ to the regional S_{Hmax} and the Struisbaai Fault is <30 $^\circ$ to the regional S_{Hmax}). This indicates the faults are well to moderately-well orientated to reactivate as normal faults in the future. The magnitude of the palaeoearthquakes (on the Blomerus and Struisbaai Faults) are considered to have been relatively large (M_w>6) due to the proposed rupture lengths of the faults, which when contrasted with seismicity patterns in other intraplate tectonic settings (such as Australia and the central U.S.), imply long recurrence intervals of between (100 ka - 1 Ma) would apply to the Southern Cape. The age of the palaeoearthquakes, the attributed earthquake recurrence interval for Southern Cape, and the well to moderately-well orientated fault geometries to the inferred prevailing stress field, provide a low to moderate earthquake hazard of a future seismic event occurring in the next 100 to 1 ka years in the Southern Cape.

The present state of active tectonics (or at least the state of elastic strain accumulation on the respective faults) within the Southern Cape is however difficult to establish from only studying neotectonic and palaeoearthquake evidence.

In terms of future work, seismic monitoring of the Blomerus, Struisbaai, and Brand-

fontein Faults would better constrain whether these faults are indeed seismically active, provided there is actual micro-seismic activity. and provide a more robust estimate of future fault reactivation potential (as already suggested by Andersen and Andreoli (1990)). Although based on the current study, such efforts should preferentially concentrate on the Blomerus Fault. The actual dating of deformed aeolianite units would provide more confined age(s) for the palaeoearthquake events and stress field related joint formation. Furthermore, if a method could be found to reliably date the breccia and gouge units found on the Heidehof and Groot Hagelkraal Farms, a far more explicit age for the palaeoearthquake on the Blomerus Fault could potentially be provided. As such, more confined ages of the preserved palaeoearthquakes, with contemporary seismic monitoring of the faults, with the analysis of neotectonic deformation features, could produce a more conclusive earthquake hazard estimate for the Southern Cape.

References

Adams, E. A. and MacKenzie, W. S. (1998). *A Colour Atlas of Carbonate Sediments and Rocks Under the Microscope*. Manson Publishing Limited.

Allen, J. R. L. (1970). The avalanching of granular solids on dune and similar slopes. *Journal of Geology*, *78*, 326 – 351.

Amadei, B. (1996). Importance of Anisotropy When Estimating and Measuring $in\ situ$ Stresses in Rock. *International Journal of Rock Mechanics and Mining Sciences & Geomechanics Abstracts*, *33*, 293 – 325.

Andersen, N. J. B. and Andreoli, M. A. G. (1990). The structural evolution of the coastal area between Danger Point and Struisbaai in the southern Cape fold belt, with implications for the siting of a nuclear power station. *South African Journal of Science*, *86*, 499 – 511.

Anderson, E. (1905). The Dynamics of Faulting. *Transactions of the Edinburgh Geological Society*, *8*, 387 – 402.

Anderson, E. (1951). *The Dynamics of Faulting and Dyke Formation with Application to Britian, 2nd Edition*. Oliver and Boyd, Edinburgh.

Andreoli, M. A. G., Doucoure, M., Van Bever Donker, J., Brandt, D., and Andersen, N. J. B. (1996). Neotectonics of Southern Africa - a review. *African Geoscience Review*, *3*, 1 – 16.

Andreoli, M. A. G., van der Vlugt, R., Norman, N. G., von Veh, M. W., and Andersen, N. J. B. (1988). Geological map of the coastal strip between Gansbaai and Waenhuiskrans, 1:50 000. Eskom Southern Cape Nuclear Siting Project. *Atomic Energy Corporation of South Africa, Pretoria*.

Arlegui, L. E. and Simón, J. L. (2001). Geometry and distribution of regional joint sets in a non-homogeneous stress field: case study in the Ebro basin (Spain). *Journal of Structural Geology*, *23*, 297 – 313.

Bard, E., Antonioli, F., and Silenzi, S. (2002). Sea-Level during the penultimate interglacial period based on a submerged stalagmite from Argentarola Cave (Italy). *Earth and Planetary Science Letters*, *196*, 135 – 146.

Bateman, M. D., Holmes, P. J., Carr, A. S., Horton, B. P., and Jaiswal, M. K. (2004). Aeolianite and barrier dune construction spanning the last two glacialŰinterglacial cycles from the southern Cape coast, South Africa. *Quaternary Science Reviews*, *23*, 1681 – 1698.

Baudon, C. and Cartwright, J. (2008). The kinematics of reactivation of normal faults using high resolution throw mapping. *Journal of Structural Geology*, *30*, 1072 – 1084.

Ben-Avraham, Z., Hartnady, C. J. H., and Kitchin, K. A. (1997). Structure and tectonics of the Agulhas-Falkland fracture zone. *Tectonophysics*, *282*, 83 – 98.

Bintanja, R., van de Waal, R. S. W., and Oerlemans, J. (2005). Modelled atmospheric temperatures and global sea levels over the past million years. *Nature*, *437*, 125 – 128.

Bird, P., Ben-Avraham, Z., Schubert, G., Andreoli, M., and Viola, G. (2006). Patterns of stress and strain rate in southern Africa. *Journal of Geophysical Research*, *111*, 1 – 14.

Blenkinsop, T. G. (2008). Relationships between faults, extension fractures and veins, and stress. *Journal of Structural Geology*, *30*, 622 – 632.

Bons, P. D., Elburg, M. A., and Gomez-Rivas, E. (2012). A review of the formation of tectonic veins and their microstructures. *Journal of Structural Geology*, *43*, 33 – 62.

Brace, W. F. (1960). An extension of the Griffith theory of fracture to rocks. *Journal of Geophysical Research*, *65*, 3477 – 3480.

Bradley, D. C. (2008). Passive margins through earth history. *Earth-Science Reviews*, *91*, 1 – 26.

Brandt, D., Andreoli, M., and McCathy, T. (2005). The Late Mesozoic palaeosoils and Cenozoic fluvial deposits at Vaalputs, Namaqualand, South Africa: Possible depositional mechanisms and their bearing on the evolution of the continental margin. *South African Journal of Geology*, *108*, 267 – 280.

Brooke, B. (2001). The distribution of carbonate eolianite. *Earth-Science Reviews*, *55*, 135 – 164.

Byerlee, J. (1978). Friction of Rocks. *Pure and Applied Geophysics*, *116*, 615 – 626.

Caine, J. S., Evans, J. P., and Forster, C. B. (1996). Fault zone architecture and permeability structure. *Geology*, *24, No. 11*, 1025 – 1028.

Caputo, R. (1995). Evolution of orthogonal sets of coeval extension joints. *Terra Nova*, *7*, 479 – 490.

Caputo, R. (2005). Stress variability and brittle tectonic structures. *Earth Science Reviews*, *70*, 103 – 127.

Carr, A. S., Bateman, M. D., Roberts, D. L., Murray-Wallace, C. V., Jacobs, Z., and Holmes, P. J. (2010). The last interglacial sea-level high stand on the southern Cape coastline of South Africa. *Quaternary Research*, *73*, 351 – 363.

Chenrai, P. (2012). DEM Application for Geological Structure Interpretation: A Case Study at the Koh Samui Area, Gulf of Thailand. *World Applied Sciences Journal*, *17*, 1516 – 1520.

Clark, P. U., Dyke, A. S., Shakun, J. D., Carlson, A. E., Clark, J., Wohlfarth, B., Mitrovica, J. X., Hostetler, S. W., and McCabe, A. M. (2009). The Last Glacial Maximum. *Science*, *325*, 710 – 714.

Cox, R. T., Van Arsdale, R. B., Harris, J. B., and Larsen, D. (2001). Neotectonics of the southeastern Reelfoot rift zone margin, central United States, and implications for regional strain accommodation. *Geology*, *29*, 419 – 422.

Davis, G. H. and Reynolds, S. J. (1996). *Structural geology of rocks and regions*, Chapter 4: Deformation Mechanisms and Microstructures, 150 – 202. John Wiley & Sons, INC.

De Beer, C. H. (2012). Evidence of Neogene to Quaternary faulting and seismogenic deformation along the Namaqualand coast, South Africa. *South African Journal of Geology*, *115.2*, 117 – 136.

Dingle, R. V. (1973). Mesozoic palaegeography of the southern Cape, South Africa. *Palaeogeography, Palaeoclimatology, Palaeoecology*, *13*, 203 – 213.

Domoney, R. N. (2009). Stress patterns in the Cape Fold Belt. *11t SAGA Biennial Technical Meeting and Exhibition, Swaziland*, *1*, 506 – 509.

Drury, S. A. (Ed.) (1993). *Image Interpretation in Geology. Second Edition*, Chapter 4: Photogeology, 69 – 109. Chapman & Hall.

Dubois, A., Odonne, F., Massonnat, G., Lebourg, T., and Fabre, R. (2002). Analogue Modelling of Fault Reactivation: Tectonic Inversion and Oblique Remobilization of Grabens. *Journal of Structural Geology*, *24*, 1741 – 1752.

Dunne, W. M. and Hancock, P. L. (1994). *Continental Deformation*, Chapter Ch. 5: Paleostress Analysis of Small-scale Brittle Structures, 101 – 120. Pergamon Press Ltd.

Engelder, T. (1987). *Fracture Mechanics of Rock*, Chapter Ch. 2: Joints and Shear Fractures in Rock, 24 – 34. Elsevier.

Engelder, T. and Geiser, P. (1980). On the Use of Regional Joint Sets as Trajectories of Paleostress Fields During the Development of the Appalachian Plateau, New York. *Journal of Geophysical Research*, *85*, 6319 – 6341.

England, P. and Jackson, J. (2011). Uncharted seismic risk. *Nature Geoscience*, *4*, 348 – 349.

Etheridge, M. A. (1986). On the Reactivation of Extensional Fault Systems. *Philosophical Transactions of the Royal Society of London. Series A, Mathematical and Physical Sciences.*, *317*, 179 – 194.

Eyal, Y., Gross, M. R., Engelder, T., and Becker, A. (2001). Joint development during fluctuation of the regional stress field in southern Israel. *Journal of Structural Geology*, *23*, 279 – 296.

Fernandes, R. M. S., Ambrosius, B. A. C., Noomen, R., Bastos, L., Combrink, L., Miranda, J. M., and Spakman, W. (2004). Angular velocities of Nubia and Somalia from continuous GPS data: implications on present-day relative kinematics. *Earth and Planetary Science Letters*, *222*, 197 – 208.

Finch, E., Hardy, S., and Gawthorpe, R. (2004). Discrete-element modelling of extensional fault-propagation folding above rigid basement fault blocks. *Basin Research*, *16*, 489 – 506.

Flemming, N. C. (1965). Form and Relation to Present Sea Level of Pleistocene Marine Erosion Features. *Journal of Geology*, *73*, 799 – 811.

Green, R. W. E. and Bloch, S. (1971). The Ceres, South Africa, earthquake of September 29, 1969: Report on some aftershocks. *Bulletin of the Seismological Society of America*, *61*, 851 – 859.

Gürpinar, A. (2005). The importance of paleoseismology in seismic hazard studies for critical facilities. *Tectonophysics*, *408*, 23 – 28.

Hälbich, I. W. (1983). *Geodynamics of the Cape Fold Belt*, Chapter Chapter 14: A Tectogenesis of the Cape Fold Belt (CFB), 165 – 175. The Geological Society of South Africa.

Hälbich, I. W., De Beer, J. H., Du Plessis, A., Dürrheim, R. J., Maher, M. J., Pitts, B. E., Smith, G., Coetzee, D. S., Cornell, D. H., Fitch, F. J., Gresse, P. G., Krynauw, J. R., Le Roux, D. M., Le Roux, J. P., Miller, J. A., Söhnge, A. P. G., and Swart, J. (1993). The Cape Fold Belt - Agulhas Bank Transect Across the Gondwana Suture in Southern Africa. In *Global Geoscience Transect 9*. American Geophysical Union.

Hancock, P. L. (1985). Brittle Microtectonics: principles and practise. *Journal of Structural Geology*, *7*, 437 – 457.

Hancock, P. L. and Engelder, T. (1989). Neotectonic Joints. *Geological Society of America Bulletin*, *101*, 1197 – 1208.

Hancock, P. L., Maddock, R., Zoback, M. L., Skipp, B., and Vita-Finzi, C. (1991). Determining Contemporary Stress Directions from Neotectonic Joint Systems. *Philosophical Transactions: Physical Sciences and Engineering*, *337*, 29 – 40.

Hanks, T. C. and Kanamori, H. (1979). A moment-magnitude scale. *Journal of Geophysical Research*, *84*, 2348 – 2350.

Haq, B. U., Hardenbol, J., and Vail, P. R. (1987). The new chronostratigraphic basis of the Cenozoic and Mesozoic sea level cycles. *Special Publications - Cushman Foundation for Foraminifera Research*, *24*, 7 – 13.

Hausegger, S., Kurz, W., Rabitsch, R., Kiechl, E., and Brosch, F. (2010). Analysis of the internal structure of a carbonate damage zone: Implications for the mechanisms of fault breccia formation and fluid flow. *Journal of Structural Geology*, *32*, 1348 – 1362.

Heidbach, O., Tingay, M., Barth, A., Reinecker, J., Kurfeß, D., and Müller, B. (2010). Global crustal stress pattern based on the World Stress Map database realease 2008. *Tectonophysics*, *482*, 3 – 5.

Heilbronner, R. and Keulen, N. (2006). Grain size and grain shape analysis of fault rocks. *Tectonophysics*, *427*, 199 – 216.

Holmes, P. J., Bateman, M. D., Carr, A. S., and Marker, M. E. (2007). The place of aeolian coversands in the geomorphic evolution of the southern Cape coast, South Africa. *South African Journal of Geology*, *110*, 125 – 136.

Hudleston, P. J. and Labao, L. (1993). Information from fold shapes. *Journal of Structural Geology*, *15*, 253 – 264.

Jaeger, J. C. and Cook, N. G. W. (1976). *Fundamentals of Rock Mechanics - Second Edition*. Chapman and Hall Limited.

Johnston, S. T. (2000). The Cape Fold Belt and Syntaxis and the rotated Falkland Islands: dextral transpressional tectonics along the southwest margin of Gondwana. *Journal of African Earth Sciences*, *31*, 1 – 13.

Kamb, W. B. (1959). Ice Petrofabric Observations from Blue Glacier, Washington, in relation to Theory and Experiment. *Journal of Geophysical Research*, *64*, 1891 – 1909.

Kanamori, H. and Brodsky, E. E. (2004). The physics of earthquakes. *Report on Progress in Physics*, *67*, 1429 – 1496.

Keefer, D. K. (2002). Investigating landslides caused by earthquakes - A historical review. *Surveys in Geophysics*, *23*, 473 – 510.

Kenner, S. J. and Segall, P. (2000). A Mechanical Model for Intraplate Earthquakes: Application to the New Madrid Seismic Zone. *Science*, *289*, 2329 – 2332.

Khadkikar, A. S. (2002). Late Quaternary neotectonic joints: Confirmation of the connection between jointing and contemporary tectonic stress. *Geophysical Research Letters*, *29*, 52 – 56.

Klappa, C. F. (1980). Rhizoliths in terrestrial carbonates: classification, recognition, genesis and significance. *Sedimentology*, *27*, 613 – 629.

Lambeck, K. and Chappell, J. (2001). Sea Level Change Through the Last Glacial Cycle. *Science*, *292*, 679 – 686.

Leeder, M. R. (2011). *Sedimentology and Sedimentary Basins. From Turbulence to Tectonics*, Chapter 7: Bedforms and Sedimentary Structures in Flows and Under Waves, 132 – 170. Blackwell Publishing Ltd.

Leroy, M., Gueydan, F., and Dauteuil, O. (2008). Uplift and strength evolution of passive margins inferred from 2-D conductive modelling. *Geophysical Journal International*, *172*, 464 – 476.

Li, Q., Liu, M., and Stein, S. (2009). Spatiotemporal Complexity of Continental Intraplate Seismicity: Insight from Geodynamic Modeling and Implications for Seismic Hazard Estimations. *Bulletin for Seismological Society of America*, *99*, 52 – 60.

Lisle, R. J. (1989). The Statistical Analysis of Orthogonal Orientation Data. *The Journal of Geology*, *97*, 360 – 364.

Lithgow-Bertelloni, C. and Silver, P. G. (1998). Dynamic topography, plate driving forces and the African superswell. *Nature*, *395*, 269 – 272.

Liu, L. and Zoback, M. D. (1997). Lithospheric Strength and Intraplate Seismicity in the New Madrid Seismic Zone. *Tectonics*, *16*, 585 – 595.

Logue, A., Heidbach, O., Andreoli, M. A. G., Hodge, M. S., and Fagereng, A. (2012). Orientation of maximum horizontal stress (SHmax) in the western and southern coastline and offshore basins of South Africa: neotectonic implications. In *Southern African Society for Quaternary Research - Biennial Congress*.

Lund, B. and Townend, J. (2007). Calculating horizontal stress orientations with full or partial knowledge of the tectonic stress tensor. *Geophysical Journal International*, *170*, 1328 – 1335.

Malan, J. A. (1989a). Lithostratigraphy of the Waenhuiskrans Formation (Bredasdorp Group). *South African Committee for Stratigraphy - Lithostratigraphic Series*, *No. 8*, 1 – 10.

Malan, J. A. (1989b). Lithostratigraphy of the Wankoe Formation (Bredasdorp Group). *South African Committee for Stratigraphy - Lithostratigraphic Series*, *No. 5*, 1 – 6.

Malan, J. A. (1990). The Stratigraphy and Sedimentology of the Bredasdorp Group, Southern Cape Province, South Africa. Master's thesis, University of Cape Town.

Malan, J. A. (1991a). Lithostratigraphy of the De Hoopvlei Formation (Bredasdorp Group). *South African Committee for Stratigraphy - Lithostratigraphic Series*, *No. 4*, 1 – 22.

Malan, J. A. (1991b). Lithostratigraphy of the Klien Brak Formation (Bredasdorp Group). *South African Committee for Stratigraphy - Lithostratigraphic Series*, *No. 13*, 1 – 13.

Marker, M. E. and Holmes, P. J. (2005). Landscape evolution and landscape sensitivity: the case of the southern Cape. *South African Journal of Science*, *101*, 53 – 60.

Maud, R. R. and Botha, G. A. (2000). *The Cenozoic of Southern Africa*, Chapter Deposits of the South Eastern and Southern Coasts, 19 – 32. Oxford University Press.

McCalpin, J. P. (2005). Late Quaternary activity of the Pajarito fault, Rio Grande rift of northern Mexico, USA. *Tectonophysics*, *408*, 213 – 236.

McCalpin, J. P. (2009). *Paleoseismology - International Geophysics Series Vol. 95*, Chapter 2A: Field Techniques in Paleoseismology - Terrestrial Environments, 29 – 118. Elsevier.

McCalpin, J. P. and Nelson, A. R. (2009). *Paleoseismology - International Geophysics Series Vol. 95*, Chapter 1: Introduction to Paleoseismology, 1 – 27. Elsevier.

McCalpin, J. P., Rockwell, T. K., and Weldon, R. J. (2009). *Paleoseismology - International Geophysics Series Vol. 95*, Chapter 6: Paleoseismology of Strike-Slip Tectonic Environments, 421 – 496. Elsevier.

McKee, E. D. (Ed.) (1979). *A Study of Global Sand Seas. Geological Survey Professional Paper 1052*, Chapter E: Sedimentary Structures in Dunes, 83 – 134. United States Government Printing Press.

Miller, C. A., James, N. P., and Bone, Y. (2012). Prolonged carbonate diagenesis under an evolving late cenozoic; Nullarbor Plain, southern Australia. *Sedimentary Geology*, *261 - 262*, 33 – 49.

Miller, D. J. and Dunne, T. (1996). Topographical perturbations of regional stress and consequent bedrock fracturing. *Journal of Geophysical Research*, *101*, 25523 – 25536.

Montenat, C., Barrier, P., Ott d'Estevou, P., and Hibsch, C. (2007). Seismites: An attempt at critical analysis and classification. *Sedimentary Geology*, *196*, 5 – 30.

Moretti, M. (2000). Soft-sediment deformation structures interpreted as seismites in middle-late Pleistocene aeolian deposits (Apulian foreland, southern Italy). *Sedimentary Geology*, *135*, 167 – 179.

Nocquet, J. M., Willis, P., and Garcia, S. (2006). Plate kinematics of Nubia-Somalia using a combined DORIS and GPS solution. *Journal of Geodesy*, *80*, 591 – 607.

Nortje, G. S., Oliver, N. H. S., Blenkinsop, T. G., Keys, D. L., McLellan, J. G., and Oxenburgh, S. (2011). *Geology of the Earthquake Source: A Volume in Honour of Rick Sibson.*,

Chapter : New faults v. fault reactivation: implications for fault cohesion, fluid flow and copper mineralization, Mount Gordon Fault Zone, Mount Isa District, Australia, 287 – 311. Geological Society, London, Special Publications.

Nyblade, A. A. and Robinson, S. W. (1994). The African Superswell. *Geophysical Research Letters*, *21*, 765 – 768.

Obermeier, S. F. (2009). *Paleoseismology - International Geophysics Series Vol. 95*, Chapter 7: Using Liquefaction-Induced and Other Soft-Sediment Features for Paleoseismic Analysis, 497 – 564. Elsevier.

Owen, G., Moretti, M., and Alfaro, P. (2011). Recognising triggers for soft-sediment deformation: Current understanding and future directions. *Sedimentary Geology*, *235*, 133 – 140.

Partridge, T. C. (1998). Of diamonds, dinosaurs and diastrophism: 150 million years of landscape evolution in Southern Africa. *South African Journal of Geology*, *101*, 167 – 184.

Partridge, T. C. and Maud, R. R. (2000). *The Cenozoic of Southern Africa*, Chapter : Macro-Scale Geomorphic Evolution of Southern Africa, 3 – 18. Oxford University Press.

Paton, D. A. (2006). Influence of crustal heterogeneity on normal fault dimensions and evolution: southern South Africa extensional system. *Journal of Structural Geology*, *28*, 868 – 886.

Paton, D. A., Macdonald, D. I. M., and Underhill, J. R. (2006). Applicability of thin or thick skinned structural models in regions of multiple inversion episodes; southern South Africa. *Journal of Structural Geology*, *28*, 1933 – 1947.

Peacock, D. C. P. (2001). The temporal relationship between joints and faults. *Journal of Structural Geology*, *23*, 329 – 341.

Pfiffner, O. A. and Ramsay, J. G. (1982). Constraints on Geological Strain Rates: Arguments From Finite Strain States of Naturally Deformed Rocks. *Journal of Geophysical Research*, *87*, 311 – 321.

Pirrotta, C. and Barbano, M. S. (2010). Analysis of deformation structures in Pliocene and Quaternary deposits of the Hyblean Plateaux (south-eastern Sicily). *Tectonophysics*, *499*, 41 – 53.

Price, N. J. and Cosgrove, J. W. (1990). *Analysis of geological structures*. Cambridge University Press.

Ramsay, J. G. (1967). *Folding and fracturing of rocks*. McGraw-Hill, New York.

Ramsay, P. J. and Cooper, J. A. G. (2002). Late Quaternary Sea-Level Change in South Africa. *Quaternary Research*, *57*, 82 – 90.

Ramsey, J. M. and Chester, F. M. (2004). Hybrid fracture and the transition from extension fracture to shear fracture. *Nature*, *428*, 63 – 66.

Reynolds, S., Hillis, R., and Paraschivoiu, E. (2003). In situ stress field, fault reactivation and seal integrity in the Bight Basin, South Australia. *Exporational Geophysics*, *34*, 174 – 181.

Roberts, D. and Myrvang, A. (2004). Contemporary stress orientation features in bedrock, Trøndelag, central Norway, and some regional implications. *Norges Geologiske Undersøkelse*, *442*, 53 – 63.

Roberts, D. L., Botha, G. A., Maud, R. R., and Pether, J. (2006). *The Geology of South Africa*, Chapter 30: Coastal Cenozoic Deposits, 605 – 628. Geological Society of South Africa, Johannesburg; Council of Geoscience, Pretoria.

Rozendaal, A., Gresse, P. G., Scheepers, R., and Le Roux, J. P. (1999). Neoproterozoic to Early Cambrian Crustal Evolution of the Pan-African Saldanian Belt, South Africa. *Precambrian Research*, *97*, 303 – 323.

Sandiford, M. (2003). *Evolution and Dynamics of the Australian Plate*, Chapter 8: Neotectonics of southeastern Australia: linking the Quaternary faulting record with seismicity and in situ stress, 101 – 113. The Geological Society of America, Inc. (GSA), and the Geological Society of Australia.

Sandiford, M. and Egholm, D. L. (2008). Enhanced intraplate seismicity along continental margins: Some causes and consequences. *Tectonophysics*, *457*, 197 – 208.

Schlische, R. W. (1995). Geometry and Origin of Fault-Related Folds in Extensional Settings. *The American Association of Petroleum Geologists (AAPG) Bulletin*, *79*, 1661 – 1678.

Scholz, C. H. (1990). *The Mechanics of Earthquakes and Faulting*. Cambridge University Press.

Scholz, C. H., Aviles, C. A., and Wesnousky, S. G. (1986). Scaling Differences Between Large Interplate and Intraplate Earthquakes. *Bulletin of the Seismological Society of America*, *76*, 65 – 70.

Secor, D. T. (1965). Role of fluid pressure in jointing. *American Journal of Science*, *263*, 633 – 646.

Shone, R. W. and Booth, P. W. K. (2005). The Cape Basin, South Africa: A review. *Journal of African Earth Sciences*, *43*, 196 – 210.

Sibson, R. H. (1977). Fault rocks and fault mechanisms. *Journal of the Geological Society*, *133*, 191 – 213.

Sibson, R. H. (1985). A note on fault reactivation. *Journal of Structural Geology*, *7*, 751 – 753.

Sibson, R. H. (1986). Earthquake and Rock Deformation in Crustal Fault Zones. *Annual Reviews of Earth and Planetary Sciences*, *14*, 149 – 175.

Sibson, R. H. (1992). Implications of fault-valve behaviour for rupture nucleation and recurrence. *Tectonophysics*, *211*, 283 – 293.

Sibson, R. H. (1998). Brittle failure mode plots for compressional and extensional tectonic regimes. *Journal of Structural Geology*, *20*, 655 – 660.

Sibson, R. H. (2002). *International Handbook of Earthquake & Engineering Seismology 81(A)*, Chapter 29: Geology of the Crustal Earthquake Source, 455 – 473. Academic Press.

Siesser, W. (1972). Petrology of the Cainozoic Coastal Limestones of the Cape Province, South Africa. *The Transactions of the Geological Society of South Africa*, *75*, 177 – 185.

Siesser, W. G. and Dingle, R. V. (1981). Tertiary Sea-Level Movements around Southern Africa. *The Journal of Geology*, *89*, 523 – 536.

Singh, M., Kijko, A., and Durrheim, R. (2009). Seismotectonic Models for South Africa: Synthesis of Geoscientific Information, Problems, and the Way Forward. *Seismological Research Letters*, *80*, 71 – 80.

Singh, M., Kijko, A., and Durrheim, R. (2011). First-order regional seismotectonic mode for South Africa. *Natural Hazards*, *59*, 383 – 400.

Söhnge, A. P. G. (1983). *Geodynamics of the Cape Fold Belt*, Chapter 1: The Cape Fold Belt - Perspective, 1 – 6. The Geological Society of South Africa.

Stewart, I. S. and Hancock, P. L. (1994). *Continental Deformation*, Chapter Ch. 18: Neotectonics, 370 – 409. Pergamon Press Ltd.

Thomson, K. (1999). Role of continental break-up, mantle plume development and fault reactivation in the evolution of the Gamtoos Basin, South Africa. *Marine and Petroleum Geology*, *16*, 409 – 429.

Trumbull, R. B., Reid, D. L., De Beer, C. H., and Romer, R. L. (2007). Magmatism and continental breakup at the west margin of southern Africa: A geochemical comparison of dolerite dikes from NW Namibia and the Western Cape. *South African Journal of Geology*, *110*, 477 – 502.

U.S. Nuclear Regulatory Commission (2007). Regulatory Guide 1.208: A Performance-based Approach to Define the Site-specific Earthquake Ground Motion. Technical report, Office of Nuclear Regulatory Research.

Van Loon, A. J. (2009). Soft-sediment deformation structures in siliciclastic sediments: an overview. *Geologos*, *15*, 3 – 55.

Viljoen, J. H. A. (1992). *Inversion Tectonics of the Cape Fold Belt, Karoo and Cretaceous Basins of Southern Africa*, Chapter 4: The stratigraphy of the Heidelberg/Riversdale Mesozoic Basin, 77 – 84. A.A. Balkema Publishers.

Viola, G., Andreoli, M. A. G., Ben-Avraham, Z., Stengel, I., and Reshef, M. (2005). Offshore mud volcanoes and onland faulting in southwestern Africa: neotectonic implications and constraints on the regional stress field. *Earth and Planetary Science Letters*, *231*, 147 – 160.

Viola, G., Kounov, A., Andreoli, M. A. G., and Mattila, J. (2012). Brittle tectonic evolution along the western margin of South Africa: More than 500 Myr of continued reactivation. *Tectonophysics*, *514 - 517*, 93 – 114.

Von Veh, M. W. (1992). *Inversion Tectonics of the Cape Fold Belt, Karoo and Cretaceous Basins of Southern Africa*, Chapter 6: Compressional and extensional tectonics in the southernmost exposures of the Cape Fold Belt, 185 – 192. A.A. Balkema Publishers.

Waelbroeck, C., Labeyrie, L., Michel, E., Duplessy, J. C., McManus, J. F., Lambeck, K., Balbon, E., and Labracherie, M. (2002). Sea-level and deep water temperature changes derived from benthic foraminifera isotope record. *Quaternary Science Reviews*, *21*, 295 – 305.

Watson, G. S. (1966). The Statistics of Orientation Data. *The Journal of Geology*, *74*, 786 – 797.

Wells, D. L. and Coppersmith, K. J. (1994). New Emperical Relationships among Magnitude, Rupture Length, Rupture Width, Rupture Area, and Surface Displacement. *Bulletin of the Seismological Society of America*, *84*, 974 – 1002.

Whitaker, A. E. and Engelder, T. (2005). Characterizing stress fields in the upper crust using joint orientation distributions. *Journal of Structural Geology*, *27*, 1778 – 1787.

White, S. H., Bretan, P. G., and Rutter, E. H. (1986). Fault-Zone Reactivation: Kinematics and Mechanisms. *Philosophical Transactions of the Royal Society of London. Series A, Mathematical and Physical Sciences*, *317*, 81 – 97.

Willsey, S. P., Umhoefer, P. J., and Hilley, G. E. (2002). Early evolution of an extensional monocline by a propagating normal fault: 3D analysis from combined field study and numerical modelling. *Journal of Structural Geology*, *24*, 651 – 669.

Zoback, M. L. (1992a). First- and Second-Order Patterns of Stress in the Lithosphere: The World Stress Map Project. *Journal of Geophysical Research*, *97*, 11 703 – 11 728.

Zoback, M. L. (1992b). Stress Field Constraints on Intraplate Seismicity in Eastern North America. *Journal of Geophysical Research*, *97*, 11 761 – 11 782.

Zoback, M. L. and Zoback, M. D. (1980). State of Stress in the Conterminous United States. *Journal of Geophysical Research*, *85*, 6113 – 6156.